Structure-guided design of novel inhibitors targeting the drug-resistant M2 proton channel from pandemic “swine” influenza

Claire Scott

Submitted in accordance with the requirements for the degree of
Doctor of Philosophy

The University of Leeds
School of Medicine

July 2016

The candidate confirms that the work submitted is her own and that appropriate credit has been given where reference has been made to the work of others.

Chapter 3

A/England/195/2009 (H1N1) M2 homology model based upon the published PDB 2RLF structure (Schnell & Chou, 2008), minimisation in octanol and the associated clip files were generated by Dr Jayakanth Kankanala. The overlay of 2RLF and E915 M2 homology model was carried out by Dr Richard Foster.

Unbiased compound docking and attrition carried out by Dr Jayakanth Kankanala.

Rapid Overlay of Compound Structures (ROCS) docking was rescored using SPROUT by Dr Katie Simmons.

Selection of analogues carried out by Dr Richard Foster.

Chapter 4

Figure 4.1: Liposome assay carried out by Ranjitha Tathineni

Figure 4.2: Liposome and plaque assays carried out by Dr Toshana Foster.

Chapter 6

A second E195 M2 homology model, based upon PDB 2L0J (Sharma *et al.*, 2010) was generated by Dr Richard Foster.

This copy has been supplied on the understanding that it is copyright material and that no quotation from the thesis may be published without proper acknowledgement.

© 2016 The University of Leeds and Claire Scott

The right of Claire Scott to be identified as Author of this work has been asserted

by her in accordance with the Copyright, Designs and Patents Act 1988.

Acknowledgements

I would like to thank my supervisor Dr Stephen Griffin for his guidance and support throughout my PhD, for listening to my ideas and believing in me. Thank you to my co-supervisor Dr Richard Foster for his training and time. For joining my supervisory team and for all of his advice I would like to thank Prof Graham Cook. I also extend my thanks to Dr Peter Marshall, my supervisor during an industrial placement year at GSK, who saw my potential and encouraged me to undertake a PhD. Thank you to Dr Laura Wetherill for her training and both technical and moral support through my first months, but also for always being willing to answer my questions and grievances throughout and thank you to Dr Matthew Bentham for, somewhat reluctantly at first, taking on some of this role. I would like to thank Dr Jayakanth Kanakanala for his invaluable training and assistance with the *in silico* work. Thank you to Dr Toshana Foster who carried out the initial experiments. For their collaboration, training and guidance, I thank Prof Wendy Barclay and Dr Ruth Elderfield from Imperial College London, without whom the project would not have progressed as far. My thanks to all past and present members of the Griffin lab, for their friendship and advice, as well as the occasional splitting of cells and routinely listening to my frustration with the liposome assay. Numerous members of the Foster lab aided me on my visits to the Chemistry department, especially when it came to using the modelling software, so thank you to them for their kind assistance and making me feel welcome, not useless. I would like to thank the virology group for listening to so many of my talks and always finding new and challenging questions to ask. Thank you to the many faces on level 5 who made it an interesting and fun place to work, helping me to get through the never ending plaque assays by supplying an equally never ending amount of baked goods and sweets. Thank you to the hiking club (LUUHC) for welcoming me when I first arrived, being the excuse why I couldn’t spend all of my weekends in the lab and to the PhD members for their empathy, but most importantly for some truly amazing friendships and memories. I would like to thank all my friends and family back home for their support over the years. A special thank you to my parents, Kim and Dave, for their unconditional support and love throughout all of my studies. Lastly, thank you to Steve (aka Bob) for ensuring that, alongside my time in the lab and writing, our lives were full of laughs and adventures.

Abstract

Antiviral drugs are essential in the early response to pandemic influenza, whilst effective vaccines are developed. The 2009 pandemic H1N1 (pH1N1) strain, and other currently circulating Influenza A viruses (IAVs), are almost ubiquitously resistant to the licensed antivirals amantadine and rimantadine, which target the M2 proton channel. Amongst the polymorphisms associated with M2 drug resistance, asparagine at position 31 (N31) is the most prevalent. With resistance to neuraminidase-targeted antivirals also on the rise there exists an urgent need to develop new inhibitors targeting resistant strains. Through the generation of a pH1N1 M2 homology *in silico* model, we have identified the first non-adamantane compounds targeting M2 that are effective against the N31 pH1N1 strain.

Controversy exists over the binding site of current adamantane based antivirals to M2, with both lumenal and peripheral sites described in the literature. The novel compounds identified herein using our *in silico* model were selected based upon a predicted preference for one or other of these binding sites. As such, these compounds represent useful tools to investigate the potential of targeting both sites in combination, which will help to mitigate potential drug resistance. A novel *in vitro* assay was established to test the functional preferences of these compounds, with the results largely supporting *in silico* predictions. Combinations of lumenally and peripherally targeted compounds resulted in synergistic effects upon infectious virus titre, whereas this was not the case for combinations of compounds predicted to bind at the same site; in the case of two lumenally targeted compounds, this resulted in antagonistic effects. These data support the presence of two drug target sites within the M2 proton channel complex. Finally, whilst resistance within M2 was readily selected against amantadine analogue M2WJ332, this was not the case for non-adamantane compounds, further emphasising the potential benefits of investigating novel compound classes.

Table of Contents

Acknowledgements .... **iii**

Abstract .... **iv**

Table of Contents .... **v**

Table of Figures .... **x**

Table of tables .... **xiv**

Abbreviations .... **xvi**

Chapter 1 Introduction **2**

- 1.1 Influenza viruses 2
- 1.2 Influenza A viruses 3
  - 1.2.1 Origin and Discovery 3
  - 1.2.2 Classification 3
  - 1.2.3 Host range 4
  - 1.2.4 Transmission 9
  - 1.2.5 Seasonal influenza A 10
  - 1.2.6 Pandemic influenza 10
- 1.3 Molecular biology of influenza A virus 12
- 1.4 Influenza A virus life cycle 14
- 1.5 Innate immunity 16
- 1.6 Influenza vaccination 17
  - 1.6.1 Current annual vaccination 18
  - 1.6.2 Universal vaccines 20
- 1.7 Influenza Antivirals 20
  - 1.7.1 M2 inhibitors 22
  - 1.7.2 Neuraminidase inhibitors (NAIs) 22
  - 1.7.3 Resistance 22
  - 1.7.4 Targeting the host 25
- 1.8 M2 26
  - 1.8.1 Mechanism of M2 proton conductance 26
  - 1.8.2 Functions of M2 during the IAV life cycle 29
  - 1.8.3 IAV M2 tetramer structures 30
  - 1.8.4 The future of M2 as a drug target 35
- 1.9 Viroporins 36
  - 1.9.1 Hepatitis C Virus (HCV) p7 37

1.9.2 Human Immunodeficiency Virus type 1 (HIV-1) Vpu 41
1.9.3 Human Respiratory Syncytial Virus (hRSV) SH 42
1.9.4 Human Papillomavirus type 16 (HPV-16) E5 43
1.10 Aims 44
Chapter 2 Materials and methods...46
2.1 Materials...46
2.1.1 Compounds 46
2.1.2 Lipids 46
2.1.3 M2 peptides 46
2.1.4 Mammalian Cell Culture...47
2.1.5 Influenza A virus 47
2.1.6 Oligonucleotides 47
2.2 *In silico* protein modelling and drug binding 47
2.2.1 E195 M2 homology model 47
2.2.2 High throughput docking using eHiTS...48
2.3 *In vitro* liposome assay 49
2.3.1 Liposome preparation 49
2.3.2 M2 activity liposome assay 50
2.4 Mammalian Cell Culture 51
2.4.1 Recovery of Cells...51
2.4.2 Maintenance and Passage of Cells...51
2.4.3 Storage of Cells 51
2.4.4 Cell plating for compound treatment and infection 51
2.5 Cell culture cytotoxicity assays 52
2.5.1 Determination of cell confluency 52
2.6 Virus production and storage...52
2.6.1 Growing virus stocks...52
2.6.2 Freezing virus for storage 53
2.7 Plaque reduction assay 53
2.7.1 Virus titration..53
2.7.2 Compound screening..54
2.7.3 Determination of IC_{50} values 54
2.7.4 Compound combinations 54
2.8 Selection of escape mutants...55
2.8.1 Serial passage using increasing compound concentrations 55

2.8.2 Plaque purification 55
2.8.3 Viral RNA Extraction 55
2.8.4 Reverse Transcription...56
2.8.5 cDNA Amplification 56
2.8.6 PCR purification..56
2.8.7 Gel electrophoresis...57
2.8.8 Sequencing..57

Chapter 3 *In silico* screening of compounds against a pH1N1 M2 homology model 59

3.1 Introduction 59
3.2 Generation of a pH1N1 M2 homology model *in silico* 60
3.2.1 Defining lumenal and peripheral binding regions..........................63
3.3 *In silico* prediction of the binding preferences for adamantane compounds...65
3.3.1 *In silico* docking of adamantane compounds to the E195 M2 homology model 65
3.3.2 Analysis of docking scores and poses of adamantane compounds..67
3.4 Unbiased screening for novel compounds targeting the rimantadine resistant M2 ion channel of pH1N1 influenza.......................................71
3.4.1 High throughput docking using eHiTs 71
3.4.2 Attrition 72
3.4.3 Specific interactions between unbiased compounds and the E195 M2 ion channel, predicted by eHiTS 72
3.5 Biased compound selection...77
3.5.1 Compound attrition 77
3.5.2 Analysis of specific interactions between compounds and residues in the M2 tetramer 81
3.6 Analogues of first generation compounds..85
3.6.1 Prediction of ligand-protein binding modes using eHiTS 85
3.6.2 Analysis of predicted docking poses and interactions of L1, L4 and P6 analogues with the lumenal binding site of the E195 M2 homology model 86
3.6.3 Analysis of predicted docking poses and interactions of L1, L4 and P6 analogues with the peripheral binding site of the E195 M2 homology model 90
3.7 Discussion..97

Chapter 4 Screening novel compounds for activity against M2 *in vitro* and effects upon virus titre in culture..103

4.1 Introduction 103

4.2 Effects of adamantane derivative compound D on M2 *in vitro* and in virus culture..107

4.3 Non-adamantane compounds are capable of inhibiting M2 *in vitro* and in virus culture 112

4.3.1 Dose dependent effects of predicted lumenal and peripheral targeted compounds on N31 CD peptide 112

4.3.2 Effect of compounds on cellular metabolism and virus titre........115

4.4 Assessing compound binding preferences *in vitro* via differential inhibition of M2 peptides..115

4.5 Dissecting binding preferences and improving potency of novel non-adamantane compounds 120

4.5.1 Does peptide preference of unbiased compounds change with alterations in chemical structure?..121

4.5.2 Do unbiased compound analogues have improved effects against E195 virus titre? 127

4.6 Effects of compounds derived from a biased screen on M2 channel activity and E195 virus titre...130

4.7 Effect of non-adamantane compounds on S31 peptide 132

4.8 Assessing potency of novel effective compounds..............................136

4.9 Discussion...140

Chapter 5 Cell culture investigations of compound specificity......................148

5.1 Introduction 148

5.2 Drug combination assays 149

5.2.1 Combination of predicted lumenally, and peripherally targeted compounds...152

5.2.2 Combination of two predicted peripherally targeted compounds 153

5.2.3 Can combination experiments resolve the preferred binding site of DL7?...155

5.2.4 Combinations of M2 and NA inhibitors 158

5.2.5 Further analysis of combination indexes 159

5.3 Generation of escape mutants to support predicted compound binding164

5.3.1 Optimisation of M2 sequencing from vRNA within infectious cell culture supernatants 165

5.3.2 Resistance selection following prolonged low MOI infection in presence of high compound concentrations..............................166

5.3.3 Selection of resistance by serial passage in increasing concentration of compound 168

5.3.4 Plaque purification 170

5.4 Discussion 176

Chapter 6 Reconciliation of *in silico* work and final discussion 187

6.1 Reconciliation of *in silico* work 187

6.1.1 Membrane minimised E195 M2 homology model 189

6.1.2 A homology model based upon a structure solved in a lipid environment 192

6.1.3 Discussion 198

6.2 Final discussion 199

Chapter 7 References 202

Appendix 230

Appendix A Supplementary Data 230

Appendix B Recipes 248

B.1 Carboxyfluorescein (CF) buffer 248

B.2 Liposome assay buffer 248

B.3 Cell culture media 248

B.4 Freezing media 248

B.5 Serum free (SF) media 248

B.6 Overlay media 248

B.7 Viral RNA extraction buffers 248

B.8 5x Superscript III (SSCIII) first strand buffer 249

B.9 PCR purification buffers 249

B.10 50x Tris-acetate-EDTA (TAE) 249

Appendix C Description and semi-quantitative analysis of compound combinations 250

Appendix D Summary of compound effects 251

Table of Figures

Figure 1.1 Schematic illustration of the Influenza A virus life cycle. 15

Figure 1.2 Molecular structures of FDA approved influenza A virus antivirals. 21

Figure 1.3 Sequence of A/England/195/2009 segment 7. 27

Figure 1.4 A selection of the published influenza A virus M2 tetramer structures. 33

Figure 3.1 Sequence and structure of the conductance domain of M2 from A/Udorn/307/1972 (H3N2) (Udorn, 2RLF) and pH1N1 A/England/195/2009 (H1N1) (E195) M2 homology model. 62

Figure 3.2 Positions of key residues within the conductance domain of M2 from A/Udorn/307/1972 (H3N2) (Udorn, 2RLF) and pH1N1 A/England/195/2009 (H1N1) (E195) M2 homology model. 64

Figure 3.3 Binding sites residues in the E195 M2 homology model. 66

Figure 3.4 Structure of adamantane containing compounds M2WJ332 and compound D. 68

Figure 3.5 *In silico* docking poses of adamantane containing compound M2WJ332 to the E195 M2 homology model based upon the published structure PDB 2RLF. 69

Figure 3.6 *In silico* docking poses of adamantane containing compound D to the E195 M2 homology model based upon the published structure PDB 2RLF. 70

Figure 3.7 Predicted docking pose and polar interactions identified between predicted lumenal binders and the lumenal binding site of the E195 M2 homology model. 73

Figure 3.8 Predicted docking pose and polar interactions identified between predicted peripheral binders and the peripheral binding site of the E195 M2 homology model. 74

Figure 3.9 *In silico d*ocking poses of biased compounds in the E195 M2 tetramer homology model. 82

Figure 3.10 Predicted interactions between DL compounds and the lumenal binding site of the E195 M2 homology model. 83

Figure 3.11 Predicted interactions between DP compounds and the peripheral binding site of the E195 M2 homology model. 84

Figure 3.12 Predicted interactions between analogues of L1 and the lumenal binding site of the E195 M2 homology model. 88

Figure 3.13 Predicted interactions between analogues of L4 and the lumenal binding site of the E195 M2 homology model. 89

Figure 3.14 Predicted interactions between analogues of P6 and the lumenal binding site of the E195 M2 homology model. 91

Figure 3.15 Predicted interactions between analogues of L1 and the peripheral binding site of the E195 M2 homology model. 92

Figure 3.16 Predicted interaction between analogues of L4 and the peripheral binding site of the E195 M2 homology model. 94

Figure 3.17 Predicted interaction between analogues of P6 and the peripheral binding site of the E195 M2 homology model. 95

Figure 4.1 M2 mediates release of CF from liposomes is enhanced at acidic pH. 105

Figure 4.2 E195 M2 conductance domain peptides maintain resistance to rimantadine, but are sensitive to novel adamantane derivatives, which also reduce E195 infectious virus titre. 106

Figure 4.3 N31 CD peptide mediated release of CF from liposomes occurs in a concentration dependent manner..109

Figure 4.4 N31 CD peptide activity is inhibited in a dose dependent manner by adamantane compound, D. 110

Figure 4.5 Compound D, but not rimantadine is capable of reducing the infectious virus titre of pH1N1 swine influenza. 111

Figure 4.6 Does dependent inhibition of an E195 M2 conductance domain peptide by lumenally targeted compounds..113

Figure 4.7 Dose dependent inhibition of an E195 M2 conductance domain peptide by peripherally targeted compounds. 114

Figure 4.8 Novel compounds reduce E195 infectious virus titre but do not have adverse effects on cellular metabolism...116

Figure 4.9 An M2 transmembrane domain peptide has reduced activity compared to conductance domain peptides...118

Figure 4.10 M2 peptides can exhibit differential sensitivity to compounds. .119

Figure 4.11 Dose dependent effect of unbiased compounds on the activity of transmembrane (TM) and conductance domain (CD), E195 M2 peptides. 122

Figure 4.12 Investigating effects of active compound analogues from original unbiased screen, on the activity of transmembrane (TM) and conductance domain (CD), E195 M2 peptides. 125

Figure 4.13 Dose dependent effects of unbiased compound analogues on the activity of transmembrane (TM) and conductance domain (CD), E195 M2 peptides. 126

Figure 4.14 Analogues of L1, L4 and P6 do not exhibit adverse effects on MDCK cell metabolism. 128

Figure 4.15 Effect of unbiased compounds and their analogues on E195 virus titre. 129

Figure 4.16 Effects of biased compounds on channel activity of transmembrane (TM) and conductance (CD) domain E195 M2 peptides *in vitro*...131

Figure 4.17 Biased screen compounds reduce E195 virus titre, without affecting MDCK cellular metabolism. 133

Figure 4.18 Dose dependent effects of biased screen compounds on CF release mediated by transmembrane (TM) and conductance (CD) domain E195 M2 peptides *in vitro*...134

Figure 4.19 Comparison of compound effects against WT (N31) and mutated (S31) conductance domain M2 peptides activity *in vitro*.........135

Figure 4.20 IC$_{50}$ curves for novel M2 inhibitors against the E195 swine influenza. 137

Figure 5.1 Effect of predicted peripheral targeting M2WJ332 in combination with predicted lumenal targeted compound L1.1 on E195 infectious virus titre 24 hpi. 154

Figure 5.2 Effect of a combination of two predicted peripheral targeted compounds on E195 infectious virus titre 24 hpi. 156

Figure 5.3 Effect of combining DL7 with predicted lumenal compound L1.1 and peripheral compound M2WJ332, on E195 infectious virus titre. 157

Figure 5.4 Zanamivir IC$_{50}$ determination against E195 virus...........................160

Figure 5.5 Effect of novel M2 inhibitor L1.1 in combination with neuraminidase inhibitor zanamivir on E195 infectious virus titre 24 hpi. 161

Figure 5.6 Optimisation of forward primer and annealing temperature. 167

Figure 5.7 Schematic representation of samples generated via serial passage method...169

Figure 5.8 Virus titre of serial passage viruses samples SP-6, SP-7 and SP-14...171

Figure 5.9 M2WJ332 serial passage M2 sequence on days 5, 6, 7, 10 and 14.172

Figure 5.10 Effect of different concentrations of compound included in the overlay during plaque purification on E195 infectious virus titre. 174

Figure 5.11 Plaque purification of M2WJ332 treated E195 virus. 175

Figure 6.1 Comparison of predicted rimantadine docking to E195 homology model and the original 2RLF structure. 188

Figure 6.2 Structures of the A/Udorn/307/1972 (H3N2) 2RLF-based A/England/195/2009 (H1N1) (E195) M2 homology models minimised in either octanol or membrane environments. 190

Figure 6.3 Structures of the conductance domain of the 2L0J structure and 2L0J-based A/England/195/2009 (H1N1) (E195) M2 homology model. ..194

Figure A.1 Effect of predicted lumenal binding compounds on CF release mediated by an E195 N31 CD peptide. 233

Figure A.2 Effect of predicted peripheral binding compounds CF release mediated by an E195 N31 CD peptide. 234

Figure A.3 Assessment of L1, L4, P1 and P6 compound purity. 235

Figure A. 4 Effect of compound analogues on MDCK cell confluency after a 48 hour incubation. 236

Figure A.5 Effect of L1, L4, P6 and selected analogues on infectious E195 virus titre. 237

Figure A.6 Effect of biased compounds on E195 virus titre. 238

Figure A.7 Effect of HMA on the CF release mediated by an E195 N31 CD peptide. 239

Figure A.8 MDCK cell confluency is unaffected by MOI 0.01 with 80 μM novel compound over 24 hours. 240

Figure A.9 Predicted interactions between compounds M2WJ332, DL7 and DP9, and the lumenal binding site of the 2L0J E195 M2 homology model. 241

Figure A.10 Predicted interactions between novel compound L4 and its analogues L4.2 and L4.4 and the lumenal binding site of the 2L0J E195 M2 homology model. 242

Figure A.11 Predicted interactions between novel compounds P6, P6.4 and L1.1, and the lumenal binding site of the 2L0J E195 M2 homology model. 243

Figure A.12 Predicted interactions between compounds M2WJ332, DL7 and DP9, and the peripheral binding site of the 2L0J E195M2 homology model. 244

Figure A.13 Predicted interactions between novel compound L4 and its analogues L4.2 and L4.4 and the peripheral binding site of the 2L0J E195 M2 homology model. 245

Figure A.14 Predicted interactions between novel compounds P6, P6.4 and L1.1, and the peripheral binding site of the 2L0J E195 M2 homology model. 246

Figure A.15 Predicted interactions between M2WJ332 and the lumenal binding and peripheral binding sites of the 2RLF E195 M2 homology model. 247

Table of tables

Table 1.1 Influenza A virus and influenza-like haemagglutinin subtypes and host species. 5

Table 1.2 Influenza A virus and influenza-like neuraminidase subtypes and host species. 6

Table 1.3 Summary of WHO recommended strains for influenza vaccines in the Northern Hemisphere from the 2008-2009 season until the 2016-2017 season. 19

Table 1.4 Published structures of influenza A virus M2 tetramers. 32

Table 1.5 Summary of selected viroporins and their characteristics. 38

Table 1.6 Summary of experimental inhibitors of selected viroporins, described in the literature. 39

Table 3.1 Predicted lumenal binders. 75

Table 3.2 Predicted peripheral binders. 76

Table 3.3 DL compound details and binding scores. 79

Table 3.4 DP compound details and binding scores. 80

Table 3.5 Docking analysis at the lumen and periphery of the E195 M2 homology model, of L1, L4 and P6 analogues. 87

Table 4.1 Structures of L1, L4, P6 and their analogues. 124

Table 4.2 Calculated IC_{50} values for novel M2 inhibitory compounds against E195 swine influenza. 138

Table 4.3 Calculated IC_{50} and IC_{90} values for novel M2 inhibitory compounds against E195 swine influenza. 138

Table 5.1 Average combination indexes for compound combinations 163

Table 5.2 Average semi-quantitative grading of compound combination effects 163

Table 6.1 Comparison of the binding of unbiased compounds to the A/England/195/2009 (H1N1) (E195) M2 homology model minimised in an octanol environment and a lipid membrane. 191

Table 6.2 Docking scores for novel compounds at each of the two proposed binding sites of the 2L0J- and 2RLF-based E195 M2 homology models. 195

Table A.1 Interactions between DL compounds and the lumenal binding site of the E195 M2 homology model. 230

Table A.2 Interactions between DP compounds and the peripheral binding site of the E195 M2 homology model. 231

Table A.3 Combination Indexes calculated for the combination of zanamivir and L1.1 when calculated using IC_{50} concentrations. 232

Table A.4 Combination Indexes calculated for the combination of zanamivir and L1.1 when calculated using micromolar concentrations. 232

Table A.5 Interpretation of combination index values. 250
Table A.6 Summary of compound data. 256

Abbreviations

α-PA	L-α-phosphatidic acid
α-PC	L-α-phosphatidyl choline
α-PE	L-α-phosphatidyl ethanolamine
λem	Emission wavelength
λex	Excitation wavelength
ºC	Degrees centigrade
2D	Two-dimensional
3’	Three prime
3D	Three-dimensional
5’	Five prime
Å	Angstrom
aa	Amino acids
ANP32A	Acidic leucine-rich nuclear phosphoprotein 32 family member A
AVE	Elution buffer (vRNA extraction)
AVL	Lysis buffer (vRNA extraction)
AW1	Wash buffer 1 (vRNA extraction)
AW2	Wash buffer 2 (vRNA extraction)
BM2	Influenza B virus M2
bp	Base pairs
C	Carboxyl
CBD	Caveolin binding domain
cDNA	Complementary deoxyribonucleic acid
CD	Conductance domain
CF	Carboxyfluorescein
CI	Combination index
cm	Centimetre(s)

CPE	Cytopathic effect
CRAC	Cholesterol recognition amino acid consensus
cRNA	Complimentary ribonucleic acid
Da	Dalton(s)
dH_2O	De-ionised water
DL1-17	Predicted lumenal binding compound based on compound D 1-17
DMEM	Dulbecco's modified eagles medium
DMSO	Dimethyl sulfoxide
DNA	Deoxyribonucleic acid
dNTPs	Deoxynucleotide triphosphates
DP1-19	Predicted peripheral binding compound based on compound D 1-17
ds	Double stranded
DTT	Dithiothreitol
E195	A/England/195/2009 (H1N1)
ED_{50}	Median effective dose
EDTA	Ethylenediaminetetraacetic acid
FCS	Foetal calf serum
FDA	Food and Drug Administration
g	Gravitational force
H+	Proton(s)
HA	Haemagglutinin
HA0	Uncleaved haemagglutinin
HCV	Hepatitis C virus
HF	High fidelity
HIV(-1)	Human immunodeficiency virus (type 1)
HMA	Hexamethylene amiloride
hpi	Hours post infection
hr	Hour(s)

HTS	High-throughput screen
HPV(-16)	Human papillomavirus (type 16)
IAV	Influenza A virus
IBV	Influenza B virus
ICV	Influenza C virus
IC_{50}	Half maximal inhibitory concentration
IFN	Interferon
IRF	Interferon regulatory factor
kDa	Kilodalton
L1-7	Predicted lumenal binding compound 1 to7
L1.1-.4	Analogues of compound L1
L4.1-.4	Analogues of compound L4
LAIV(s)	Live attenuated influenza vaccine(s)
LC3	Microtubule-associated protein 1A/1B-light chain 3
(V)LP	(virus) like particle
M1	Matrix protein 1
M2	Matrix protein 2
M2e	Matrix protein 2 extracellular domain
MAVS	Mitochondrial antiviral signalling
MD	Molecular dynamics
MDCK	Madin-Darby Canine Kidney
MHC	Major histocompatibility complex
ml	Millilitre(s)
mM	Millimolar
mV	Millivolt(s)
MW	Molecular weight
N	Amino
NA	Neuraminidase

NAI	Neuraminidase inhibitor
NEAA	Non-essential amino acids
ng	Nanogram(s)
NLRs	NOD-like receptors
nm	Nanometer(s)
nM	Nanomolar
NMR	Nuclear magnetic resonance
NN-DGJ	N-(n-Nonyl)-deoxygalactonojirimycin
NN-DNJ	N-(n-Nonyl)-deoxynojirimycin
NOD	Nucleotide oligomerisation domain
NP	Nucleoprotein
NS1	Non-structural protein 1
NS2	Non-structural protein 2, also known as nuclear export protein (NEP)
OD	Optical density (nm)
OPLS	Optimised Potentials for Liquid Simulations
P1-6	Predicted peripheral binding compound 1 to 6
P6.1-.4	Analogues of compound P6
PA	Polymerase acidic
PA-N155	Polymerase acidic N-terminal truncation at residue 155
PA-N182	Polymerase acidic N-terminal truncation at residue 182
PA-X	Polymerase acidic frame shift
PAMPs	Pathogen associated molecular patterns
PB	Binding Buffer (PCR purification)
PB1	Polymerase basic 1
PB1-F2	Polymerase basic 1 frameshift
PB2	Polymerase basic 2
PBS	Phosphate buffered saline
pCD	Plasmacytoid dendritic cells

PCR	Polymerase chain reaction
PDB	Protein Data Bank
PE	Elution buffer (PCR purification)
PFA	Paraformaldehyde
pfu	Plaque forming unit
pfu/ml	Plaque forming units per ml
pH	-$\log_{10}$ concentration of hydrogen ions
Phusion	Phusion® high fidelity polymerase
pH1N1	Pandemic H1N1
pK_a	-$\log_{10}$ acid dissociation constant
pM	Picomolar
RCSB	Research Collaboratory for Structural Bioinformatics
RdRp	RNA dependent RNA polymerase
RIG-I	Retinoic acid-inducible gene 1
Rim	Rimantadine
RMSD	Root mean square deviation
RNA	Ribonucleic acid
ROCS	Rapid overlay of compound structures
rpm	Revolutions per minute
RT	Room temperature
RT-PCR	Reverse-transcription polymerase chain reaction
s	Second(s)
SAR	Structure-activity relationship(s)
SF	Serum free
ss	Single stranded
SSCIII	SuperScript® III
ssNMR	Solid state nuclear magnetic resonance
TAE	Tris-acetate-EDTA

TEVC	Two-electrode voltage clamp
TM(D)	Transmembrane (domain)
TPCK	L-1-Tosylamide-2-phenylethyl chloromethyl ketone (trypsin)
U	Unit(s)
Udorn	A/Udorn/307/1972 (H3N2)
µg	Microgram(s)
µg/µl	Mirogram(s) per microlitre
µl	Microlitre(s)
µm	Micrometre
µM	Micromolar
Uml^{-1}	Unit(s) per millilitre
V	Volts
v/v	Volume per volume
VLP	Virus-like particle
vRNA	Viral ribonucleic acid
vRNP	Viral ribonucleoprotein
WT	Wildtype
w/v	Weight per volume
w/w	Weight per weight
Zan	Zanamivir

Chapter 1

Introduction

Chapter 1 Introduction

Influenza A viruses (IAVs) are a common respiratory pathogen. Seasonal influenza epidemics, which occur during the winter months, result in between 250,000 and 500,000 deaths annually worldwide; current vaccination strategies are able to control the spread of infection. In addition to these seasonal strains, sporadic emergence of IAV pandemic strains occurs due to antigenic shift resulting from virus recombination involving two or more strains, one of which generally originating from an animal host. When this happens there is potential for great impact; of the four pandemics in the past 100 years the 1918 “Spanish ‘flu” was the most devastating resulting in at least 50 million deaths (Johnson & Mueller, 2002). Effective vaccines cannot currently be developed quickly enough to prevent the spread of pandemics due to rapid emergence of such strains. In these scenarios antiviral prophylaxis is the primary defence.

There are two classes of antivirals licensed for the treatment of IAVs, targeting either the neuraminidase (NA) protein or the matrix protein 2 (M2) ion channel. Due to the process of antigenic drift and selective pressure from the use of antiviral monotherapy, many of the strains circulating today are resistant to available antiviral treatments, in particular licensed M2 inhibitors. Thus, the threat of pandemics and resistance of circulating strains to current therapies drives an urgent need to develop novel antivirals. The ability of novel compounds to target the resistant strains is vital as the last pandemic strain from 2009 was found to be resistant to M2 inhibitors when it entered the human population.

1.1 Influenza viruses

The three genera of influenza viruses: A, B and C, are all capable of infecting humans and are part of the *Orthomyxoviridae* family of enveloped, single stranded, negative sense RNA viruses. There are three other genera in the *Orthomyxoviridae* family: *Isavirus*, *Quaranjavirus,* including the *Johnston Atoll* and *Lake Chad virus* species and *Thogotovirus* which contains *Dhori virus* amongst others. Influenza B viruses (IBVs) infect humans in seasonal epidemics and are capable of causing severe disease. In addition to humans, IBVs have also been isolated from seals (Osterhaus *et al.*, 2000), yet pandemics have not arisen despite this animal reservoir being present. IBVs are not split into subgroups, but are identified by strain. One strain of IBV was included in the annual trivalent vaccine, but this has been increased to two strains in the latest quadrivalent vaccines (Table 1.3). In addition to vaccines, neuraminidase inhibitors (NAIs) can be used against IBVs (Gubareva *et al.*, 2000). IBVs also encode a proton channel, BM2. Like M2 from IAVs, BM2 has a HxxxW motif responsible for conductance (Pinto & Lamb, 2006), yet sequence divergence between M2 of IAV and BM2 means that the licensed M2 antivirals (amantadine and rimantadine) are not effective against IBV (Pielak & Chou, 2011; Pinto & Lamb, 2006).

Unlike IAVs and IBVs, influenza C viruses (ICVs) have not been associated with epidemics. Combined with normally subclinical symptoms of infection, this means ICVs are not included in the annual vaccines and antivirals are rarely prescribed. Reports have been made of ICVs being isolated from pigs (Yuanji *et al.*, 1983), but there have been no pandemics recorded to date.

1.2 **Influenza A viruses**

1.2.1 Origin and Discovery

It is difficult to pinpoint the time when influenza first entered the human population, but it is hypothesised that this coincided with the domestication of animals such as birds and swine. There is a consensus that a pandemic in 1580 was the first that could be attributed to influenza, originating in the Asia Minor and South Africa and spreading to the southern Mediterranean (Pyle, 1986). Until the 1930s when influenza virus was first isolated from infected patients (Smith *et al.*, 1933), diagnosis was simply based on symptoms. There are now a variety of laboratory tests available (George, 2012), including immunoassays and rapid antigen testing, that use nasal or nasopharyngeal samples, but virus culture and polymerase chain reaction (PCR) are still required to establish the virus strain.

1.2.2 Classification

There are three integral membrane proteins encoded by IAVs: haemagglutinin (HA), neuraminidase and M2. The two glycoproteins HA and NA, involved in entry and release respectively, are used to categorise IAVs into subtypes. Commonly reverse-transcription polymerase chain reaction (RT-PCR) is used to subtype IAV, moving away from previous serological methods, such as hemagglutination inhibition. To date there are 18 HA and 11 NA subtypes identified for IAV, denoted H1-H18 and N1-N11 respectively, the combination of the HA and NA provide the subtype.

All influenza viruses are classified into strains, according to a standardised naming convention (WHO, 1980), composing five elements. Firstly the antigenic type (A/B/C), followed by the species of the host (if human this is omitted). This is followed by geographic origin, strain number and year of isolation. In the case of IAV this is then followed by the subtype in parentheses. For example: B/Brisbane/60/2008, A/England/195/2009 (H1N1) or A/mallard/Sweden/133546/2011 (H10N4).

1.2.3 Host range

The three main host species of IAVs are considered to be birds, humans and pigs, but certain subtypes are also able to infect a wide variety of mammalian species including sea mammals, dogs, horses and ferrets (Table 1.1 and Table 1.2). Until recently it was thought that all IAV strains were capable of infecting migratory birds and consequently these were thought to be the reservoir host from which all strains emerged. However, the recent discovery of H17, H18, N10 and N11, which to date have only been identified from bats (Tong *et al.*, 2012; Tong *et al.*, 2013) questioned this. Recent analysis of these new HA and NA proteins (reviewed in (Wu *et al.*, 2014c)) suggests that these are not true IAV proteins and as such H17N10 and H18N11 are considered “influenza-like viruses” (Wu *et al.*, 2014c). It must be noted that reassortment of these novel HA or NA segments may lead to a zoonotic virus capable of infecting avian or mammalian species. Many of the proteins of IAV have been implicated as host range determinants, of most note are haemagglutinin and polymerase basic protein 2 (PB2).

1.2.3.1 Haemagglutinin

Discounting H17 and H18, all 16 NA subtypes of IAVs are known to infect birds, whilst only H1, H2 and H3 are currently transmissible from human to human. In addition to this, H5, H7 and H9 subtypes have been isolated from infected humans, with the 1997 H5N1 and 2013-2016 H7N9 outbreaks resulting in fatalities (Cases, 1998; Gao *et al.*, 2013; Lin *et al.*, 2016). However, at present there is limited evidence for the human to human transmission of these subtypes. There have been cases where the source of infection is unknown, and one reported case of a H7N9 related death, in which the patient is thought to have contracted the virus from an infected relative, as they themselves had no direct contact with infected poultry (BMJ, 2013). Additionally, there have been reports of family clusters of H5N1 that could have been caused by human to human transmission (Wang *et al.*, 2008; Yang *et al.*, 2007). All known human HA subtypes are known to also infect swine and in addition H4, H6 and H11 can transmit between pigs.

Subtype	Avian	Human	Swine	Other
H1	🦆	👫	🐖	🐕 🦭 🦦
H2	🦆	👫	🐖	
H3	🦆	👫	🐖	🐎 🐕 🦭 🦦
H4	🦆		🐖	🦭
H5	🦆	👫	🐖	🐕 🦦
H6	🦆		🐖	🐕
H7	🦆	👫	🐖	🐎 🦭
H8	🦆			
H9	🦆	👫	🐖	
H10	🦆	👫	🐖	🦭
H11	🦆		🐖	
H12	🦆			
H13	🦆			🦭
H14	🦆			
H15	🦆			
H16	🦆			
H17				🦇
H18				🦇

Table 1.1 Influenza A virus and influenza-like haemagglutinin subtypes and host species.

All 18 known subtypes of haemagglutinin are listed with their respective host species. Only avian, human, swine, bat, equine, canine, sea mammal and ferret hosts are shown, based on strains available on the Influenza Research Database (www.fludb.org).

Subtype	Avian	Human	Swine	Other
N1	🦆	👫	🐖	🐕 🦭 🦦
N2	🦆	👫	🐖	🐕 🦭 🦦
N3	🦆	👫	🐖	🦭
N4	🦆			
N5	🦆		🐖	🦭
N6	🦆	👫	🐖	🦭
N7	🦆	👫	🐖	🐎 🦭
N8	🦆	👫	🐖	🐎 🐕 🦭
N9	🦆	👫		🦭
N10				🦇
N11				🦇

Table 1.2 Influenza A virus and influenza-like neuraminidase subtypes and host species.

All 11 known subtypes of neuraminidase are listed with their respective host species. Only avian, human, swine, bat, equine, canine, sea mammal and ferret hosts are shown, based on strains available on the Influenza Research Database (www.fludb.org).

Host species specificity of IAVs can, in part, be determined by HA surface glycoproteins, which bind to sialic acid on the surface of host cells to initiate entry (Section 1.4), this tropism is affected by the linkages of sialic acids. Avian influenza viruses demonstrate a higher affinity for sialic acid with α(2,3) linkages, whilst human viruses preferentially bind sialic acid with α(2,6) linkages (Matrosovich *et al.*, 1997; Rogers & Paulson, 1983). In humans the primary site of infection is the upper respiratory tract, where the epithelial cells mainly possess α(2,6) glycans (Baum & Paulson, 1989; Thompson *et al.*, 2006; van Riel *et al.*, 2010). However, α(2,3) linkages are found in the lower respiratory tract of humans (Shinya *et al.*, 2006) and it is here that some avian H5N1 viruses replicate most efficiently (Van Riel *et al.*, 2006). Conversely, in birds the primary site of infection is the gut, where epithelial cells predominately have α(2,3) glycans (Stevens *et al.*, 2006). Epithelial cells of the swine respiratory tract contain both sialic acids with α(2,3) and α(2,6) linkages (Ito *et al.*, 1998). As a result swine are able to act as “mixing vessels” (Castrucci *et al.*, 1993; Lowen *et al.*, 2007; Scholtissek *et al.*, 1985), allowing genetic reassortment of viruses leading to pandemics. However, introduction of a novel HA alone is not sufficient to give rise to pandemic strains as additional mutations in the HA gene are required to allow human receptor binding. Residues implicated in human receptor binding specificity span residues 100-300 of HA and include 190, 225, 226 and 228 (Gamblin *et al.*, 2004; Matrosovich *et al.*, 1997). The HA sequence of the pandemic A/California/04/2009 (H1N1) strain was analysed and the E225D mutation, conferring α(2,6) glycan binding and human-adaption, was observed (Soundararajan *et al.*, 2009), but a lysine at residue 145 is thought to compensate for the E225D mutation, meaning it can additionally bind α(2,3) glycans.

“Gain of function” experiments, over which there has been much debate, represent one method of investigating the avian strains such as H5N1 and H7N9. By artificially inducing changes that make these highly pathogenic avian strains more transmissible and infectious to humans, it is possible to study potential evolution of the virus, as well as aid work on developing vaccines and antivirals. The debate arises as these viruses also pose a potential deadly threat to the human population. When four mutations were made within the H5 of H5N1 it meant this segment could be reassorted with segment seven of pH1N1 to become transmissible between ferrets via the airborne route (Imai *et al.*, 2012). It was later demonstrated that four mutations in H5, and a fifth in PB2 had the same effect, without the need for recombination with a human transmissible virus (Herfst *et al.*, 2012).

1.2.3.2 Neuraminidase

NA host adaption has also been observed during pandemics, as the ability of this enzyme to cleave α(2,6) glycans is essential for the virus to replicate in humans. The 1957 H2N2 pandemic was the first recorded incidence of N2 viruses infecting humans and there was neuraminidase activity only against α(2,3) glycans (Baum & Paulson, 1991; Kobasa *et al.*, 1999). However, by 1972 N2 virus strains circulating in humans had gained the ability to cleave α(2,3) and α(2,6) glycans. Residues 275 and 431 have been specifically linked to this, with early human isolates of human N2 and avian viruses possessing an isoleucine at position 275, whereas in later human isolates I275V was present (Kobasa *et al.*, 1999).

1.2.3.3 Polymerase basic protein 2 (PB2)

In addition to the ability to bind and be released from sialic acid on the surface of the host cell, viruses also need to be able to replicate in the host cell. In this regard, the most important determinant of host range is the viral polymerase, PB2 (Almond, 1977). The best characterised polymorphism is at residue 627, in avian strains this is usually a glutamic acid, but upon serial passage in mammalian cells the E627K mutation is selected (Subbarao & Murphy, 1993).

The E627K mutation has been linked to modulation of RIG-I. RIG-I is an RNA helicase, present in the cytoplasm, with a role as a sensor for viruses (section 1.5). Short 5' triphosphate-dsRNA has been shown to be a ligand for RIG-I (Hornung *et al.*, 2006; Schmidt *et al.*, 2009), the "panhandle" of vRNA features this structure (Schlee *et al.*, 2009). Avian IAV nucleocapsids possessing E627 are more prone to recognition by RIG-I, the E627K mutation modulates this recognition (Weber *et al.*, 2015), permitting the virus to replicate in mammalian cells. Host factor ANP32A has also been implicated in host restriction of viral polymerase. Avian PB2 (E627) has suboptimal function in mammalian cells (Long *et al.*, 2016). However, addition of an avian ANP32A to mammalian cells was able to rescue the activity of avian IAV polymerase, to a similar extent as an E627A adaptation (Long *et al.*, 2016).

The E627K mutation allows strains to efficiently replicate at the lower temperature of the human respiratory tract (Massin *et al.*, 2001) and results in increased replication, pathogenicity and transmission in animal models (Shinya *et al.*, 2004; Steel *et al.*, 2009). However, E627 was present in the 2009 pandemic H1N1 (pH1N1) swine flu, but instead mutations at residues 590 and 591 are thought to allow replication in humans (Mehle & Doudna, 2009).

1.2.4 Transmission

Despite the long history of influenza research there is still controversy over the mode of virus transmission, with debate over whether transmission via the airborne route or via droplet or contact routes (or a combination) is the most important for implementing intervention. There are numerous studies published on this topic many using animal models and artificial inoculation, which limit the extrapolation of these finding to natural human infection.

It has been demonstrated that influenza virus can survive as an aerosol (Hemmes *et al.*, 1960; Mitchell & Guerin, 1972; Wells & Brown, 1936), however viruses were artificially aerosolised, then during, or after, recovery were diluted in liquid before infectivity was tested and not direct subsequent infection. It has also been shown that influenza can survive on surfaces both in a controlled laboratory setting with direct inoculation of surfaces (Bean *et al.*, 1982) and in environmental settings where household and day care fomites were tested for naturally occurring inoculation (Boone & Gerba, 2005). Similarly to the survival in aerosol studies, direct subsequent infection caused by virus on fomites was not shown.

The airborne hypothesis is supported by a study that demonstrated virus can be transmitted from infected mice to mice with which they have no direct contact (Schulman & Kilbourne, 1962). They also showed that the rate of transmission is not significantly different to when the two groups are housed together in direct contract.

Avian influenza virus can be isolated from the cloaca of birds and is excreted in their faecal matter (Webster *et al.*, 1976). The virus reaches the intestine where it replicates via the digestive tract (Webster *et al.*, 1978), supporting transmission via a faecal-oral route. It has also been demonstrated that avian IAVs can contaminate water supplies and be transmitted via a waterborne route (Markwell & Shortridge, 1982).

Studies of transmission of IAVs in humans have been carried out. The findings of nine observational studies of natural outbreaks have been reviewed (Brankston *et al.*, 2007) and it was concluded that there was generally a lack of controls to eliminate influence of airborne transmission. Notwithstanding, evidence suggested that, in general, droplet or contact transmission predominates. When it comes to transmission of avian strains of IAV to humans, for example the Hong Kong 1997 outbreak, close contact with infected poultry or their faeces appears to be the most important factor (Bridges *et al.*, 2002; Mounts *et al.*, 1999), yet multiple routes of transmission may be involved (Hayden & Croisier, 2005).

1.2.5 Seasonal influenza A

The seasonality of influenza A and B epidemics was first reported in 1981 (Hope-Simpson, 1981). The exact reason for this association with the colder months is unknown, but many explanations have been proposed including diminished vitamin D (Cannell *et al.*, 2006), reductions in humidity (Lowen *et al.*, 2007; Shaman & Kohn, 2009) and temperature (Lowen *et al.*, 2007).

The circulating viruses naturally mutate due to the infidelity of the polymerase. High mutation rates of 1/67000 (Parvin *et al.*, 1986) to 1/13700 base pairs (bp) (Drake, 1993) have been reported, equivalent to up to one mutation per round of replication. Silent mutations, that do not result in an amino acid change, are unlikely to result in a fitness cost, but nonsense mutations that result in a premature truncation of the protein are likely to be lethal to the virus (Wu *et al.*, 2014a). Sequence homology can reveal highly conserved residues, that could be involved in essential functions, but that is not necessarily the case. Depending on the site and type of the mutation, viral fitness may be affected. Detrimental mutations, that affect the ability of the virus to either infect or replicate, are unlikely to result in a novel virus that will replace the original wildtype (WT). However, mutations can arise that do not cause a reduction in viral fitness and even result in an advantage e.g. evasion of the immune system (Archetti & Horsfall, 1950; Hamre *et al.*, 1958). In these instances the mutated virus will be able to compete and reassort with the WT. Accumulation of point mutations in HA (Laver & Webster, 1968) and NA (Paniker, 1968; Schulman & Kilbourne, 1969) result in a phenomenon known as antigenic drift, where the immune system is less able to recognise the new virus. It is due to this antigenic drift that current influenza vaccines are updated annually.

1.2.6 Pandemic influenza

In addition to seasonal influenza, sporadically pandemic strains also emerge; these are attributed to antigenic shift and mean that the strain can jump from one species host to another. When the human population is exposed to a new HA / NA combination there is no pre-existing immunity, allowing the virus to replicate and spread effectively.

In the 20th century there were three influenza pandemics: the 1918 “Spanish ‘flu” (H1N1), 1957 “Asian ‘flu” (H2N2) and 1968 “Hong Kong ‘flu” (H3N2). The 1918 Spanish flu has been reported to be one of the most devastating diseases in recorded history, with conservative estimates linking over 50 million deaths between 1918 and 1920 to the virus (Johnson & Mueller, 2002), with the possibility that the true figure could be double that. To put this in perspective, this was treble the number of people killed by the concurrent WW1. As a result, Spanish flu caused a dramatic decrease in life expectancy, not seen by any other disease or event in recorded history. At the time of the pandemic, influenza viruses had yet to be isolated, however it was noted in post-mortem examinations that bacterial infections of the lung were commonplace amongst those who lost their lives. Recent analysis of these examination results and lung sections taken at the time, confirm high incidence of bacterial co-infection (Morens *et al.*, 2008).

One causation of antigenic shift is genetic reassortment or recombination. Genetic reassortment is a valuable method employed by IAV to expedite evolution, and it is this phenomenon that has been linked to the pandemics over the last 100 years. Shortly after the discovery that the IAV genome is made up of at least seven RNA segments (Bean & Simpson, 1976; McGeoch *et al.*, 1976; Palese & Schulman, 1976; Pons, 1977), it was hypothesised that novel combinations could arise if two viruses simultaneously infected the same host. Reassortment between the segments occurs as a result of simultaneous infection of a single cell with two or more distinct IAV strains. The resulting novel strain packages a new combination of genome segments.

Accordingly, comparison of the 1968 Hong Kong pandemic and previously circulating IAV strains, revealed that the HA and NA varied independently. NA was antigenically identical to previous strains, but the HA was considerably different (Coleman *et al.*, 1968; Schulman & Kilbourne, 1969). The ability of two influenza viruses to recombine in nature was first shown in 1978. Two avian viruses, isolated from wild birds were shown to have indistinguishable HA, whereas this was not the case for NA, supporting previous serological data (Desselberger *et al.*, 1978). In the case of the 1968 Hong Kong pandemic, it was later identified that a number of the genomic segments originated from avian IAV strains (Kawaoka *et al.*, 1989; Scholtissek *et al.*, 1978), supporting the theory of reassortment between avian and human strains.

Swine are the classic “mixing vessels” for IAVs (Castrucci *et al.*, 1993; Ito *et al.*, 1998; Scholtissek *et al.*, 1985). Due to the epithelial cells in respiratory tract containing both sialic acids with α(2,3) and α(2,6) linkages (Ito *et al.*, 1998), they are capable of being co-infected with an avian and a human strain of IAV. The potential of chickens to act as mixing vessel was raised, after discovery that both receptors are co-expressed in many organs of these birds (Kuchipudi *et al.*, 2009).

Unlike the 1957 and 1968 pandemics, which were caused by reassortment between human and avian strains (Kawaoka *et al.*, 1989), sequence analysis of the 1918 pandemic strain suggested this strain was an entirely avian-like virus that mutated to allow infection of humans (Taubenberger *et al.*, 2005). Similarly the 1997 Hong Kong H5N1 virus, which infected 18 humans and resulted in 6 deaths (Chan, 2002), was found to be of solely avian origin, without an intermediate mammalian host or mixing vessel (Claas *et al.*, 1998; Subbarao *et al.*, 1998).

1.3 **Molecular biology of influenza A virus**

In the 1960s it was identified that the IAV genome was made up of a number of RNA segments, with initial reports indicating 5 segments (Duesberg, 1968; Pons & Hirst, 1968). This number was then increased to between 7 and 9 (Palese & Schulman, 1976), before it was settled that eight separate RNA segments make up the IAV genome (Bean & Simpson, 1976; McGeoch *et al.*, 1976; Pons, 1977). All eight segments have partial complementarity at the 5’ and 3’ ends, which come together and form a “panhandle”, with partial double helical structures (Cheong *et al.*, 1996; Desselberger *et al.*, 1980; Hsu *et al.*, 1987; Robertson, 1979). These sequences are involved in transcription initiation (Fodor *et al.*, 1994; Fodor *et al.*, 1993; Seong & Brownlee, 1992), as well as termination and polyadenylation (Li & Palese, 1994).

The consensus remained that each RNA segment produced a single transcript and protein, with segments being assigned to the known viral proteins including haemagglutinin, neuraminidase, nucleocapsid (NP) and matrix (McGeoch *et al.*, 1976). It was also recognised that there were also non-structural proteins encoded that do not form part of the virus particle (Skehel, 1972). In the late 1970s the one RNA to one protein hypothesis was coming under scrutiny, and in 1979 evidence suggested that segment 8 encoded two proteins (Lamb & Choppin, 1979): non-structural proteins 1 and 2 (NS1 and NS2). From the title of the paper it is clear it was thought that this was the only segment that encoded more than one protein, however it did not take long for it to be discovered that segment 7 also had this capacity, when a second open reading frame was discovered (Allen *et al.*, 1980; Winter & Fields, 1980). Along with segment 7 encoding the matrix protein 1 (M1), M2 was determined to be encoded by the second open reading frame and its amino acid sequence was said not to exceed 97 aa, due to a termination codon (Lamb & Lai, 1981).

The eleventh protein of IAVs was not discovered until much later (Chen *et al.*, 2001), this is most likely due to the fact that polymerase basic protein 1 frameshift 2 (PB1-F2) is not essential for the virus replication cycle, but instead induces apoptosis of immune cells (Chen *et al.*, 2001). An N-terminal truncation of PB1 forms the twelfth identified polypeptide (Wise *et al.*, 2009), PB1 N40 like PB1-FS2 is nonessential for virus viability in culture. Three additional proteins have been identified in the past five years, all are encoded by segment 3 and are variations of polymerase A (PA): PA-X results from a frame shift of PA and has implications on host cell response to IAV infection (Jagger *et al.*, 2012), whilst PA-N155 and PA-N182 are both N-terminal truncated versions of PA (Muramoto *et al.*, 2013).

Of the IAV structural proteins, the three integral membrane proteins; haemagglutinin, neuraminidase and M2, are encoded by segments 4, 6 and 7, respectively. HA and NA are both glycoproteins and make up the majority of the surface proteins with approximately 500 and 100 proteins present, respectively. This is compared to the relative low 20-60 copy number of M2. Additionally, M1 plays vital roles in virus uncoating and assembly and NP binds and encapsidates the vRNA. The heterotrimeric influenza A RNA-dependent RNA polymerase (RdRp) consists of PA, PB1 and PB2. Each of the eight RNA segments has its own polymerase complex, bound to the termini of the vRNA and are individually encapsidated by NP, forming viral ribonucleoproteins (vRNPs) (Compans & Duesberg, 1972; Heggeness *et al.*, 1982).

After viral replication each of the eight segments needs to be packaged into progeny virions, each containing one copy of each segment. Transmission electron microscopy of virions showed a distinct pattern of vRNPs (Noda *et al.*, 2006), indicating the process of packaging is not random. It has also been shown that regions at both the 5’ and 3’ ends of vRNA are important for the correct incorporation of segments, first identified for HA, NA and NS segments (Fujii *et al.*, 2005; Fujii *et al.*, 2003; Watanabe *et al.*, 2003). In addition to these genome incorporation signals, a genome-bundling signal has been identified with a role of ensuring that a complete set of vRNPs are present in the nascent virion (Goto *et al.*, 2013).

Two distinct morphologies exist for IAV virions, spherical (Williams & Wyckoff, 1945) and filamentous (Chu *et al.*, 1949; Dawson & Elford, 1949). The significance of each type remains unclear, but it has generally been observed that filamentous virions are evident in low passage numbers, whilst spherical morphologies are established after several rounds of passage in eggs or cell lines. Both morphologies possess organised structures of their eight RNA segments (Noda *et al.*, 2006).

Segment 8 encodes NS1 and NS2. NS1 is a multifunctional, but non-essential, virulence factor with the ability to bind RNA and proteins. Roles of NS1 include; increasing expression of viral proteins due to preferential translation of viral mRNAs (Burgui *et al.*, 2003; De La Luna *et al.*, 1995) and antagonising the host immune response. NS1 has a crucial role in counteracting the host interferon (IFN) response

(Garcí *et al.*, 1998; Kochs *et al.*, 2007) and also inhibits or suppresses RIG-I mediated responses (Gack *et al.*, 2009; Mibayashi *et al.*, 2007; Rückle *et al.*, 2012) (section 1.5). NS2, also known as nuclear export protein (NEP), has, as its name suggests, a role in mediating the export of vRNPs from the nucleus to the cytoplasm (O'Neill *et al.*, 1998). However, independent of this, NS2 also has roles in viral replication and transcription (Robb *et al.*, 2009). Originally thought to be non-structural, NS2 is now considered a structural protein (Richardson & Akkina, 1991; Yasuda *et al.*, 1993), found interacting with M1 in the virion.

1.4 **Influenza A virus life cycle**

The life cycle of IAVs can be divided into four parts; firstly attachment, entry and uncoating, then protein synthesis, nucleic acid synthesis and finally assembly and budding. A schematic representation of the lifecycle of spherical virions is presented in Figure 1.1 and the process has been reviewed by Samji and Eisfeld (Eisfeld *et al.*, 2015; Samji, 2009). The first stage of the life cycle is initiated when the virus uses its HA to attach to sialic acid on the host cell membrane, this is followed by receptor mediated endocytosis (Matlin *et al.*, 1981; Patterson *et al.*, 1979). The HA at this stage is a precursor HA0, which needs to be cleaved by a host protease into HA1 and HA2 (Klenk *et al.*, 1975; Lazarowitz & Choppin, 1975). This exposes the fusion peptide, which then inserts into the endosomal membrane and facilitates fusion with the viral envelope. Prior to HA0 cleavage it undergoes a conformational change and this is facilitated by the low pH environment of the endosome (Bullough *et al.*, 1994; Maeda & Ohnishi, 1980; White *et al.*, 1981). The acidic environment also activates the M2 proton channel (Pinto *et al.*, 1992), which enables proton transport along the pH gradient between the acidic endosome and the viral core. This acidification plays a part in causing dissociation of M1 from the viral envelope and vRNPs (Li *et al.*, 2014a; Stauffer *et al.*, 2014).

IAVs, unlike most RNA viruses, transcribe and replicate their genome in the nucleus. The vRNPs, once released from M1, are transported to the nucleus (Martin & Helenius, 1991), via a process that is reliant on the nuclear localisation signals found in NP (O'Neill *et al.*, 1995) and host cell trafficking. Once in the nucleus, negative sense viral RNA (vRNA) is used as a template to transcribe mRNA. The endonuclease activity of the PA subunit of the viral RdRp is able to “cap-snatch” from cellular mRNA (Dias *et al.*, 2009; Herz *et al.*, 1981). This aids both the transport of viral mRNA into the cytoplasm followed by subsequent translation by the cellular ribosomes, and inhibition of host cell

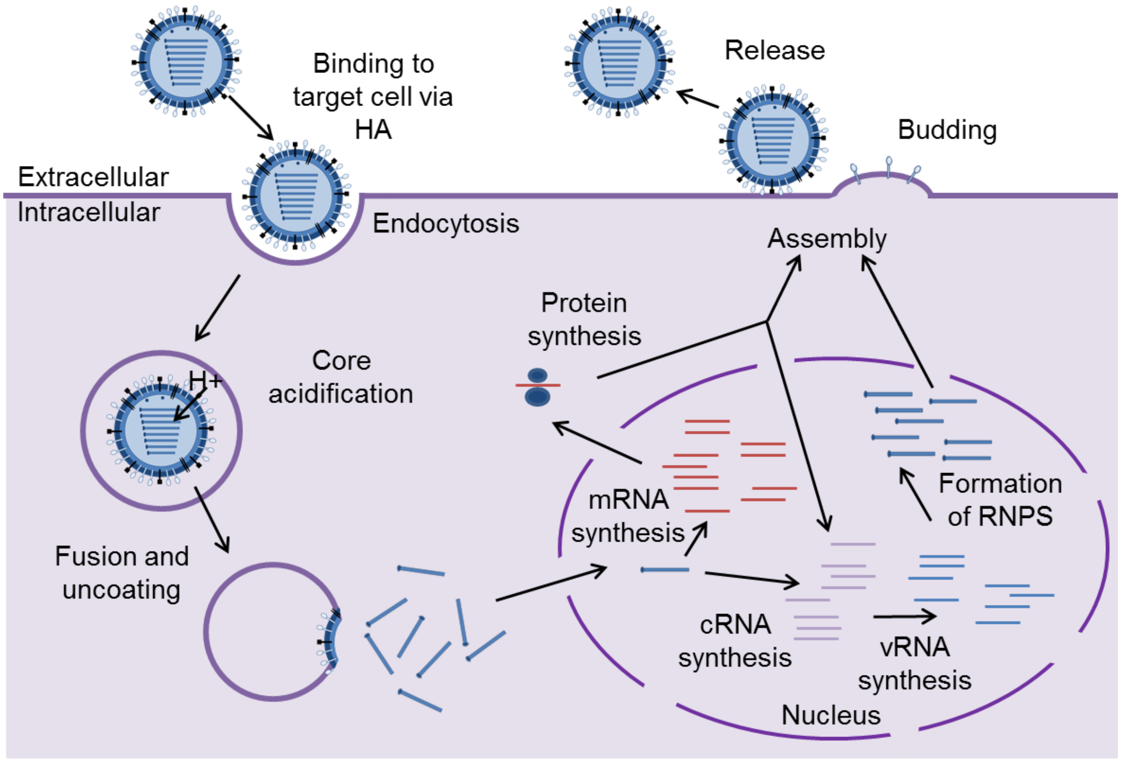
Binding to target cell via HA
Release
Budding
Extracellular
Intracellular
Endocytosis
Assembly
Protein synthesis
Core acidification
H+
mRNA synthesis
Formation of RNPS
Fusion and uncoating
cRNA synthesis
vRNA synthesis
Nucleus

Figure 1.1 Schematic illustration of the Influenza A virus life cycle.

Schematic depicting the stages of the IAV life cycle. Starting with viral attachment and entry, through nucleic acid and protein synthesis and ending with assembly, budding and release. Nucleic acid is colour coded: vRNA – blue, mRNA – red and cRNA – purple.

gene expression. Newly synthesised viral proteins (PA, PB1, PB2 and NP) are then transported back to the nucleus to take part in genome replication. In order to replicate the viral genome, vRNA is first copied into cRNA, before a new vRNA copy is synthesised and can form part of the vRNPs. The resultant progeny vRNPs are then transported back to the cytoplasm and subsequently to the plasma membrane on Rab11 vesicles (Amorim *et al.*, 2011; Eisfeld *et al.*, 2011), which is the site of virion assembly.

Viral envelope protein synthesis begins in the cytoplasm, it then moves to the endoplasmic reticulum where the proteins are also glycosylated, and folded into their 3D structures. They are then transported to the plasma membrane via the Golgi and *trans*-Golgi network. M2 present in the membrane of the *trans*-Golgi derived vesicles functions to counteract the acidification caused by cellular proton pumps (Ciampor *et al.*, 1992; Sugrue *et al.*, 1990). This is necessary to prevent acid-induced premature fusion, due to activation of cleaved HA in some strains including some H7 strains, which possess a multibasic cleavage site targeted by furin and other proteases (Grambas & Hay, 1992; Stieneke-Gröber *et al.*, 1992; Sugrue *et al.*, 1990).

At the plasma membrane, M1 interacts with HA and NA, then vRNPs interacts with this complex to form nascent virions. Virus budding then takes place, the newly formed virus particles are still attached to the host cell via sialic acid, which the NA enzyme cleaves, releasing the virion (Palese *et al.*, 1974).

1.5 **Innate immunity**

The innate immune response has an important role in the recognition and control of virus infection, but some exaggerated innate immune responses can lead to further pathology. An overview of the innate immune response to influenza can be found in recent reviews (Iwasaki & Pillai, 2014; Pulendran & Maddur, 2014). Recognition of pathogen associated molecular patterns (PAMPs), using pattern recognition receptors (PRRs) is an antiviral strategy of the innate immune system. Many classes of PRRs recognise IAV, these include: retinoic acid-inducible gene 1 (RIG-I), Toll-like receptors (TLRs) and nucleotide oligomerisation domain (NOD)-like receptors (NLRs).

During IAV infection, TLR signalling induces type-I IFNs and proinflammatory cytokines, with the purpose of restricting viral replication/dissemination, and linking to an adaptive immune response. TLR7 recognition of ssRNA leads to an IFN-α response from plasmacytoid dendritic cells (pDC) (Lund *et al.*, 2004), whereas the recognition of dsRNA by TLR3 primarily mediates a proinflammatory response in lung epithelial cells (Le Goffic *et al.*, 2007).

RIG-I recognises the 5’ triphosphate in the “panhandle” structure of vRNPs (Schlee *et al.*, 2009; Schmidt *et al.*, 2009) and leads to type-1 interferon production via binding the adapter mitochondrial antiviral signalling (MAVS) protein. In turn this leads to phosphorylation of interferon regulatory factor 3/7 (IRF3/7) and IκB. Phosphorylation of IκB is required for the activation of NF-κB, which together with IRF3/7 direct IFN transcription (Loo & Gale, 2011).

Some NLRs, in addition to triggering proinflammatory signalling pathways, have been implicated in the “inflammasome” (Franchi *et al.*, 2009), with the ion channel activity of M2 playing a role in its activation (Ichinohe *et al.*, 2010). As a result, this causes activation of caspase-1 and maturation of proinflammatory cytokines (Yu & Finlay, 2008).

1.6 **Influenza vaccination**

In the decade after influenza virus was first isolated (Smith *et al.*, 1933), studies on the potential for vaccination were undertaken with volunteers infected with either untreated active virus, that had been passaged through mice (Francis & Magill, 1937) or artificially cultivated using eggs (Thomas & Magill, 1936). Later vaccination went on to include both IAV and IBV strains (Francis *et al.*, 1946).

The humoral response plays an important role in prevention of, and recovery from, viral infection and this is the response that IAV vaccination aims to evoke. In the case of influenza infection a neutralisation response to the surface glycoproteins is desirable. Antibodies against HA interfere with binding of the virus to cell surface receptors (Virelizier, 1975), whilst anti-NA antibodies prevent release of influenza and therefore subsequent infection within the respiratory tract (Webster & Laver, 1967). During natural infection and after vaccination, HA exhibits immunodominance over NA (Johansson & Cox, 2011; Kilbourne, 1976; Oxford *et al.*, 1979). Monoclonal antibodies against the third integral membrane protein, M2, have also been shown to reduce levels of IAV replication in mice (Treanor *et al.*, 1990).

1.6.1 Current annual vaccination

Antibodies are able to provide long lasting protection against infection. However, as antigens vary both between influenza strains and also change via the process of antigenic drift, there is often little cross-protection between strains and as a result vaccination occurs annually. Predictions of the prevalent strains are made many months in advance of the onset of the winter epidemic. Due to the limited changes to the vaccine year on year, new vaccines tend to get approval quickly.

Broadly, the currently available vaccines can be split into inactivated and live-attenuated influenza vaccines (LAIVs). Trivalent vaccines protecting against two strains of IAV and a single IBV strain are being phased out, replaced with new quadrivalent vaccines that contain a second IBV strain. A list of the northern hemisphere vaccine strains since the 2008/2009 season is given in Table 1.3.

The first inactivated vaccines used whole viruses, treated with formalin to cause cross-linking and conformational changes of viral proteins, leading to inactivation (Francis Jr *et al.*, 1945; Stanley, 1945). Such modification of HA and NA can result in reduced immunogenicity. Split vaccines are inactivated by disruption of the particles using detergents and/or solvents, but still contain all of the viral proteins (Barry *et al.*, 1974; McKeage, 2013). Subunit vaccines are produced in a similar method as split vaccines, but are purified to only contain the HA and NA (Ruben & Jackson, 1972). Influenza virus-like particles (VLPs), or “virosomes”, mimic the external surface of IAV, without any of the internal components. VLPs are essentially unilamellar vesicles composed of phospholipids with HA and NA membrane proteins inserted, therefore retaining cell binding and fusion capabilities (Glück *et al.*, 1992; Mischler & Metcalfe, 2002).

Unlike the inactivated vaccines, LAIVs are administered intranasally, providing a better mimic of natural infection. They are licensed for use in patients between the ages of 2 and 49, as they have been found to be less efficacious in the older population (Ambrose *et al.*, 2011; Belshe *et al.*, 1998). For the influenza season 2015/2016, the LAIV was the vaccine of choice for national childhood flu immunisation programme, recommended by Public Health England. Despite much evidence supporting their superiority over inactivated vaccines, there are reports suggesting this results in increased local mucosal response, but rarely a systemic humoral response and seroconversion (Barría *et al.*, 2013).

Vaccine season	Vaccine type	Strains included
2008/2009	Trivalent	A/Brisbane/59/2007 (H1N1)-like; A/Brisbane/10/2007 (H3N2)-like; B/Florida/4/2006-like.
2009/2010	Trivalent	A/Brisbane/59/2007 (H1N1)-like; A/Brisbane/10/2007 (H3N2)-like; B/Brisbane/60/2008-like.
2010/2011	Trivalent	A/California/7/2009 (H1N1)-like; A/Perth/16/2009 (H3N2)-like; B/Brisbane/60/2008-like.
2011/2012	Trivalent	A/California/7/2009 (H1N1)-like; A/Perth/16/2009 (H3N2)-like; B/Brisbane/60/2008-like.
2012/2013	Trivalent	A/California/7/2009 (H1N1)pdm09-like; A/Victoria/361/2011 (H3N2)-like; B/Wisconsin/1/2010-like.
2013/2014	Trivalent	A/California/7/2009 (H1N1)pdm09-like; A/Texas/50/2012 (H3N2); B/Massachusetts/2/2012-like.
2014/2015	Trivalent	A/California/7/2009 (H1N1)pdm09-like; A/Texas/50/2012 (H3N2)-like; B/Massachusetts/2/2012-like. (B/Brisbane/60/2008-like).
2015/2016	Trivalent	A/California/7/2009 (pH1N1)-like; A/Switzerland/9715293/2013 (H3N2)-like; B/Phuket/3073/2013-like. (B/Brisbane/60/2008-like).
2016/2017	Trivalent	A/California/7/2009 (pH1N1)-like; A/Hong Kong/4801/2014 (H3N2)-like; B/Brisbane/60/2008-like. (B/Phuket/3073/2013-like).

Table 1.3 Summary of WHO recommended strains for influenza vaccines in the Northern Hemisphere from the 2008-2009 season until the 2016-2017 season.

Influenza B virus strains only present in the quadrivalent vaccine are in parentheses.

1.6.2 Universal vaccines

Universal vaccines would eliminate the requirement to produce annual vaccines based on the circulating strains. In order to achieve this, vaccines need to elicit an immune response to a less genetically diverse target. One approach still uses HA as the antigen, but instead targets a response to the conserved stalk instead of the more divergent globular head (Krammer *et al.*, 2013; Margine *et al.*, 2013; Steel *et al.*, 2010).

M2 is another viral target being investigated, with the extracellular domain (M2e) being well conserved among different IAV strains. However, immunity induced to M2e as a result of natural infection or conventional vaccines is poor (Black *et al.*, 1993b; Feng *et al.*, 2006; Treanor *et al.*, 1990). Due to its short length, only 23 aa, the M2e is regularly fused to a carrier protein (De Filette *et al.*, 2005; Neirynck *et al.*, 1999) or is expressed using VLPs (Kim *et al.*, 2014; Kim *et al.*, 2012), which has resulted in improved immunogenicity.

Another approach is to use vaccines to encourage cytotoxic T-cell responses. These aim to confer broader specificity and longer lasting immunity compared to antibodies (McMichael *et al.*, 1983), by targeting conserved viral proteins (Townsend & Skehel, 1982; Yewdell *et al.*, 1985). M1 and NP have been found to be the most immunodominant targets during natural infection (Lee *et al.*, 2008). M1 and NP were included in a novel vaccine based upon a Vaccinia virus vector and produced a potent T cell response (Berthoud *et al.*, 2011; Lillie *et al.*, 2012). The addition of adjuvants to influenza vaccines has also been shown to improve T cell response in mice (Wack *et al.*, 2008).

There is promise that one day a universal vaccine will be available in the clinic. Unlike the annual vaccines used currently, that are approved relatively quickly, due to many decades of expertise and clinical use, a universal vaccine will need to undergo extensive clinical trials and require a new FDA approval, which could take many years.

1.7 Influenza Antivirals

Two classes of antivirals are currently licensed for the treatment of IAVs. Zanamivir (“Relenza”, GlaxoSmithKline), oseltamivir (“Tamiflu”, Roche) and peramivir (“Peramiflu”, “Rapivab” or “Rapiacta”, BioCryst Pharmaceuticals) target the neuraminidase enzyme, and amantadine (“Symmetrel”, Endo Pharmaceuticals) and rimantadine (“Flumadine”, Forest Pharmaceuticals) target the M2 ion channel (Figure 1.2).

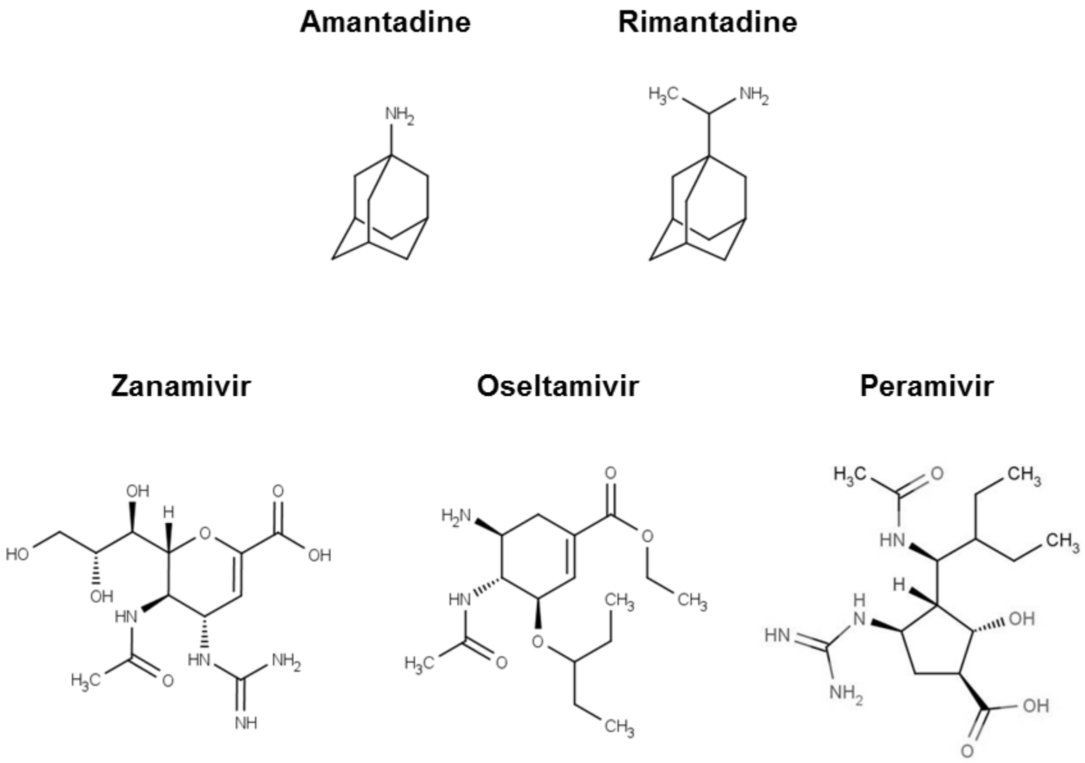

Amantadine **Rimantadine**

Zanamivir **Oseltamivir** **Peramivir**

NH2
H3C
NH2
OH
H
O
O
HO
OH
OH
HN
H3C
O
HN
NH2
NH
H2N
O
O
HN
CH3
CH3
H3C
O
O
CH3
H3C
O
CH3
HN
CH3
H
H
N
OH
HN
NH2
OH
O

Figure 1.2 Molecular structures of FDA approved influenza A virus antivirals.

Amantadine and rimantadine target the M2 ion channel, whilst zanamivir, oseltamivir and peramivir target the neuraminidase enzyme.

1.7.1 M2 inhibitors

Amantadine was the first antiviral licensed for use against IAVs in the 1960s, but at the time, its precise target was unknown. By the end of the decade it had been proposed, through time of addition studies in a single cycle replication assay, that amantadine was effective during an early stage of the virus life cycle i.e. virus uncoating (Kato & Eggers, 1969). M2 was only identified as the target of amantadine when resistance was selected *in vitro* and the virus genomic RNA was sequenced (Hay *et al.*, 1985; Hay *et al.*, 1986). The methylated derivative of amantadine, rimantadine was licensed at a later date. Both of these compounds are only effective against certain strains of IAV and are not licensed for treatment of IBVs.

1.7.2 Neuraminidase inhibitors (NAIs)

The premise of NAIs is that they mimic sialic acid, the natural substrate of neuraminidase; therefore, compete for the enzyme active site. In 1993 it was first demonstrated that sialic acid based inhibitors were able to inhibit the enzymatic activity of NA and, more importantly, as a consequence are effective against IAV in culture and in animal models (von Itzstein *et al.*, 1993). Zanamivir, which is administered either intravenously or inhaled (Cass *et al.*, 1999) and oseltamivir, which is taken orally (Davies, 2010), were licensed at the turn of the 21st Century and remain the only licensed NAIs in the UK. There has been a widespread practice of stockpiling NAIs, for use during the emergence of a pandemic. As a result of the UK spending over £400 million on a oseltamivir stockpile (Van Noorden, 2014), there is controversy over the benefits of this strategy.

Further NAIs have been developed, with peramivir licensed by the Food and Drug Administration (FDA) in the USA for emergency use during the 2009 pandemic (Birnkrant & Cox, 2009). Peramivir, administered intravenously, was later approved in 2014 for use in adults and has been shown to be effective against avian strains *in vitro,* and *in vivo* (Farooqui *et al.*, 2015; Hurt *et al.*, 2007).

1.7.3 Resistance

Resistance is a major clinical issue with regards to IAVs. As a consequence of the lack of proof reading capabilities of the viral polymerase (Drake, 1993; Parvin *et al.*, 1986), there is a large pool of mutated virus ready to expand when a selection pressure is applied. Use of antivirals, particularly as monotherapies, only serves to increase the selective pressure on the virus to evolve. Resistance to both classes of IAV antivirals exists, but it is far more widespread with respect to M2 inhibitors. As such the licensed M2 inhibitors are no longer recommended for prophylactic treatment (Fiore *et al.*, 2011), leaving NAIs as the standard of care.

Development of resistance to amantadine *in vitro* lead to identification of M2 as the viral target for the compound (Hay *et al.*, 1985; Hay *et al.*, 1986), with V27A, A30T, S31N and G34A implicated in different strains. Subsequently, L26F and L38F polymorphisms have also been shown to confer adamantane resistance (Black *et al.*, 1993a; Wang *et al.*, 1993). The first observation of amantadine resistance in clinical isolates was in the late 1980s (Belshe *et al.*, 1988; Pemberton *et al.*, 1986). However, sequence analysis revealed that the polymorphisms associated with resistance were present in circulating strains long before the development of adamantanes as antivirals (Furuse *et al.*, 2009), including in the A/Puerto Rico/8/1934 (H1N1) strain. Viruses containing the S31N polymorphism are also seen to be commonly circulating in regions of the world where adamantane compounds have never been used in humans (Furuse *et al.*, 2009), further suggesting this mutation is well tolerated, confers no loss of fitness and can occur spontaneously.

Since the turn of the millennium, the incidence of rimantadine resistance among circulating seasonal strains of H1N1 and H3N2 has increased, it is also the case in avian and swine isolates (Furuse *et al.*, 2009). The most predominant resistance polymorphism is S31N (Furuse *et al.*, 2009), but it has been reported that the total incidence of resistance and relative prevalence of each polymorphism can depend on virus subtype (Control & Prevention, 2008; Saito *et al.*, 2003). In 2009, when the pandemic H1N1 swine influenza strain entered the human population, it was already resistant to amantadine and rimantadine, with > 99.9 % of virus isolates sequenced containing N31 (Gubareva *et al.*, 2010). Conversely, when the avian H5N1 virus first infected humans in 1997 it was amantadine sensitive (Cheung *et al.*, 2006), but within five years the prevalence of resistance reached 95 % (Govorkova *et al.*, 2013).

Although uncommon, there have been reports of dual resistant V27A/S31N or L26F/S31N viruses (Dong *et al.*, 2015; Durrant *et al.*, 2015; Furuse *et al.*, 2009; Garcia & Aris-Brosou, 2014). Like individual resistance polymorphisms dual V27A/S31N sequences have been identified from isolates prior to the use of antivirals, with their prevalence increasing with the single polymorphisms (Furuse *et al.*, 2009). Due to the minimal fitness cost of these mutations they are likely to remain in circulating strains.

Since the NAIs zanamivir and oseltamivir were first used in the clinic, susceptibility surveillance has been carried out. By 2003, despite no naturally occurring resistance in

IAVs, it had been established that, as with M2 inhibitors, resistance polymorphisms varied between subtypes, as well as varying between the two drugs (McKimm-Breschkin *et al.*, 2003; Saito *et al.*, 2003). In both Europe and United States, the 2007-2008 IAV season saw a prevalence of the H274Y polymorphism conferring oseltamivir resistance in the circulating H1N1 strains, but these strains remained sensitive to zanamivir and M2 inhibitors (Control & Prevention, 2008; Lackenby *et al.*, 2008). The following year the oseltamivir resistant strain was the predominant H1N1 strain in the northern hemisphere. It was displaced in the winter 2009-2010 by the pandemic H1N1, which was sensitive to both licensed NAIs, but resistant to M2 inhibitors (Gubareva *et al.*, 2010; McKimm-Breschkin, 2013). The H274Y polymorphism was detected in some pH1N1 patients who were given a reduced prophylaxis dose of oseltamivir (Gubareva *et al.*, 2010). In the southern hemisphere the same mutation was found in 2011, in isolates from untreated individuals (Butler *et al.*, 2014). Peramivir susceptibility is also reduced by the H274Y polymorphism (Memoli *et al.*, 2010).

Zanamivir resistance in IAV strains was identified in isolates from 2006-2008 (Hurt *et al.*, 2009). However, zanamivir resistance had previously been reported in IBV (Gubareva *et al.*, 1998). Sequencing of an immunocompromised child infected with IBV after prolonged treatment identified a R152K mutation in the NA active site; in addition a mutation in HA was also detected (Gubareva *et al.*, 1998). The mutation in HA was considered to be a compensatory mutation, reducing the HA affinity for cell surface receptors, thus allowing virus to be released from cells even with reduced NA activity caused by zanamivir.

1.7.3.1 New antiviral targets

In addition to M2 and NA there are many other potential proteins on IAVs and numerous steps of the life cycle that can be targeted with antivirals. A review of the current and new therapeutic approaches targeted by antivirals has been carried out by Loregian and colleagues (Loregian *et al.*, 2014). In one study, over 1000 compounds, of which the majority had previously been tested clinically in humans or in animals, were screened for anti-influenza activity. Dozens of compounds affecting many different stages of the life cycle were identified (An *et al.*, 2014). Amantadine analogues, harbouring changes to the cyclic ring were found to be effective against an amantadine resistant H1N1 strain, yet upon investigation were shown to target HA, rather than M2 (Torres *et al.*, 2014).

The potential of inhibiting fusion has been investigated using multiple approaches. Peptides based on HA1 and HA2 subunits have been shown to bind the HA stalk potentially preventing the HA conformational change required for fusion (López-

Martínez *et al.*, 2013). Additionally, small molecules that prevent the lipid mixing stage of fusion (Rowse *et al.*, 2015a; Rowse *et al.*, 2015b), or inhibition of the protease mediated cleavage of HA have been studied (Hamilton *et al.*, 2014). In Russia, arbidol, which prevents the pH-induced conformational change in HA, has been approved for use in treatment of IAV and IBV (Leneva *et al.*, 2009). Arbidol has been found to have broad antiviral activity with effects upon other enveloped viruses, such as hepatitis C virus (HCV) (Teissier *et al.*, 2011).

Inhibitors of the PA replicase subunit have been identified by *in silico* modelling, with both the endonuclease activity of PA (Yan *et al.*, 2014) and its interaction with PB1 targeted by novel compounds (Tintori *et al.*, 2014). A small molecule has also been identified which inhibits the activity of the vRNP complex, by binding to NP (Kakisaka *et al.*, 2015). Additionally, favipiravir, which targets the IAV RdRP, is undergoing clinical trials (Baranovich *et al.*, 2013; Furuta *et al.*, 2013) and was licenced in Japan during 2014. Favipiravir has also shown efficacy against other RNA viruses, including its use most recently during the Ebolavirus outbreak in Western Africa (Sissoko *et al.*, 2016).

1.7.4 Targeting the host

Antivirals targeting host cellular functions possess the potential advantage of minimising the effects of IAV genetic variability, both in terms of genetic drift, but also strain differences. However, this strategy also has disadvantages, including potential for off-target effects. Many cellular pathways and functions have been targeted, for example the MAPK/ERK protein kinase cascade and the NF-κB pathway (Lee & Yen, 2012; Loregian *et al.*, 2014). Some compounds are global inhibitors of viral replication, including human RIG-I agonists (Goulet *et al.*, 2013; Lin *et al.*, 2012; Ranjan *et al.*, 2010) and IFN inducers (Martínez-Gil *et al.*, 2012; Ortigoza *et al.*, 2012).

Iminosugars have also been shown to be effective against a range of enveloped viruses including HIV-1 and Dengue (Fleet *et al.*, 1988; Jacob & Bryant, 1993; Wu *et al.*, 2002; Zitzmann *et al.*, 1999). However, inhibition of host α-glucosidases using alkylated iminosugars has been shown to have a strain-specific effect on IAVs, by altering the glycan processing of HA and NA (Hussain *et al.*, 2014). IAV replication has also been shown to be dependent on the PI3K-AKT-mTOR pathway (Murray *et al.*, 2012), with NS1 phosphorylation decreased when Akt kinase activity is inhibited by a peptide (Hirata *et al.*, 2014).

1.8 M2

M2 was discovered as the second protein encoded by segment 7, with differential splicing of the mRNA transcript producing a 97 aa product (Lamb *et al.*, 1981), details are shown in Figure 1.3. This integral membrane protein has three domains: a highly conserved N-terminal ectodomain that extends into the extracellular space (aa 1-23), followed by a transmembrane (TM) domain (aa 24-46) and then a cytoplasmic domain (aa 47-97) (Lamb *et al.*, 1985; Pielak & Chou, 2011). M2 can oligomerise into disulphide-linked tetramers (Sugrue & Hay, 1991), that comprise part of the infectious virion (Zebedee & Lamb, 1988) and are present on the surface of infected cells (Lamb *et al.*, 1985). In the mid-1980s, over a decade after it was first licensed, the target of amantadine was revealed to be M2 (Hay *et al.*, 1985; Hay *et al.*, 1986).

1.8.1 Mechanism of M2 proton conductance

The ion channel activity of IAV M2 was first demonstrated using electrophysiology studies, where a preference for monovalent cations was discovered (Pinto *et al.*, 1992). It has been shown that the TM domain is the minimal unit required for proton conductance and this domain is also inhibited by amantadine, albeit with reduced conductance compared to full length protein (Ma *et al.*, 2009). Whilst, the longer conductance domain (CD), which includes residues to the C-terminal of the TM domain (aa 21-61), has activity “indistinguishable from that of full length M2” (Ma *et al.*, 2009).

As M2 is expressed on the surface of the cells, it could be expected that, if all channels were constitutively active, this would result in deleterious effects upon the cell. It was therefore a reasonable hypothesis that M2 exists in two states: open / activated and closed / inactive. As M2 had been proposed to act in two intracellular compartments, the late endosome and the *trans*-Golgi, both of which contain lumens that exist at acidic pH, it was logical to assess whether low pH was responsible for M2 activation. Accordingly, reducing the external buffer pH of *Xenopus* oocytes from pH 7.5 to 6.2 resulted in a seven-fold increase in inward current, which remained inhibited by 100 µM amantadine (Pinto *et al.*, 1992). Due to the fact that histidine (H37) is the only charged residue within the transmembrane domain of M2, it was hypothesised that this residue may be involved in channel gating/activation. Accordingly, a H37A mutant protein expressed in oocytes resulted in a non-specific five-fold increase in current at neutral pH (Pinto *et al.*, 1992). Furthermore, no increase in current was observed when the external buffer pH was reduced for the H37A mutant (Pinto *et al.*, 1992).

A

AAG**ATGAGTC TTCTAACCGA GGTCGAAAC**G TACGTTCTTT 40
CTATCATCCC GTCAGGCCCC CTCAAAGCCG AGATCGCGCA 80
GAGACTGGAA AGTGTCTTTG CAGGAAAGAA CACAGATCTT 120
GAGGCTCTCA TGGAATGGCT AAAGACAAGA CCAATCTTGT 160
CACCTCTGAC TAAGGGAATT TTAGGATTTG TGTTCACGCT 200
CACCGTGCCC AGTGAGCGAG GACTGCAGCG TAGACGCTTT 240
GTCCAAAATG CCCTAAATGG GAATGGGGAC CCGAACAACA 280
TGGATAGAGC AGTTAAACTA TACAAGAAGC TCAAAAGAGA 320
AATAACGTTC CATGGGGCCA AGGAGGTGTC ACTAAGCTAT 360
TCAACTGGTG CACTTGCCAG TTGCATGGGC CTCATATACA 400
ACAGGATGGG AACAGTGACC ACAGAAGCTG CTTTTGGTCT 440
AGTGTGTGCC ACTTGTGAAC AGATTGCTGA TTCACAGCAT 480
CGGTCTCACA GACAGATGGC TACTACCACC AATCCACTAA 520
TCAGGCATGA AAACAGAATG GTGCTGGCTA GCACTACGGC 560
AAAGGCTATG GAACAGATGG CTGGATCGAG TGAACAGGCA 600
GCGGAGGCCA TGGAGGTTGC TAATCAGACT AGGCAGATGG 640
TACATGCAAT GAGAACTATT GGGACTCATC CTAGCTCCAG 680
TGCTGGTCTG AAAGATGACC TTCTTGAAAA TTTGCAG**GCC** 720
TACCAGAAGC GAATGGGAGT GCAGATGCAG CGATTCAAGT 760
GATCCTCTCG TCATTGCAGC AAATATCATT GGGATCTTGC 800
ACCTGATATT GTGGATTACT GATCGTCTTT TTTTCAAATG 840
TATTTATCGT CGCTTTAAAT ACGGTTTGAA AAGAGGGCCT 880
TCTACGGAAG GAGTGCCTGA GTCCATGAGG GAAGAATATC 920
AACAGGAACA GCAGAGTGCT GTGGATGTTG ACGATGGTCA 960
TTTTGTCAAC ATAGAGCTAG AGTAAAAAAC TACCTTGTTT 1000
CTA 1003

B

MSLLTEVETP TRSEWECRCS DSSDPLVIAA NIIGILHLIL 40
WITDRLFFKC IYRRFKYGLK RGPSTEGVPE SMREEYQQEQ 80
QSAVDVDDGH FVNIELE 97

C

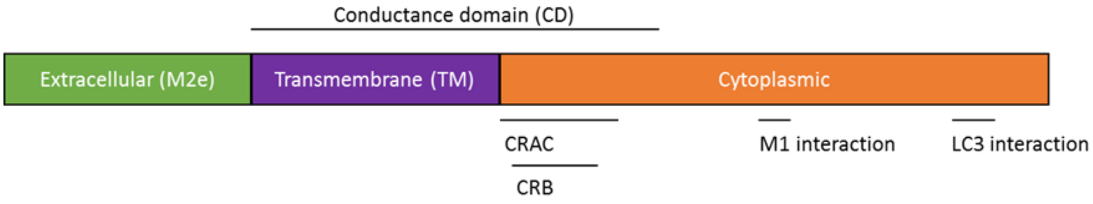

Figure 1.3 Sequence of A/England/195/2009 segment 7.

A) The nucleotide sequence of A/England/195/2009 segment 7 was downloaded from the Influenza Research Database (www.fludb.org), Sequence Accession: GQ166660. In red are nucleotides untranslated in M1 and M2. M1 coding sequence is coloured blue. M2 coding sequence is in bold and the M2 intron is underlined. B) The corresponding amino acid sequence of M2 and C) schematic representation of its domains and motifs, with domains colour coded: ectodomain (green), transmembrane domain (purple) and cytoplasmic domain (orange).

Using planar lipid bilayers, experiments demonstrating acid activation, amantadine sensitivity and cation selectivity of M2 ion channels were repeated (Duff & Ashley, 1992; Tosteson *et al.*, 1994). Further work using H37E and H37G mutants of M2, which remain negatively charged or uncharged respectively, when the pH is lowered to between pH 5-7, demonstrated the key role of histidine, as mutants were not activated by acidic pH, but were constitutively active (Wang *et al.*, 1995). Expression of mutated M2 resulted in oocytes with morphological changes consistent with ion channel-induced deterioration, even at neutral pH. This was in contrast to WT M2 which only caused these effects following prolonged incubation in acidic buffers, in the absence of amantadine (Wang *et al.*, 1995). Activation resulted from protonation of a binding site, with pK_a = 5.8, providing further support for H37 being responsible for the channel activation, as this is the only residue within the TM capable of being protonated in this pH range (Wang *et al.*, 1995).

The mechanism of M2 proton conduction has been long debated, since it was first proposed that proton conductance is not by the free passage of hydronium ions, but instead by interaction with titratable groups on M2 (Mould *et al.*, 2000). One mechanism is based upon a “dimer of dimers” (Hu *et al.*, 2006) structure and the second a “histidine-box” (Acharya *et al.*, 2010).

The channel is closed at physiological pH, but already two of the H37 residues are protonated forming two imidazole-imidazolium dimers (Hu *et al.*, 2006). This “dimer of dimers” structure of the channel causes the homotetramer to have two-fold symmetry, considered to be a stable state, with a hydrogen bond within each dimer (Hu *et al.*, 2006). The dimers are both proposed to form at pK_a = 8.2, suggesting high affinity for H+ and also cooperative binding to result in the two-fold symmetry of the closed channel; it is therefore a third protonation event that results in the activation of the channel (Hu *et al.*, 2006). Binding of a third proton to the third histidine is proposed to disrupt the stable dimer of dimers structure. The resultant high-energy metastable state is willing to give up one H+, in order to return to the favourable state and as such conductance through the channel occurs (Hu *et al.*, 2006).

A four-fold symmetry X-ray structure of the M2 TM domain (3LBW), combined with molecular dynamics (MD) simulations, lead to the proposal of the histidine-box model (Acharya *et al.*, 2010). The third protonation state is still considered important for conductance, but it is suggested that protons delocalise over the entire histidine-box and the surrounding well-ordered water clusters, as opposed to being associated with discrete residues (Acharya *et al.*, 2010). A separate MD simulation study suggests both the dimer of dimers and histidine-box configurations of M2 tetramers play a role in conductance (Dong *et al.*, 2013).

The four histidine residues are responsible for the pH dependent activation of M2, but tryptophan 41 has also been implicated in the control of channel conductance, by acting as a molecular gate (Tang *et al.*, 2002). A model for M2 activation showed that at high pH the indole groups of W41 obstruct the channel. As the pH is reduced a conformational change occurs and the indole groups rotate and permit conductance (Tang *et al.*, 2002). It is suggested that H37 and W41, part of the HxxxW motif, are involved in direct hydrogen bonding, resulting in the opening and conductance of the channel at reduced pH (Sharma *et al.*, 2010). A third residue, D44, has also been implicated with a role in the activity of M2 (Betakova *et al.*, 2005). D44 acts to stabilise the W41 gate, maintaining its asymmetry and resultant conductance of protons from the acidic external environment (Ma *et al.*, 2013). V27 has also been proposed to act a secondary gate at the N-terminal end of the channel (Sharma *et al.*, 2010; Yi *et al.*, 2008).

1.8.2 Functions of M2 during the IAV life cycle

It has been suggested that M2 may not be essential, as virus lacking M2 ion channel activity can still undergo multiple rounds of replication in tissue culture (Watanabe *et al.*, 2001), although this viral replication is severely attenuated (Takeda *et al.*, 2002). However, M2 inhibitors are capable of reducing infectious titres *in vitro* and have been efficacious in the clinical setting. Combined with the fact that M2, produced by splicing of segment 7, is highly conserved, it is therefore unlikely that M2 expression will have been maintained if it was not essential to the virus life cycle.

The addition of amantadine at different stages of the life cycle played a leading part in revealing the roles of M2. Amantadine treatment was not found to completely block virus infection, but instead slowed down the penetration of IAV into host cells (Davies *et al.*, 1964a), it was hypothesised that the virus remained attached to the host cell membrane (Hoffmann *et al.*, 1965). Technical advances meant it was later possible to distinguish between penetration and uncoating, thereby revealing that amantadine prevented the latter, uncoating (Kato & Eggers, 1969).

In a subset of viruses, M2 ion channel activity is also required later in the life cycle. Using H7 viruses, it was demonstrated that amantadine led to acidification of intracellular vesicles compared with untreated controls. This acidification resulted in a conformational change of HA, blocking release of virus (Sugrue *et al.*, 1990). This event was shown to occur within the *trans*-Golgi (Ciampor *et al.*, 1992), implicating M2 in the protection of newly synthesised HA from premature acid-activated fusion (Grambas & Hay, 1992). This function is dependent on whether the HA0 has a monobasic or multibasic cleavage site. Mammalian strains and low pathogenic avian influenza have monobasic sites, which get cleaved extracellularly and as such limits their spread. On the other hand, highly pathogenic avian influenza contain a multibasic cleavage site (R-X-K/R-R) which gets cleaved intracellularly by proteases such as furin, heightening the ability to systemically spread (Stieneke-Gröber *et al.*, 1992). When HA has been cleaved intracellularly, M2, antagonising V-ATPase, blocks the conformational change that results in premature fusion, enabling progeny virions to be infectious upon release (Grambas & Hay, 1992).

M2 has also been shown to have roles unrelated to its ion channel activity, these are highlighted in Figure 1.3C. Some of these roles involve virus assembly, with t M2e being required for M2 incorporation into the virion (Park *et al.*, 1998) and the cholesterol recognition amino acid consensus (CRAC) motif being implicated in membrane curvature and budding from cholesterol rich lipid rafts at the apical surface of the cell (Rossman *et al.*, 2010; Schroeder *et al.*, 2005), The possession of a caveolin binding domain (CBD) is thought to also aid recruitment to lipid rafts (Zou *et al.*, 2009). The CRAC domain has been shown to have a role in virulence (Stewart *et al.*, 2010). The cytoplasmic tail of M2 has been shown to be involved in virus assembly, aiding incorporation of vRNPs by interacting with M1 (Chen *et al.*, 2008). The cytoplasmic tail of M2 has also been shown to interact with microtubule associated protein LC3. As a result of this, it is redistributed to the plasma membrane facilitating transmission and stability of progeny virions (Beale *et al.*, 2014). In addition, M2 has been shown to subvert autophagy, with the N-terminal 60 residues able to bind the autophagy-related Beclin-1 protein (Gannagé *et al.*, 2009), allowing survival of infected cells. In the case of filamentous IAV, when virus entry is not by clathrin-mediated endocytosis, but instead micropinocytosis, the intact virions are then trafficked to acidified late endosomes, where M2 curvature leads to fragmentation of the virion, aiding fusion with endosomal membrane (Rossman *et al.*, 2012).

1.8.3 IAV M2 tetramer structures

In 2002 the first structure of the IAV M2 tetramer was published (Nishimura *et al.*, 2002). To date there are 20 M2 structures deposited on the Research Collaboratory for Structural Bioinformatics (RSCB) Protein Data Bank (PDB) website (http://www.rcsb.org/pdb/home/home.do - accessed May 2016), none of which are full length structures. Selected structures are shown in Figure 1.4 and details of all structures can be found Table 1.4. In spite of this wealth of structural information, controversy exists over the binding site of antiviral compounds, stemming from two opposing drug-bound structures being published in 2008 (Schnell & Chou, 2008; Stouffer *et al.*, 2008).

DeGrado's lab published an X-ray crystal structure (PDB 3C9J) of the TM domain (aa 22-46), solved in the presence of a single molecule of amantadine bound within the channel lumen (Stouffer *et al.*, 2008). There were two possible orientations of amantadine, the most favourable being with the amine group pointing inwards towards, but not directly contacting H37, and with the adamantyl cage towards the N-terminal region of the lumen, in proximity to S31 (Stouffer *et al.*, 2008). However, Chou's lab solved a solution NMR structure (PDB 2RLF) of the conductance domain (aa 23-60) in the presence of rimantadine (Schnell & Chou, 2008). Unlike the lumenal binding seen in 3C9J, four molecules of rimantadine were bound around the periphery in close proximity to D44, on the lipid facing side of the channel. This allosteric method of adamantane binding was in fact first proposed over a decade earlier, due to findings that suggests amantadine was most effective against the closed conformation of the tetramer (Tosteson *et al.*, 1994).

The X-ray structure of the TM domain (3C9J) was solved in a bilayer-like environment at pH 5.3 and so represents the open conformation of the tetramer (Stouffer *et al.*, 2008). Amantadine physically occluded the lumen, in close proximity to residues linked with amantadine resistance. The four chains formed a cone like structure that was most constricted at the N-terminus and wider towards H37 and W41 at the C-terminus. In the same study, a second structure was also solved at pH 7.3, in the absence of amantadine (PDB 3BKD). The two structures are very similar at the proposed drug binding site (aa 27-34), with the pore being slightly narrower at neutral pH; however, there are greater differences observed at the C terminus with a larger opening at low pH, representing a stable open conformation (Stouffer *et al.*, 2008). Even in the neutral pH structure, that should be representative of a closed tetramer, the gating W41 residues are on average ~9.5 Å apart. This could be due to the electrostatic repulsion of the charged H37 residues, meaning looser helical packing in the context of the short TM domain peptide.

The solution NMR structure (2RLF) used a CD peptide and as such covers more of the protein sequence than 3C9J. The additional residues may act to stabilise the structure, but also mean that the experimental structure theoretically better reflects that of the native protein. These additional residues also make up the majority of the proposed

PDB ID	Residues	Artificial Mutations	Ligand	Method	pH	Reference
1NYJ	22-46	-	-	Solid state NMR	7.0	(Nishimura *et al.*, 2002)
2H95	26-43	-	-	Solid state NMR	8.8	(Hu *et al.*, 2007a)
2KAD	22-46	L40A	Amantadine	Solid state NMR	7.5	(Cady *et al.*, 2009)
2KIH	23-60	C19S, S31N, C50S	-	Solution NMR	-	(Pielak *et al.*, 2009)
2KQT	22-46	-	Amantadine	Solid state NMR	7.5	(Cady *et al.*, 2010)
2KWX	23-60	V27A, C50S	-	Solution NMR	7.5	(Pielak & Chou, 2010)
2L0J	22-62	C50S	-	Solid state NMR	7.5	(Sharma *et al.*, 2010)
2LY0	19-49	C19S	M2WJ332	Solution NMR	6.8	(Wang *et al.*, 2013b)
2MUV	19-49	C19S	Compound 11	Solution NMR	6.8	(Wu *et al.*, 2014b)
2MUW	19-49	C19S, N31S	Compound 11	Solution NMR	7.5	(Wu *et al.*, 2014b)
2N70	18-60	C19S, S31N, C50S	-	Solid state NMR	6.5	(Andreas *et al.*, 2015)
2RLF	23-60	C19S, C50S	Rimantadine	Solution NMR	7.5	(Schnell & Chou, 2008)
3BKD	22-46	-	-	X-ray crystallography	7.3	(Stouffer *et al.*, 2008)
3C9J	22-46	G34A	Amantadine	X-ray crystallography	5.3	(Stouffer *et al.*, 2008)
3LBW	25-46	G34A	-	X-ray crystallography	6.5	(Acharya *et al.*, 2010)
4QK7	22-46	-	-	X-ray crystallography	8.0	(Thomaston *et al.*, 2015)
4QKC	22-46	-	-	X-ray crystallography	5.5	(Thomaston *et al.*, 2015)
4QKL	22-46	-	-	X-ray crystallography	8.0	(Thomaston *et al.*, 2015)
4QKM	22-46	-	-	X-ray crystallography	5.5	(Thomaston *et al.*, 2015)
5C02	22-46	S31N	-	X-ray crystallography	8.0	(Thomaston & DeGrado, 2016)

Table 1.4 Published structures of influenza A virus M2 tetramers.

Details of all IAV M2 tetramer structures available from RCSB protein data bank (PDB). These are identified by their unique PDB IDs. Additional details of amino acid residues of the tetramer, artificial mutations, ligands bound and method of structural determination are included alongside the original publication citation. M2WJ332 and compound 11 are adamantane compounds.

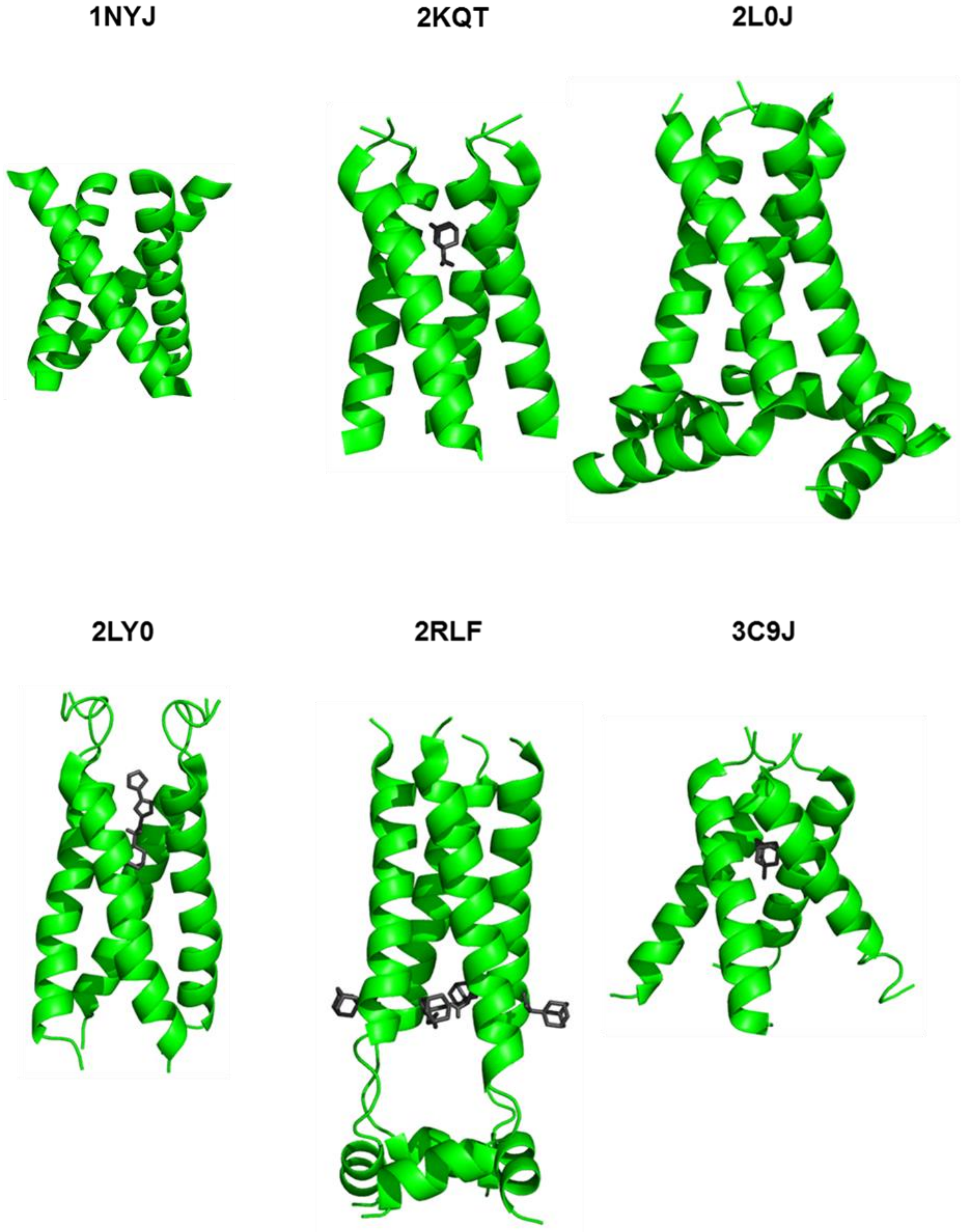

1NYJ

2KQT

2L0J

2LY0

2RLF

3C9J

Figure 1.4 A selection of the published influenza A virus M2 tetramer structures.

Structures of six published M2 tetramers, depicted as cartoons. 1NYJ solution NMR structure of residues 22-46, 2KQT solid state NMR (ssNMR) 22-46 with amantadine bound, 2L0J ssNMR 22-63, 2LY0 solution NMR 19-49 with M2WJ332 bound, 2RLF solution NMR 26-60 with rimantadine bound and 3C9J X-ray crystallography 22-46 with amantadine bound.

peripheral adamantane binding site (Schnell & Chou, 2008), which is only partially represented by the TM peptide used in 3C9J. This lipid facing binding site would mean that rimantadine exerts an allosteric mechanism of inhibition, stabilising the closed conformation of M2. The paper proposes that resistance mutations located at pore lining residues in fact result in a destabilisation of the closed state (Schnell & Chou, 2008), a year later this was supported by a second paper (Pielak *et al.*, 2009). Previous work, using spin-labelled amantadine, demonstrated the high membrane partition coefficient of the M2 inhibitor, causing it to concentrate in the membrane (Subczynski *et al.*, 1998). It must also be noted that as 2RLF was solved at pH 7.5, the structure is of the closed form of the M2 tetramer (Schnell & Chou, 2008). As such, constrictions at V27 result in a pore diameter of ~ 3.1 Å, insufficient for rimantadine to occupy the proposed lumenal binding site. In comparison to 3C9J the diameter of the pore is also smaller at the C-terminal end; this may not be solely due to the pH, but also that the presence of the additional residues of the conductance domain, adding to the stability of the tetramer, counteracting the electrostatic repulsion of charged histidine residues (Schnell & Chou, 2008).

The DeGrado group refined their model of the TM domain in 2010 (PDB 2KQT), reporting a high affinity lumenal amantadine binding site and a second lower affinity peripheral binding site (Cady *et al.*, 2010). The primary binding site was consistent with that previously reported (3C9J), where a single molecule of amantadine binds in close proximity to S31 (Cady *et al.*, 2010; Stouffer *et al.*, 2008). Increasing the concentration of amantadine in the bilayer revealed the second, lower affinity site, allowing an additional four molecules to bind in proximity to D44, without displacing the lumenally bound amantadine (Cady *et al.*, 2010). However, this low affinity might in part be explained by the use of a TM peptide rather than a CD peptide, meaning either fewer or weaker interactions are made to the tetramer. Interestingly, amantadine was still capable of binding to the lumen of the TM domain tetramer, even when the structure was solved at pH 7.5 (Cady *et al.*, 2010), compared to the acidic pH of 3C9J (Stouffer *et al.*, 2008). The NMR data for amantadine at the lumenal binding site showed the potential for the drug to undergo rotation, possibly due to dynamic interactions with the binding site (Cady *et al.*, 2010). This demonstrated a potential lack of specificity of adamantane compounds.

Both the 2RLF and the 3C9J structures have their merits, but also their limitations. The CD structure of 2RLF has the benefit of spanning more of the sequence and as such allowing investigation of the peripheral site and potentially a more native state of the protein. However, potentially as a consequence of the neutral pH used, the pore diameter is too narrow to assess lumenal binding. Conversely, the TM 3C9J structure omits a portion of the peripheral binding site, but the study looked at both open and closed conformations by using different pH environments.

1.8.4 The future of M2 as a drug target

Resistance to the current adamantane M2 antivirals, amantadine and rimantadine is widespread and linked to various amino acid substitutions (Black *et al.*, 1993a; Hay *et al.*, 1985; Hay *et al.*, 1986; Wang *et al.*, 1993), but most notably V27A and S31N. This resistance has been attributed to two things. Firstly, a lack of specificity due to the large hydrophobic cage and minimal function groups, linked to weaker binding and a reduced barrier to resistance, and secondly their use as monotherapies. However, the successful use of M2 inhibitors in the past demonstrated that it is a valid target for IAV antivirals, and for this reason much work has been undertaken to design new M2-targeted inhibitors.

Amantadine and rimantadine contain only one pharmacophore i.e. one group of atoms responsible for ligand interaction and drug action. This limits the points of specific interactions they can make with the M2 tetramer to just one. Some groups have taken the strategy of adding a second pharmacophore to the adamantane scaffold in order to improve efficacy (Du *et al.*, 2010; Tran *et al.*, 2011; Wang *et al.*, 2013a; Wang *et al.*, 2013b; Wu *et al.*, 2014b). The effects of amantadine derivatives with changes to the cage structure have also been investigated, but despite effects against S31 and N31 M2 channels in electrophysiology studies, plaque assays used only a WT S31 strain (Duque *et al.*, 2011). Undertaking modifications of adamantanes has yielded inhibitors with effects against WT and S31N viruses (Wang *et al.*, 2013a; Wang *et al.*, 2013b) or M2 in two-electrode voltage clamp (TEVC) assays (Wu *et al.*, 2014b). Of note is M2WJ332, an adamantane compound which has experimental activity against a rimantadine-resistant N31 IAV strain; this compound has also been shown to bind within the lumen of a M2 TM tetramer (Wang *et al.*, 2013b). Further amantadine analogues, with a potential effect on pH1N1 swine influenza (N31), have been identified by *in silico* docking but have not been tested *in vitro* or *in vivo* (Du et al., 2010; Tran et al., 2011). Aminoadamantanes have been shown to be efficacious against pH1N1 and A/Puerto Rico/8/1934 (H1N1) viruses, but not A/WSN/1933 (H1N1), despite all three strains containing N31 M2 (Kolocouris *et al.*, 2014). However, with electrophysiology studies using N31 M2 showing no blockade, it has been postulated that these adamantane derivatives target a different IAV protein.

The potential of non-adamantane inhibitors has also been explored. One line of investigation started from the discovery of spirene-containing compound, BL-1743, as an inhibitor of mutant N31S A/WSN/1933 (H1N1) M2 in 1995 (Kurtz *et al.*, 1995). This was the first non-adamantane inhibitor of M2 identified. BL-1743 was shown to be effective against IAVs that are amantadine sensitive, but it was ineffective against naturally occurring resistant strains (Tu *et al.*, 1996). Interestingly, a novel I35T polymorphism in M2 conferred BL-1743, but not amantadine resistance, suggesting a different binding mode (Tu *et al.*, 1996). Derivatives of BL-1743 have demonstrated the potential of this class of compound to be used against rimantadine sensitive (Balannik *et al.*, 2009; Wang *et al.*, 2009) and resistant strains containing either L26F or V27A polymorphisms, but were found to be ineffective against S31N mutants (Balannik *et al.*, 2009).

Subsequently, other scaffolds and compound classes have been investigated, including amines. Screening of a small primary amine library resulted in identification of a number of compounds effective against amantadine sensitive, but not amantadine resistant IAV strains (Hu *et al.*, 2010). Modification of the top hit, through structure activity relationship (SAR) studies, produced imines with improved efficacy, but compounds were still only effective against WT M2 viruses (Zhao *et al.*, 2011). Polycyclic amines targeting M2 have shown efficacy in TEVC and plaque assays (Rey-Carrizo *et al.*, 2014). Whilst antiviral activity was seen against A/Puerto Rico/8/1934 (H1N1), a virus strain containing the dual V27A/S31N mutation; in TEVC assays only 1 % inhibition was recorded for the N31 peptide, compared to 96 % for V27A. Polycyclic pyrrolidine derivatives were also investigated and likewise were only seen to affect the V27A resistance polymorphism (Rey-Carrizo *et al.*, 2013). Spirane amine compounds were effective against WT and L26F and V27A mutants (Wang *et al.*, 2011).

Additional non-adamantane compounds; hexamethylene amiloride (HMA) and triazine derivatives, have also shown antiviral effects against S31 IAV strains. Despite showing good efficacy against WT M2 in TEVC assays, their effects were limited against S31N M2 (Balgi *et al.*, 2013). In the current literature there are no reports of non-adamantane compounds with efficacy against the most prevalent resistance polymorphism S31N.

1.9 **Viroporins**

Viroporins are a family of small, hydrophobic membrane proteins, encoded by a range of viruses that modify membrane permeability. Electrophysiology studies using *Xenopus* oocytes identified IAV M2 as the first virally encoded protein to directly exhibit channel activity (Pinto *et al.*, 1992). This corroborated the observation made over a decade earlier that virus infection led to increased permeability of the cell membrane to ions and small molecules (Carrasco, 1978). In the years following, many other clinically relevant viruses were found to encode viroporins, including human respiratory syncytial virus (hRSV) (Perez *et al.*, 1997), poliovirus (Aldabe *et al.*, 1996; Lama & Carrasco, 1992), HCV (Griffin *et al.*, 2003) and human immunodeficiency virus type 1 (HIV-1) (Ewart *et al.*, 1996; Schubert *et al.*, 1996b). More recently viroporins from DNA viruses have also been identified (Suzuki *et al.*, 2010; Wetherill *et al.*, 2012). A non-exhaustive list of viroporins and their characteristics can be found in Table 1.5.

Viroporins are made up of monomers, typically below 120 aa in length, which oligomerise primarily via hydrophobic interactions. Whilst the IAV M2 monomer has a single transmembrane domain (TMD) α-helix, some viroporins have multi-pass TMDs. Oligomers range from the simplest single TMD, tetrameric structure of IAV M2 (Sakaguchi *et al.*, 1997), to the human papillomavirus type 16 (HPV-16) E5 viroporin, predicted as being a hexameric channel with each monomer having three TMDs, giving a total of 18 TM passes (Wetherill *et al.*, 2012).

Limited sequence homology exists between viroporins, yet despite this, HCV p7 and IAV M2 have been shown to have analogous functions and be *trans*-complementary *in vitro* (Bentham *et al.*, 2013; Griffin, 2004; Wozniak *et al.*, 2010), as have HIV-1 Vpu and Sindbis virus 6K (Carrasco, 2001). Viroporins were originally thought to solely be involved in mediating virus entry and/or exit. However, as the family has expanded, new functions have been identified, with the ion channel activity in most cases being essential to the virus life cycle. In many cases viroporin proteins have additional roles, unrelated to their ion channel activity and involving extra-membranous domains; as such, these functions limit the ability of one viroporin to replace the function of one from another virus.

The potential of viroporins as antiviral targets is demonstrated by M2 licensed inhibitors amantadine and rimantadine, with many more potential inhibitors, from multiple classes of compounds, being identified via *in silico* and *in vitro* means (Section 1.8.4). A selection of compounds that have demonstrated the ability to target other viroporins as antivirals are summarised in Table 1.6.

1.9.1 Hepatitis C Virus (HCV) p7

HCV protein p7 was discovered by characterising the inefficient cleavage of its polyprotein by signal peptidase (Lin *et al.*, 1994; Mizushima *et al.*, 1994). The 63 amino

Virus genome	Virus	Viroporin	Amino acids	Ion specificity	Role of channel function
ssRNA (+)	Poliovirus	2B	97	Ca^{2+}	Particle production
	HCV	p7	63	H^+	Particle production, entry (suspected)
ssRNA (-)	hRSV	SH	64-65	K^+/Na^+	TNF antagonist, pathogenesis
	IAV	M2	97	H^+	Entry, particle production (some)
	IBV	BM2	100	H^+	Entry
ssRNA (RT)	HIV-1	Vpu	81	K^+/Na^+	Particle production
dsDNA	HPV-16	E5	83	Unknown	Oncogenesis, signalling / trafficking

Table 1.5 Summary of selected viroporins and their characteristics.

The viroporins from positive sense (+), negative sense (-) and reverse transcription (RT) selected single-stranded RNA (ssRNA) viruses and double stranded DNA (dsDNA) viruses, with name, amino acid length, consensus on ion channel specificity and known function of the channel. Adapted from (Scott & Griffin, 2015).

Class	Compound ID	Structure	Viroporin target	Reference
Adamantane	Amantadine	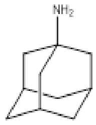	HCV p7	(Griffin *et al.*, 2003)
	Rimantadine	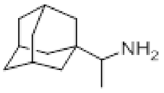	HCV p7	(Griffin *et al.*, 2008)
	Compound H	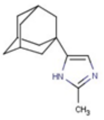	HCV p7	(Foster *et al.*, 2011)
Iminosugar	NN-DNJ	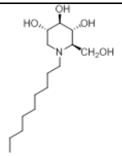	HCV p7	(Pavlovic *et al.*, 2003)
	NN-DGJ	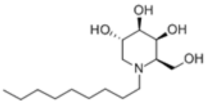	HCV p7	(Pavlovic *et al.*, 2003)
Amiloride	HMA	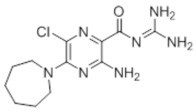	HIV-1 Vpu	(Ewart *et al.*, 2002)
			HCV p7	(Premkumar *et al.*, 2004)
	BIT225	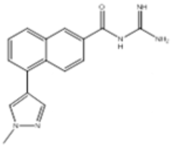	HCV p7	(Luscombe *et al.*, 2010)
			HIV-1 Vpu	(Khoury *et al.*, 2010)
Other	CD	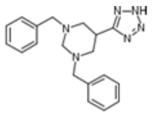	HCV p7	(Foster *et al.*, 2011)
	LDS19/21	Unknown	HCV p7	(Foster *et al.*, 2014)
	MV006	Unknown	HPV-16 E5	(Wetherill *et al.*, 2012)
	Pyronin B	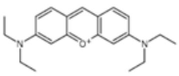	hRSV SH	(Li *et al.*, 2014b)

Table 1.6 Summary of experimental inhibitors of selected viroporins, described in the literature.

Prototypic and derivative inhibitors of viroporins from HCV, HIV-1, HPV-16 and hRSV. Adapted from (Scott & Griffin, 2015).

acid, highly hydrophobic protein is predicted to have two TMDs, separated by a short loop of conserved basic residues (Carrere-Kremer *et al.*, 2002; Luik *et al.*, 2009). Predominantly, p7 resides in endoplasmic reticulum membranes, but evidence of cell surface expression has also been presented in over-expression studies (Carrere-Kremer *et al.*, 2002; Haqshenas *et al.*, 2007; Wozniak *et al.*, 2010).

HCV p7 is able to oligomerise, forming complexes with either hexameric or heptameric stoichiometry (Clarke *et al.*, 2006; Griffin *et al.*, 2003; Luik *et al.*, 2009). Two solution NMR structures of p7 monomers revealed a hairpin structure (PDB 2MTS and 3ZD0) (Cook *et al.*, 2013; Foster *et al.*, 2014). The conformation of these structures varies slightly, most likely due to differences in pH (PDB 2MTS, pH 4.0 and PDB 3ZD0, pH 7.0). An *in silico* model of the channel was generated from the 3ZD0 monomer and resulted in a heptameric oligomer, retaining the lumenal facing orientation of key residues H17 and F25 (Foster *et al.*, 2014). A hexameric NMR structure has also been published (PDB 2M6X), but in contrast to the hairpin conformation of the monomer structures, a “staple-like” monomer was determined (OuYang *et al.*, 2013). Whether hairpin monomers under conformational rearrangement to form staple-like structures upon oligomerisation is unknown. Another point to consider is the genotype of HCV used in the structural studies, the monomers are genotype 1b, whilst it is a genotype 5a complex and this could be the source of the discrepancies. An earlier electron microscopy study of genotype 2a p7 hexameric channels revealed a structure with both termini exposed, and consistent with the hairpin conformation of the monomers (Luik *et al.*, 2009). Until further oligomer structures are solved it will be difficult to determine the source of the variation.

It has been demonstrated that p7 has amantadine-sensitive ion channel activity *in vitro* (Griffin *et a*l., 2003). However, it was later demonstrated that the amantadine sensitivity of p7 was determined by genotype (Griffin *et al.*, 2008; Steinmann *et al.*, 2007b). The p7 channel was shown to be selective for cations including Na^+, K^+ and Ca^{2+} (Clarke *et al.*, 2006; Griffin *et al.*, 2003; Pavlovic *et al.*, 2003; Premkumar *et al.*, 2004) and have the ability to functionally replace IAV M2 in cell culture (Griffin *et al*., 2004). It is this ability to conduct protons that, to date, is the only known biologically relevant function of p7 channel activity (Wozniak *et al.*, 2010). Reminiscent of IAV M2, it has been shown that reduced pH can activate p7 (StGelais *et al.*, 2007; Wozniak *et al.*, 2010), but this is not the case for all HCV genotypes (Atkins *et al.*, 2014; Li *et al.*, 2012).

An infectious culture model for HCV revealed the essential role of p7 in production of infectious particles (Jones *et al.*, 2007; Steinmann *et al.*, 2007a; Wozniak *et al.*, 2010). Here, p7 proton channel activity is required to deacidify intracellular compartments in order to protect nascent virus particles (Wozniak *et al.*, 2010), potentially similar to the role M2 plays in protection of HA in some strains of IAV (Grambas & Hay, 1992; Sugrue *et al.*, 1990). A second, and controversial, role of p7 channel activity during virus entry has been postulated, supported by an enhancement of HCV-like particle uptake by hepatocytes, when p7 is present (Saunier *et al.*, 2003) and effective use of specific p7 inhibitors when present during the infection process (Baumert *et al.*, 2016; Griffin *et al.*, 2008). Channel independent roles have also been demonstrated for p7, including during assembly of the capsid and envelopment (Gentzsch *et al.*, 2013). Interactions between p7 and other virus proteins, notably NS2 are thought to be responsible for additional roles in the life cycle (Boson *et al.*, 2011; Hagen *et al.*, 2014; Jirasko *et al.*, 2008; Jirasko *et al.*, 2010; Ma *et al.*, 2011; Tedbury *et al.*, 2011).

Following the finding that licensed IAV M2 antiviral amantadine has been shown to inhibit p7 channel activity (Griffin *et al.*, 2003), and *in vivo* studies in chimpanzees demonstrating the viroporin was essential for HCV infectivity (Sakai *et al.*, 2003), interest for developing antivirals targeting p7 grew. Many different classes of inhibitory compound have been identified as targeting p7. The channel activity of p7 has also been shown to be inhibited by rimantadine (Griffin *et al.*, 2008) and another adamantane derivative compound H (Foster *et al.*, 2011). Additionally amiloride analogues, HMA and BIT225, are able to inhibit HCV p7 (Ewart *et al.*, 2002; Khoury *et al.*, 2010; Luscombe *et al.*, 2010; Premkumar *et al.*, 2004). Long chain alkylated iminosugar derivatives demonstrate antiviral effects on HCV, being proposed to inhibit p7 by interfering with oligomerisation (Foster *et al.*, 2011), in addition to inhibiting host endoplasmic reticulum α-glucosidases (Pavlovic *et al.*, 2003; Steinmann *et al.*, 2007b). Identified through *in silico* docking to a peripheral site on the p7 heptamer, novel compound CD was shown to inhibit the conductance of p7 (Foster *et al.*, 2011). Resistance to p7 inhibitors has also been shown, with the L20F and F25A polymorphisms conferring resistance to adamantanes and iminosugars, respectively (Foster *et al.*, 2014; Foster *et al.*, 2011). Mutant L20F HCV was resistant to novel compound CD(Foster *et al.*, 2011). However, compounds LDS19 and LDS21 are affective against L20F genotype 1b mutants, but genotype 2a mutants had increased susceptibility to these compounds (Foster *et al.*, 2014), further demonstrating the differential effects inhibitors have on different HCV genotypes.

1.9.2 Human Immunodeficiency Virus type 1 (HIV-1) Vpu

HIV-1, as well as related simian immunodeficiency viruses, encodes the 16 kDa multifunctional protein Vpu (Cohen *et al.*, 1988; Strebel *et al.*, 1988). Vpu is an 81 amino acid, type-1 integral membrane protein capable of homo-oligomerising (Maldarelli *et al.*, 1993). It has a pentameric structure predicted by molecular dynamics (Grice *et al.*, 1997) and shown by NMR studies (Park *et al.*, 2003; Sharpe *et al.*, 2006). It is not a component of the virion and is not required for efficient virus replication in culture (Du *et al.*, 1993), but scrambling of the TMD of Vpu results in reduced pathogenicity (Hout *et al.*, 2005; Schubert *et al.*, 1996a).

Vpu has a role in regulating the degradation of CD4 (Willey *et al.*, 1992), linked to phosphorylation of serine residues in its cytoplasmic domain (Paul & Jabbar, 1997). It also antagonises the restriction factor tetherin, permitting release of the virus from the cell surface (Neil *et al.*, 2008). The N-terminal domain of Vpu has also been associated with immune evasion, via inhibiting NF-κB activation and its suppression antiapoptotic factors or interfering with major histocompatibility complex (MHC) class I biosynthesis (Akari *et al.*, 2001; Bour *et al.*, 2001; Kerkau *et al.*, 1997).

The ion channel activity of Vpu has been demonstrated via electrophysiology studies (Schubert *et al.*, 1996b) and N-terminal peptides were demonstrated to have cation selectivity (Ewart *et al.*, 1996). *In vitro* Vpu TMD peptides adopt an almost pore-like character (Mehnert *et al.*, 2007). However, evidence of preferential cation conductance, a critical role of the lumen lining residue S23 and the potential for W22 to be either pore or lipid facing implies that the channel is both selective and gated (Cordes *et al.*, 2001; Grice *et al.*, 1997; Park *et al.*, 2003; Sharpe *et al.*, 2006).

Adamantane compounds capable of inhibiting IAV M2 and HCV p7 are not effective against Vpu (Ewart *et al.*, 2002). Whilst amiloride derivatives BIT225 and HMA, but not amiloride itself, are capable of blocking the ion channel activity of Vpu (Ewart *et al.*, 2002; Luscombe *et al.*, 2010). HMA inhibited budding of HIV-LPs from the surface of cells *in vitro* (Ewart et al., 2002), and it has since been identified that the channel activity of Vpu may enhance particle release by via depolarisation-stimulated exocytosis (Hsu *et al.*, 2010).

1.9.3 Human Respiratory Syncytial Virus (hRSV) SH

Human RSV encodes SH, a small hydrophobic protein, 64-65 aa in length. SH is predicted to contain a single TMD, with pentameric (Collins & Mottet, 1993; Gan *et al.*, 2008; Gan *et al.*, 2012) and hexameric complexes reported (Carter *et al.*, 2010). SH is not required for virus replication in culture, but SH-deleted viruses are attenuated (Bukreyev *et al.*, 1997; Karron *et al.*, 1997). The SH protein has been implicated in subverting apoptosis, by antagonising TNF-α signalling (Fuentes *et al.*, 2007). It has also been shown to promote bacterial membrane permeability (Perez *et al.*, 1997), with both TMD and full length peptides having been shown to form cation selective channels *in vitro* (Gan *et al*., 2008). Conserved W15, H22 and H51 residues have been implicated in channel gating and activity, with deletion of both histidines resulting in a non-functional channel (Gan *et al.*, 2012). However, unlike IAV M2, reduction in pH, causing histidine protonation results in reduced cation transport (Gan *et al.*, 2008).

The activity of SH is inhibited by pyronin B, when used *in vitro* and in culture (Li *et al.*, 2014b). Pyronin B was found to bind to the conserved C-terminal end of the TMD of a SH monomer, these data were supported by work in bicelles (Li *et al.*, 2014b). This finding provides a viable start point for the development of RSV antivirals targeting SH.

1.9.4 Human Papillomavirus type 16 (HPV-16) E5

HPVs are non-enveloped DNA viruses. HPV-16 is one of the most studied types and is known to be potently oncogenic. HPV-16 E5 consist of 83 amino acids and is highly hydrophobic (Halbert & Galloway, 1988). The oncogenic potential of E5 was first highlighted in the 1990s, but it remains the least well characterised of the three HPV oncoproteins (Leechanachai *et al.*, 1992; Leptak *et al.*, 1991; Pim *et al.*, 1992; Straight *et al.*, 1993; Valle & Banks, 1995).

The monomers of E5 have three TMDs (Krawczyk *et al.*, 2010; Wetherill *et al.*, 2012), with the multiple hydrophobic regions promoting oligomerisation (Gieswein *et al.*, 2003). No published structure of E5 monomers or the oligomer exists. However, expression of recombinant E5 resulted in formation of a single oligomeric species, indicative of a hexameric complex, which formed channels of defined lumenal diameter and stoichiometry (Wetherill *et al.*, 2012).

The channel activity of E5 *in vitro* was increased by a reduction in pH, suggesting a potential acid activation mechanism. Activity was sensitive to rimantadine, but not amantadine (Wetherill *et al.*, 2012). Novel compound MV006, selected via *in silico* modelling, exerted greater effects than adamantanes *in vitro* (Wetherill *et al.*, 2012) and when used in cell culture resulted in reduced E5-mediated effects on cellular signalling (Pim *et al.*, 1992; Suprynowicz *et al.*, 2010; Wetherill *et al.*, 2012). This implies that channel activity is related to oncogenic function.

1.10 **Aims**

The Influenza A virus M2 proton channel is a proven antiviral target, but due to widespread resistance in circulating strains, including the 2009 swine influenza pH1N1 swine influenza, licensed adamantane compounds (amantadine and rimantadine) are no longer recommended for clinical use. Controversy exists over the binding site and mode of action of adamantane compounds, with structures supporting both a pore-blocking lumenal binding site and allosteric peripheral binding published in the literature. This project sought to address this controversy and determine whether both sites are able to be targeted. Through the use of rational, structure-guided drug design, this project set out to discover novel inhibitors of N31-containing pH1N1 M2. By designing compounds predicted to make specific interactions with either the lumenal, or the peripheral site, we could generate tools to further investigate the potential benefits of having drugs specifically targeting each site. We hypothesised that it would be possible to inhibit both sites and that this novel combination therapy could both achieve improved antiviral potency, as well as combatting the emergence of future resistant strains.

.

Chapter 2

Materials and methods

Chapter 2 Materials and methods

2.1 Materials

2.1.1 Compounds

M2WJ332 ((3S,5S,7S)-N-{[5-(thiophen-2-yl)-1,2-oxazol-3-yl]methyl}tricycle[3.3.1.1~3,7 ~]decan-1-aminium) and compound H (5-(1-adamantyl)-2-methyl-1H-imidazole) were synthesised by Dr Jayakanth Kankanala. Rimantadine hydrochloride ((RS)-1-(1-adamantyl)ethanamine) and zanamivir ((2R,3R,4S)-3-acetamido-4-(diaminomethylideneamino)-2-[(1R,2R)-1,2,3-trihydroxypropyl]-3,4-dihydro-2H-pyran-6-carboxylic acid) were purchased from Sigma, all other compounds were purchased from ChemBridge.

Compounds were resuspended in dimethyl sulfoxide (DMSO) to 10-100 mM, aliquoted, and stored at –20 ºC, or –80 ºC for long term storage.

2.1.2 Lipids

Lipids were purchased from Avanti Polar Lipids: L-α-phosphatidic acid (α-PA), L-α-phosphatidyl choline (α-PC) and L-α-phosphatidyl ethanolamine with lissamine rhodamine B labelled head groups (α-PE). All were derived from chicken eggs and supplied in chloroform.

2.1.3 M2 peptides

M2 peptides were purchased from Peptides International and were provided lyophilised as a TFA salt. These comprised conductance domain (CD) peptides for both wild type (WT) N31 and mutant S31 M2 from E195, and a WT transmembrane (TM) domain peptide. Details of their sequence are noted below:

H-RCSDSSDPLVIAASIIGILHLILWITDRLFFKCIYRRFKYGLK-NH2 (S31 CD, 18-60aa)

H-RCSDSSDPLVIAANIIGILHLILWITDRLFFKCIYRRFKYGLK-NH2 (N31 CD, 18-60aa)

H-RCSDSSDPLVIAANIIGILHLILWITDRL-NH2 (N31 TM, 18-46aa)

2.1.4 Mammalian Cell Culture

Madin-Darby Canine Kidney (MDCK) cells, passage 6, were kindly provided by Prof. Wendy Barclay (Imperial College London) and were regularly checked to ensure they were free of mycoplasma infection.

2.1.5 Influenza A virus

A/England/195/2009 (E195) influenza A virus was kindly provided by Prof. Wendy Barclay (Imperial College London), as a frozen viral stock derived from MDCK cells at 6 $x10^6$ pfu/ml. New stocks were generated in house at 5 $x10^5$ pfu/ml.

2.1.6 Oligonucleotides

DNA oligonucleotide primers were manually designed and purchased from either Sigma Aldrich or Eurofins Genomics. Lyophilised primers were resuspended to a concentration of 100 mM in dH_2O and stored at –20 ºC. These were used for reverse transcription and cDNA amplification, in order to gather sequence information for M2.

pH1N1_s7_fwd: 5'-AAGATGAGTCTTCTAACCG-3’

pH1N1_s7_F2: 5’-AAGATGAGTCTTCTAACCGAGG-3’

pH1N1_s7_Fint: 5’-GGCTAGCACTACGGC-3’

Flu_s7_fwd: 5'-AGCAAAAGCAGGTAG-3’

Flu_s7_R2: 5’-AGTAGAAACAAGGTAGTTTTTTACTCTAGC-3’

2.2 *In silico* protein modelling and drug binding

2.2.1 E195 M2 homology model

Published M2 tetramer structures were downloaded from the website of the Research Collaboratory for Structural Bioinformatics (RCSB), protein data bank (PDB) (http://www.rcsb.org/pdb/home/home.do).

An *in silico* homology model of conductance domain of E195 M2 was generated using the solution NMR structure of A/Udorn/307/1972 H3N2 (PDB 2RLF, Schnell and Chou (2008)) as a template and A/England/195/2009 as the target. Prime and Maestro (Schrödinger) were used for homology modelling, with the model minimised in an octanol environment (Dr Jayakanth Kankanala). This homology model was later re-minimised in a lipid membrane environment, using an Optimised Potentials for Liquid Simulations (OPLS) force field and used for docking of unbiased compound analogues.

A second homology model using PDB 2L0J (Sharma *et al.*, 2010) as a template was made, using the SWISS-MODEL (ExPASy) web server and was minimised in an octanol environment using Maestro (Dr Richard Foster).

2.2.2 High throughput docking using eHiTS

Two binding regions (clip files) were defined using Maestro software, the lumen concentrated on pore lining residues at the N-terminal end of the TM domain (V27, A30, N31, I33 and (G34) and the periphery on lipid facing residues at the C-terminal of the TM domain (W41, I42, T43, D44, R45 and F48) (Figure 3.3).

2.2.2.1 Unbiased screen

Open access small molecules libraries were used for molecular binding studies, eHiTS (SimBioSys Inc.) was used to dock compounds onto the two clip files of the pH1N1 homology model. The top 1000 compound based on eHiTS score, at each site, were manually assessed for their binding pose and drug-like qualities. Seven predicted lumenal binding compounds L1-L7 and six peripheral binding compounds P1-P6 were selected for testing (Dr Jayakanth Kankanala).

2.2.2.2 Biased screen

A rapid overlay of chemical structure (ROCS) search based on compound D (Figure 3.4) was carried out using ROCS (OpenEye Scientific) software. The top 1000 hits were docked using eHiTS, against the clip files for the proposed lumenal and peripheral binding sites. Compound docking at both sites was validated using SPROUT (Keymodule Ltd.) software (Dr Katie Simmons).

A protocol of attrition was carried out to select DL and DP compounds, focussing on docking scores, molecular weight and specific interactions with the M2 tetramer. Full details are listed in (Section 3.5.1). Briefly, compounds were selected based on agreement between the two binding scores, molecular weight and specific interactions with the protein.

2.2.2.3 Analogues

Analogues of selected compounds were found via the online tool eMolecules (www.emolecules.com). Selected compounds were subsequently docked against the 2RLF-based E195 M2 homology model using eHiTS.

2.3 *In vitro* liposome assay

2.3.1 Liposome preparation

Lipids (Avanti polar lipids) were thawed on ice and added to a glass tube. 50 µl α-PA, 50 µl α-PC and 5 µl α- PE were mixed, to give a final mixture containing 1 mg of lipid, containing 0.5 % w/w α-PE with lissamine rhodamine B labelled head groups. Chloroform was evaporated from the lipids using a stream of nitrogen, before placing in a vacuum for 4 hours (hr) at room temperature (RT). Lipids were rehydrated to 2 mgml^{-1}, in a self-quenching concentration of carboxyfluorescein (CF) buffer (Appendix B.1 Carboxyfluorescein (CF) buffer) and vigorously shaken overnight at RT.

Lipids were briefly vortexed and a 3 µl pre-extrusion sample was taken prior to 15 passes through an Avanti extruder and a 0.4 µm filter, at 37 ˚C. Unilamellar liposomes were washed four times with liposome assay buffer (Appendix B.2 Liposome assay buffer) and purified via centrifugation at 49,000 rpm (104,000 x *g*) for 15 minutes (min) at 25 ˚C, using a TLA 110 rota in a Beckman Coulter Optima Max 130,000 RPM ultracentrifuge. The final liposome pellet was resuspended liposome assay buffer (0.5 ml).

To determine the concentration of liposomes, pre-extrusion sample (3 µl diluted 1:20) and post-extrusion samples (3 µl neat liposomes) were assessed for rhodamine absorbance (OD_{570}), using a NanoDrop (Thermo Scientific). Absorbance values were then substituted into the equation below:

$$Liposome\ concentration\ (mM) = \frac{\text{2.75 mM (average lipid molarity)}}{OD_{570}\ \text{pre extrusion}\ \times \text{diltuion factor (20)}} \times OD_{570}\ \text{post extrustion}$$

2.3.2 M2 activity liposome assay

The E195 M2 peptides (Section 2.1.3) were reconstituted to 1 mM in methanol (MeOH). From this stock further dilutions were made in MeOH; a maximum of 5 µl MeOH per well for a given peptide concentration.

Unilamellar liposomes, containing 50 mM CF, a self-quenching concentration, were assembled from lipids as described in section 2.3.1. Real time assays were carried out in black-walled, flat-bottomed black-base 96 well plates (Grenier Bio One). 50 µM liposomes (determined by rhodamine absorbance, section 2.3.1) and up to 50 nM peptide in a volume of 5 µl MeOH were used in experiments. Reactions were made up to a total of 100 µl using liposome assay buffer. Liposomes alone were used as a baseline for fluorescence, liposomes + 5 % v/v MeOH was used a negative control and 0.5 % v/v Triton TX-100 (Triton), which lyses liposomes, was used for gain adjustment, setting a level of 90 % fluorescence.

CF release measured by increased fluorescence was taken as an indicator of peptide induced membrane permeability. A set of 30 or 63 readings (λex = 485 nm, λem = 520 nm) were made at 43 second (s) intervals using a FLUOstar Galaxy plate-reader (BMG Labtech). Assays were carried out at RT, with the plate kept on ice for 2-5 min after gain adjustment and while the peptide +/- drug was added (Section 2.3.2.1). All samples were repeated in duplicate on the plate and each experiment repeated three times (unless otherwise stated). Baseline readings of liposomes alone were subtracted from each of the wells when calculating end point results.

2.3.2.1 Inhibition assays

A maximum of 1 % v/v DMSO was added to each reaction, with stock inhibitor concentrations diluted accordingly. Compounds or a DMSO control were preincubated with peptides for 20 min at RT (except in the case of rimantadine which was preincubated for 1 hr, as minimal effects were seen after 20 min), prior to their addition to chilled liposome suspensions diluted in assay buffer.

End point values were taken and liposome alone values subtracted for each condition. Data from duplicate wells was then averaged and normalised to the peptide + DMSO control. Values were then averaged across replicate experiments and standard errors calculated. Paired t-tests were then used to assess statistical significance between the peptide + DMSO control and the compound treated peptide.

2.4 **Mammalian Cell Culture**

2.4.1 Recovery of Cells

MDCK cells (Section 0) were removed from liquid nitrogen and thawed immediately in a 37 ˚C water bath. Cells were then transferred to a 15 ml falcon tube and 10-12 ml of cell culture media (Appendix B.3 Cell culture media) was added, prior to centrifugation at 1500 x *g* for 5 min, using an Eppendorf 5810 R centrifuge. The cell pellet was then resuspended in 5 ml of media and transferred to a T25 tissue culture flask (Corning®, canted neck, vented cap) and incubated at 37 ˚C in 5 % CO_2. 24 hr later, cells were transferred (section 2.4.2) to a T75 tissue culture flask (Corning®, canted neck, vented cap).

2.4.2 Maintenance and Passage of Cells

MDCK cells were maintained in “complete” Dulbecco’s modified essential cell culture media (Appendix B.3 Cell culture media) at 37 ˚C in 5 % CO_2. Cells were passaged every 2-3 days by washing twice in phosphate buffered saline (PBS), followed by incubation in trypsin (Trypsin- Ethylenediaminetetraacetic acid (EDTA) solution, Sigma) for 5-10 min, until cells became detached from the flask. Trypsin was then neutralised with an equal volume of complete cell culture media. Subcultivation ratios of between 1:2 to 1:10 were used to maintain MDCK cells, remaining cells were plated, frozen for storage or discarded.

2.4.3 Storage of Cells

MDCK cells from early passage were centrifuged at 1500 x *g* for 5 min. The cell pellet was then resuspended in freezing media (Appendix B.4 Freezing media) at a density of $1x10^6$ / ml. Cell aliquots were frozen slowly, by being wrapped in paper and placed in a polystyrene box at -80 ˚C, after 48 hr cells were transferred to liquid nitrogen for storage.

2.4.4 Cell plating for compound treatment and infection

Cells were passaged as described in section 2.4.2. The number of MDCK cells plated for each experiment are detailed here: cytotoxicity assay 2.5 $x10^4$ / well (96 well), plaque reduction assay 5 $x10^5$ / well (12 well), generation of escape mutants 1.25 $x10^6$

/ well (6 well). Cells were allowed to settle for at least four hr before treatment with compounds or infection.

2.5 Cell culture cytotoxicity assays

MDCK cells were seeded into flat-bottomed clear 96 well plates (Corning® Costar®) and incubated overnight at 37 ºC, 5 % CO_2. The next morning, media was removed and cells were treated with dilutions of compounds up to 160 µM in cell culture media (Appendix B.3 Cell culture media), with a final concentration of 0.2-0.8 % v/v DMSO. Cells were incubated with the compound for 48-72 hr at 37 ºC, 5 % CO_2.

3-(4, 5-dimethyl-2-thiazolyl)-2, 5-diphenyl-2H-tetrazolium bromide (MTT), a tetrazolium dye, was used as a colourimetric indicator of cellular metabolism, as MTT is reduced to formazan by cellular oxidoreductase enzymes, a colour change occurs. A stock solution (2.5 $mgml^{-1}$) used to add 50 µg MTT to each of the wells and incubated at 37 ºC, 5 % CO_2 for 4 hr. Media was then replaced by 75 µl of DMSO and incubated at 37 ºC for 5 min prior to reading absorbance at 550 nm. Data was normalised to cells treated with the appropriate DMSO control (0.2-0.8 % v/v).

2.5.1 Determination of cell confluency

Cellular confluency after drug treatment was assessed using the IncuCyte ZOOM® (Essen Bioscience). Each well of a tissue culture plate was divided into squares and a measurement of the percentage of the each square occupied by a cell was made under phase. Wells of identical condition were then averaged and standard deviations calculated.

2.6 Virus production and storage

2.6.1 Growing virus stocks

MDCK cells were seeded, with $3\text{-}6 \times 10^6$ per T75 flask and allowed to settle for at least 4 hr. Cells were washed twice in PBS, prior to the addition of A/England/195/2009 virus diluted in serum free (SF) media (Appendix B.5 Serum free (SF) media) to a multiplicity of infection (MOI) < 0.01. After a one hr infection at 37 ºC, 5 % CO_2, virus containing media was replaced with SF media with the addition of 1 $µgml^{-1}$ L-(tosylamido-2-

phenyl) ethyl chloromethyl ketone (TPCK) trypsin (Worthington Biochemical Company) and returned to 37 ºC, 5 % CO_2. Once a cytopathic effect (CPE) of between 40 and 70 % was observed virus containing media was removed for clarification and storage.

2.6.2 Freezing virus for storage

Virus-containing supernatants were clarified by centrifugation (800 x *g* 10 min, 4 ˚C) in an Eppendorf 5810 R centrifuge, transferred to 1.5 ml Eppendorf tubes, and then snap frozen using a dry ice and ethanol / methanol bath. Once frozen, the tubes were stored at – 80 ˚C.

2.7 Plaque reduction assay

Initial plaque reduction assays looking at 24 and 48 hr post infection (hpi) were carried out at Imperial College London, where training for this methodology was given by Dr Ruth Elderfield. The assay was then established within the laboratory at the University of Leeds. Subsequent experiments, using the optimised time point of 24 hpi, were carried out at the University of Leeds.

2.7.1 Virus titration

35 µl of stock virus or virus-containing supernatant samples virus containing media samples were serially diluted in 315 µl SF media. Dilutions from 10^{-1} to 10^{-4} were then used to infect MDCK cells that had been washed twice in PBS, 4 hr after seeding in 12 well plates (Corning® Costar®) at 5 $x10^5$ / well. Infections were carried out for 1 hr at 37 ºC, 5 % CO_2, with manual shaking every 15 min. Media was then removed and a 3:7 mixture of 2% w/v agar (Oxoid™ Purified Agar) and overlay media (Appendix B.6 Overlay media) containing 2 μgml^{-1} TPCK trypsin was added to cells. Once the agar had set, plates were inverted and incubated at 37 ºC, 5 % CO_2 for 72 hr to allow plaques to form. After removal of the agar, cells were fixed in 2 ml 4 % paraformaldehyde (PFA, Sigma) in PBS for 1 hr, then stained with 1 ml of 1 % v/v crystal violet solution (Sigma) for 5 min. Plaques were then counted and virus titres calculated. Each condition was carried out in triplicate within an experiment, with average titres and standard deviations calculated. Paired t-tests were carried out to assess statistical significance between DMSO control treated virus and other compounds.

2.7.2 Compound screening

IAV was diluted in SF media to a multiplicity of infection (MOI) of 0.01 or 0.001 and preincubated with 80 µM compound for 30 min on ice. This virus + compound mix was used for a one hr infection of MDCK cells, on the producer plate. Virus containing media was then removed and replaced with SF media with the addition of 1 µgml^{-1} TPCK trypsin and 80 µM compound before incubation of the producer plate at 37 ºC, 5 % CO_2.

At 24 hpi the media was removed for titration, as described in Section 2.7.1. Initial experiments continued to 48 hpi, with 100 µl of media removed at 24 hpi for titration, but additionally being replaced with 100 µl SF media containing compound and a further sample taken from the producer plate at 48 hpi. Once samples are taken these producer plates were either discarded or fixed in 4 % PFA.

2.7.3 Determination of IC_{50} values

To determine the half maximal inhibitory concentration (IC_{50}) of plaque formation, half-$\log_{10}$ dilutions were made from 80 µM, down to 80 nM, except in the case of zanamivir where $\log_{10}$ dilutions were made from 80 µM, down to 80 pM. A MOI of 0.01 was used and the infection carried out as described in Section 2.7.2, with virus titrated 24 hpi.

2.7.4 Compound combinations

Combinations of two M2 targeted compounds, or an M2 targeted compound and the licensed neuraminidase inhibitor zanamivir were tested. Combination matrices were set up across a range from 0, 0.2, 1 and 5 µM, or based upon doses corresponding to multiples of the compound IC_{50} value, with the 0, 0 combination as DMSO control. Experiments were carried out as described in Section 2.7.2. Virus titres were normalised to the DMSO control, set to 100 % relative virus titre.

CompuSyn (ComboSyn, Inc., www.combosyn.com) software was used to analyse the effects of combinations of compounds on infectious virus titre and determine antagonistic, additive or synergistic combination (Chou, 2006).

2.8 Selection of escape mutants

2.8.1 Serial passage using increasing compound concentrations

MDCK cells were seeded into 6 well plates and allowed to settle for at least 4 hr at 37 ºC, 5 % CO_2. The initial infection with Influenza virus was carried out as described in section 2.7, with 2.5 µM compound at MOI 0.001. At 24 hpi virus containing media was removed, 1/10th volume was used infect freshly seeded MDCK cells and the remainder was snap frozen (Section 2.6.2). This process was repeated, each time increasing the concentration of compound present in the media two-fold, until 80 µM was reached.

The titre of viral supernatants was determined, at selected time points, via plaque assay as described in section 2.7. These supernatants could then be used at MOI 0.001, with fresh 80 µM compound, in subsequent infections.

Full details of compound concentrations, infections, sample nomenclature handling are detailed in Figure 5.7.

2.8.2 Plaque purification

MDCK cells were seeded in 12 well plates and allowed to settle for at least 4 hr at 37 ºC, 5 % CO_2. Virus was diluted 1:250 in SF media containing between 5 and 80 µM compound and used to infect cells for one hr, before cells were set under overlay media, containing 2 µg/ml TPCK, 0 – 80 µM compound and agar.

72 hpi, agar plugs were picked and placed in 300 µl SF media for 2 hr prior to being used to infect fresh MCDK cells, in the presence or absence of compound (5 – 80 µM) for one hr at 37 ºC, 5 % CO_2. Once infectious supernatant was removed, it was replaced with SF media + 1 µg/ml TPCK and 0 – 80 µM compound and plates returned to 37 ºC, 5 % CO_2. Once > 40 % CPE was observed, infectious supernatant was clarified (Section 2.6.2), prior to vRNA extraction.

2.8.3 Viral RNA Extraction

Viral RNA (vRNA) was extracted from clarified supernatants using a QIAamp Viral RNA Mini Kit (QIAGEN). Briefly 140 µl of viral supernatant was added to 560 µl lysis buffer (AVL, appendix B.7.1 Lysis buffer (AVL)) containing carrier RNA and mixed by pulse-vortexing for 15 s, prior to a 10 min incubation at RT. 560 µl of ethanol was then added, followed by pulse-vortexing for 15 s. The sample was then applied to a QIAMP mini column, prior to centrifugation at 6000 x *g* for 1 min and the filtrate discarded. 500 µl wash buffer 1 (AW1, appendix B.7.2 Wash buffer 1 (AW1) (concentrate)) was then added and sample centrifuged at 6000 x *g* for 1 min. 500 µl wash buffer 2 (AW2, appendix B.7.3 Wash buffer 2 (AW2) (concentrate)) was then added followed by centrifugation at 17,900 x *g* for 3 min. vRNA was then eluted into a clean eppendorf by application of elution buffer (AVE, appendix B.7.4 Elution buffer (AVE)) (60 µl) for 1 min, prior to subsequent centrifugation at 6000 x *g* for 1 min. Eluted vRNA kept at –20 ˚C for short term storage, or transferred to -80 ˚C for long term storage.

2.8.4 Reverse Transcription

vRNA was synthesised into first strand cDNA using SuperScript® III (SSCIII) (Invitrogen™) and a pH1N1 segment 7 specific forward primer (pH1N1_s7_fwd, section 2.1.6). Each reaction used 4 µl of vRNA as a template and contained 500 nM primer and 500 nM dNTPs and made to 9 µl with dH_2O. This was incubated at 65 ºC for 5 min, and then placed on ice for 1 min. A mixture containing 14.3 mM dithiothreitol (DTT), 1 x concentration of “first strand buffer” (Appendix B.8 5x Superscript III (SSCIII) first strand buffer), 40 U (units) RNase OUT™ (Invitrogen™) ribonuclease inhibitor and 200 U SSCIII was then added to make the total reaction volume up to 20 µl. The reaction was incubated at 55 ˚C for 50 min, then 70 ˚C for 15 min, before being kept at 4 ˚C. A negative control, of vRNA but no SSCIII was included in each experiment.

2.8.5 cDNA Amplification

cDNA was amplified via polymerase chain reaction (PCR) using the proof reading Phusion® high fidelity (HF) polymerase (Phusion) (New England Biolabs). Each 50 µl reaction contained 4 µl of cDNA, 1 x HF buffer, 200 µM dNTPs, 500 nM of forward primer pH1N1_s7_fwd, 500 nM reverse primer (Flu_s7_R2, section 2.1.6) and 1 U Phusion®. A negative control reaction, containing enzyme, but no cDNA was included.

Reactions were heated to 98 ºC for 30 s, followed by 35 cycles of the following steps; denaturation at 98 ºC for 10 s, annealing at 48 ºC for 30 s and extension at 72 ºC for 40 s. A final incubation at 72 ºC for 7 min was used to ensure completion of any partial copies and clearance of replication machinery from the nascent cDNA.

2.8.6 PCR purification

Amplified cDNA was purified using a QIAquick PCR Purification Kit (QIAGEN). Briefly 5 volumes of binding buffer (PB, appendix B9.1 Binding buffer (PB)) were added to the

PCR reaction and mixed prior to addition to a QIAquick column and subsequent centrifugation at 17,900 x *g* for 1 min to allow the DNA to bind. The column was washed with 750 µl elution buffer (PE, Appendix B9.2 Elution buffer (PE)). DNA was then eluted into a clean eppendorf by addition of water (50 µl) for 1 min, prior to centrifugation at 17,900 x *g* for 1 min. Eluted DNA concentrations were determined by gel electrophoresis (Section 2.8.7) and samples were stored at –20 ºC.

2.8.7 Gel electrophoresis

Molten 0.8 % UltraPure™ agarose (Invitrogen™) was prepared in 1 x Tris-acetate-EDTA (TAE, appendix B.10 50x Tris-acetate-EDTA (TAE)) and added to a casting plate with 0.01 % v/v ethidium bromide (Invitrogen™) and allowed to set at room temperature. The gel was transferred to a gel tank (BioRad) and submerged in 1 x TAE. HyperLadder™ 1 kb (BioLine) was used as a reference and 10 µl of samples were typically added to each well. The samples were run for 20 – 40 min with a constant voltage of 120 V applied. DNA was visualised and images captured on a UV lightbox using Gel Doc™ (BioRad).

2.8.8 Sequencing

The Mix2Seq kit (Eurofins Genomics) and service was used, with forward internal primer pH1N1_s7_Fint or reverse primer Flu_s7_R2 (section 2.1.6). PCR purified cDNA (50-100 ng) was mixed with 2 µl primer (10 µM) and made to a total of 17 µl before submission to Eurofins Genomics.

Chapter 3

In silico screening of compounds against a pH1N1 M2 homology model

Chapter 3 *In silico* screening of compounds against a pH1N1 M2 homology model

3.1 Introduction

Drug discovery and design encompasses a large variety of methodologies and approaches, with *in silico* pharmacology being increasingly utilised. One of the first applications of this approach was quantitative structure–activity relationships, where the structure of chemical compounds was quantitatively linked to pharmacological effects on systems (Cherkasov *et al.*, 2014; Winkler, 2002). As technology advanced, *in silico* pharmacology followed, with 3D modelling of compounds and virtual high-throughput screens (HTS) available to complement biological testing and protein modelling. All of these aspects of *in silico* pharmacology were utilised during this project, and are described in this chapter.

The premise of this project was a programme of structure-guided design for novel inhibitors targeting the drug-resistant M2 proton channel from pandemic swine influenza, using the A/England/195 2009 (H1N1) strain (E195) as the basis. As such, a 3D structure of the M2 tetramer was required. To date, there are 20 structures of IAV M2 tetramers deposited in the RSCB PDB (www.rcsb.org/pdb/home/home.do; accessed May 2016, details in Table 1.4). These structures include many different strains of IAV, some with compounds bound, and others without. Furthermore, the majority of structures have been solved at neutral pH, and thus represent the closed channel. None of the structures span the entire 97 amino acids of M2, instead they usually comprise peptides covering either the transmembrane (TM) domain or the conductance domain (CD). There are several reasons for this: firstly it is difficult to synthesise large quantities of pure protein. In addition, micelle-membrane protein complexes are very large and the helical secondary structure of some membrane proteins can lead to poor spectral dispersal, aggravated by the highly repetitive hydrophobic amino acid sequence (Montaville & Jamin, 2010; Sanders & Sönnichsen, 2006). Finally, the CD has the same activity as full length M2 (Ma *et al.*, 2009) and as such contains the functionally important residues required for conductance, as well as all known resistance polymorphisms.

Recently there has been a move towards the longer CD peptide (Andreas *et al.*, 2015; Sharma *et al.*, 2010), with groups who had previously published TM structures now adopting extended peptides (Wang *et al.*, 2013b; Wu *et al.*, 2014b). This can in part be attributed to improvements in NMR methodologies for membrane proteins. It is becoming more widely accepted that the CD peptide provides a more native-like structure of the tetramer, with numerous groups having also observed binding at the peripheral site (Cady *et al.*, 2010; Schnell & Chou, 2008).

There are several published experimental structures for rimantadine resistant variants such as V27A (Pielak & Chou, 2010) (PDB 2KWX) and S31N (Andreas *et al.*, 2015; Pielak *et al.*, 2009; Wang *et al.*, 2013b) (PDBs 2N70, 2KIH and 2LY0), but none of the published structures use the amino acid sequence of pH1N1 M2. Thus, to identify novel inhibitors of pH1N1 M2, it was necessary to adopt a homology model approach. Homology modelling of proteins relies upon published sequence and structural data, in addition to specialised programs. SWISS-MODEL (Arnold *et al.*, 2006) is one example of an online tool in which a template structure (such as a PDB file) can be used in conjunction with the sequence of a target protein to generate a homology model. This model can then be exported for energy minimisation and compound docking.

The availability of open-access virtual compound libraries, such as those used in this work (Section 2.2.2), enables virtual HTS to be carried out, where tens of thousands of compounds can be docked against a 3D protein structure or model. The ability to gather predicted binding and interaction information, combined with a representative score for each compound, precludes the need to purchase and biologically test such large numbers of compounds. In addition, online resources such as eMolecules are readily accessible and capable of searching databases of millions of commercially available compounds; eMolecules was used to search for chemically and structurally related analogues of query compounds, to aid structure activity relationship (SAR) studies.

This chapter describes and discusses the *in silico* work underpinning the selection of novel M2 targeted compounds for biological testing against M2 peptides *in vitro and* pH1N1 swine ‘flu in culture.

3.2 **Generation of a pH1N1 M2 homology model *in silico***

At the beginning of this work, the only M2 tetramer structure spanning the CD and with a bound ligand (rimantadine) was 2RLF (Schnell & Chou, 2008), shown in Figure 3.1B. This structure was used as a template to generate the pH1N1 (E195) M2 homology model. This structure contains the TM domain and CD residues 23-60 (no coordinates were determined for residues 18-22), for this reason it was possible to investigate the presence of the potential peripheral binding site, alongside the proposed lumenal binding site.

In the region of 23-60, the 2RLF sequence varies from that of A/Udorn/307/1972 (H3N2) (Udorn) at position 50, where a serine is used in place of a cysteine (C50S), this is common in structural studies of influenza M2 (Acharya *et al.*, 2010; Pielak & Chou, 2010; Pielak *et al.*, 2009; Sharma *et al.*, 2010), along with C19S (Pielak *et al.*, 2009; Wang *et al.*, 2013b; Wu *et al.*, 2014b). Replacing these cysteine residues with serines is done to reduce palmitoylation and aid protein refolding when expressed in bacteria.

To generate a homology model, the PDB 2RLF file was downloaded from the PDB website (www.rcsb.org/) and opened in Prime (Schrödinger) software. The published structure 2RLF was obtained with a ligand present; four molecules of rimantadine are bound around the periphery (Figure 1.4). These were removed to form the 2RLF M2 structure seen in Figure 3.1B. This file, lacking the ligands, was used for the generation of the homology model.

The M2 sequence from strain A/England/195/2009 (H1N1) (E195), collected in April 2009, was obtained from the online influenza research database (Genbank Accession number GQ166660). Figure 3.1A shows that there are 7 amino acid substitutions (shown in red) required to change the Udorn sequence used in the 2RLF structure into E195: V28A, S31N, L43T, S50C, F54R, E56K and H57Y. These amino acid substitutions were manually entered for each chain of the tetramer to make the sequence for E195 M2. Following this, it was necessary to refine this model using a process known as minimising. This minimises the energy of the protein using force fields to find the most favourable state. The minimisation process can result in different conformations based on the solvent selected; octanol was selected as it provides a good mimic of the amphipathic environment of the cell membrane (Karle *et al.*, 1998).

The resultant 3D structure is shown in Figure 3.1C, alongside the published 2RLF structure (Figure 3.1B) and an overlaid image of both (Figure 3.1D). There was strong alignment between the two structures, with an alignment score of 0.225 and a root mean square deviation (RMSD) of 2.370 Å. Figure 3.1A highlights four residues in orange that are important for compound binding; residues 31 and 37 form part of the lumenal binding site (Stouffer *et al.*, 2008), whilst residues 41 and 44 are part of the peripheral binding pocket (Schnell & Chou, 2008). The position of these four residues are highlighted in the 2RLF structure and the E195 M2 homology model (Figure 3.2A). In the 2RLF structure residue 31 was a serine, but has been replaced by an asparagine in the homology model, to represent the rimantadine resistant pH1N1 sequence. The

A

2RLF	SDPLVVAASIIGILHLILWILDRLFFKSIYRFFEHGLK
E195	SDPLVIAANIIGILHLILWITDRLFFKCIYRRFKYGLK

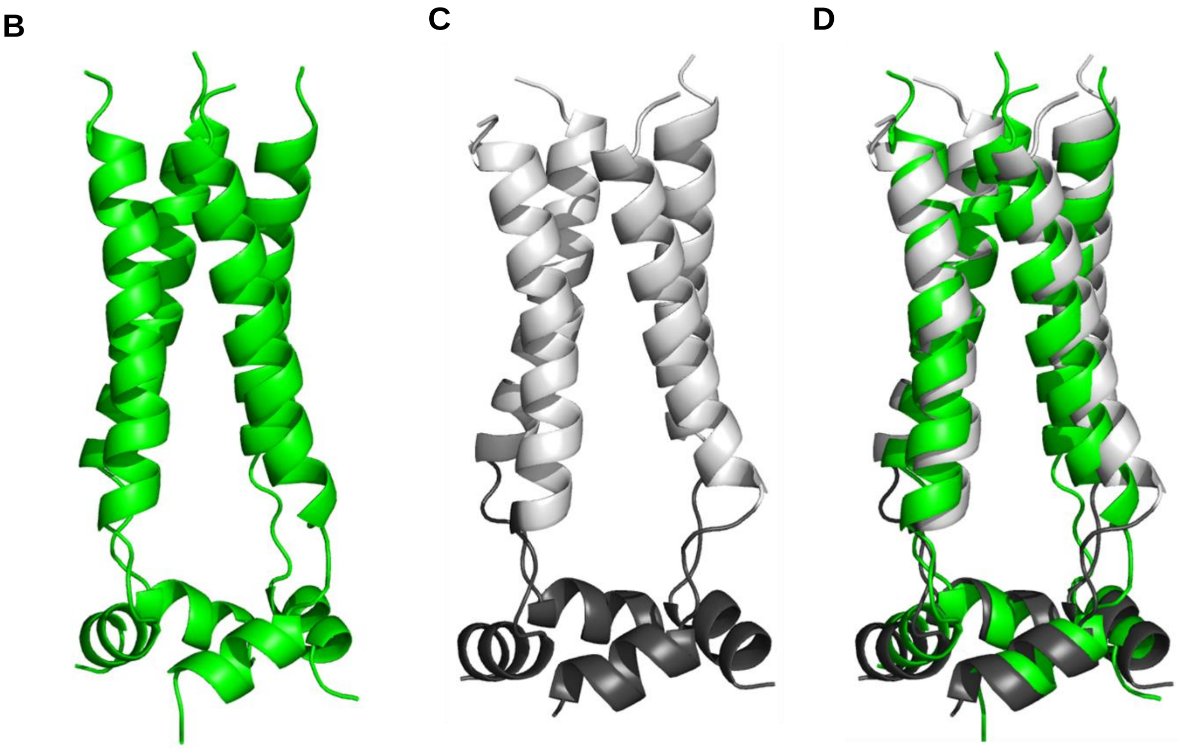

Figure 3.1 Sequence and structure of the conductance domain of M2 from A/Udorn/307/1972 (H3N2) (Udorn, 2RLF) and pH1N1 A/England/195/2009 (H1N1) (E195) M2 homology model.

Structures of conductance domain of M2 from A/Udorn/307/1972 (H3N2) (Udorn, 2RLF) (green) and pH1N1 A/England/195/2009 (H1N1) (E195) (residues 23-46 light grey and 47-60 dark grey). A) Primary structure residues 23-60 of the M2 from of 2RLF and E195, in orange key residues (S31, H37, W41 and D44), in red the seven changes made between 2RLF and the E195 M2 homology model. B and C) Secondary structure depicted using cartoons for α-helices, for 2RLF and E915 M2 homology model, respectively. D) Overlaid structures. Dr Jayakanth Kankanala generated the homology model and Dr Richard Foster overlaid the structures.

CD structure of PDB 2KIH had a S31N mutation (Pielak *et al.*, 2009), however the lack of ligand bound to the tetramer meant this structure was not chosen. Pielak and colleagues report that the N31 mutation perturbs the packing of the helices and, as such, both disrupts the lipid-facing peripheral binding site indirectly and is less stable overall (Pielak *et al.*, 2009).

The backbone structure at position 31 remains unchanged between 2RLF and the E195 M2 homology model and the amide group of asparagine protrudes in similar direction to the hydroxyl group (Figure 3.2A). The carboxyl group of residue D44 of the 2RLF structure was rotated outwards, away from the lumenal space and this angle was maintained in the E195 M2 homology model (Figure 3.2A). It was with residues H37 and W41 where the greatest divergence was seen; these are residues with large ring structures that project into the channel lumen and are known to play a role in proton sensing and gating, respectively (Wang *et al.*, 1995) (Tang *et al.*, 2002). In the 2RLF structure the H37 side chains stick out from the α-helices at an almost perpendicular angle, with the imidazole ring towards the adjacent chain (Figure 3.2B and C). In the case of the histidine residues of the E195 M2 homology model, their position was less consistent between chains, with the imidazole group of the H37 from chain C protruding into the lumenal space more than the others (Figure 3.2B and D). The S31N polymorphism may have implications on the configuration of H37 residues, due to the looser packed helices at the C-terminal of the channel (Pielak *et al.*, 2009). Likewise the indole ring of W41 from the 2RLF structure was angled downwards and sits towards the previous chain and the lumenal space (Figure 3.2B and C). In the E195 M2 homology model the indole rings of chains A and C protruded into the centre of the channel opening (Figure 3.2B and D), narrowing the lumenal diameter at this location.

3.2.1 Defining lumenal and peripheral binding regions

Having generated the E195 M2 homology model based on the 2RLF structure of M2 (Figure 3.1C), “clip files” were generated for each of the two proposed binding sites. These clip files were then used to concentrate compound docking to specific regions of the model. Residues implicated in the binding of amantadine (Stouffer *et al.*, 2008) or rimantadine (Schnell & Chou, 2008) at the lumenal and peripheral binding sites, respectively, were used as the basis for selection of residues for the clip files and depicted in Figure 3.3.

The lumenal binding site concentrated on residues lining the pore, namely residues 27, 30, 31 and 34 (Stouffer *et al.*, 2008) and residue 33 at the N-terminus of CD peptide, with the clip file containing residues from all chains (Chain A: V27, N31 and I33. Chain

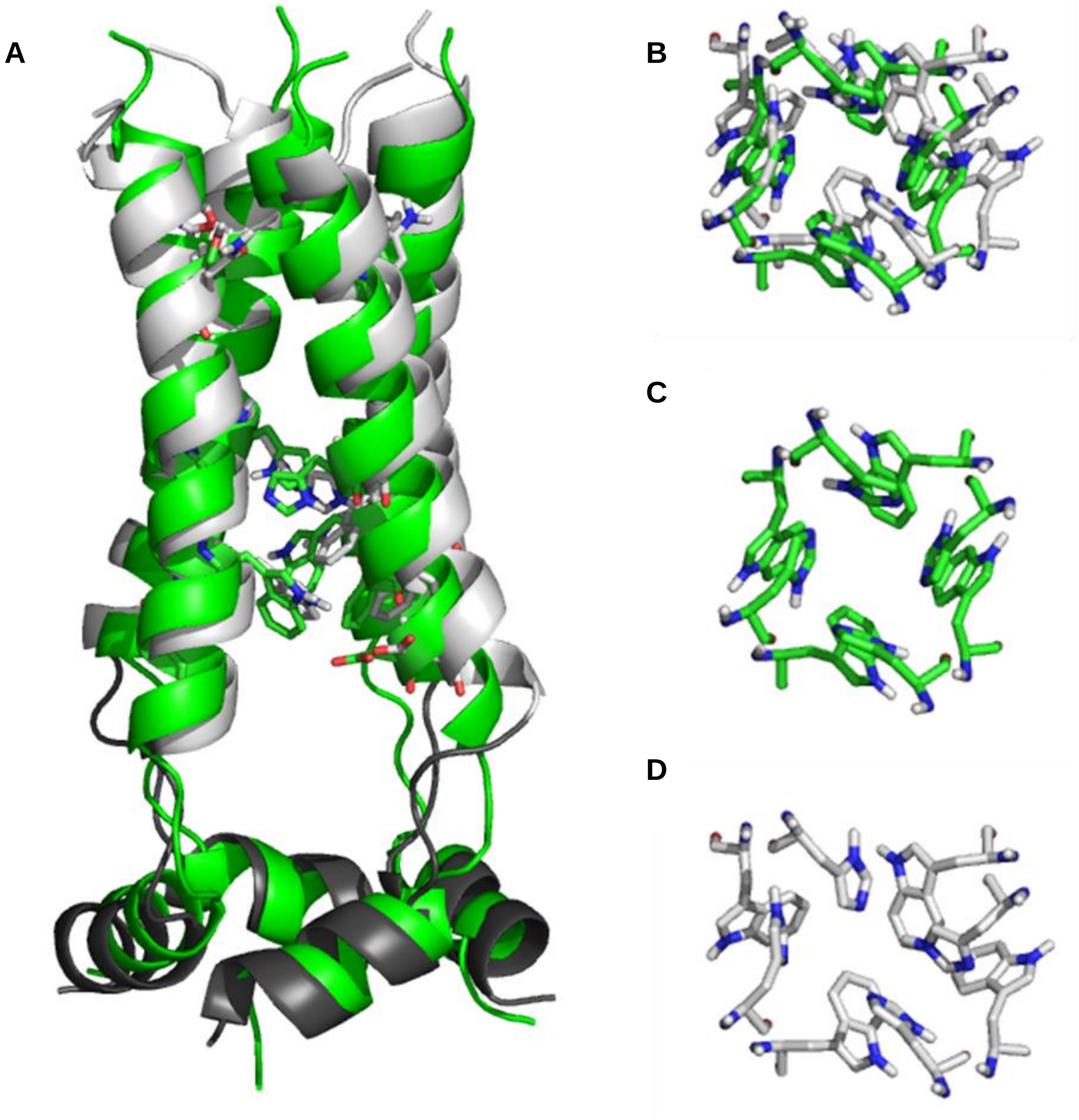

Figure 3.2 Positions of key residues within the conductance domain of M2 from A/Udorn/307/1972 (H3N2) (Udorn, 2RLF) and pH1N1 A/England/195/2009 (H1N1) (E195) M2 homology model.

2RLF (green) and E195 M2 homology model (grey). A) Overlay of 2RLF and E195 M2 conductance domains (residues 23-60) shown as cartoon, with residues 31, 37, 41 and 44 shown as sticks. Top down view of H37 and W41 residues as sticks, B) overlay of 2RLF and E195 M2 homology model, C) 2RLF and D) E195 M2 homology model.

B: V27, A30 and I33. Chain C: V27, A30 and I32. Chain D: V27, N31 and G34). The peripheral site clip file contained only residues from two adjacent chains (Chain A: W41, I42 and R45 and Chain D: I39, L40, W41, T43, D44 and F48), including aa 40-45 found to interact with rimantadine (Schnell & Chou, 2008).

The position of residues that form the two clip files are shown in Figure 3.3A and Figure 3.3B. The lumenal binding site (magenta) side chains were predominantly pore facing (Figure 3.3A and Figure 3.3C), whereas the peripheral site (cyan) side chains bridged between the adjacent chains (Figure 3.3A) and were seen on the external surface of the tetramer (Figure 3.3B). Rotating the tetramer through 90˚ further demonstrated that the residues of the lumenal binding site spanned all four chains and centred around the visible pore (Figure 3.3C), whilst the peripheral binding site was concentrated between two chains (Figure 3.3D).

3.3 *In silico* prediction of the binding preferences for adamantane compounds

Two adamantane compounds M2WJ332 and compound D (Figure 3.4), have previously been shown to target M2 and reduce virus titre in culture. M2WJ332 was identified during a program of testing adamantane analogues against influenza A (Wang *et al.*, 2013b), where it was seen to cause a reduction in titre of an amantadine resistant (N31) strain of IAV (A/WSN/1933 (H1N1)). Compound D was first studied as a potential inhibitor of the p7 viroporin of HCV (Foster *et al.*, 2011), before being shown to have efficacy against pH1N1 E195 (Foster, unpublished). These two compounds were chosen to test the ability of the E195 M2 *in silico* homology model system to distinguish between binding at the two proposed binding sites.

3.3.1 *In silico* docking of adamantane compounds to the E195 M2 homology model

Compound D and M2WJ332 were drawn using the “2D Sketcher” function in Maestro. Each of the two resultant structures was then converted using the ligand preparation “LigPrep” function into a three dimensional (3D) structure, that was energy minimised and which maintained chirality. The LigPrep file containing the 3D structures and the two clip files were then used in eHiTS (SymBioSys Inc.) to predict binding to the E195 M2 homology model. eHiTS docking and scoring software provides a “statistically

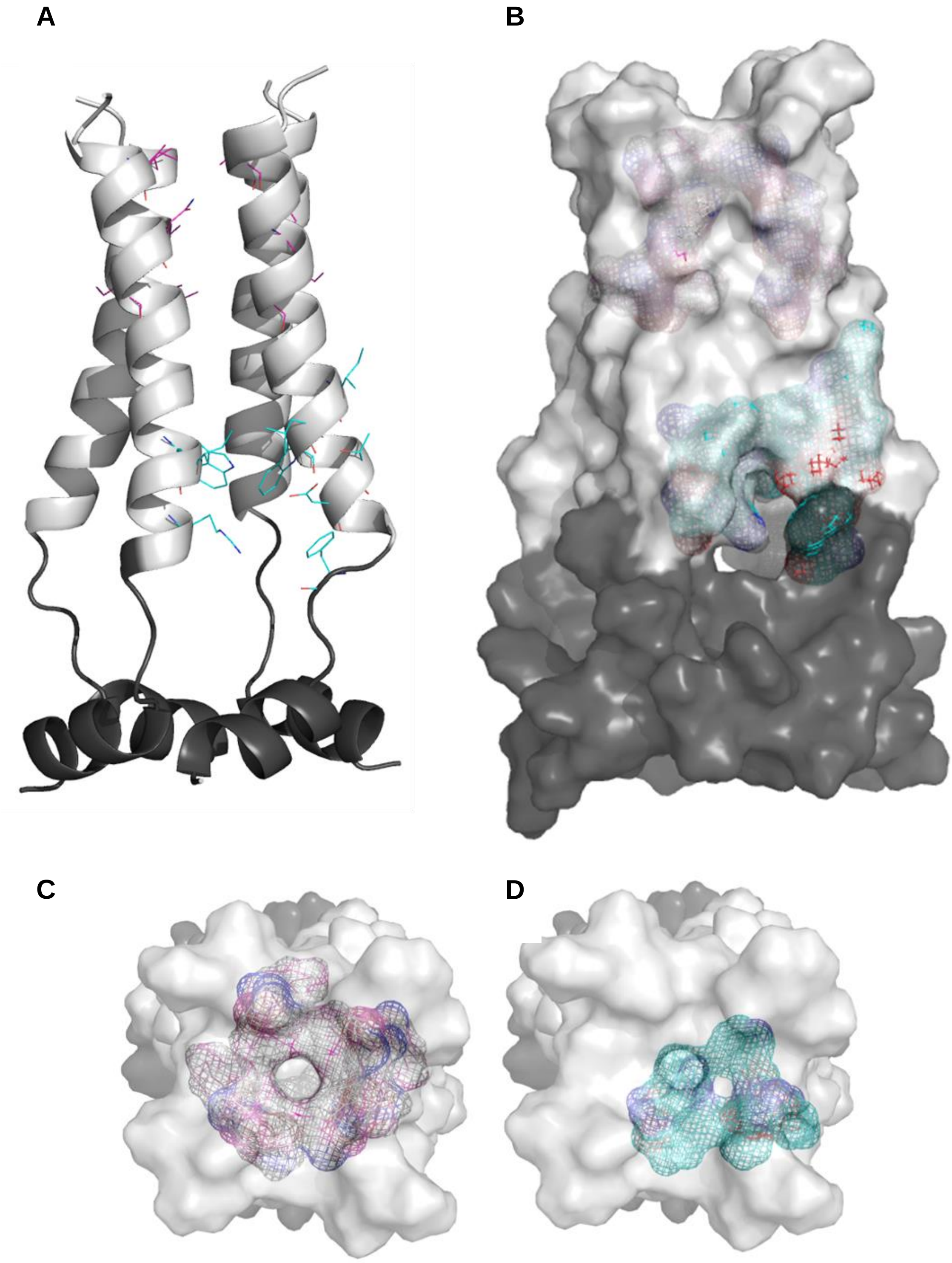

Figure 3.3 Binding sites residues in the E195 M2 homology model.

A) E195 M2 homology model depicted as a cartoon, with binding residues as lines. Transparent surface representations of the homology model, with binding sites shown as mesh B), with aerial views of binding sites C) lumen and D) periphery. Transmembrane residues (23-46) (light grey), additional conductance domain residues (47-60) (dark grey). Lumenal (magenta) and peripheral (cyan) binding site residues are coloured by element.

derived empirical scoring function” (Zsoldos *et al.*, 2006), coined an “eHiTS score”.

Through its novel algorithm eHiTS identifies rotatable bonds within ligands, which it then removes leaving a collection of rigid fragments, for which thousands of poses are generated and scored. The software then rebuilds the compound using different combinations of the fragment poses and the individual scores of each fragment combined to give a score entire ligand (Zsoldos *et al.*, 2006). The eHiTS scores are arbitrary, but can give an indication of a predicted $\log_{10}$ IC_{50} value; scores are negative and the further from zero the more potent the compound is predicted to be, due to a greater number or stronger interactions with the target protein.

3.3.2 Analysis of docking scores and poses of adamantane compounds

M2WJ332 and compound D are both predicted to bind at both of the proposed binding sites (Figure 3.5 and Figure 3.6). eHiTS scores for M2WJ332 were -3.992 and -3.430 for the lumenal and peripheral binding sites, respectively and for compound D they were -3.841 and -2.949. It was not possible to directly compare the eHiTS scores at the two sites and determine if binding at one site was more probable or favourable. The reasons behind this are two-fold; firstly the peripheral binding site is made up of residues from two adjacent amino acid chains, whereas the lumenal binding site can include residues from all four chains. Therefore, compounds may have the ability to bind with a greater number of residues and, as such, improve their score. Secondly, in nature, IAV M2 exists in a membrane, meaning the external portions of the helices of the TM domain are in a hydrophobic environment and some of the additional residues that make up the conductance domain are also likely to be lipid facing. In the E195 M2 homology model, the external environment is octanol and as such compounds binding at the peripheral site are likely to encounter a hydrophobic penalty during the *in silico* docking that would not be present in nature.

Examining the docking poses of the compounds at each site using Pymol software revealed that both bind at the lumenal binding site with the cage-like structure of the adamantane group closest to the N-terminal opening of the channel (Figure 3.5A and Figure 3.6A), as is the case for amantadine in PDB 3C9J (Stouffer *et al.*, 2008), whereas in the published structure of M2WJ323 the cage is deepest within the channel (Wang *et al.*, 2013b). Both compounds formed at least one hydrogen bond with residue N31 at this site (Figure 3.5B and Figure 3.6B). As depicted in Figure 3.5B, M2WJ332 extended beyond N31, towards the N-terminus, with V27 being the most proximal residue to the adamantane group, but no additional polar interactions were predicted using Pymol.

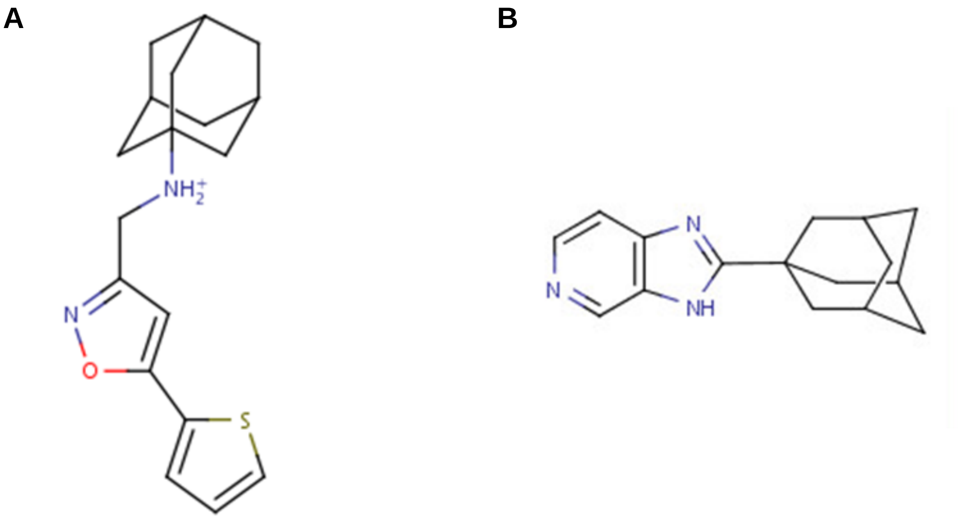

Figure 3.4 Structure of adamantane containing compounds M2WJ332 and compound D.

Shorthand formulas of adamantane containing compounds (A) M2WJ332 ((3S,5S,7S)-N-{[5-(thiophen-2-yl)-1,2-oxazol-3-yl]methyl}tricycle[3.3.1.1~3,7 ~]decan-1-aminium) (Wang et al., 2013b) and (B) compound D (2-(1-adamantyl)-3H-imidazo[4,5-c]pyridine) (Foster et al., 2011), previously reported to target M2 of rimantadine resistant strains of Influenza A viruses (Foster, unpublished; Wang et al., 2013b).

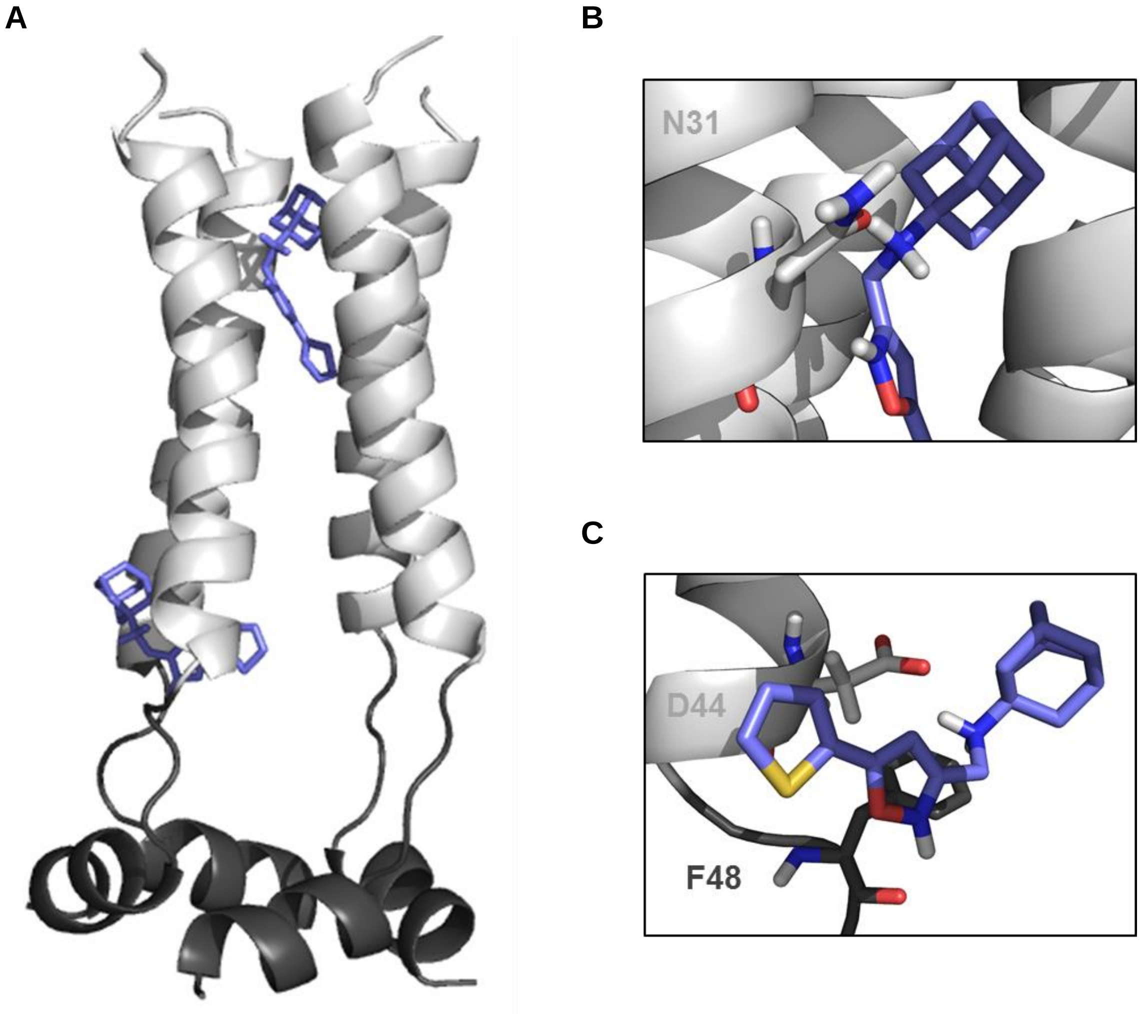

Figure 3.5 ***In silico*** **docking poses of adamantane containing compound M2WJ332 to the E195 M2 homology model based upon the published structure PDB 2RLF.**

A) Adamantane compound M2WJ332 was docked against the E195 M2 homology model and is predicted to bind to both of the proposed binding sites. Hydrogen bonds (yellow dashed lines) between M2WJ332 and the protein or solvent at the B) lumenal and C) peripheral binding site are shown. M2 conductance domain tetramer depicted as cartoons, residues 23-46 (transmembrane) light grey and 47-60 dark grey. M2WJ332 (blue) and labelled amino acids are depicted as sticks.

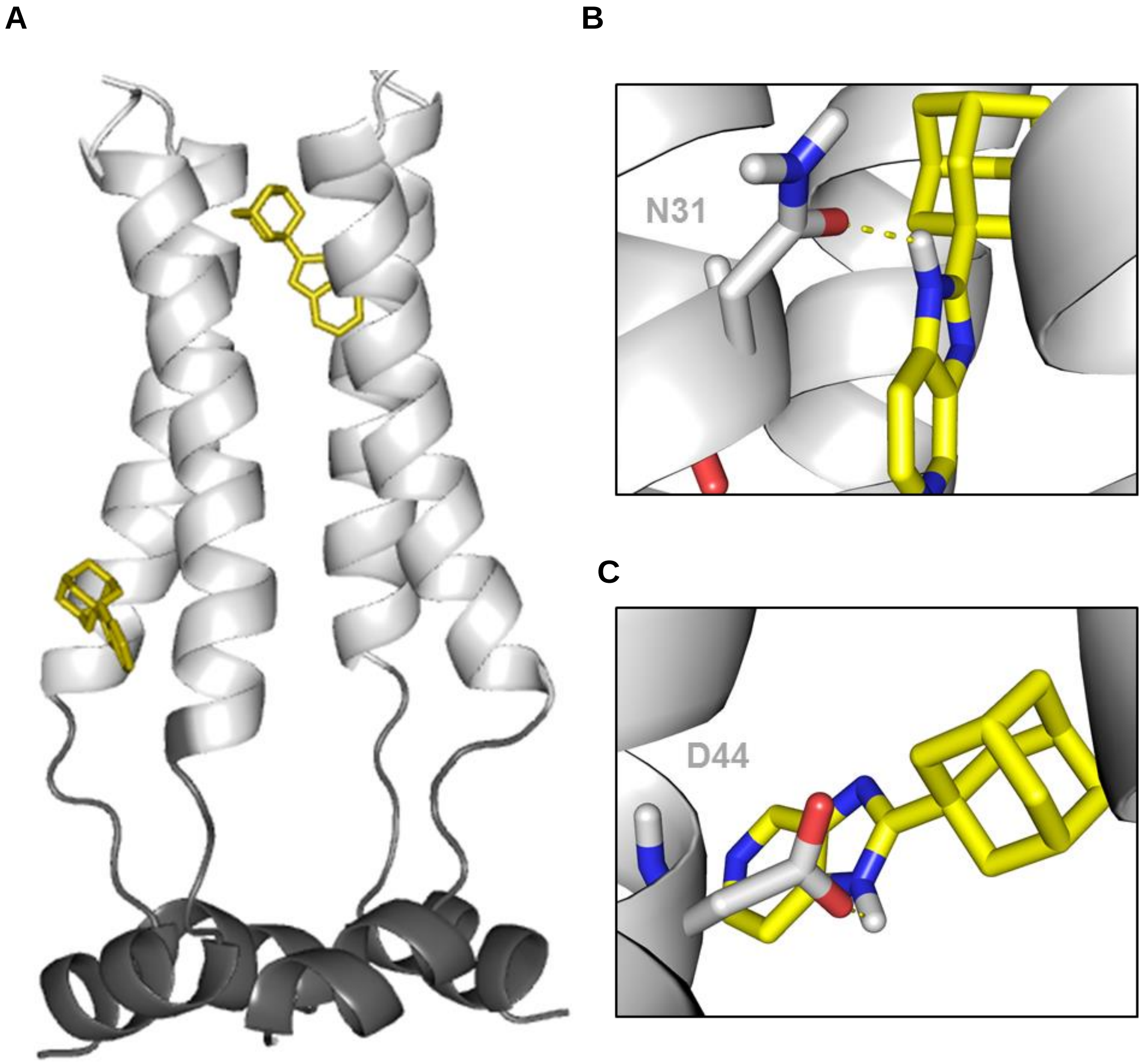

Figure 3.6 *In silico* docking poses of adamantane containing compound D to the E195 M2 homology model based upon the published structure PDB 2RLF.

A) Adamantane containing compound D was docked against the E195 M2 homology model and is predicted to bind to both of the proposed binding sites. Hydrogen bond (yellow dashed lines) between compound D and the B) lumenal and C) peripheral binding site are shown. M2 conductance domain tetramer depicted as cartoons, residues 23-46 (transmembrane) light grey and 47-60 dark grey. Compound D (yellow) and interacting amino acids are depicted as sticks.

At the peripheral binding site only compound D was predicted to make a hydrogen bond to D44 of the protein (Figure 3.6C). M2WJ332 was in close proximity to a D44 residue (Figure 3.5C), but was not predicted to partake in any hydrogen bonding. The entirety of compound D docked around the external portion of the proposed peripheral binding site between the two chains (Figure 3.6A and C). However, M2WJ332 docked between the two chains, with the adamantane cage in a similar locality, but the thiophene (sulphur containing) group extended inwards towards the pore (Figure 3.5A and C). In this instance the homology model was not able to discriminate binding of these adamantane compounds at each site. The common feature between these two compounds is the adamantyl group, essentially a hydrophobic hydrocarbon cage, which was not predicted to partake in any specific polar interaction with the protein (Figure 3.5 and Figure 3.6); it could be for this reason that both compounds were predicted to bind at both sites. If this hydrophobic cage was substituted for a hydrocarbon ring (e.g. with methoxyl or amine groups generating a pharmacophore able to make polar interaction with the protein), then it is hypothesised that the resultant specific interaction may lead to a preference for one site. For this reason it was decided that none of our novel compounds would contain this adamantyl group.

3.4 Unbiased screening for novel compounds targeting the rimantadine resistant M2 ion channel of pH1N1 influenza

Traditionally, searches for inhibitors of rimantadine resistant M2 have focussed on analysing analogues of the licensed adamantane antivirals (Kolocouris *et al.*, 2014; Wang *et al.*, 2013a; Wang *et al.*, 2013b; Wu *et al.*, 2014b). However, one of our strategies was to move away from this class of molecule. Instead, open access small molecule libraries were utilised to provide a wide range of structurally diverse scaffolds.

3.4.1 High throughput docking using eHiTs

An open access small molecule library, ChemBridge Diversity Set, containing over 45,000 compounds was selected for the docking. Using the LigPrep function of Maestro, over 80,000 conformers were generated and subsequently docked against the two clip files defining the lumenal and peripheral binding regions of the E195 M2 homology model (section 3.2.1), using eHiTS software. Each conformer had an eHiTS score generated for each of the two proposed binding sites.

3.4.2 Attrition

It was necessary to cut down the results to a number feasible for *in vitro* testing, via a process of attrition. eHiTS scores were used to rank the results and the top 1000 at each site were taken forward. In addition to eHiTS score, manual analysis of “drug-like” properties including those outlined in the “rules of five” (Lipinski *et al.*, 2012), were taken into account. Finally predicted binding poses were examined and any compounds seen to be present at both sites were eliminated.

As a result of this process a list of compounds that are predicted to bind one site, but not the other was generated. Compounds L1-7 and P1-6 were identified as candidates for further investigation, for the lumenal and peripheral binding sites, respectively. Compound structures, molecular weights (MW) and eHiTS binding scores are detailed in Table 3.1 and Table 3.2.

3.4.3 Specific interactions between unbiased compounds and the E195 M2 ion channel, predicted by eHiTS

PyMol was used to visualise the predicted docking pose of each of the predicted lumenal (Figure 3.7) and peripheral (Figure 3.8) binders and to identify polar contacts (depicted by yellow dashed lines) between the compounds and the protein or surrounding solvent. Residues N31, G34, H37 and L38 at the lumenal binding site and R45, F48 and K39 at the peripheral binding site were seen to make polar contacts.

Predicted lumenal binders were seen to dock into the homology model in proximity to N31 (Figure 3.7). In the majority of cases, they did not extend into the channel further than residue G34, but L6 was shown to interact with residue L38. Predicted lumenal compounds L2, L4 and L6 participated in polar interaction with the lumenal binding site (Figure 3.7), whereas L1, L3, L5 and L7 only made polar contacts to the solvent. The docking of peripheral binders was concentrated in the pocket between R45, F48 and K39 (Figure 3.8). A common feature in P compounds was a “linker”, a linear stretch of atoms linking larger cyclic or aromatic components. The predicted polar interactions of P5 (assessed via PyMol) exclusively involved this linker region and in compounds P1 and P4, polar contacts were found for this linker region and other functional groups (Figure 3.8). Compounds P4 and P6 both contain sulphonamide groups that were involved in polar interactions with R45. Neither P2, nor P3 were predicted to participate in any polar contacts. eHiTS scores take into account many more types of interaction than those identified using PyMol and it was the eHiTS score that had the biggest influence on selection of compounds for subsequent testing in biological experiments.

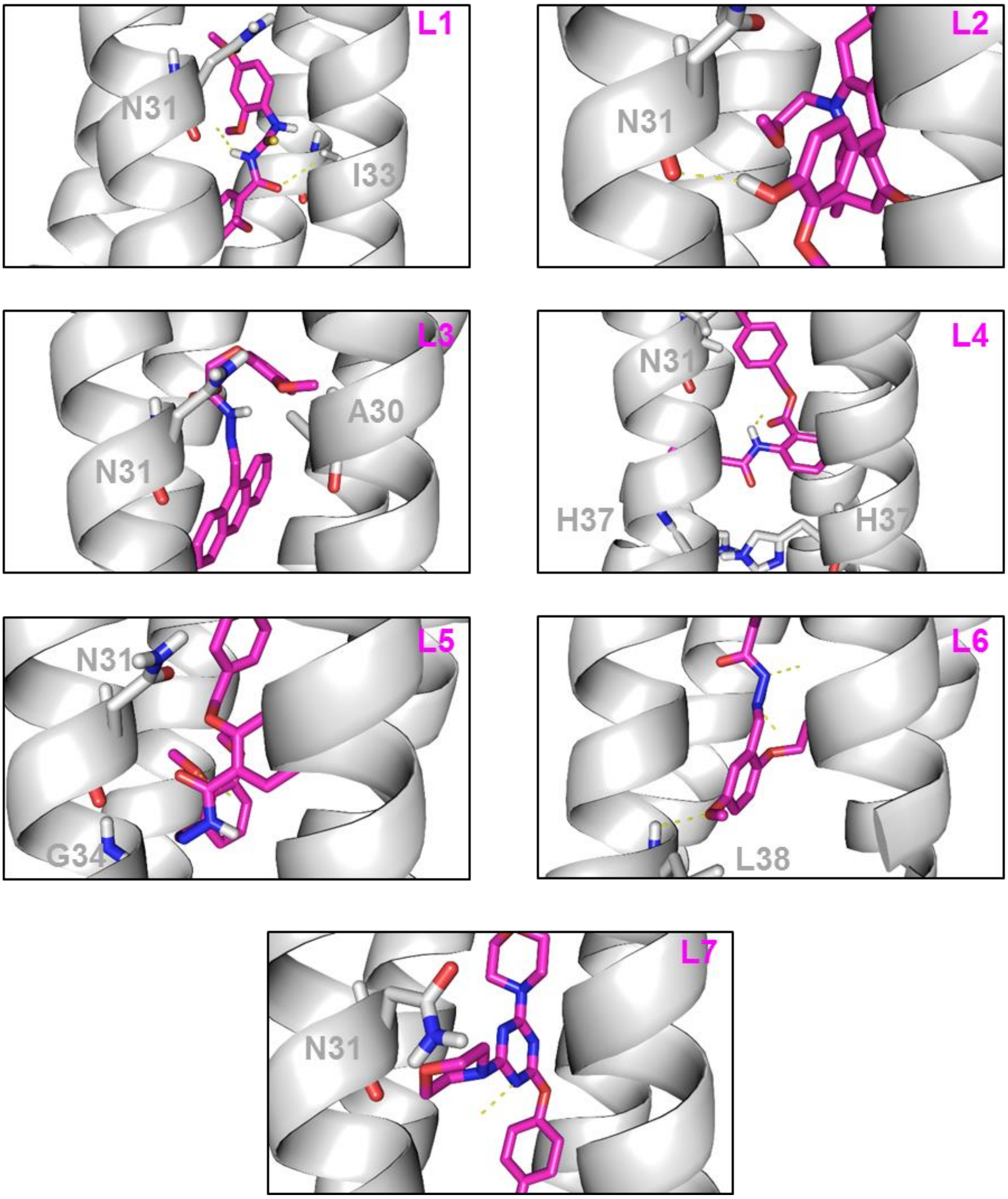
L1
N31
I33
L2
N31
L3
A30
N31
L4
N31
H37
H37
L5
N31
G34
L6
L38
L7
N31

Figure 3.7 Predicted docking pose and polar interactions identified between predicted lumenal binders and the lumenal binding site of the E195 M2 homology model.

Polar contacts (yellow dashed lines) were identified between novel non-adamantane compounds and the M2 tetramer of the E195 M2 homology model and/or the surrounding solvent. Compounds (L1-L7) and residues either shown to participate in polar contacts or in close proximity to the compounds are depicted as sticks and are coloured by element, with only polar hydrogens shown.

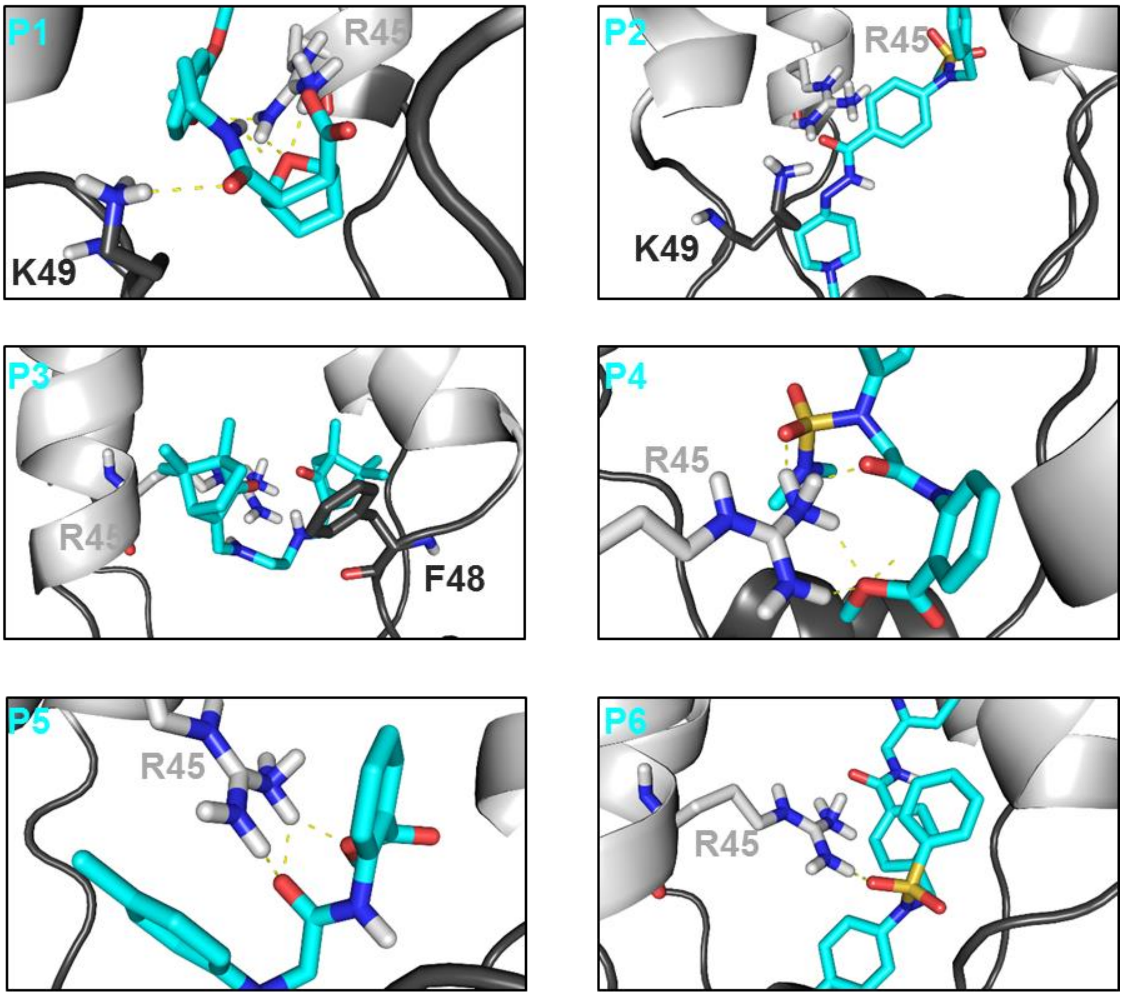

Figure 3.8 Predicted docking pose and polar interactions identified between predicted peripheral binders and the peripheral binding site of the E195 M2 homology model.

Polar contacts (yellow dashed lines) were identified between novel non-adamantane compounds and the M2 tetramer of the E195 M2 homology model. Compounds (P1-P6) and residues either shown to participate in polar contacts or in close proximity to the compounds are depicted as sticks and are coloured by element, with only polar hydrogens shown.

Compound ID	Compound structure	Molecular Weight	eHiTS Score
L1	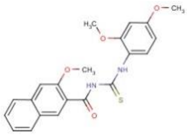	396.468	-5.138
L2	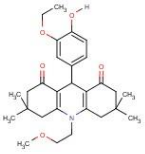	467.606	-4.988
L3	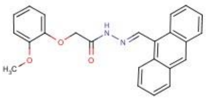	384.435	-4.827
L4	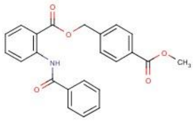	389.407	-5.233
L5	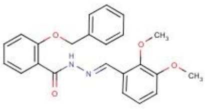	390.439	-5.108
L6	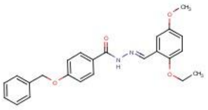	404.466	-4.805
L7	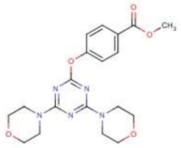	401.423	-4.603

Table 3.1 Predicted lumenal binders.

Details of compound ID, 2D structure, molecular weight (Da) and eHiTS scores for binding at the proposed lumenal binding site of the E195 M2 homology model.

Compound ID	Compound structure	Molecular Weight	eHiTS Score
P1	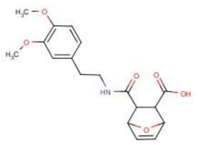	347.371	-4.211
P2	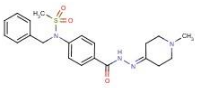	414.530	-4.785
P3	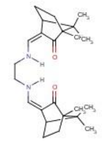	384.567	-5.427
P4	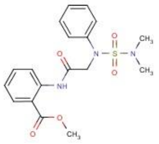	391.450	-4.421
P5	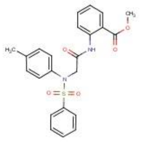	438.506	-4.308
P6	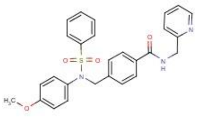	487.582	-4.122

Table 3.2 Predicted peripheral binders.

Details of compound ID, 2D structure, molecular weight (Da) and eHiTS scores for binding at the proposed peripheral binding site of the E195 M2 homology model.

3.5 **Biased compound selection**

In addition to this unbiased compound screen, a biased approach was employed. The premise was that, by limiting a search to compounds with similar molecular shape and volume to a known inhibitor of the M2 channel, we could enrich our screen. Compound D was chosen as the basis of the Rapid Overlay of Chemical Structure (ROCS) (OpenEye Scientific) search. This was due to preliminary data showing effects against pH1N1 'flu (Figure 4.2D) and the lack of a linker. Our *in silico* data showed compound D had the potential to bind to both the lumenal and peripheral binding sites (Figure 3.6), hence theoretically refinements of the structure could be made to allow specific binding at one or other of the sites. The ChemBridge Diversity Set (accessed January 2014) was searched, and the top 1000 results from the library (which did not include any adamantane containing compounds), were docked against the clip files described in section 3.2.1 using eHiTS. The poses were also re-scored using a second docking programme (SPROUT (SimBioSys Inc.) (performed by Dr Katie Simmons).

3.5.1 Compound attrition

A protocol for reducing the number of compounds taken forward for *in vitro* testing was established. This was done individually for the two binding sites. Attrition began by looking for agreement between the docking scores from eHiTS and SPROUT; the difference between the two scores was calculated and the 25 % of compounds with the greatest difference were eliminated. Secondly, an arbitrary cut off for eHiTS score was set at ≤ -4.5 (predicted IC_{50} 10-100 µM), leaving 552 compounds for the peripheral site and 244 at the lumen. At this point, 16 compounds were disregarded from the peripheral list as they had a MW < 225 daltons (Da) and were likely to be of too low a molecular weight to demonstrate selectivity; there were no compounds in the lumenal list with MW < 225 Da.

Compounds were then assessed for non-covalent interactions made with the M2 binding site. A default tolerance of 4 Å was set for interaction distances, adjustments of this distance could result in increased or decreased interactions including:

- Dipole-dipole interactions – weak interactions between polar groups, when the alignment and attraction of the molecules reduces the potential energy.
- Hydrogen bonds – a strong form of dipole-dipole interaction that occurs when a hydrogen atom covalently bonded to a strongly electronegative atom (donor)

such as oxygen, nitrogen or fluorine, is in close range of another electronegative atom with a lone pair of electrons (acceptor).

- Salt bridges – contain a hydrogen bond and an electrostatic interaction, and as such are stronger than hydrogen bonds alone. They occur between two ionised groups, typically involving amino acids arginine, lysine, aspartic acid, glutamic acid or histidine. Protons migrate from a carboxylic acid to an amine.
- π-π stacking – is a non-covalent interaction occurring between two aromatic rings, with p-orbital electrons.
- π-cation interactions – are non-covalent interactions that occur between the face of an electron rich group, such as an aromatic ring or ethylene, and an adjacent cation.

After all interactions were manually noted for each compound, those compounds with fewer than 2 or 3 interactions for the peripheral and lumenal binding site, respectively, were eliminated. This left 360 lumenal and 194 peripheral compounds. Dipole-dipole interactions were only seen at the lumenal binding site. These interactions are weaker than all of the other interactions taken into account. Compounds at the lumenal binding site have the capability of binding to all four chains, as opposed to the peripheral compounds having a maximum of two chains to interact with. For these reasons, there was a requirement for more interactions per compound at the lumenal binding site. In addition, peripheral binding compounds can be subject to a hydrophobic penalty, if exposed to the octanol environment outside of the membrane.

At this stage, compounds which remained on the lists for both binding sites were discounted for further study, as they would not be suitable for investigating preferential binding. The remaining compounds were then assessed for “drug-like” properties, including potential to form covalent bonds to the protein, potential for formation of reactive metabolites and toxicity, those falling short were eliminated from further investigation.

The number of compounds remaining at this stage still exceeded the number desirable to take forward into *in vitro* screening. Hence, compounds for each site were ranked on their eHiTS score divided by molecular weight (eHiTS/MW). Compounds with the high eHiTS/MW are more efficient binders and consequently have a better potential for optimisation to drugs. The top 20 compounds at each site were selected and those that were available were purchased from ChemBridge. Details of nomenclature, MW and docking scores are listed in Table 3.3 and Table 3.4 for predicted lumenal (DL prefix) and peripheral (prefix DP) binding compounds, respectively.

ID	MW	eHiTS Score	SPROUT score	eHiTS/MW
DL1	249.313	-4.694	-5.980	-0.019
DL2	285.346	-5.111	-6.930	-0.018
DL3	285.346	-5.095	-6.520	-0.018
DL4	277.283	-4.782	-5.410	-0.017
DL5	329.79	-5.586	-7.250	-0.017
DL6	296.713	-4.942	-4.900	-0.017
DL7	300.405	-4.982	-6.030	-0.017
DL8	299.377	-4.899	-6.640	-0.016
DL9	292.725	-4.735	-5.980	-0.016
DL10	304.349	-4.848	-6.640	-0.016
DL11	325.795	-5.163	-6.940	-0.016
DL12	296.395	-4.678	-5.350	-0.016
DL13	294.335	-4.591	-5.570	-0.016
DL14	339.181	-5.290	-6.160	-0.016
DL15	332.742	-5.183	-6.760	-0.016
DL16	341.458	-5.301	-6.110	-0.016
DL17	354.409	-5.481	-6.580	-0.015

Table 3.3 DL compound details and binding scores.

Details of novel compounds, with similar structure to compound D, predicted to bind exclusively to the lumenal binding site of the E195 M2 homology model. Compound nomenclature (ID), molecular weight (MW) and their predicted binding scores (eHiTS score and SPROUT score) to the lumenal binding site and eHiTS score divided by MW (eHiTS/MW). Structures of all DL compounds can be found in Appendix Table A.6.

ID	MW	eHiTS Score	SPROUT score	eHiTS/MW
DP1	234.258	-5.179	-5.780	-0.022
DP2	234.262	-5.173	-5.550	-0.022
DP3	238.294	-5.230	-5.200	-0.022
DP4	211.22	-4.583	-4.770	-0.022
DP5	251.353	-5.411	-6.750	-0.022
DP6	215.276	-4.580	-5.210	-0.021
DP7	251.309	-5.345	-5.790	-0.021
DP8	256.305	-5.435	-5.930	-0.021
DP9	235.286	-4.986	-6.500	-0.021
DP10	246.269	-5.159	-6.220	-0.021
DP11	231.258	-4.815	-5.870	-0.021
DP12	271.345	-5.627	-5.720	-0.021
DP13	223.279	-4.623	-5.760	-0.021
DP14	297.401	-6.157	-7.250	-0.021
DP15	236.234	-4.886	-5.240	-0.021
DP16	224.263	-4.610	-5.990	-0.021
DP17	239.234	-4.901	-6.050	-0.020
DP18	224.287	-4.590	-5.710	-0.020
DP19	226.324	-4.598	-6.090	-0.020

Table 3.4 DP compound details and binding scores.

Details of novel compounds, with similar structure to compound D, predicted to bind exclusively to the peripheral binding site of the E195 M2 homology model. Compound nomenclature (ID), molecular weight (MW) and their predicted binding scores (eHiTS score and SPROUT score) to the peripheral binding site and eHiTS score divided by MW (eHiTS/MW). Structures of all DP compounds can be found in Appendix Table A.6.

3.5.2 Analysis of specific interactions between compounds and residues in the M2 tetramer

During the process of attrition (section 3.4.2), a number of interactions between compound and protein were analysed. A summary of the different types of interaction and the residues and chains involved for each of the tested compounds are detailed in Appendix Table A.1 and Table A.2, with binding poses and interactions for DL1, DL3, DL7, DL11, DP9 and DP14 depicted in Figure 3.9, Figure 3.10 and Figure 3.11.

The binding poses of compounds DL1, DL3, DL7, DL11, DP9 and DP14 were visualised in PyMol (Figure 3.9). Identification of polar contacts, using a heuristic technique and default PyMol settings for distance (3.6 Å), predicted the direct polar interaction of DP9, via a hydrogen bond, to residue W41 of the protein. Manual analysis of the eHiTS data also identified this interaction (Figure 3.11). All of the DL compounds were predicted to participate in weak dipole-dipole interactions with the M2 tetramer (Figure 3.10), these were not illustrated in PyMol (Figure 3.9).

The docking poses of DL1 and DL11 showed that they bound near the neck of the channel, with the lower portion of their structures in the locality of N31 (Figure 3.9). Looking at the 2D interaction maps the binding site for DL1 solely and DL11 predominately consisted of N31 residues (Figure 3.10). This was in comparison to DL3 and DL7 that docked further down the channel close to H37 (Figure 3.9) and both compounds participated in π-π interactions with the H37 from chain C (Figure 3.10).

Compounds DP9 and DP14 had similar docking poses that spanned between two adjacent helical chains, below residue W41 (Figure 3.9), with which they both interacted; DP9 via a hydrogen bond and DP14 via π-π interactions (Figure 3.11). Residue W41 was the most N-terminal amino acid within the M2 tetramer that either of these DP compounds interacted with. The most C-terminal residue was also common between DP9 and DP14, with both making π-π interactions with F48. Both compounds also made π-π interactions with R45, in addition DP14 also made a π-cation interaction with this residue (Figure 3.11).

The lumenal binding site consisted of all four chains (Figure 3.10) and polar residues from all chains showed a potential for dipole-dipole interactions with the compound, but π-π interactions and hydrogen bonds were predicted between DL compounds and chain C and D, respectively. DL3 and DL7 (Figure 3.10) interacted with M2 via π-π interactions with H37 from chain C, whilst DL12 interacted with the N31 residue of chain D via a hydrogen bond (Appendix Table A.1).

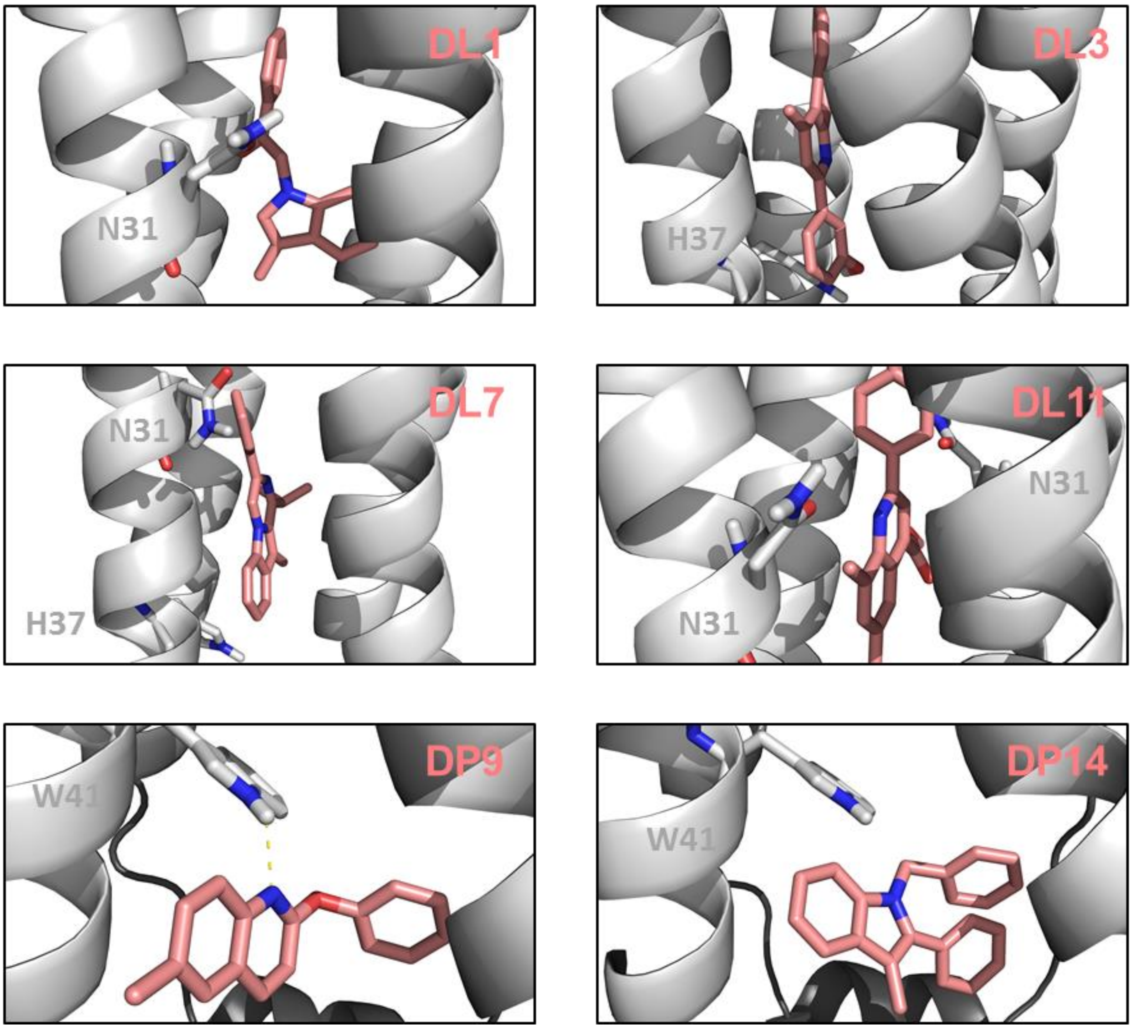
DL1
N31
DL3
H37
N31
DL7
H37
DL11
N31
N31
W41
DP9
W41
DP14

Figure 3.9 *In silico d*ocking poses of biased compounds in the E195 M2 tetramer homology model.

Docking poses of predicted lumenal binders DL1, DL3, DL7 and DP11 and peripheral binders DP9 and DP14, with polar contacts shown (yellow dashed lines). 3D structures of compounds are shown as sticks (salmon) and the M2 tetramer as a cartoon (grey) with selected residues represented as sticks, stick representations are coloured by element.

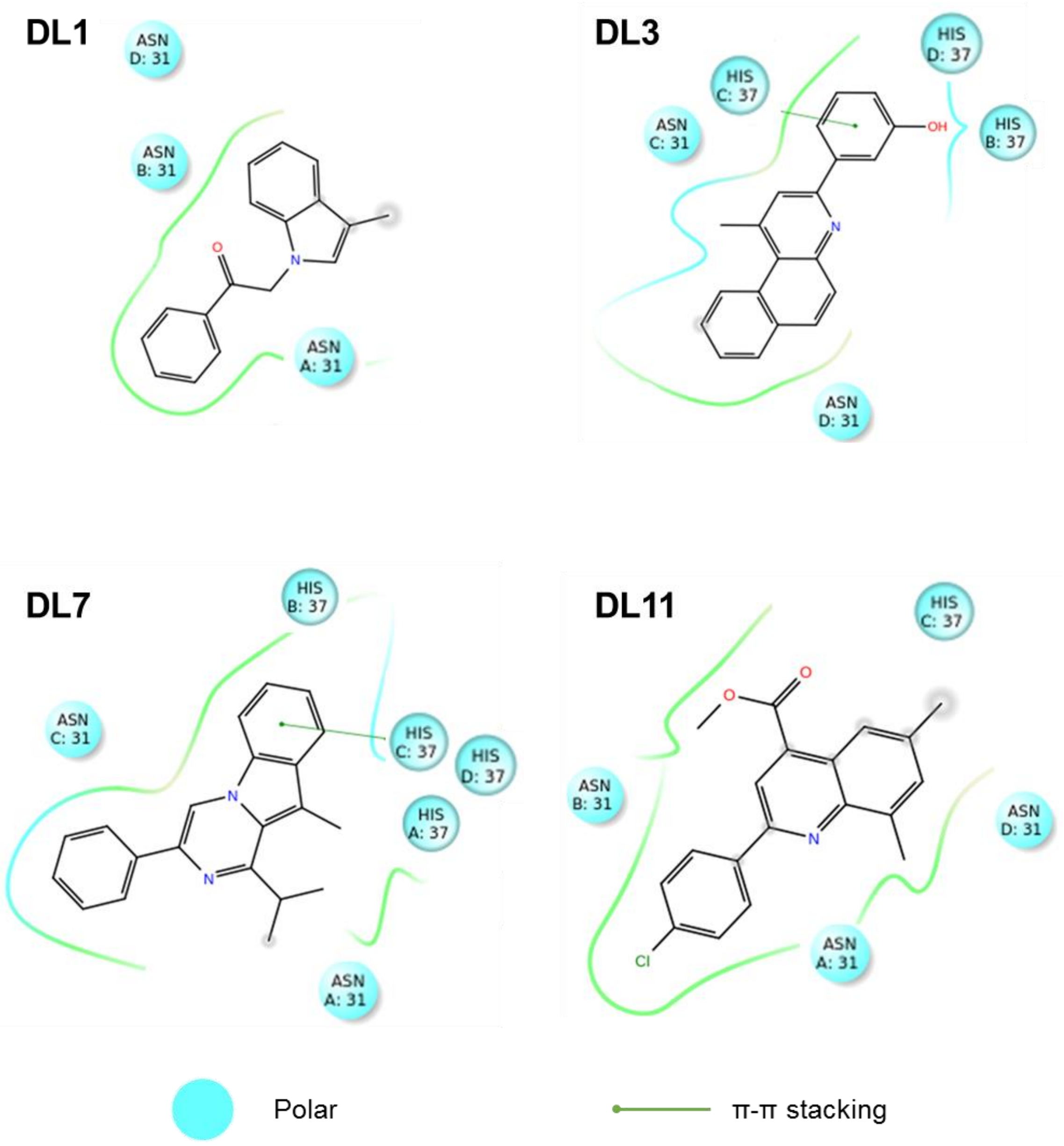
DL1
ASN D: 31
ASN B: 31
O
N
ASN A: 31
DL3
HIS D: 37
HIS C: 37
ASN C: 31
OH
HIS B: 37
N
ASN D: 31
DL7
HIS B: 37
ASN C: 31
HIS C: 37
HIS D: 37
N
HIS A: 37
N
ASN A: 31
DL11
HIS C: 37
O
O
ASN B: 31
N
ASN D: 31
Cl
ASN A: 31
Polar
π-π stacking

Figure 3.10 Predicted interactions between DL compounds and the lumenal binding site of the E195 M2 homology model.

2D structures of DL1, DL3, DL7 and DL11 and the polar residues (blue circles) of the M2 tetramer they interact with are shown. π-π interactions (green lines) to the M2 tetramer are highlighted. Residues are labelled with the three letter code, chain and residue number.

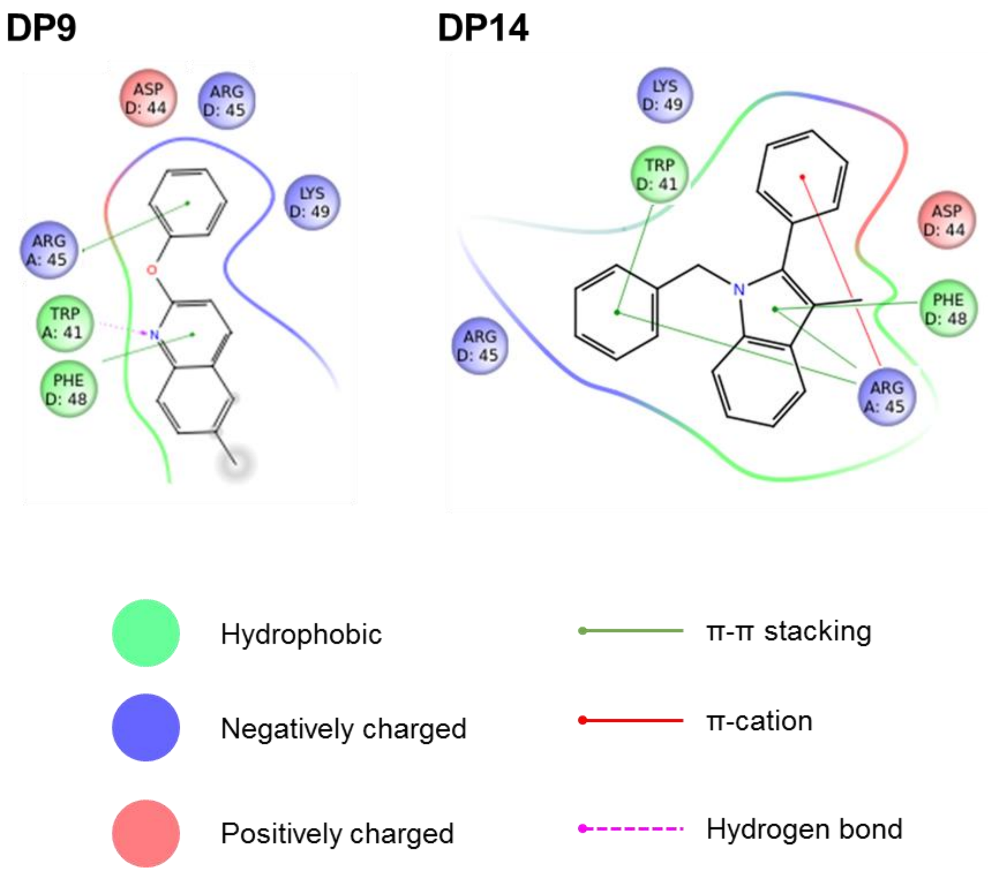
DP9
ASP D: 44
ARG D: 45
LYS D: 49
ARG A: 45
TRP A: 41
PHE D: 48
O
N
DP14
LYS D: 49
TRP D: 41
ASP D: 44
PHE D: 48
ARG D: 45
ARG A: 45
N
Hydrophobic
Negatively charged
Positively charged
π-π stacking
π-cation
Hydrogen bond

Figure 3.11 Predicted interactions between DP compounds and the peripheral binding site of the E195 M2 homology model.

2D structures of DP9 and DP14 and residues (circles) of the M2 tetramer they interact with are shown. π-π stacking (green lines), π-cation (red lines) and hydrogen bond (dashed magenta lines) interactions are highlighted. Amino acids involved in interactions with compounds are coloured as being either hydrophobic (lime green), negatively (blue) or positively charged (red), they are labelled with the three letter code, chain and residue number.

At the peripheral binding site there were only two chains that made up the binding site (Chains A and D). However, a wider number of residues were predicted to be involved in interactions, W41, D44, R45 and F48, compared to only N31 and H37 at the lumenal binding site. As seen for DL compounds at the lumenal binding site, π-π interactions and hydrogen bonds were identified for DP compounds, but additional π-cation interactions and salt bridges were predicted. π-cation interactions were the most common form of interaction predicted between DP compounds and the peripheral binding site, with only DP8 and DP9 not predicted to interact using them (Figure 3.11). Salt bridges were only predicted to involve residue D44 from chain D and hydrogen bonds to either residue W41 or R45 on chain A.

3.6 Analogues of first generation compounds

To investigate SAR for compounds L1, L4 and P6 an online search for analogues of was carried out using eMolecules software. Individually the 2D structures of each compound was constructed in the software, then a search carried out to identify similar compounds; each resultant structure was given a similarity score of between 0.8 and 1.0, with 1.0 being identical to the input structure. In addition to this, details of suppliers and product codes were listed.

Each parental compound returned numerous analogues. These were narrowed down by exclusively concentrating on compounds available from ChemBridge, the source of the compounds we had purchased previously. In cases where greater than four analogues were identified, Lipinski’s “rule of five” (Lipinski *et al.*, 2012) and other analysis of “drug-like” qualities, were used to decide upon which to take forward. Analogues of L1 are denoted L1.1 – L1.4 and the same nomenclature are used for L4 and P6 analogues.

3.6.1 Prediction of ligand-protein binding modes using eHiTS

In the original, unbiased *in silico* eHiTS screen (Section 3.4.1), all of the tens of thousands of compounds were docked against both the lumenal and peripheral binding sites. During the attrition process compounds present in the top 1000 (ranked by eHiTS score) for both sites were eliminated. The aim was to identify novel compounds with a specific preference for one site, before assessing their activity against the M2 peptide and E195 virus. As a result of this attrition L1 and L4 were predicted to bind in the lumenal binding site of the E195 M2 homology model and P6 at the peripheral binding site.

Likewise, analogues of unbiased compounds were docked against both sites. However, in contrast to the original, unbiased screen, the docking poses and eHiTS scores for analogues were analysed at both sites (Table 3.5). This was done in order to assess whether changes in chemical structure between analogues affects interactions or binding poses at a particular site, potentially altering the binding specificity. As discussed previously (section 3.3.2), as eHiTS scores cannot be directly compared between sites, it is not possible to determine the preferred binding site of an individual compounds from the docking scores. However, binding site preferences were to be tested experimentally and correlated back to the *in silico* docking scores and poses.

3.6.2 Analysis of predicted docking poses and interactions of L1, L4 and P6 analogues with the lumenal binding site of the E195 M2 homology model

No hydrogen bonds were shown in the docking pose of L1 in the lumenal binding site of the E195 M2 homology model (Figure 3.7). This was also the case for all four of its analogues (Figure 3.12B), for which polar contacts only with solvent were observed using PyMol. The 2D interaction maps also showed a lack of hydrogen bonds between L1 analogues and the tetramer (Figure 3.12). Analogue compounds L1.1 and L1.2 retain the napthyl ring seen in L1 and only differ by the removal of one or other of the methoxy groups at the other end of the molecule. However, the predicted binding poses varied greatly. Like L1, L1.2 still had the napthyl ring further down the channel towards H37, whereas L1.1 had the napthyl ring towards the neck of the channel, in proximity to N31 (Figure 3.12). The orientation of L1.3 had the sulphur atom above the adjacent aromatic ring (Figure 3.12B), as opposed to L1 where it was underneath (Figure 3.7). For L1.4 the molecule was inverted with the aromatic with two methoxy groups now deeper in the channel (Figure 3.12B) than the sulphur atom.

Compound L4 docked into the lumen with its ester group closest to the neck of the channel (Figure 3.7), whilst L4.3, which lacks the aromatic ring with an ester group, docked even closer to the neck of the channel. The two aromatic rings of L4.3 were sat vertically in the channel (Figure 3.13B), whereas for L4 these ring were essentially in the same horizontal plane. Neither L4, nor L4.3 was predicted to make any hydrogen bonds with the lumenal binding site (Figure 3.13). L4.4 only lacks this ester group, not the aromatic ring and was seen in PyMol to form direct interactions to the N31 residue

Compound ID	CB ID	eHiTS score	
		Lumen	Periphery
L1.1	6607593	-3.682	-3.113
L1.2	6598617	-3.152	-3.112
L1.3	6945470	-2.797	-2.784
L1.4	7642465	-3.519	-2.707
L4.1	6302982	-3.615	-3.958
L4.2	7999011	-3.942	-3.400
L4.3	5128188	-4.033	-3.333
L4.4	7749703	-3.038	-3.483
P6.1	6479640	-4.919	-4.900
P6.2	6470103	-3.275	-4.542
P6.3	5732197	-4.546	-4.097
P6.4	5861836	-1.803	-3.551

Table 3.5 Docking analysis at the lumen and periphery of the E195 M2 homology model, of L1, L4 and P6 analogues.

Four analogues each of L1, L4 and P6 were docked against the proposed lumenal and peripheral binding sites of the E195 M2 homology model, using eHiTS software. eHiTS scores for both lumenal and peripheral binding sites are listed alongside compound nomenclature.

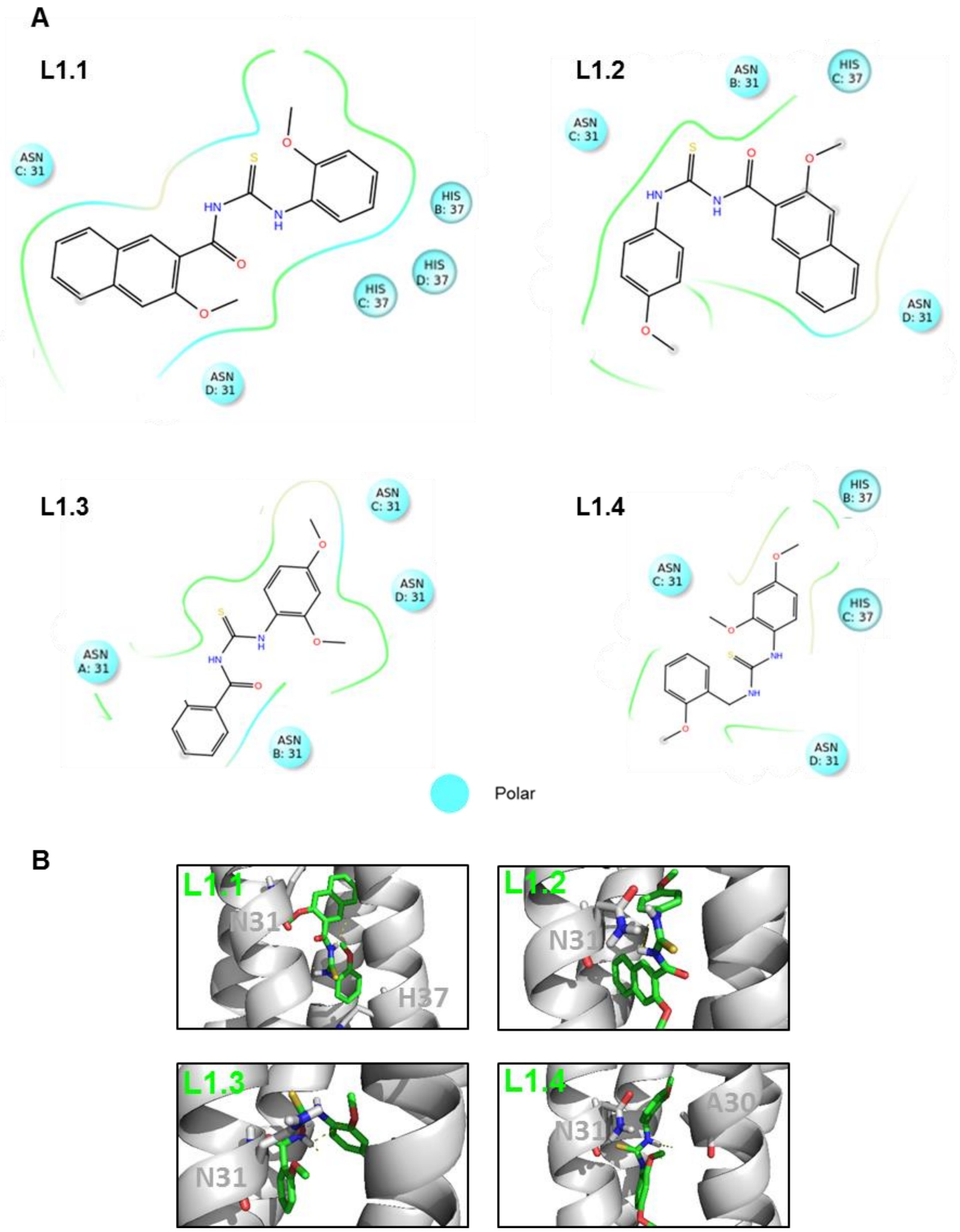
A
L1.1
ASN C: 31
HIS B: 37
HIS D: 37
HIS C: 37
ASN D: 31
L1.2
ASN B: 31
HIS C: 37
ASN C: 31
ASN D: 31
L1.3
ASN C: 31
ASN D: 31
ASN A: 31
ASN B: 31
L1.4
HIS B: 37
ASN C: 31
HIS C: 37
ASN D: 31
Polar
B
L1.1
N31
H37
L1.2
N31
L1.3
N31
L1.4
N31
A30

Figure 3.12 Predicted interactions between analogues of L1 and the lumenal binding site of the E195 M2 homology model.

A) 2D structures of L1.1, L1.2, L1.3 and L1.4 and the residues (circles) of the M2 tetramer they interact with are shown. Polar interactions (to cyan circled residues). Residues are labelled with the three letter code, chain and residue number. B) Docking poses of compounds L1.1-4 (green) within the lumenal binding site of M2 (grey). Selected residues represented as sticks, stick representations are coloured by element and polar contacts (yellow dashed lines) to the protein or solvent highlighted.

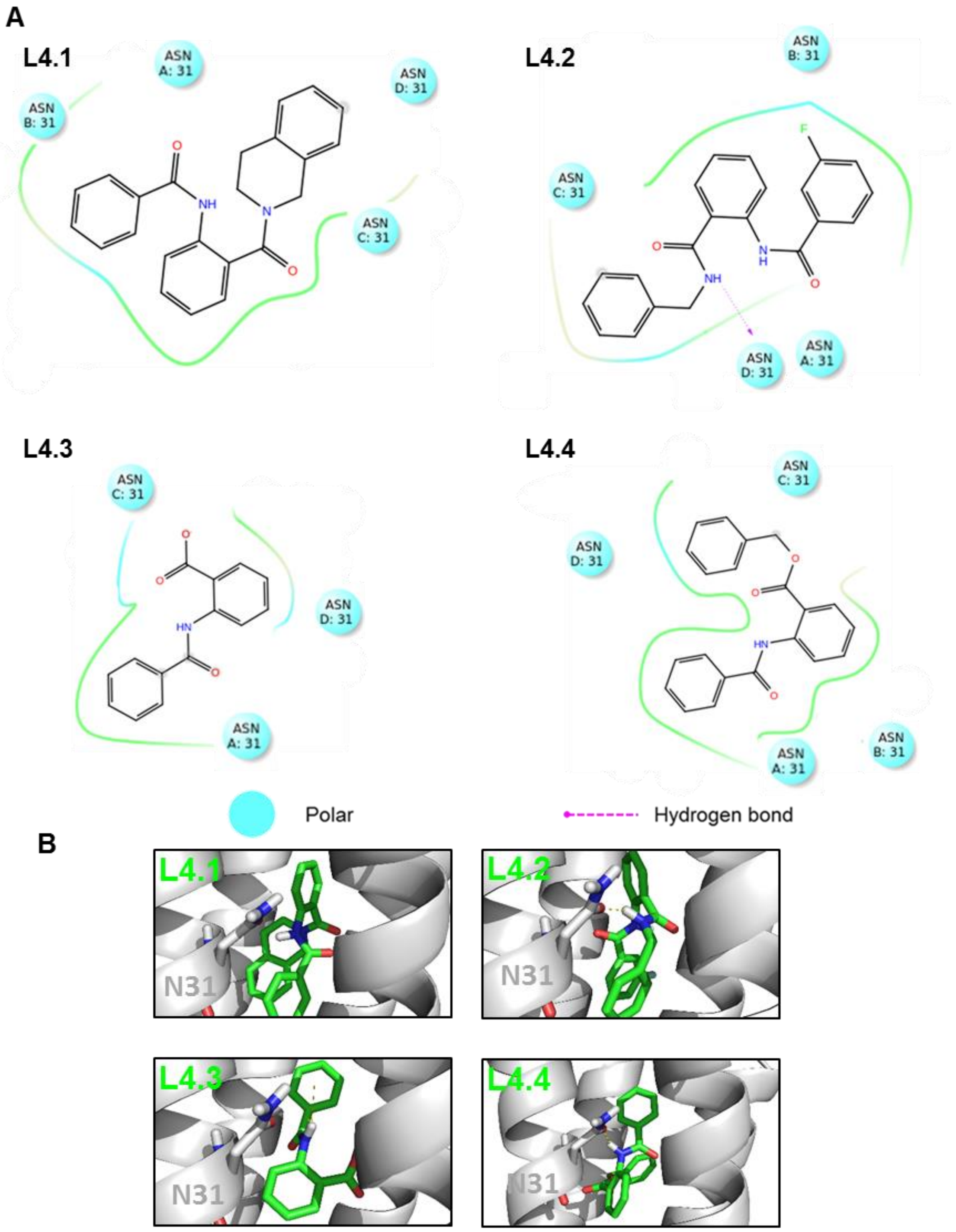
A
L4.1
ASN A: 31
ASN D: 31
ASN B: 31
ASN C: 31
L4.2
ASN B: 31
ASN C: 31
ASN D: 31
ASN A: 31
L4.3
ASN C: 31
ASN D: 31
ASN A: 31
L4.4
ASN C: 31
ASN D: 31
ASN A: 31
ASN B: 31
Polar
Hydrogen bond
B
L4.1
N31
L4.2
N31
L4.3
N31
L4.4
N31

Figure 3.13 Predicted interactions between analogues of L4 and the lumenal binding site of the E195 M2 homology model.

A) 2D structures of L4.1, L4.2, L4.3 and L4.4 and the residues (circles) of the M2 tetramer they interact with are shown. Polar interactions (to cyan circled residues). Residues are labelled with the three letter code, chain and residue number. B) Docking poses of compounds L4.1-4 (green) within the lumenal binding site of M2 (grey). Selected residues represented as sticks, stick representations are coloured by element and polar contacts (yellow dashed lines) to the protein or solvent highlighted.

of chain D (Figure 3.13B). Despite its structural similarity to L4, the binding pose of this compound also varied greatly from that observed for L4. The aromatic ring was still in proximity to N31 residues, but the other end of the molecule was docked higher in the channel close to residue V27 (Figure 3.13B), as opposed to between I33 and H37 as it was for L4 (Figure 3.7). The central aromatic group of L4 was found in the region of residue G34 in the lumenal binding site. For compound L4.1 this aromatic group was the portion of the molecule closest to the neck of the channel at V27 (Figure 3.13B). Of the four L4 analogues, L4.2 was the only one that is predicted to form a hydrogen bond to the lumenal binding site of M2, interacting directly with N31 (Figure 3.13).

There was no data supporting that P6 docked in the lumenal binding site, as it did not feature in the top 1000 eHiTS scores for that site, during the original screening. However, it was possible to establish likely docking poses for its analogues at this site. Analogues P6.3 and P6.4 were predicted to form specific π-π interactions with H37 in the lumenal binding site (Figure 3.14A), with P6.3 seen to also have polar contacts with I35 (Figure 3.14B). In the case of P6.4, it was the aromatic group attached to the sulphur atom that participated in the π-π interaction, yet this was not the case for P6.3 (Figure 3.14A). On the other hand, P6.1 and P6.2 were only predicted to make weak dipole-dipole interactions with residues N31 and H37 of E195 M2 (Figure 3.14).

3.6.3 Analysis of predicted docking poses and interactions of L1, L4 and P6 analogues with the peripheral binding site of the E195 M2 homology model

Despite L1 not being predicted to bind at the peripheral binding site, all of the L1 analogues were predicted to make polar contacts with D44 (Figure 3.15B) at the peripheral binding site, using PyMol. In addition L1.1 was predicted to directly interact with R45. The 2D interactions map did not predict L1.3 interacting with the peripheral binding site by strong polar interactions (Figure 3.15A), contrary to what PyMol predicted (Figure 3.15B).The predicted polar interactions seen in the docking pose of L1.1 were seen to be hydrogen bonds to residues D44 and R45 (Figure 3.15A). The 2D interaction map of L1.1 showed it also made π-π stacking and π-cation interactions to residue R45 (Figure 3.15A). Analogue L1.2 also interacted with the protein by π-π stacking and π-cation interactions with R45, as well as π-π stacking to F48 and a hydrogen bond to W41 of chain A (Figure 3.15), not to D44 as predicted in the docking pose (Figure 3.15B). Focussing on the 2D interaction map, L1.4 was predicted to interact with F48 from chain D via π-π stacking interactions (Figure 3.15) and to D44 via a hydrogen bond, as highlighted in the docking pose (Figure 3.15B).

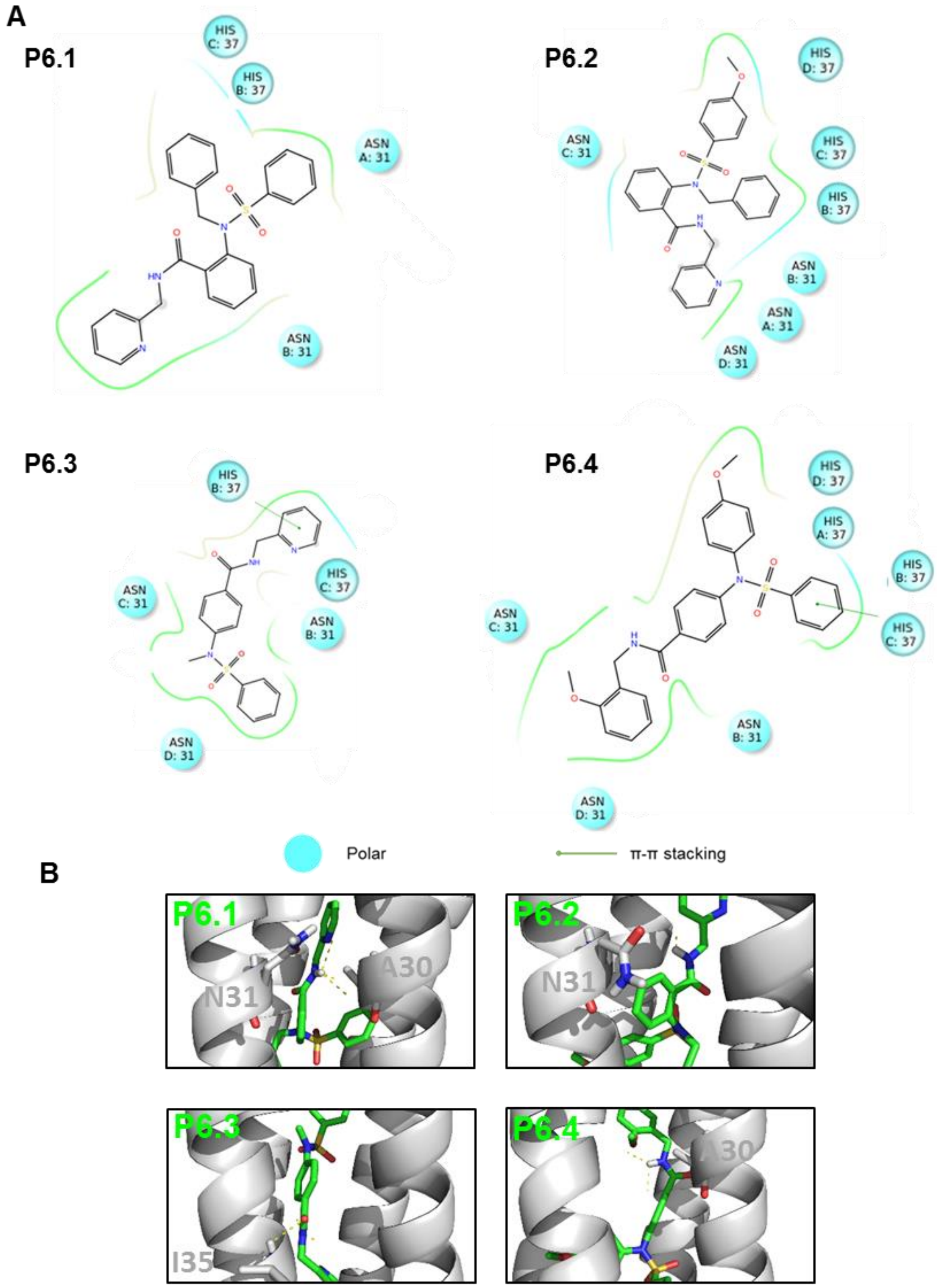
A
P6.1
HIS C: 37
HIS B: 37
ASN A: 31
ASN B: 31
P6.2
HIS D: 37
ASN C: 31
HIS C: 37
HIS B: 37
ASN B: 31
ASN A: 31
ASN D: 31
P6.3
HIS B: 37
ASN C: 31
HIS C: 37
ASN B: 31
ASN D: 31
P6.4
HIS D: 37
HIS A: 37
HIS B: 37
HIS C: 37
ASN C: 31
ASN B: 31
ASN D: 31
Polar
π-π stacking
B
P6.1
N31
A30
P6.2
N31
P6.3
I35
P6.4
A30

Figure 3.14 Predicted interactions between analogues of P6 and the lumenal binding site of the E195 M2 homology model.

A) 2D structures of P6.1, P6.2, L4.3 and P6.4 and the residues (circles) of the M2 tetramer they interact with are shown. Polar interactions (to cyan circled residues). Residues are labelled with the three letter code, chain and residue number. B) Docking poses of compounds P6.1-4 (green) within the lumenal binding site of M2 (grey). Selected residues represented as sticks, stick representations are coloured by element and polar contacts (yellow dashed lines) to the protein or solvent highlighted.

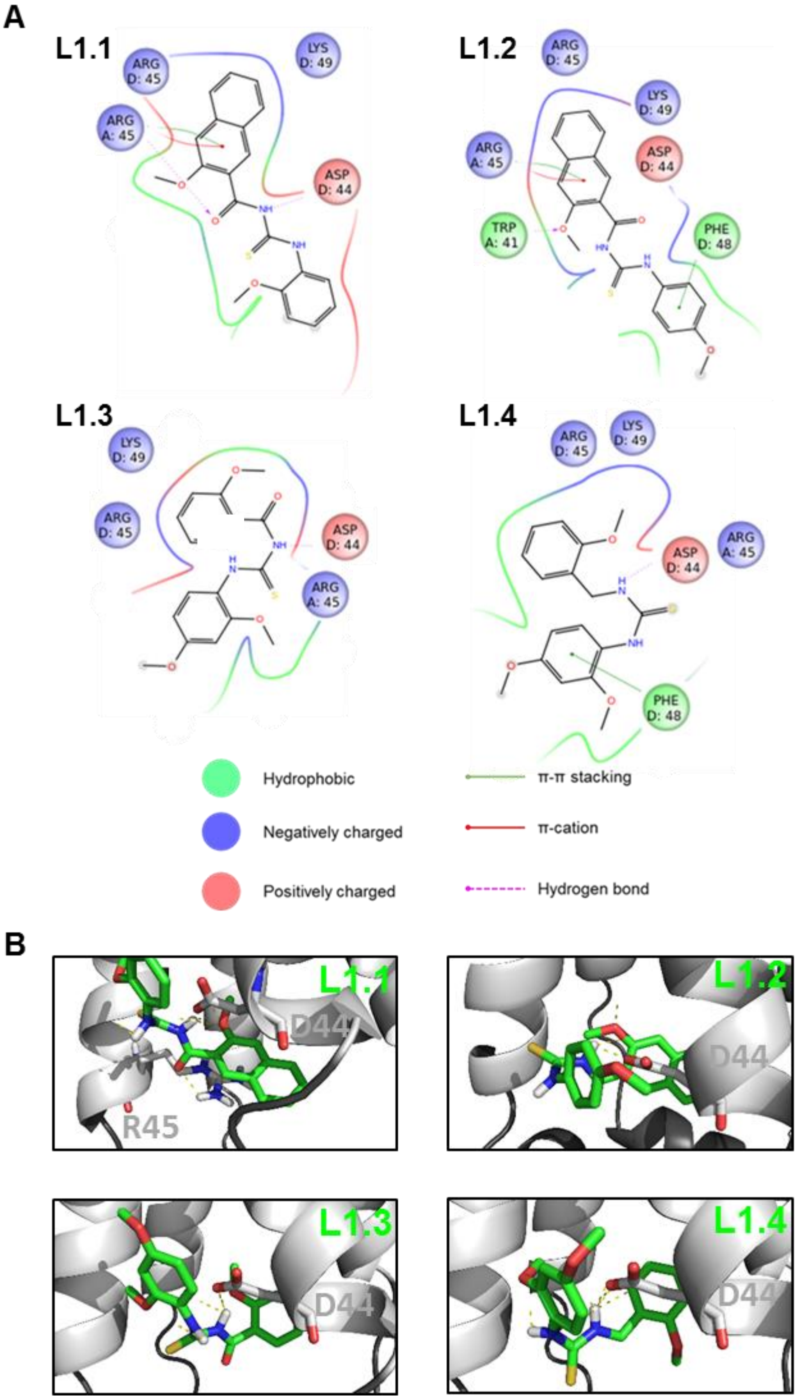
A
L1.1
ARG D: 45
LYS D: 49
ARG A: 45
ASP D: 44
L1.2
ARG D: 45
LYS D: 49
ARG A: 45
ASP D: 44
TRP A: 41
PHE D: 48
L1.3
LYS D: 49
ARG D: 45
ASP D: 44
ARG A: 45
L1.4
ARG D: 45
LYS D: 49
ARG A: 45
ASP D: 44
PHE D: 48
Hydrophobic
Negatively charged
Positively charged
π-π stacking
π-cation
Hydrogen bond
B
L1.1
D44
R45
L1.2
D44
L1.3
D44
L1.4
D44

Figure 3.15 Predicted interactions between analogues of L1 and the peripheral binding site of the E195 M2 homology model.

A) 2D structures of L1.1, L1.2, L1.3 and L1.4 and the residues (circles) of the M2 tetramer they interact with are shown (hydrophobic - lime green, negatively - blue or positively charged - red). π-π stacking (green lines), π-cation (red lines) and hydrogen bond (dashed magenta lines) interactions are highlighted. B) Docking poses of compounds L1.1-4 (green) within the peripheral binding site of M2 (grey). Selected residues represented as sticks, stick representations are coloured by element and polar contacts (yellow dashed lines) to the protein or solvent highlighted.

Analogue L4.1 was predicted to form a single π-cation interaction with R45 (Figure 3.16A), this was compared to all other L4 analogues which were predicted to partake in at least four direct interactions with the peripheral binding site. The binding pose of L4.1 indicated two polar contacts to the peripheral binding site, to W41 and D44 (Figure 3.16B), neither were predicted in the 2D interaction map (Figure 3.16A). Residue D44 was not involved in the polar interactions predicted in the 2D map of L4.2. Instead, residues R45 and F48 each interacted with the L4.2 via a π-π stacking interaction and R45 also by two π-cation interactions (Figure 3.16A). Analogue L4.3 was predicted to interact with three residues of the peripheral binding site; D44 via a hydrogen bond as predicted in the docking pose (Figure 3.16B), W41 via π-π stacking and R45 via a π-cation interaction and a salt bridge (Figure 3.16A). L4.4 was predicted to partake in three π-π stacking interactions, one with each of the residues W41, R45 and F48. Furthermore, a π-cation interaction with R45 was predicted (Figure 3.16A), in addition to the hydrogen bond to D44, as seen in the docking pose (Figure 3.16B).

Of the three parental compounds, only P6 was predicted to dock into the peripheral binding site of the E195 M2 homology model during the original unbiased docking (Figure 3.8). Compound P6 was predicted to have direct polar contacts with R45, via an oxygen atom from a sulphonamide. A sulphonamide was present in all four of the analogues investigated. However, in the docking poses the sulphonamide was not predicted to interact with the peripheral binding site (Figure 3.17B). Of the four analogues, PyMol only predicted an interaction between the peripheral binding site and P6.4, via the D44 residue of M2 (Figure 3.17B). Whereas the 2D interaction map of P6.4 predicted interactions to residues R45 and F48, but not D44 (Figure 3.17A). Analogue P6.1 was predicted to partake in π-π stacking interactions with W41 residues from both chains A and D, and to F48 of chain D, alongside a π-cation interaction with R45 (Figure 3.17A). Both P6.2 and P6.3 were predicted to take part in a π-π stacking interaction with residue F48, with P6.2 making further interactions with W41 and R45 (Figure 3.17A).

Compared to the predictions for the lumenal binding site, at the peripheral binding site there was greater disparity between the predictions of the docking pose and polar contacts (PyMol) and the 2D interaction maps (Maestro). At the lumenal binding site the 2D interaction maps rarely indicated strong polar interactions with the protein, with most interactions seen to be weak dipole-dipole interactions. PyMol indicated that only three analogues, L4.2, L4.4 and P6.3, made polar contacts to residues of the lumenal binding site; 2D interaction maps also predicted L4.2 and P6.3 took part in interactions; additionally interactions were seen for P6.4, but not L4.4.

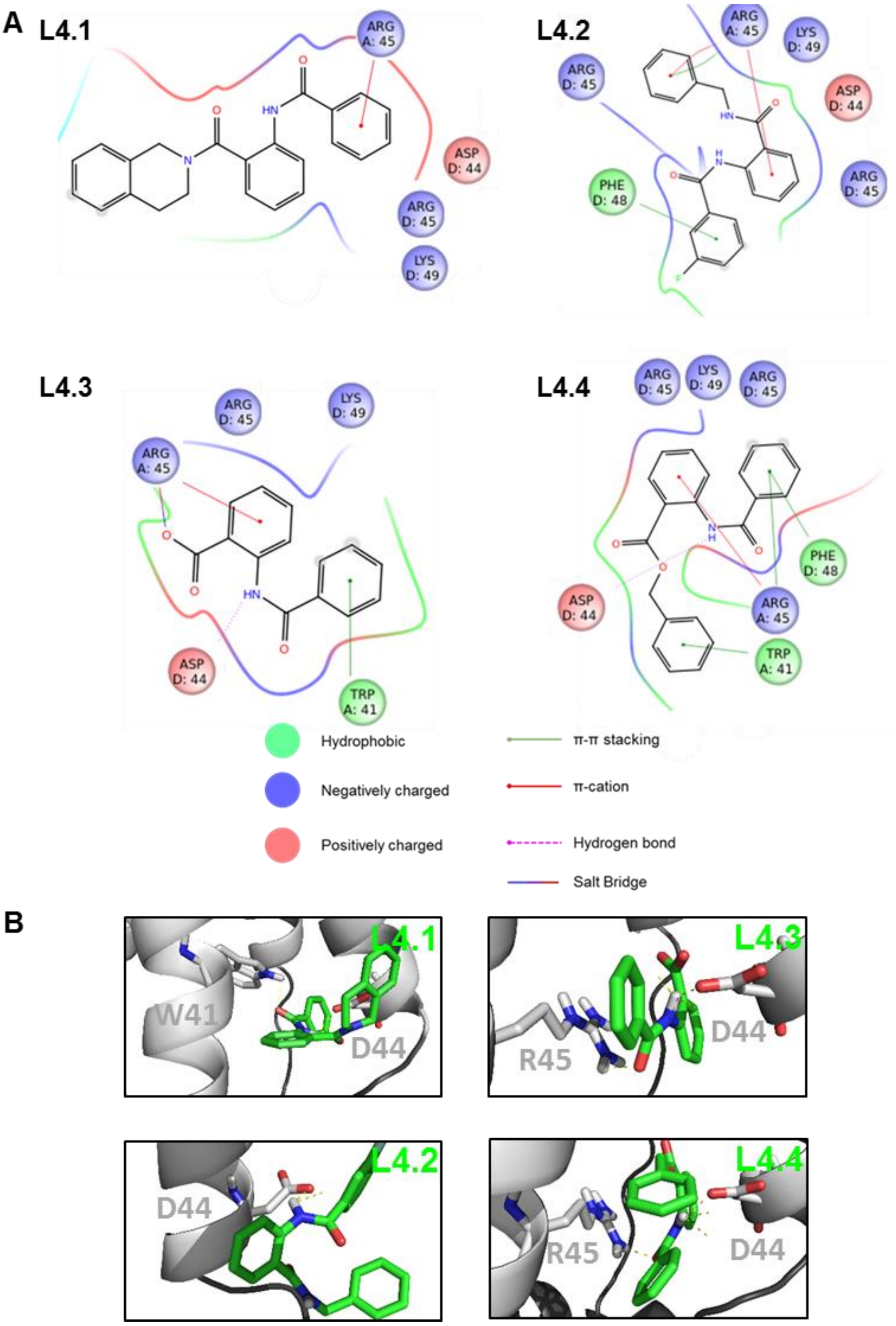
A
L4.1
ARG A: 45
ASP D: 44
ARG D: 45
LYS D: 49
L4.2
ARG A: 45
LYS D: 49
ARG D: 45
ASP D: 44
PHE D: 48
ARG D: 45
L4.3
ARG D: 45
LYS D: 49
ARG A: 45
ASP D: 44
TRP A: 41
L4.4
ARG D: 45
LYS D: 49
ARG D: 45
PHE D: 48
ASP D: 44
ARG A: 45
TRP A: 41
Hydrophobic
Negatively charged
Positively charged
π-π stacking
π-cation
Hydrogen bond
Salt Bridge
B
L4.1
W41
D44
L4.3
R45
D44
L4.2
D44
L4.4
R45
D44

Figure 3.16 Predicted interaction between analogues of L4 and the peripheral binding site of the E195 M2 homology model.

A) 2D structures of L4.1, L4.2, L4.3 and L4.4 and residues (circles) of the M2 tetramer they interact with are shown (hydrophobic - lime green, negatively - blue or positively charged - red). π-π stacking (green lines), π-cation (red lines) hydrogen bond (dashed magenta lines) and salt bridge (blue-red gradient line) interactions are highlighted. B) Docking poses of compounds L4.1-4 (green) within the peripheral binding site of M2 (grey). Selected residues represented as sticks, stick representations are coloured by element and polar contacts (yellow dashed lines) to the protein or solvent highlighted.

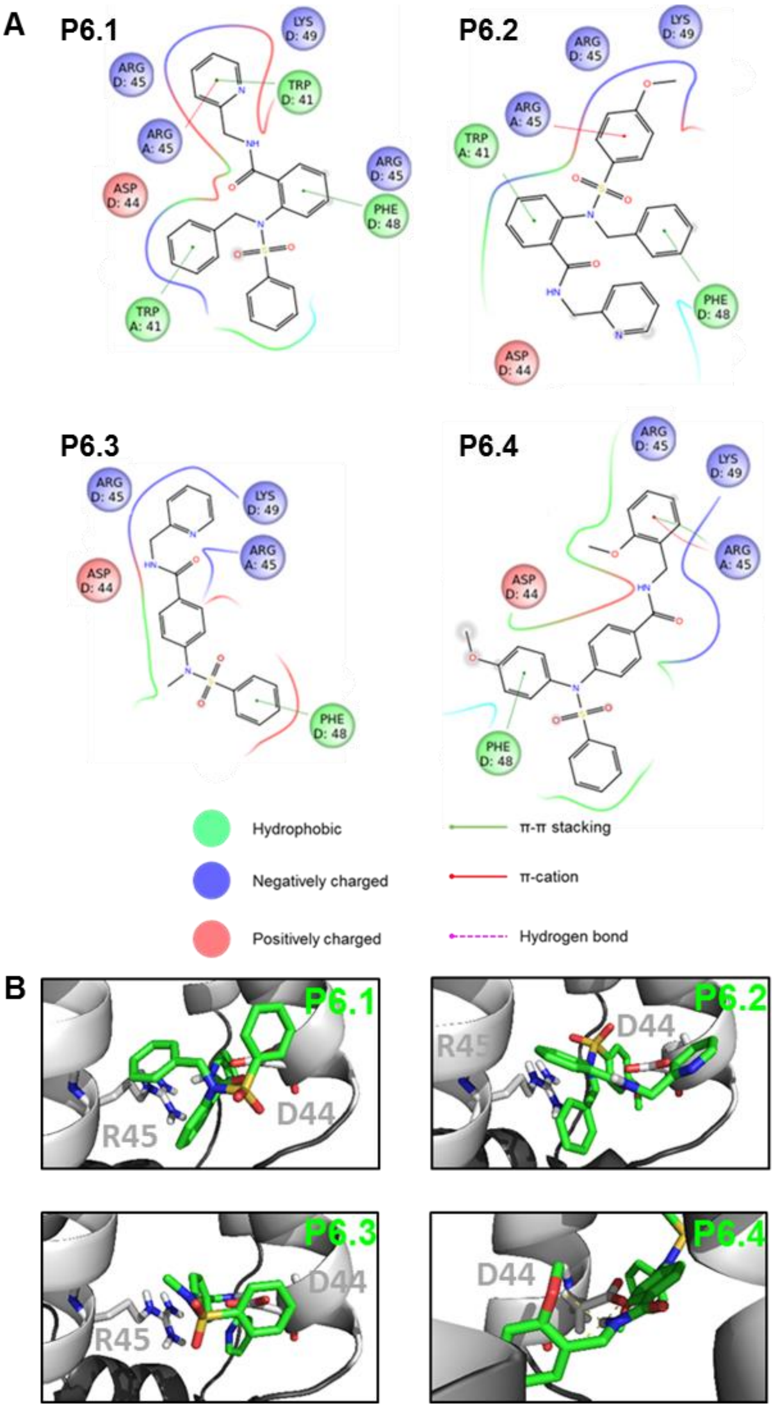
A
P6.1
LYS D: 49
ARG D: 45
TRP D: 41
ARG A: 45
ASP D: 44
ARG D: 45
PHE D: 48
TRP A: 41
P6.2
LYS D: 49
ARG D: 45
ARG A: 45
TRP A: 41
PHE D: 48
ASP D: 44
P6.3
ARG D: 45
LYS D: 49
ARG A: 45
ASP D: 44
PHE D: 48
P6.4
ARG D: 45
LYS D: 49
ARG A: 45
ASP D: 44
PHE D: 48
Hydrophobic
Negatively charged
Positively charged
π-π stacking
π-cation
Hydrogen bond
B
P6.1
R45
D44
P6.2
D44
R45
P6.3
D44
R45
P6.4
D44

Figure 3.17 Predicted interaction between analogues of P6 and the peripheral binding site of the E195 M2 homology model.

A) 2D structures of P6.1, P6.2, P6.3 and P6.4 and residues (circles) of the M2 tetramer they interact with are shown (hydrophobic - lime green, negatively - blue or positively charged - red). π-π stacking (green lines), π-cation (red lines) and hydrogen bond (dashed magenta lines) interactions are highlighted. B) Docking poses of compounds P6.1-4 (green) within the peripheral binding site of M2 (grey). Selected residues represented as sticks, stick representations are coloured by element and polar contacts (yellow dashed lines) to the protein or solvent highlighted.

Strong interactions (π-π stacking, π-cation, hydrogen bonds and salt bridges) were predicted to all but one of the twelve analogues docked at the peripheral binding site (Figure 3.15, Figure 3.16 and Figure 3.17). This could be attributed to the fact that residues at this site were more likely to be charged or contain an aromatic ring. PyMol did predict that a larger number of the analogues were involved in polar contacts with the peripheral binding site, with the three analogues of P6 being the only compounds not seen to interact (Figure 3.17B). All of the interacting compounds were predicted to use D44, in some cases in addition to another residue, for polar contacts (Figure 3.15B, Figure 3.16B and Figure 3.17B). However, the 2D interaction maps only corroborated hydrogen bonds to D44 in four of these nine analogues (Figure 3.15A, Figure 3.16A and Figure 3.17).

3.7 **Discussion**

To reduce the number of compounds down to a realistic list for experimental testing, analysis of the *in silico* results was paramount. Both binding specificities and drug like qualities of the compounds were carefully examined prior to screening.

The generation of an *in silico* homology model of E195 M2 based upon the published structure of the conductance domain of a Udorn H3N2 strain (Schnell & Chou, 2008) enabled virtual HTS of novel compounds against both of the proposed binding sites of M2. Two independent *in silico* screens were carried out and both identified non-adamantane compounds that were predicted to interact specifically with residues of either the proposed lumenal or peripheral binding sites of the E195 M2 homology model. Analysis of analogue compounds revealed further information on these specific interactions and binding poses.

The generation of homology models, when protein structural information is unavailable, is a relatively quick and inexpensive way to produce a 3D structure of a protein (Vyas *et al.*, 2012; Wiltgen & Tilz, 2009) and has applications to drug discovery. The more homology between the template and target sequence the more reliable the model is predicted to be. There were 7 aa substitutions required to match the E195 sequence. Of these substitutions S31N was of the greatest importance, due to its role in rimantadine resistance (Hay *et al.*, 1986); the bulkier side chain of asparagine has been associated with looser packing of the tetramer and disruption of the proposed peripheral binding site (Pielak *et al.*, 2009). The effects of the S31N mutation on the proposed lumenal binding site are less dramatic, with slight constriction of the pore, but no overall impact on the structure of the channel pore (Pielak *et al.*, 2009; Stouffer *et al.*, 2008). Accordingly, the *in silico* minimisation of the resultant model lead to changes in the backbone structure of the tetramer (Figure 3.1) and caused the orientation of H37 and W41 side chains to alter (Figure 3.2).

In addition to S31N, two further amino acid substitutions formed part of, or were in close proximity to, proposed binding sites. V28I is proximal to the lumenal binding site, and L43T is predicted to form part of the peripheral binding site. Replacing V28 with an isoleucine, another hydrophobic amino acid, did not greatly alter the structure of the channel or affect potential interactions with lumenal binding compounds. L43 forms part of the hydrophobic wall of the peripheral binding pocket (Schnell & Chou, 2008); replacing this with the polar residue threonine will potentially increase the size of the polar patch able to interact with peripherally targeted compounds. However, the compound docking analysed in this chapter did not identify any strong polar or hydrophobic interactions between compounds and T43. The remaining four substitutions all lie to the C-terminus of residues reported to be involved in peripheral binding (Schnell & Chou, 2008) and the most C-terminal residue included in the clip file for this site. This does not exempt these changes from having effects upon compound binding, especially at the peripheral binding site. However, due to the limited availability of CD structures of the M2 tetramer, generation of a homology model and amino acid substitutions were unavoidable in the pursuit of a model for a structure-guided search for novel inhibitors. At the time of performing this study, all other CD structures deposited to the PDB lacked a ligand (Pielak & Chou, 2010; Pielak *et al.*, 2009; Sharma *et al.*, 2010), so 2RLF (Schnell & Chou, 2008) was deemed most appropriate to use. Providing some precedent of our choice of 2RLF as a template, other groups have also built pH1N1 swine influenza M2 homology models and undertaken *in silico* docking (Du *et al.*, 2010; Tran *et al.*, 2011). As with our investigation, Tran and colleagues took into account binding at both of the proposed sites of M2 (Tran *et al.*, 2011), whereas Du *et al.* concentrated on the peripheral site only (Du *et al.*, 2010).

Clip files were generated and used to specify the two proposed binding sites of M2 (Section 3.2.1). The purpose of this was to concentrate docking to regions proposed as binding sites for amantadine and rimantadine, including residues seen to directly interact with the compounds (Schnell & Chou, 2008; Stouffer *et al.*, 2008). This approach inherently applied bias to the docking, yet without this there was potential for compounds to dock to any region of the tetramer. This is including at the termini, which would not represent valid poses as in nature additional amino acids would exist at either end of the polypeptide chain. However, there is potential that the use of clip files could result in further, novel binding sites, and consequently compounds targeting these sites, being excluded from analysis. Docking tools such as AutoDock (Scripps), used in other docking studies of IAV M2 (Du *et al.*, 2010; Tran *et al.*, 2011), have minimised user input for defining a binding site, meaning that all potential sites are considered, and as such reduce bias (Goodsell & Olson, 1990), but both methods are valid and have identified novel inhibitors. Additionally, eHiTS has the capability of using large compound libraries in addition to a smaller targeted collection such as the analogues (Section 3.6.1), enabling clip files and docking parameters to remain constant throughout the project.

The M2 tetramer has four potential peripheral binding sites (Schnell & Chou, 2008), one between each pair of adjacent chains. The E195 M2 homology model, like the 2RLF structure does not have perfect four-fold symmetry, such that concentrating the clip file on one particular site between only one pair of chains (A and D) may not have allowed for all potential docking poses. Undertaking *in silico* docking to each of these four sites would have resulted in a larger data set, potentially with additional docking poses. However, it is likely that this would have been repetitive and due to this largely uninformative.

Docking adamantane containing compounds M2WJ332 (Wang *et al.*, 2013b) and compound D into the E195 M2 homology model (section 3.3) highlighted that the characteristic large hydrophobic cage-like structure is not predicted to make any polar contacts to the protein (Figure 3.5 and Figure 3.6). For this reason, instead of simply adding complexity or a second pharmacophore to this cage structure (Du *et al.*, 2010; Wang *et al.*, 2013a; Wang *et al.*, 2013b), we wanted to test a more diverse range of structures. We started with an unbiased screen, to not put any restrictions on shape or chemical groups of compounds (Section 3.4). In addition we carried out a biased screen. This used adamantane compound D as a starting point, due to its predicted ability to bind to both sites weakly. Thus, we aimed to improve selectivity by carrying out divergent SAR and selecting compounds with similar shape and pharmacophore to compound D, but lacking the adamantane cage (Section 3.5). The unbiased screen gave rise to two specific, divergent series (DL and DP), both from a single starting compound.

All compounds from the two large screens (Sections 3.4.1 and 3.5) were docked to both the lumenal and peripheral clip files and then during attrition those predicted to bind to both sites were eliminated during the analysis. For the unbiased screen the top 1000 compounds at each site (ranked by eHiTS score) were included in the analysis; this reduced the number of compounds docking at both sites. Compared to the initial unbiased screen (Section 3.4.1), the number of compounds used in the biased screen was limited to 1000, a number more appropriate for a manual comparison and analysis of the docking. During the biased screen, in addition to eHiTS, a second docking tool was used and corroboration of the eHiTS and SPROUT scores provided an extra level of confidence in the *in silico* docking predictions. During the attrition of the biased screen, the dismissal of compounds remaining in the lists for both sites was carried out both after ranking by eHiTS score and manual assessment of interactions to the protein. This was done in order to select out compounds with a specific preference to one site or the other and as a result being capable of investigating the possibility of targeting the two proposed binding sites of the M2 tetramer independently.

In the case of investigating the binding of L1, L4 and P6 analogues (Section 3.6.1), eHiTS scores were generated for both sites for each of the 12 analogues (Table 3.5). *In silico* docking scores can be compared between compounds within a single site, but cannot be used to compare binding of a single compound at each of the sites and as such could not be used to predict if one binding site was more favourable. The intention of this docking was not to eliminate any compounds from biological testing, but to analyse if any changes in structure affected the predicted binding poses of compound. All compounds were assessed for their effects on CF release, mediated by TM and CD N31 M2 peptides (Figure 4.12 and Figure 4.13) and this experimental data was used to define binding preferences.

Two programs were used to visualise and analyse docking of compounds to the E195 M2 homology model. 2D interaction maps were generated in Maestro software using the data generated from the eHiTS docking, these illustrations depicted interactions between individual functional groups of the compound and specific residues of the protein. Weak dipole-dipole interactions are inferred by the presence of polar residues in proximity to the compound, whilst stronger interactions of π-π stacking, π-cation, hydrogen bonds or salt bridges are clearly labelled. In the case of the attrition of biased compounds (Section 3.5.1) it was these 2D maps that were used to assess the interactions between the compound and M2. In this work the primary function of PyMol software was in the visualisation of the most energetically favourable docking pose for each compound at a specific site. A feature of PyMol allows you to “find” “polar contacts” between the compound and the protein, as well as to the solvent, these are shown as yellow dashed lines in all of the docking poses (Figure 3.5, Figure 3.6 ,Figure 3.9 and Figure 3.12-Figure 3.16). The two software programs inevitably have different parameters including distance, for predicting interactions. Additionally PyMol is more akin to looking for hydrogen bonds, whereas Maestro looks for a wider range of polar and hydrophobic contacts e.g. π-π stacking interactions. For this reason PyMol was used for visualising likely docking poses, whereas Maestro was relied upon as the source of interaction data.

Another method available for *in silico* identification of novel inhibitors is molecular dynamic (Inamdar *et al.*, 2014) simulation, which was first used in the 1970s (McCammon *et al.*, 1977). Unlike homology models generated from published structures, proteins are not rigid structures. MD simulations allow for dynamic motions and conformations (Karplus & McCammon, 2002) and take into account the motion as a function of time. Inhibitors of drug-resistant M2 have been designed by MD simulations (Wang *et al.*, 2011). The basis of the Wang *et al.* work was not the published CD structure 2RLF (Schnell & Chou, 2008), as used in this project and in the generation of other pH1N1 M2 homology models (Du *et al.*, 2010; Tran *et al.*, 2011). Wang and colleagues instead employed the X-ray crystallographic TM structure 3LBW (Acharya *et al.*, 2010) and therefore investigation of the proposed peripheral binding site was not undertaken (Wang *et al.*, 2011). The drug-resistance polymorphisms used as the focus of the study was V27A, with identification of a series of spirane amine compounds found to be effective against WT, V27A and L26F peptides in a TEVC assay (Wang *et al.*, 2011). Nevertheless, this class of compound were not seen to be effective against S31N M2, considered the most clinically relevant polymorphism.

High-throughput identification of novel inhibitors does not necessarily require *in silico* studies. This is highlighted by the use of a yeast growth restoration assay (Balgi *et al.*, 2013), in which both adamantane derivatives and non-adamantane compounds were identified as potential M2 inhibitors. When expressed in yeast, M2 led to a reduction in yeast growth observed at 48 hours, that in the case of WT M2 could be restored by addition of amantadine (Balgi *et al.*, 2013); employing the 384-well setup allowed for screening of over 200,000 compounds, with 21 active compounds identified. The initial screen was performed using WT M2, with hits then being used against S31N, V27A and L26F, none of which were able to inhibit the most prevalent S31N resistance polymorphism (Balgi *et al.*, 2013); as such, these compounds do not represent a significant improvement on licensed M2 antivirals.

Through the utilisation of an *in silico* homology model, we have handpicked compounds for experimental investigation against drug-resistant N31 M2 from pH1N1 swine influenza. Predictions were made as to the preference in binding site and proposed efficacy, which needed to be tested. Assessment of effects on different M2 peptides *in vitro*, alongside antiviral efficacy can be used to validate or improve the methodology of the *in silico* work.

Chapter 4

Screening novel compounds for activity against M2 *in vitro* and effects upon virus titre in culture

Chapter 4 Screening novel compounds for activity against M2 *in vitro* and effects upon virus titre in culture

4.1 Introduction

M2 is the best characterised viroporin to date, with numerous studies of its function and inhibition being published since 1992, when electrophysiology studies in *Xenopus laevis* oocytes revealed its function as an ion channel (Pinto *et al.*, 1992). In addition, electrophysiology studies have been instrumental in uncovering more about M2, including its activation by low pH (Pinto *et al.*, 1992), preference for conducting protons (Balannik *et al.*, 2010; Shimbo *et al.*, 1996), the minimal functional unit for conductance (Ma *et al.*, 2009) and key functional residues, including the H37 proton sensor (Wang *et al.*, 1995) and the W41 gate (Tang *et al.*, 2002).

Alongside these studies, *in vitro* methods for assessing M2 ion channel activity and inhibition have been used; one advantage of *in vitro* methods over electrophysiology studies is that there is no influence of endogenous ion channels that are present in oocytes. Since the 1990s when planar lipid bilayers were first used to assess adamantane effects on proton conductance (Duff & Ashley, 1992), this system has been used to study many other viroporins including HIV-1 Vpu (Ewart *et al.*, 1996), Alphavirus 6k (Melton *et al.*, 2002), HCV p7 (Clarke *et al.*, 2006; Griffin *et al.*, 2003; Pavlovic *et al.*, 2003; Premkumar *et al.*, 2004) and Dengue M protein C-terminal peptide (Premkumar *et al.*, 2005). Liposomes can be used in place of planar bilayers and resultant recordings can give an overview of channel populations, as opposed to single, or a handful of channels when analysed in bilayers. M2 conductance has previously been investigated in this way (Lin *et al.*, 1997; Peterson *et al.*, 2011; Schroeder *et al.*, 1994).

In addition to assessing ion conductance, liposomes can also be filled with self-quenching dyes such as carboxyfluorescein (CF) (Blumenthal *et al.*, 1977), which upon release into the external buffer, dilute and fluoresce, giving an indirect readout of ion channel activity. Originally used to assess the activity of melittin (Schwarz *et al.*, 1992), a peptide found in bee venom, this system was adopted for studying viroporins in 2007 when it was first used to study HCV p7 (StGelais *et al.*, 2007). Following this, hRSV SH (Carter *et al.*, 2010) and HPV-16 E5 (Wetherill *et al.*, 2012) have also been shown to mediate a dose-dependent release of CF from liposomes.

The system does have its limitations. In the instance of M2, there is naturally selectivity for conducting protons, CF with a MW of 376.62 is undoubtedly much larger and more in scale with scale of M2 inhibitors. However, it has been demonstrated that the release of CF from liposomes mimics the activation and inhibition characteristic of viroporin channel activity. In the case of HCV p7 and HPV-16 E5, viroporin-mediated release of CF is enhanced at acidic pH (StGelais *et al.*, 2007; Wetherill *et al.*, 2012). Work in the laboratory had previously demonstrated that M2 peptides in this system are also pH activated (Figure 4.1) (Atkins *et al.*, 2014) and responsive to inhibitors (Figure 4.2). Additionally, the lipid constituents of the liposomes used do not always best represent the environment in which the viroporin naturally occurs, with a viral envelope rich in cholesterol and sphingomyelin (Klenk *et al.*, 1972). There has to be a balance between a lipid composition in which the viroporin can oligomerise and function and one that allows for stability to provide reproducibility within an assay system. In order to develop a HTS for analysing p7 inhibition Gervais and colleagues investigated different lipid compositions (Gervais *et al.*, 2011). Optimisation of lipid composition of liposome was not carried out in this work, but may have resulted in improved stability and formation of channels better resembling their native state. Despite this the use of peptides to investigate the functional activity and inhibition of viroporins such as M2 is a valuable tool; the ability to incorporate specific mutations (such as those implicated in resistance), into the sequence can reveal more about mechanisms of action of compounds. It is, however, still important to demonstrate that the results can be replicated in the context of virus infection. For this reason, after each *in vitro* screen of compounds we ensured that effective compounds were tested in plaque assays, to test whether the reduction of M2 activity was translatable to a reduction in virus titre.

The primary strain for our investigations was chosen to be E195 pH1N1, due to its prevalence in the population for a number of years following its emergence in the 2009 pandemic. E195 also retains the common polymorphism conferring resistance to currently licensed M2 antivirals.

Prior to studies presented herein, preliminary work had already begun to start optimising an M2 *in vitro* dye release assay, and to screen existing viroporin inhibitors against pH1N1 swine ‘flu. The liposome dye release assay was adapted to use M2 conductance domain peptides. At neutral pH M2 is highly active, but as with M2 in the virion (Pinto *et al.*, 1992), activity is enhanced by acidic pH (Figure 4.1). This method is also appropriate for testing inhibitors, validated by tests using the licensed M2 antiviral rimantadine. Wild-type E195 M2 is naturally rimantadine resistant due to presence of N31; testing a conductance domain peptide (N31 CD), demonstrated that the CF release was unaffected by the presence of rimantadine (Figure 4.2B). This was in

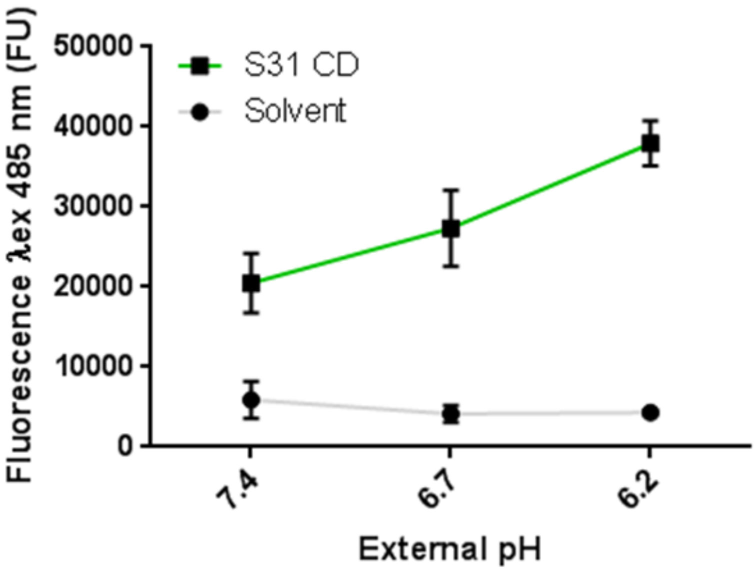

Figure 4.1 M2 mediates release of CF from liposomes is enhanced at acidic pH.

An E195 M2 conductance domain peptide was assessed by end point fluorescence in buffers of decreasing pH. 62.5 µM S31 CD or solvent (5 % v/v MeOH). To re-solubilise carboxyfluorescein the pH was re-buffered to pH 7.4, liposomes were then removed by ultracentrifugation prior to fluorimetry (λex = 485 nm, λem = 520 nm). Data represents two separate experiments, with conditions repeated in triplicate within each experiment. Error bars represent standard error of the mean. Shown with permission from Ranjitha Tathineni and Dr Stephen Griffin.

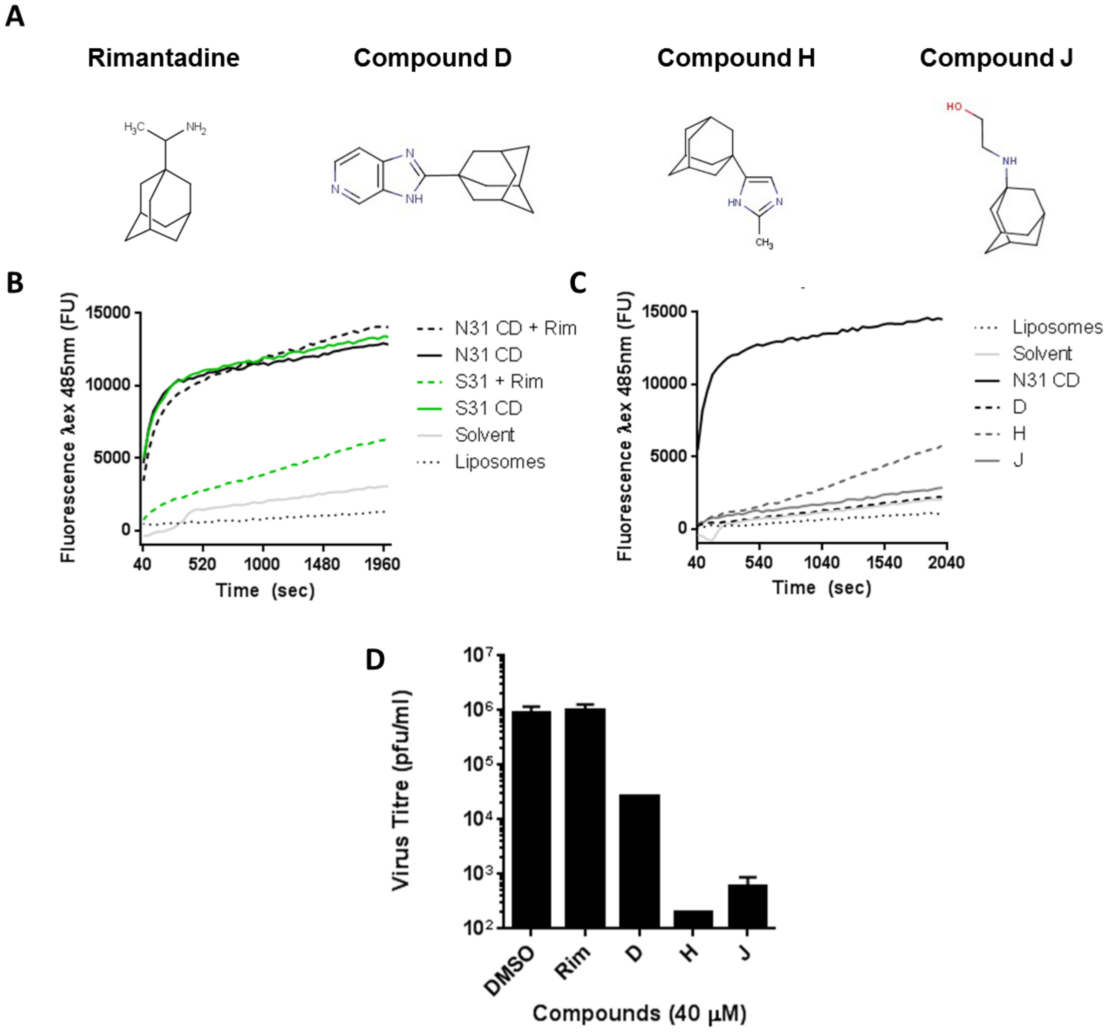

Figure 4.2 E195 M2 conductance domain peptides maintain resistance to rimantadine, but are sensitive to novel adamantane derivatives, which also reduce E195 infectious virus titre.

A) Molecular structures of rimantadine, compound D, H and J. B) Conductance domain peptides of wild-type E195 M2 (N31 CD, black) and the N31S mutant (S31 CD, green) result in release of CF from liposomes. Rimantadine (Rim, dashed lines) reduces the CF mediated release by the S31 peptide, but not the N31 peptide. C) Novel compounds all reduce N31 CD mediated CF release. D) E195 infectious virus titre is reduced by novel inhibitors, but not Rim. CF mediated release measured by fluorimetry (λex = 485 nm, λem = 520 nm) and recorded in real time. Liposomes alone (liposomes) and liposomes + 5 % v/v MeOH (solvent) were included as controls. Peptides used at 10 nM (5 % v/v MeOH) and compounds at 40 μM (1 % v/v DMSO. Virus titres were established 24 hours post an infection of MOI 0.001. Error bars represent standard deviation, within one experimental repeat, DMSO and Rim in triplicate wells, D and H single well and J duplicate wells. Work performed by Dr Toshana Foster.

comparison to a rimantadine “sensitive” peptide (S31 CD), which when preincubated with 40 µM rimantadine induced a marked decrease in fluorescence (Figure 4.2B). Thus, despite not directly assessing M2 proton conductance, the dye release assay appeared to be capable of demonstrating specific inhibition of channel activity.

Initial testing of compounds included a selection of adamantane derivatives, which had previously been tested against HCV p7 *in vitro* and infectious HCV in culture (Foster *et al.*, 2011). Adamantane derivatives compounds D, H and J (Figure 4.2A) all resulted in a reduction in N31 CD mediated fluorescence (Figure 4.2C) and infectious virus titre compared to the DMSO control (Figure 4.2D). Preincubation of N31 CD peptide with compound D reduced fluorescence to a similar level as the solvent control, whereas compound H had the least dramatic effect on CF release but the fluorescence was still more than halved (Figure 4.2C).

Concurrently, other groups were also investigating the effects of adamantane analogues on the replication of amantadine-resistant strains of IAV and found compounds effective against some S31N strains (Kolocouris *et al.*, 2014; Wang *et al.*, 2013a; Wang *et al.*, 2013b; Wu *et al.*, 2014b). A number of studies have also investigated non-adamantane inhibitors of M2. Amine compounds have been found to target M2, but to date this class of compound have only been able to inhibit amantadine-sensitive and not amantadine-resistant strains of IAV (Hu *et al.*, 2010; Zhao *et al.*, 2011). Additionally, the spirene-containing compound, BL-1743 has been shown to be effective against IAV that is amantadine-sensitive, but ineffective against naturally occurring amantadine resistant strains (Tu *et al.*, 1996). However, resistance to BL-1743 can be conferred by an I35T mutation, which does not result in amantadine resistance, supporting a different binding mode compared to adamantanes (Tu *et al.*, 1996). Spiran amine 8, a derivative of BL-1743, is effective against WT M2, as well as L26F and V27A amantadine-resistant mutants (Balannik *et al.*, 2009). However, it is not effective against S31N the most prevalent polymorphism (Balannik *et al.*, 2009). To our knowledge there are no reports of non-adamantane compounds that are effective against M2 containing N31.

4.2 Effects of adamantane derivative compound D on M2 *in vitro* and in virus culture

Both real-time traces and end point data demonstrated a dose-dependent increase in CF release mediated by E195 M2 from liposomes, with increasing concentrations of

N31 CD peptide (Figure 4.3). Unlike the preliminary studies which used 10 nM N31 CD peptide and resulted in approximately 12000 FU above liposome background (Figure 4.2), when using the new E195 N31 CD peptide batch there was repeatedly background fluorescence, but comparable fluorescence readings above background were recorded. This increased background fluorescence could be attributed to different batches of lipids. A linear relationship between end point fluorescence readings and peptide concentration was observed up until 30 nM, when the increase in fluorescence slowed and there was no increase between 40 and 50 nM (Figure 4.3B). To allow for a larger window of effect and to remain within the linear range, initial inhibition studies were carried out using 25 nM peptide.

The real-time traces showed that across all concentrations of peptide and controls, fluorescence values plateaued long before the final recorded time point (Figure 4.3A). The reproducibility of this maximum reading and the incomplete data for the exponential phase resulted in the decision to use the end point value as the primary readout from dye release experiments. Subtraction of the liposome alone reading was carried out to negate the effect of background fluorescence. To simplify the comparison between inhibition studies, these values were then normalised to the value for peptide + DMSO, which was set 100 % relative CF release. At the highest concentrations of N31 CD the fluorescence readouts were less than those measured from Triton (Figure 4.3A), confirming that liposomes are in excess of M2.

Titrations of compound D were re-optimised for the new peptide batch (Figure 4.4). Inhibition was seen to be dose-dependent; however, at none of the concentrations tested was the reduction in CF release statistically significant, with p values of 0.082 and 0.070 for 50 and 100 µM, respectively. Nonetheless at 100 µM compound D, CF release was reduced to almost 40 % of the control, whereas previously 40 µM resulted in the fluorescence readings being almost identical to that of the baseline solvent control (Figure 4.2C). This can likely be attributed to the higher concentration of peptide used in the second batch. Use of compound D enabled a direct comparison between peptide batches, with the second batch of N31 CD peptide used in all further work.

No adverse effects on MDCK cellular metabolism were measured when 10 – 80 µM of either rimantadine or compound D were incubated with MDCK cells for 72 hours (Figure 4.5A). However, whilst rimantadine was unable to reduce the virus titre at 24 hpi, 80 µM compound D resulted in a two $\log_{10}$ reduction in infectious virus titre (Figure 4.5B). This was a greater reduction compared with when 40 µM was tested previously (Figure 4.2D).

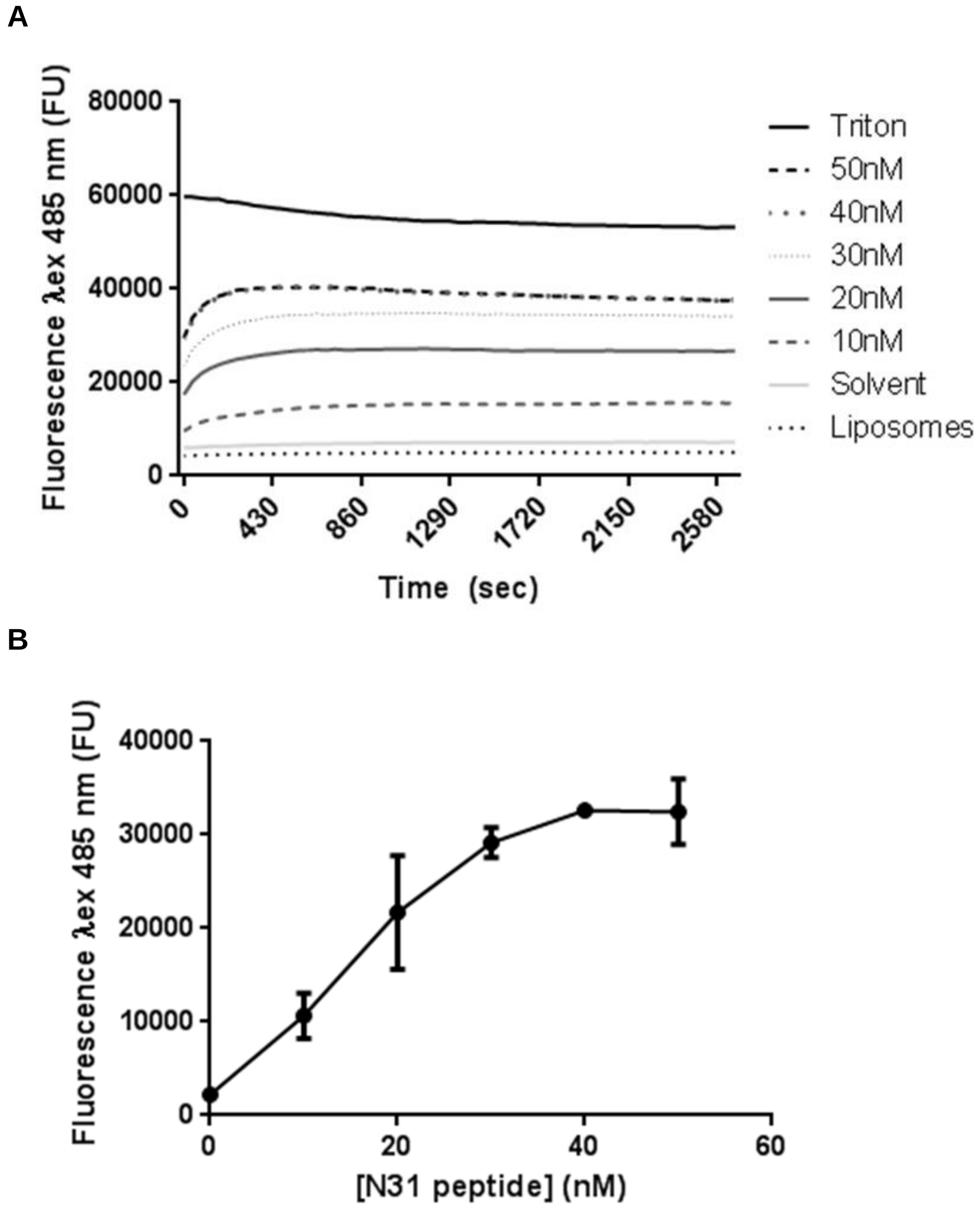

Figure 4.3 N31 CD peptide mediated release of CF from liposomes occurs in a concentration dependent manner.

A) CF release from liposomes, measured by fluorimetry (λex = 485 nm, λem = 520 nm), was recorded in real time. Fluorescence readings for liposomes alone (liposomes), liposomes plus solvent (solvent, 5 % v/v MeOH) and Triton-X 100 (5 % v/v, Triton) were included as controls. The effects of between 10 and 50 nM of a pH1N1 CD peptide (N31 peptide), in 5 % v/v MeOH, were measured. B) End point values, calculated by subtraction of liposome only values. Data is from a single experiment, with conditions carried out in duplicate, error bars represent standard deviation.

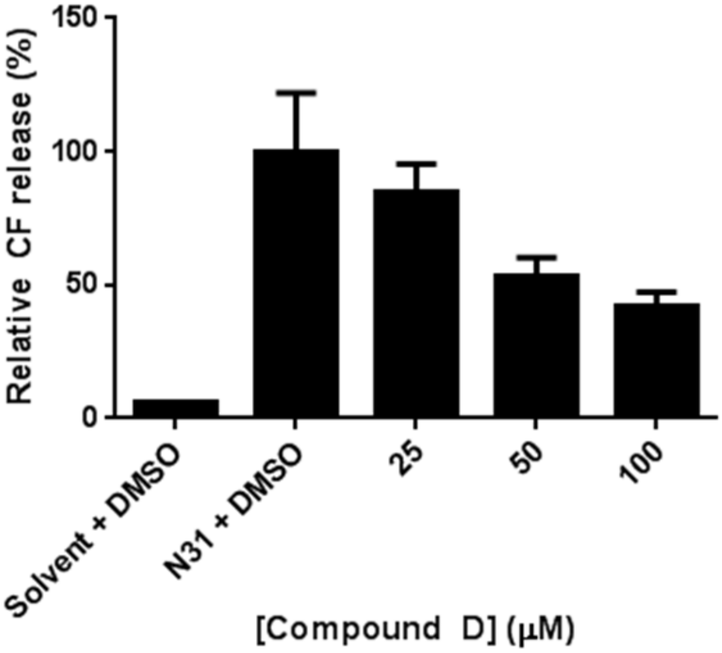

Figure 4.4 N31 CD peptide activity is inhibited in a dose dependent manner by adamantane compound, D.

Increasing concentrations of compound D (25, 50 and 100 µM, 1 % v/v DMSO) were preincubated with 25 nM N31 CD peptide (5 % v/v MeOH). CF release from liposomes was then measured by fluorimetry (λex = 485 nm, λem = 520 nm). End point values, with liposomes alone subtracted, then normalised to N31 + DMSO and relative CF release plotted. Error bars represent standard deviation of the mean, from duplicate wells of a single experiment.

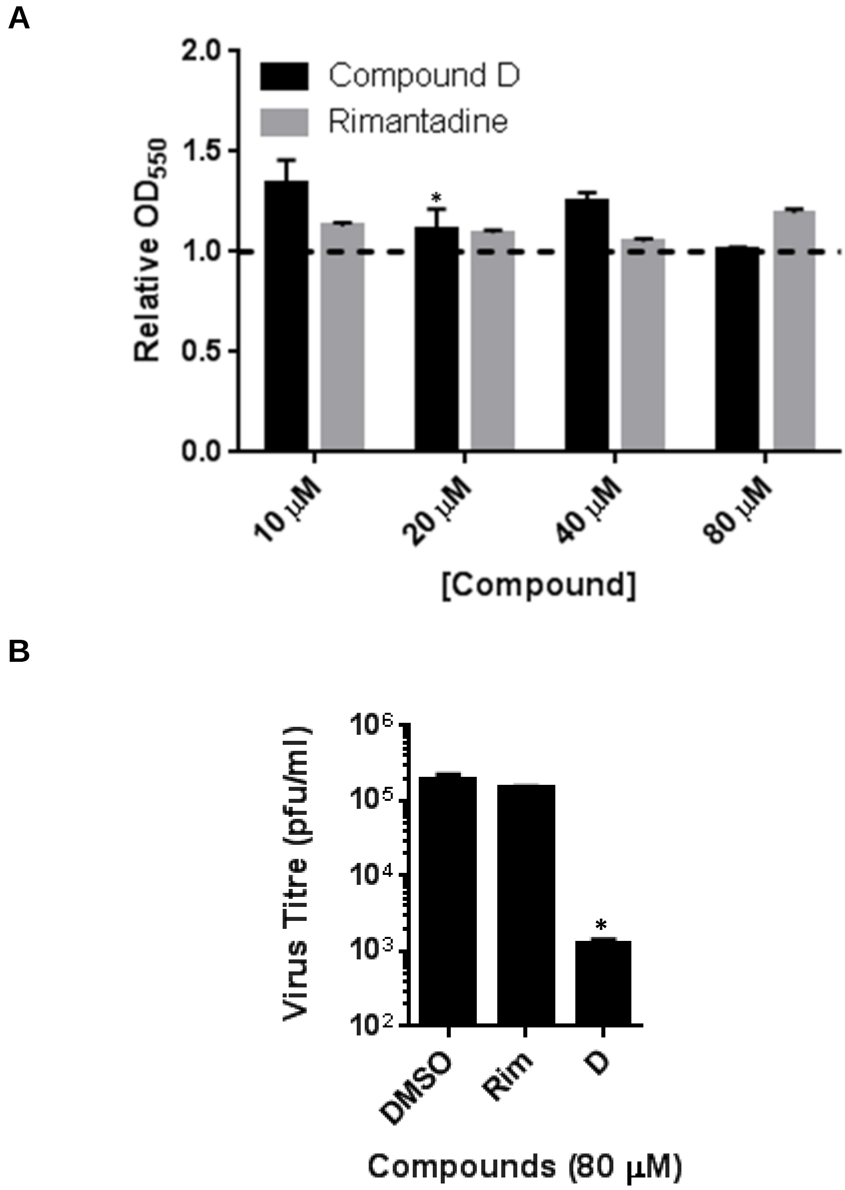

Figure 4.5 Compound D, but not rimantadine is capable of reducing the infectious virus titre of pH1N1 swine influenza.

A) Effects of rimantadine and compound D on MDCK cellular metabolism were investigated via MTT assay over 72 hours, results were normalised against the appropriate DMSO control (0.2-0.8 % v/v). Error bars represent standard deviation across three or four wells, from one experimental repeat. B) E195 virus titre is reduced by compound D (D), but not rimantadine (Rim), 24 hours post an infection of MOI 0.001. Error bars represent standard deviation over three wells, within one experimental repeat. Paired t-tests were carried out to assess statistical significance between DMSO and compounds (= $p \leq 0.05$)*

4.3 Non-adamantane compounds are capable of inhibiting M2 *in vitro* and in virus culture

The *in silico* docking of compound D was inconclusive (Figure 3.6), potentially due to the hydrophobic nature of the adamantane core. Moving away from adamantane containing compounds was seen as an important step in investigating the potential for two druggable binding sites on the E195 M2 ion channel. An unbiased *in silico* screen (Section 3.4) identified compounds predicted to bind exclusively to either the proposed lumenal or peripheral binding sites of E195 M2 (Figure 3.7 and Figure 3.8). These compounds did not contain the adamantane cage found in licensed antivirals amantadine and rimantadine, or experimental compounds such as compound D or M2WJ332 (Wang *et al.*, 2013b). At the time of writing, non-adamantane compounds have been shown to be capable of inhibiting rimantadine-sensitive, as well as rimantadine-resistant L26F and V27A M2, but not S31N (Balannik *et al.*, 2009; Hu *et al.*, 2010; Tu *et al.*, 1996; Zhao *et al.*, 2011). The *in vitro* dye release assay was used to identify compounds capable of reducing the activity of rimantadine resistant N31 M2, prior to testing against full length virus in culture.

4.3.1 Dose dependent effects of predicted lumenal and peripheral targeted compounds on N31 CD peptide

Compounds were screened for their ability to reduce the channel activity of the E195 conductance domain peptide (N31 CD). From thirteen unbiased compounds initially tested, seven caused a statistically significant, dose dependent reduction in M2 mediated CF release from liposomes. This greater than 50 % hit rate, is higher than usually expected with screening, supporting our use of the *in silico* homology model and virtual HTS to enrich screening pools. Of the seven compounds, four compounds were predicted to bind at the lumen (Figure 4.6) and three were predicted to bind at the periphery (Figure 4.7). Data for the six compounds that did not result in a reduction in the channel activity of N31 CD can be found in the appendix (Figure A.1 and Figure A.2).

Comparing the four predicted lumenal targeting compounds L1, L4, L6 and L7 (Figure 4.6), L6 demonstrated the greatest effect on CF release with a 50 % reduction in relative CF release at 20 µM and 75 % reductions at 40 and 80 µM. Compound L1 did not demonstrate a typical dose response, with the value at 20 µM lower those at both of the higher concentrations tested. However, as the reduction in CF release was significant at all of the concentrations tested, L1 was taken forwards for testing against

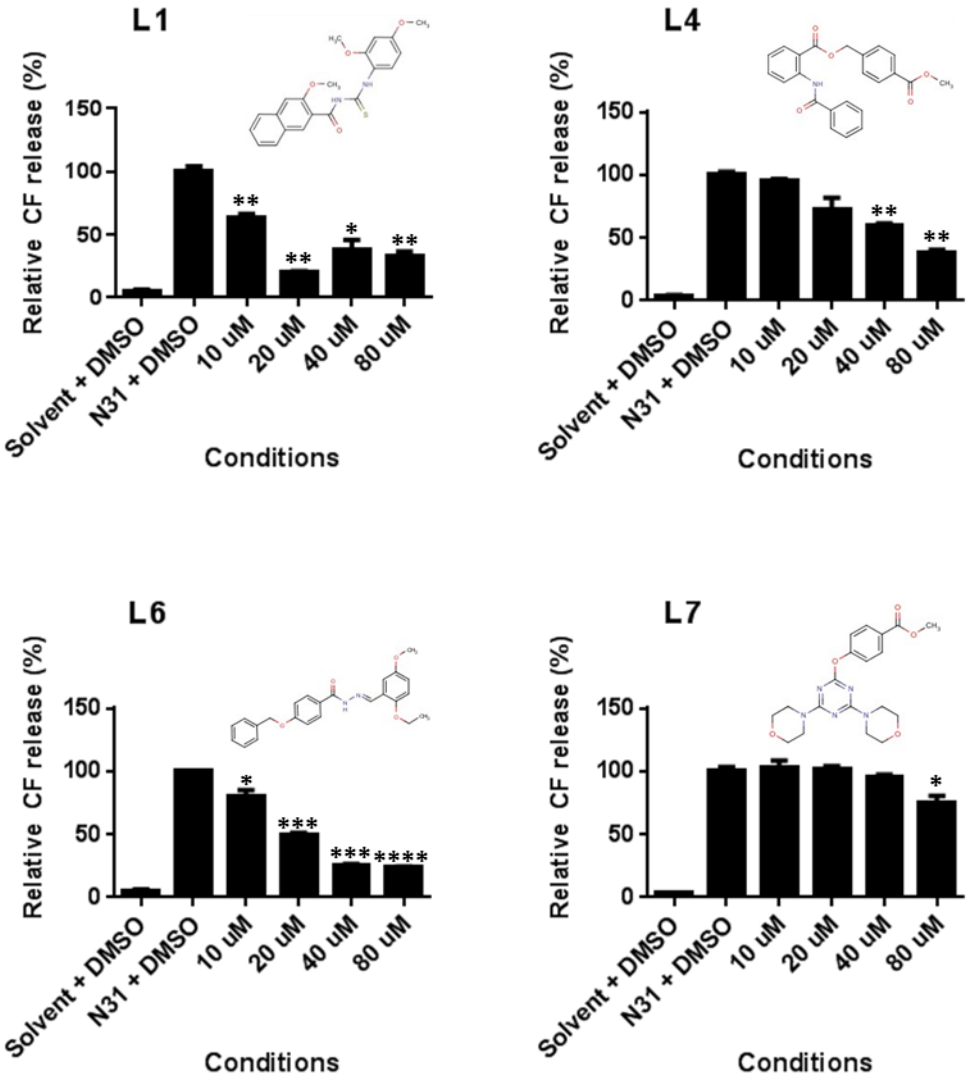

.

Figure 4.6 Does dependent inhibition of an E195 M2 conductance domain peptide by lumenally targeted compounds.

Increasing concentrations of predicted lumenal targeting compounds L1, L4, L6 and L7 (10, 20, 40 and 80 µM, 1 % v/v DMSO) were preincubated with 25 nM N31 CD peptide (5 % v/v MeOH). CF release from liposomes was then measured by fluorimetry (λex = 485 nm, λem = 520 nm). Structures of compounds are shown alongside the data. End point values, with liposomes alone subtracted, then normalised to peptide + DMSO (N31 + DMSO) and relative CF release plotted. Error bars represent standard deviation of the mean, from duplicate wells of a single experiment. Paired t-tests were carried out, on raw values, to assess statistical significance between N31 + DMSO and each compound (= $p \leq 0.05$, ** = $p \leq 0.01$, *** = $p \leq 0.001$,**** = $p \leq 0.0001$).*

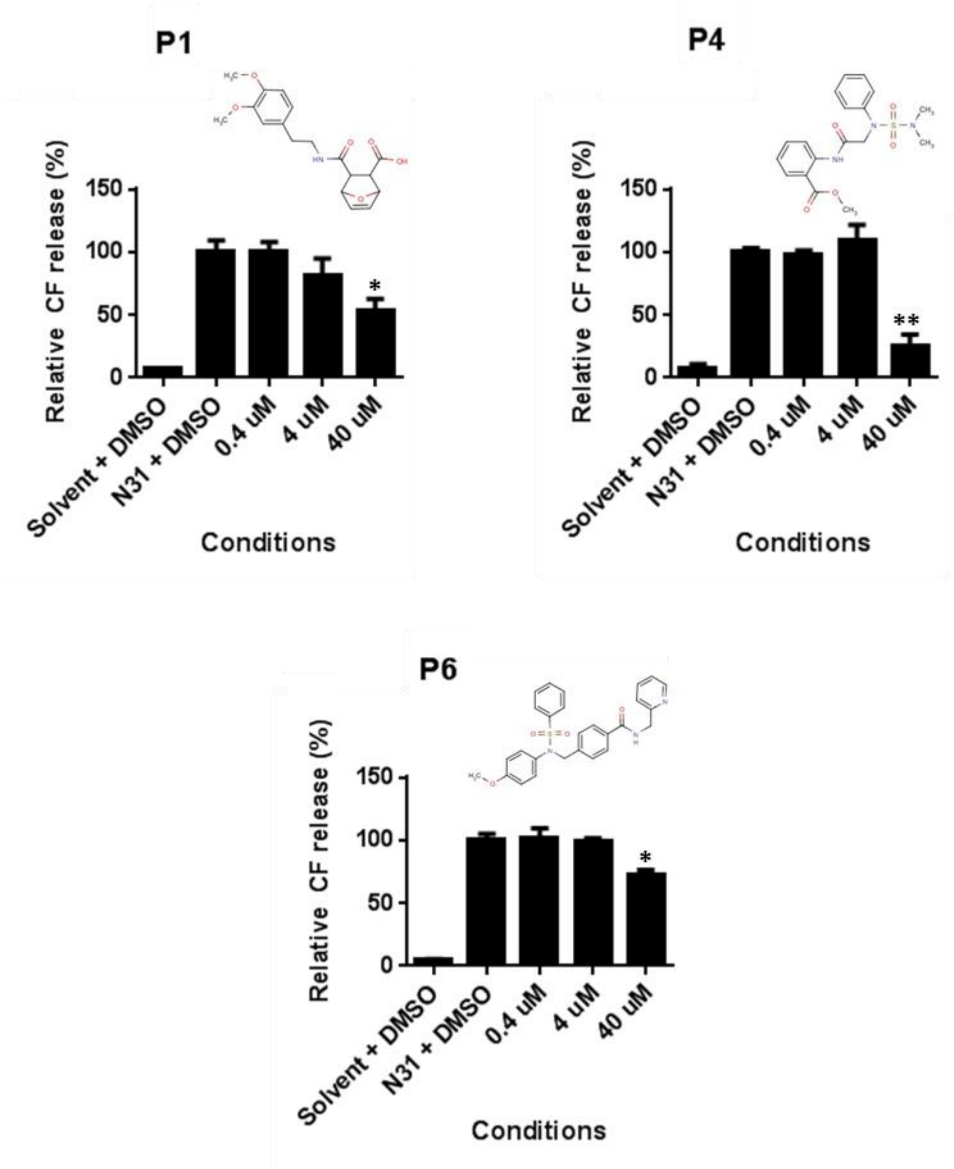

Figure 4.7 Dose dependent inhibition of an E195 M2 conductance domain peptide by peripherally targeted compounds.

Increasing concentrations of predicted peripheral targeting compounds P1, P4 and P6 (10, 20, 40 and 80 µM, 1 % v/v DMSO) were preincubated with 25 nM N31 CD peptide (5 % v/v MeOH). CF release from liposomes was then measured by fluorimetry (λex = 485 nm, λem = 520 nm). Structures of compounds are shown alongside the data. End point values, with liposomes alone subtracted, then normalised to peptide + DMSO (N31 + DMSO) and relative CF release plotted. Error bars represent standard deviation of the mean, from duplicate wells of a single experiment. Paired t-tests were carried out, on raw values, to assess statistical significance between N31 + DMSO and each compound (= p ≤ 0.05, ** = p ≤ 0.01).*

virus. Both L4 and L7 showed a dose-dependent effect of M2 mediated CF release. For L4 this effect became significant at 40 µM, whereas for L7 it was only the top concentration of 80 µM that was calculated to be significant, when compared to the DMSO control (Figure 4.6). Of the predicted peripherally targeted compound, P1, P4 and P6 all exerted statistically significant effects at 40 µM, at this concentration P4 resulted in the greatest reduction in CF release (Figure 4.7).

4.3.2 Effect of compounds on cellular metabolism and virus titre

Compounds seen to exhibit an inhibitory effect on channel activity *in vitro* (Figure 4.6 and Figure 4.7) were then tested for effects on cellular metabolism via an MTT assay (Figure 4.8A). No adverse effects were seen after 72 hours, when using any of the compounds up to a concentration of 80 µM, so all were taken forward and their effects on virus replication in culture investigated.

E195 virus plaque assays using 80 µM of the non-adamantane compounds were carried out, using compound D as a positive control. Virus titre at 24 and 48 hpi was compared to that of virus treated with DMSO (Figure 4.8B); at 24 hpi all compounds showed a statistically significant reduction in virus titre, but at 48 hpi any measured reduction was no longer a statistically significant, likely due to high levels of CPE. Apart from compounds P4 and P6, 80 µM treatment resulted in a greater than $\log_{10}$ drop in infectious virus titre 24 hpi (Figure 4.8B), with L1 having the greatest reduction of all compounds tested.

4.4 Assessing compound binding preferences *in vitro* via differential inhibition of M2 peptides

Hitherto, *in vitro* work solely used a N31 conductance domain peptide for assessing effects of novel inhibitors on M2 mediated CF release from liposomes (Figure 4.6 and Figure 4.7). Use of an S31 conductance domain (S31 CD) peptide should provide evidence pertaining to the effect of compounds on a rimantadine-sensitive strain of IAV. Furthermore, the N31 transmembrane (N31 TM) peptide (aa 18-46) lacks a portion of the peripheral binding site (Figure 3.3). Thus peripherally targeted compounds should preferentially inhibit the N31 CD peptide, compared to the N31 TM peptide, whilst lumenally targeted compounds should exert similar effects on both peptides.

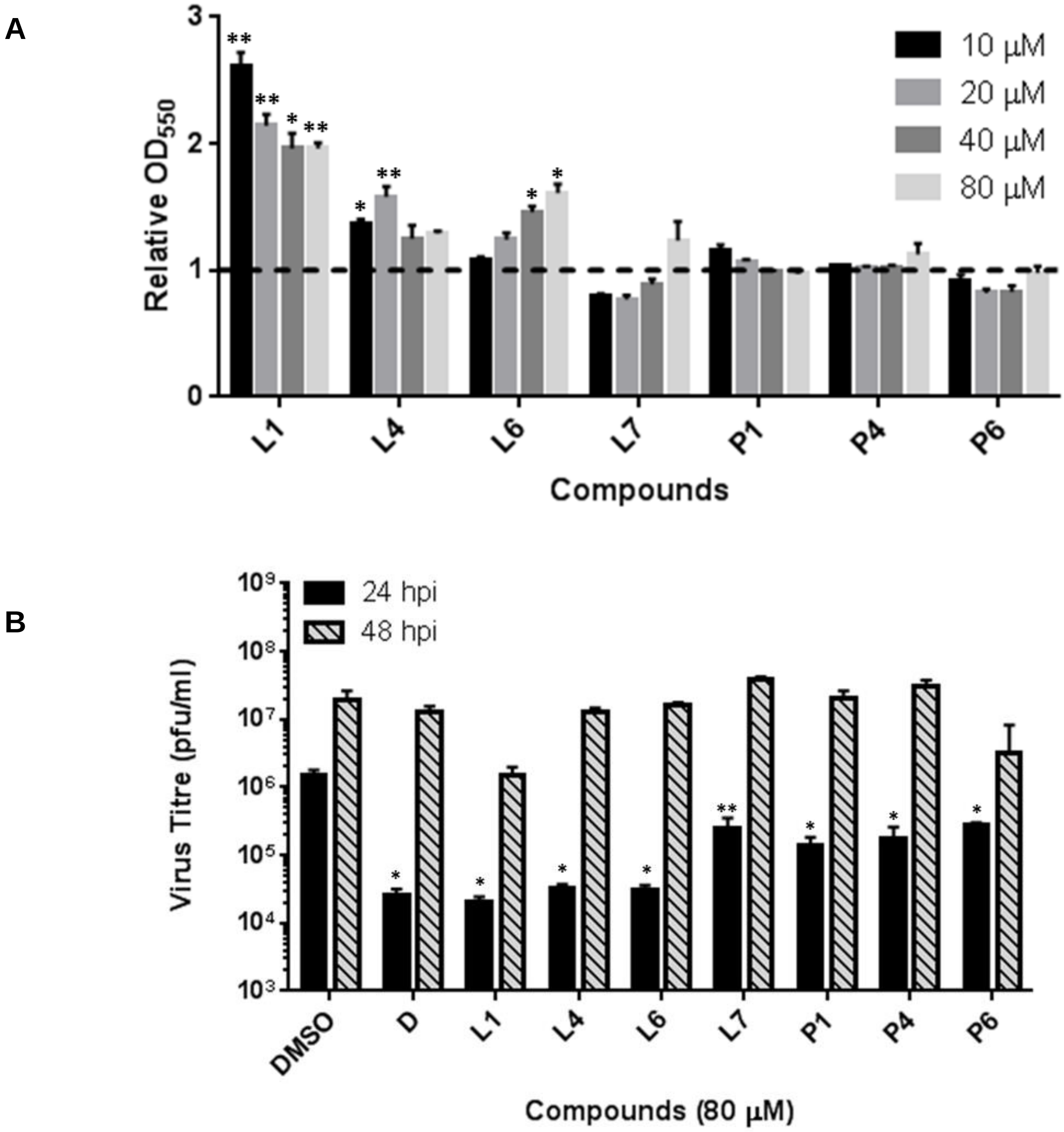

Figure 4.8 Novel compounds reduce E195 infectious virus titre but do not have adverse effects on cellular metabolism.

A) Effect of increasing concentrations of novel non-adamantane compounds on MDCK cellular metabolism after 72 hours, measured via MTT assay. Results were normalised against the appropriate DMSO control (0.2-0.8 % v/v). Error bars represent standard deviation across three or four wells, from one experimental repeat. B) E195 infectious virus titre is reduced by novel compounds at 24 hours post an infection of MOI 0.001, but at 48 hpi this effect is not significant. Data shown is the mean of three wells from a single experimental repeat, but is representative of two experimental repeats. Error bars represent standard deviation across three wells. Paired t-tests were carried out to assess statistical significance compared to DMSO (= p ≤ 0.05, ** = p ≤ 0.01).*

To date, there has been no direct comparison in terms of binding of compounds to or inhibition of the two peptides. As a consequence, the controversy over the site and mode of action of M2 inhibitors has remained. Transmembrane peptides have been used in a number of structural studies, where drug binding was observed in the lumen (Cady *et al.*, 2009; Stouffer *et al.*, 2008; Wang *et al.*, 2013b; Wu *et al.*, 2014b). To date there is only one drug bound M2 tetramer structure that utilised the conductance domain peptide (Schnell & Chou, 2008), where four molecules of rimantadine were bound at the periphery. In the context of a TM channel secondary, low affinity binding of amantadine was observed at a peripheral site (Cady *et al.*, 2010), in addition to the lumenal binding site, following lipid saturation.

To compare between CD and TM peptides, it was necessary to determine the specific activity of each; fresh stocks of N31 CD and S31 CD were purchased, alongside the new N31 TM peptide synthesis. Increasing concentration of each peptide (10-80 nM for CD peptides and 40-320 nM for TM peptide) were tested in the *in vitro* dye release assay. Both N31 CD and S31 CD peptides had comparable fluorescence readouts across all concentrations tested, whilst N31 TM had reduced fluorescence at equivalent concentrations (Figure 4.9). As mentioned previously, the degree of CF release from liposomes, measured by fluorimetry, was lower with the new synthesis of N31 CD peptide (Section 4.2), for this reason it is not possible to compare between the two data sets. In peptide comparison studies, 40 nM CD peptides and 320 nM TM peptide were used when testing inhibitors, as these reproducibly gave comparable fluorescence readings. In the case of CD peptides 40 nM was well within the linear range (Figure 4.9), meaning liposomes were in excess; this cannot be confirmed for the N31 TM peptide as 320 nM was the highest concentration tested, but as this represented an equivalent CF release it is unlikely to have reached saturation.

The E195 M2 is naturally resistant to rimantadine as it contains N31. The E195 M2 CD peptide showed a reduced response to rimantadine, compared to an S31 equivalent, in the *in vitro* dye release assay (Figure 4.2) and this result was reproduced using higher concentrations of the second batch of M2 peptides (Figure 4.10A). A statistically significant and dose responsive reduction in channel activity, compared to the DMSO control, was observed when incubating the S31 CD peptide with rimantadine, but no significant reduction in N31 CD peptide activity was measured. Due to the increased concentration and subsequently increased CF release mediated by the second batch peptides, it was also necessary to increase the concentration of rimantadine to see an effect. Importantly, statistically significant effects and greater reductions in CF were commonly seen at much lower concentrations for novel non-adamantane compounds

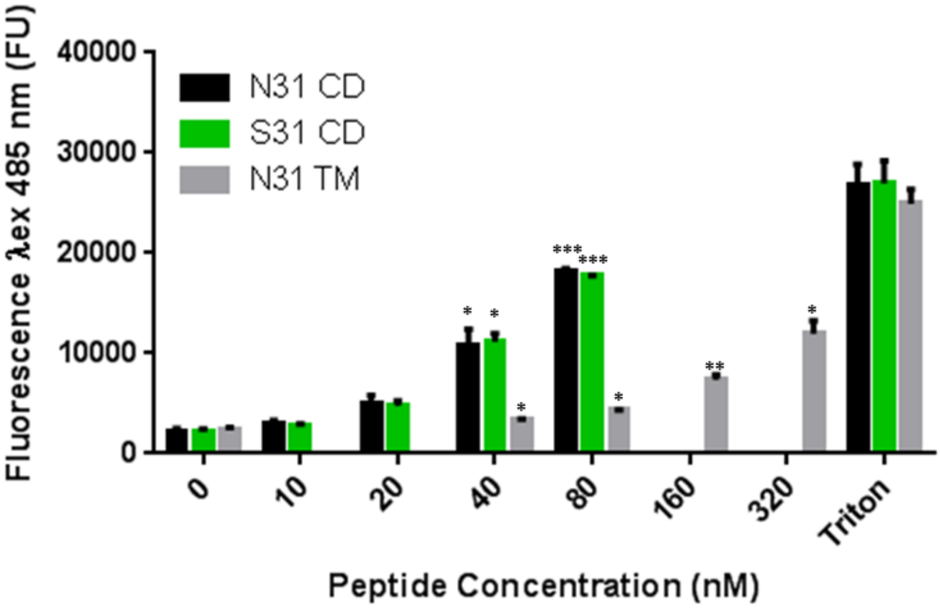

Figure 4.9 An M2 transmembrane domain peptide has reduced activity compared to conductance domain peptides.

CF release from liposomes, measured by fluorimetry (λex = 485 nm, λem = 520 nm), was recorded in real time for increasing concentrations of three M2 peptides (5 % v/v MeOH). N31 and S31 conductance domain peptides (N31 CD and S31 CD) were tested alongside an N31 transmembrane peptide (N31 TM). End point values, calculated by subtraction of liposome only values are shown. Triton-X 100 (5 % v/v, Triton), which lyses liposomes was used as a positive control. Data is from a single experiment carried out in duplicate, error bars represent standard deviation. Paired t-tests were carried out, on raw values once liposome background was subtracted, to assess statistical significance between the solvent control and each concentration of peptide (= $p \leq 0.05$, ** = $p \leq 0.01$, *** = $p \leq 0.001$).*

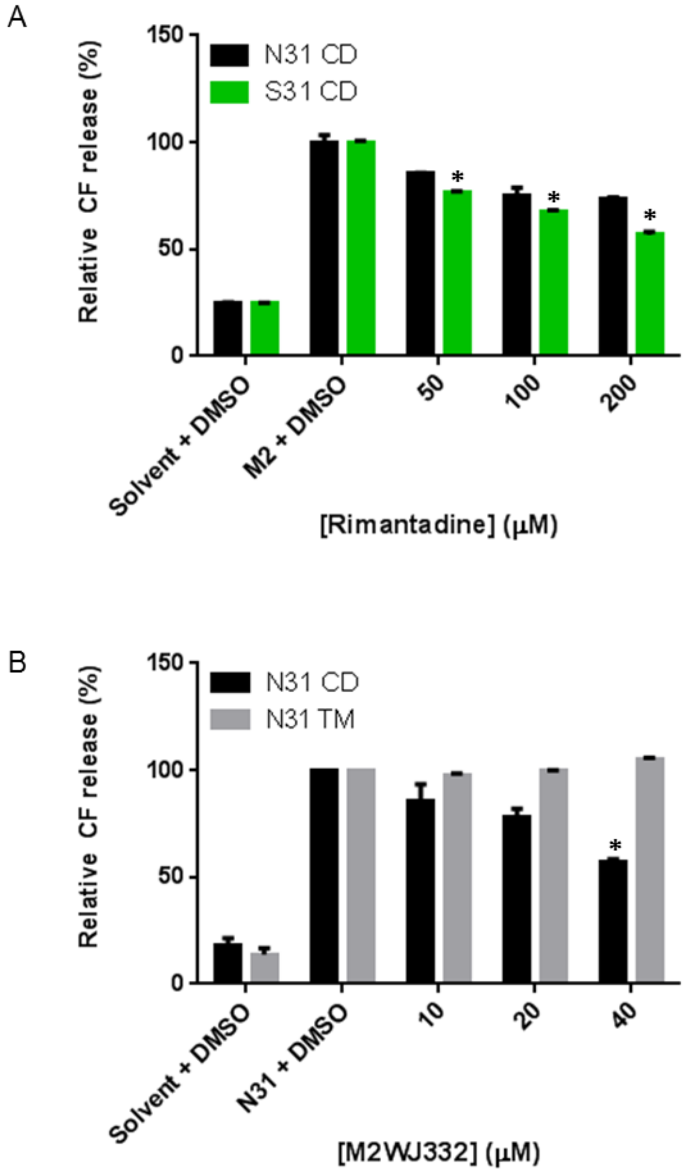

Figure 4.10 M2 peptides can exhibit differential sensitivity to compounds.

Effect of compounds on M2 meditated CF release, measured by fluorimetry (λex = 485 nm, λem = 520 nm), was recorded. End point values, calculated by subtraction of liposome only values and normalised to the peptide + DMSO are plotted. A) Effect of preincubation (for 1 hour) of increasing concentrations of rimantadine (1 % v/v DMSO) on activity of 40 nM conductance domain peptides (N31 CD and S31 CD, 5 % v/v MeOH). Data is from one duplicate experiment. B) Effect of M2WJ332 on activity of 320 nM transmembrane (TM) and 40 nM conductance (CD) domain N31 peptides (5 % v/v MeOH). Data is the average of two separate duplicate experiments. Error bars represent standard deviation. Paired t-tests were used to determine statistical difference between peptide + DMSO and each concentration of compound (= p ≤ 0.05).*

(Figure 4.6 and Figure 4.7), hence there was improved potency with novel compounds compared to rimantadine.

M2WJ332 has been shown to inhibit N31 M2 in electrophysiology studies and plaque assay using a H3N2 N31 IAV strain (Wang *et al.*, 2013b). NMR studies have shown it bound within the lumen of the M2 TM domain tetramer (PDB 2LY0). This study used a TM domain structure, but full length M2 in their electrophysiology and virus culture work. As our *in silico* docking was unable to determine the preferred binding site (Figure 3.5), it was decided to test the binding site preference of M2WJ332 utilising the *in vitro* dye release assay, by comparing CD and TM peptides. Surprisingly, when preincubated with either N31 CD or N31 TM peptides M2WJ332 demonstrated a preferential inhibition of the N31 CD peptide. CF release mediated by N31 CD was reduced with increasing concentrations of M2WJ332 (Figure 4.10B) and with comparable potency to novel non-adamantane compounds (Figure 4.6 and Figure 4.7), whereas the N31 TM peptide was unaffected. This data suggests M2WJ332 has a functional preference for the peripheral binding site, present in its entirety in the CD peptide, and in direct contrast to the published NMR structure (PDB 2LY0) (Wang *et al.*, 2013b).

4.5 Dissecting binding preferences and improving potency of novel non-adamantane compounds

The *in silico* unbiased screen (Section 3.4) selected novel compounds, including those capable of inhibiting N31 M2 in isolation during *in vitro* assays (Figure 4.6 and Figure 4.7). To our knowledge, these were the first non-adamantane compounds able to reduce infectious titre of a rimantadine-resistant virus N31 strain (Figure 4.8). Following the demonstration that compounds can have different effects on the two M2 peptides (Figure 4.10), predicted lumenal binders L1 and L4, alongside predicted peripheral binder P6 were assessed for their ability to reduce activity of the N31 TM versus N31 CD peptides. The hypothesis stood that compounds binding at the peripheral binding site would exert greater effects on the CD peptide compared to the TM peptide, as a portion of the peripheral binding site is absent from the TM peptide (Figure 3.3); as such the TM peptide was considered to have a “partial” peripheral binding site.

The effects of unbiased compounds L1, L4 and P6 on N31 CD peptide (Figure 4.6 and Figure 4.7) were reproduced. All three compounds showed a dose dependent reduction in CF release that was significant compared to the DMSO control above 20 µM (Figure 4.11) and in the case of L1 was also significant at 10 µM, the lowest concentration tested. The reduction in relative CF release was much improved compared to measurements for rimantadine against the S31 peptide; novel compounds resulted in a greater than 50 % reduction at 40 µM (Figure 4.11), this degree of reduction was not reached even when using 200 µM rimantadine against S31 M2 (Figure 4.10A). Likewise at 40 µM, M2WJ332 did not result in even a 50 % reduction in CF release mediated by N31 CD (Figure 4.10B), despite it being effective in virus culture, supporting that improvement is achievable by diverging away from adamantane derivatives.

Both of the compounds predicted to be lumenal binders by *in silico* docking (Figure 3.7), L1 and L4, exerted similar effects on both N31 CD and TM peptides across the concentration range tested (Figure 4.11). These data supported the binding of L1 and L4 at the lumenal binding site. Compound P6 was assigned as a peripheral binder based upon *in silico* docking (Figure 3.8). At 20 µM P6 significantly reduced N31 CD mediated CF release, but not that mediated by the N31 TM peptide (Figure 4.11). However, at higher concentrations P6 reduced, to a similar extent, the CF release by each peptide (Figure 4.11). This is compared to M2WJ332 which demonstrated a clear preference for the CD peptide (Figure 4.10B). We hypothesise, that an ability to inhibit the CD peptide at low concentrations and both peptides at higher concentrations, may suggest that P6 was a peripheral binder. At higher concentrations of compound, P6 can interact with the partial peripheral binding site to still exert some effect. It cannot be ruled out that P6 does interact with the lumenal binding site, ambiguity warranted further investigation, via SAR analysis.

4.5.1 Does peptide preference of unbiased compounds change with alterations in chemical structure?

Limited SAR studies were carried out to investigate which chemical groups were important for activity and peptide preference of unbiased non-adamantane compounds. From the seven novel compounds shown to have an effect against E195 infectious virus titre (Figure 4.8B), three compounds were selected based upon the reproducibility of *in vitro* results, purity of compound (using Liquid Chromatography Mass Spectrometry (Dr Charlotte Revill), Appendix Figure A.3) and potential for SAR. Four analogues were selected for each of L1, L4 and P6 (Table 4.1) and screened at 40 µM for their effects on N31 CD and TM peptides.

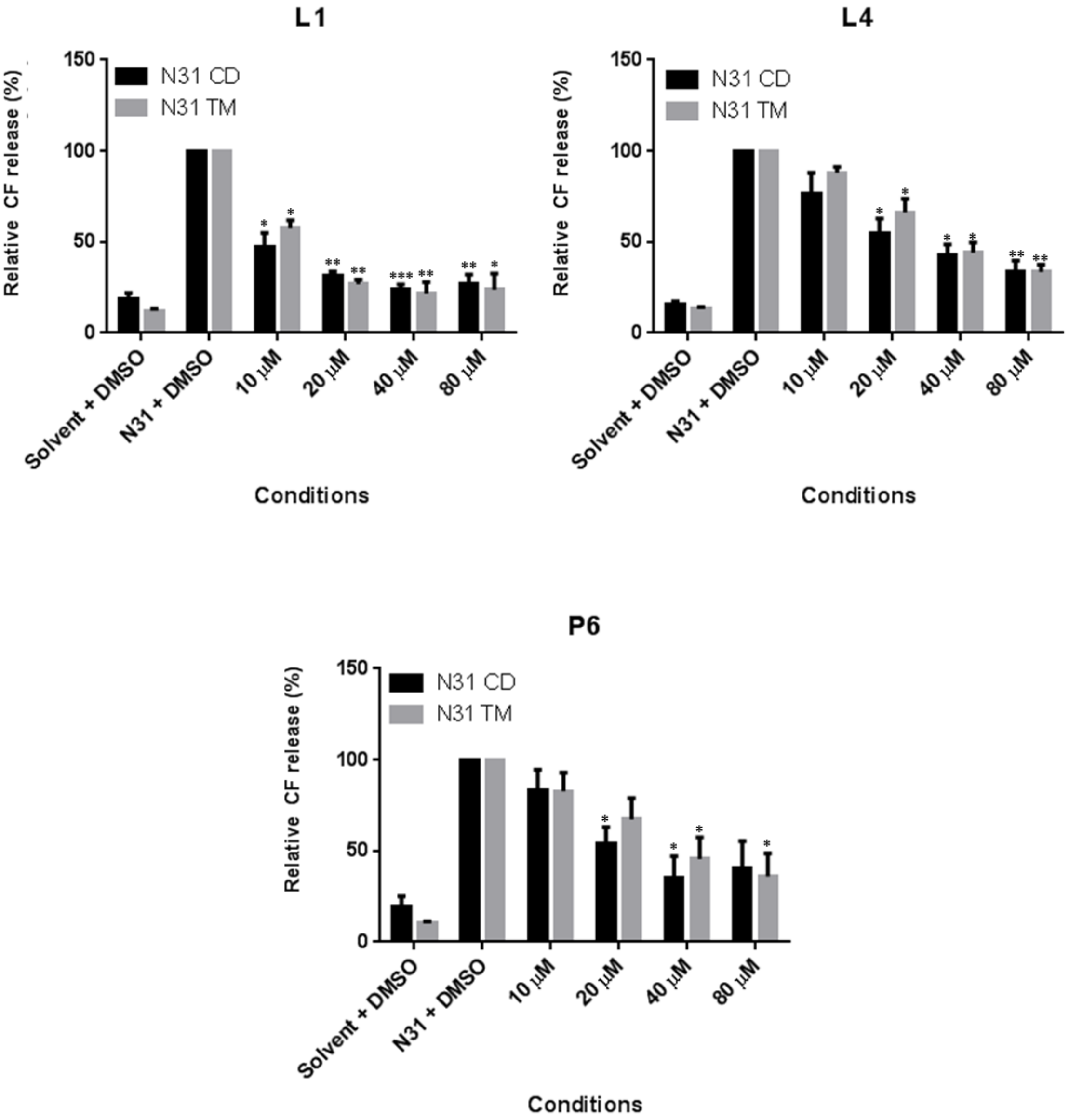

Figure 4.11 Dose dependent effect of unbiased compounds on the activity of transmembrane (TM) and conductance domain (CD), E195 M2 peptides.

Compound in 1 % v/v DMSO were preincubated with N31 peptides in 5 % v/v MeOH. Liposome subtracted end point data was normalised to the N31 + DMSO value, to assess effects on ion channel activity. Data shown is the average of three independent duplicate experiments. Error bars represent standard error between the means of thee experiment. Paired t-tests were used to determine statistical difference between N31 + DMSO and each concentration of compound (= p ≤ 0.05, ** = p ≤ 0.01).*

Analogues L1.1 and L1.2 only differ very slightly from the original compound structure, each lacking one of the methoxy groups present on the single benzene ring of L1 (Table 4.1). These changes had little effect on the ability of the compounds to inhibit both CD and TM peptides (Figure 4.12). Compounds L1.3 and L1.4 were not able to significantly affect M2 mediated CF release (Figure 4.12) and both had more drastic changes to their chemical structures, notably the napthyl ring being replaced by a single aromatic ring. The predicted docking poses for L1.3 and L1.4 were also quite different from that of L1 (Figure 3.7 and Figure 3.12), which could also explain the loss of activity against E195 M2 peptides.

None of changes introduced to L4 to generate analogues improved *in vitro* activity against either peptide (Figure 4.12). The benzyl ester of L4 was found to be important for activity, as when it was removed in L4.3 (a carboxylic acid, Table 4.1), there was complete ablation of inhibitory activity (Figure 4.12). Similarly, replacement of the ester for the amide in L4.1, also showed no effects upon M2 mediated CF release. However L4.4, which only lacked the ester group and not the aromatic ring, maintained its inhibitory activity against each of the peptides (Figure 4.12). In the 40 µM screen L4.2 only significantly reduced the CF release mediated by the CD peptide (Figure 4.12), suggesting the chemical structural changes altered the binding site of the compound, from lumenal to peripheral. This was not predicted from *in silico* docking, where L4.2 was the only one of the L4 analogues predicted to make a strong interaction with the lumenal binding site (Figure 3.16).

Of the four P6 analogues, P6.4 was the only analogue to exert inhibitory effects on the M2 peptides, showing a statistically significant reduction in CF release mediated by both CD and TM peptides (Figure 4.12). It was perhaps not surprising that the other P6 analogues failed to demonstrate activity, as they were quite structurally distinct from the parental compound. Compared to the parental compound that possessed a pyridine ring, in P6.4 this was replaced with a methoxybenzene group, this change was however predicted to quite dramatically change the predicted binding pose of the compound at the peripheral binding site (Figure 3.8 and Figure 3.17).

To further investigate the potential changes in site preference, analogues L1.1, L1.2, L4.2 and P6.4 were tested at a range of concentrations against both N31 CD and TM peptides (Figure 4.13), to assess any concentration dependent effects. Both L1.1 and L1.2 both showed comparable dose dependent effects on both peptides (Figure 4.13), echoing what was recorded for L1 (Figure 4.11).

L1	L4	P6
Original L1 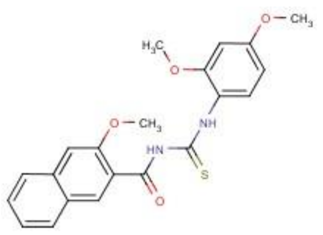	**Original L4** 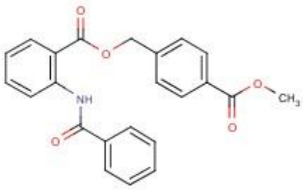	**Original P6** 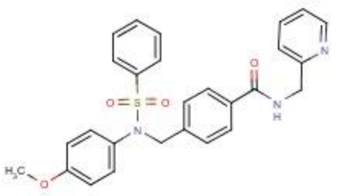
L1.1 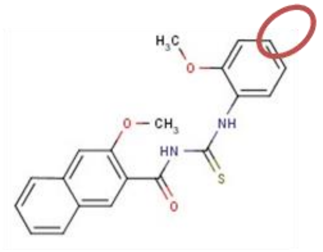	**L4.1** 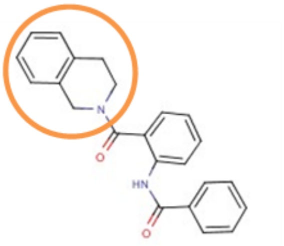	**P6.1** 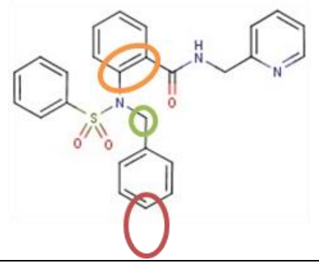
L1.2 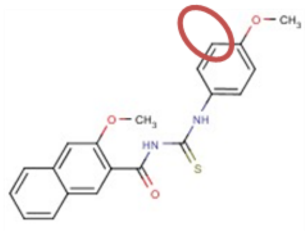	**L4.2** 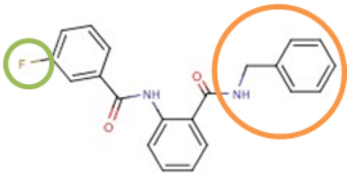	**P6.2** 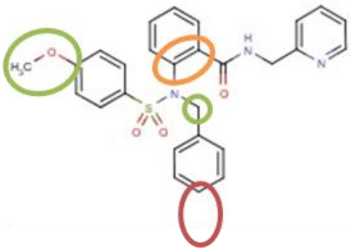
L1.3 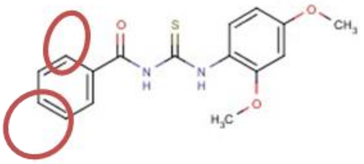	**L4.3** 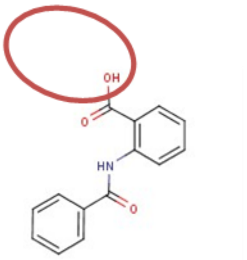	**P6.3** 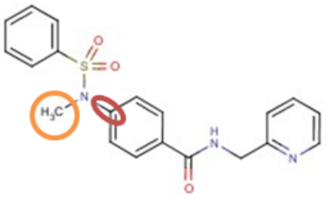
L1.4 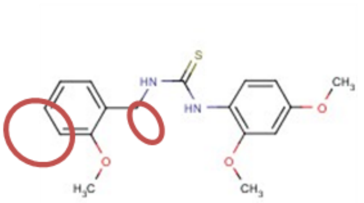	**L4.4** 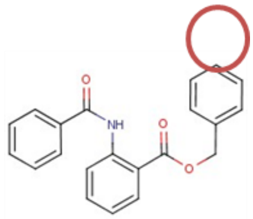	**P6.4** 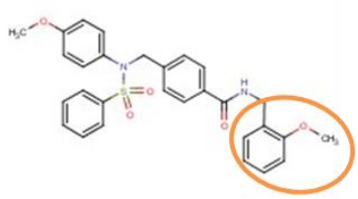

Table 4.1 Structures of L1, L4, P6 and their analogues.

2D representations of the molecular structures of L1, L4 and P6, alongside their respective analogues L1.1-L1.4, L4.1-L4.4 and P6.1-P6.4. Coloured circles represent groups or bonds that have been removed (red), altered (orange) or added (green).

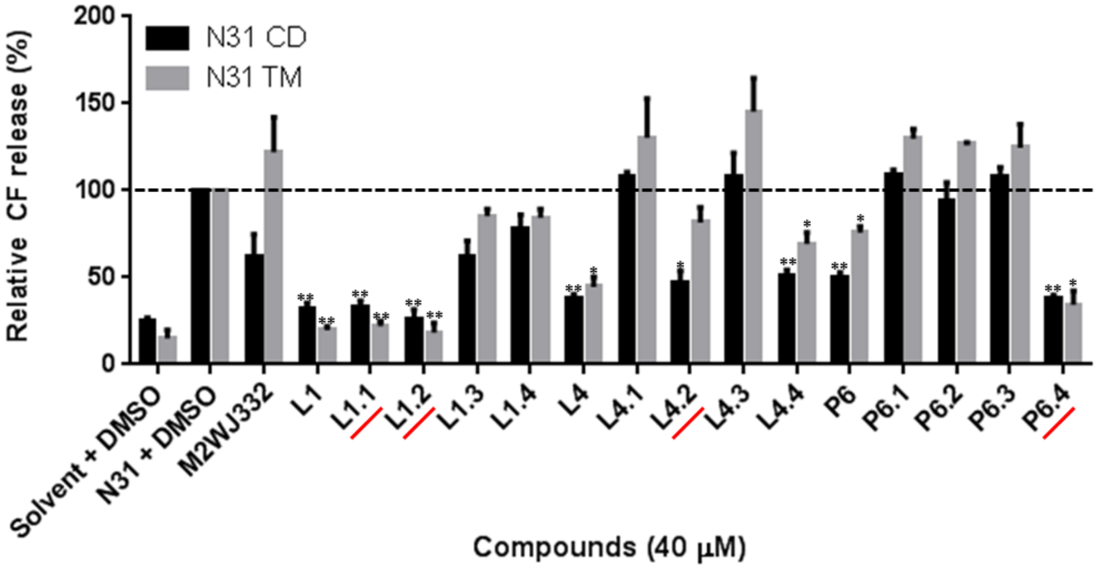

Figure 4.12 Investigating effects of active compound analogues from original unbiased screen, on the activity of transmembrane (TM) and conductance domain (CD), E195 M2 peptides.

Comparison of effects of the activity of two peptides, 40 nM N31 CD and 320 nM N31 TM. Screen of four analogues for each compound at a single concentration, compounds in 1 % v/v DMSO were preincubated with peptide in 5 % v/v MeOH. Liposome subtracted end point value were normalised to N31 + DMSO. Compound ID taken forward to cell culture testing are underlined in red. Data is the average of three separate duplicate experiments. Errors bars represent standard error. Paired t-tests were used to determine statistical difference between DMSO and each concentration of compound (= p ≤ 0.05, ** = p ≤ 0.01).*

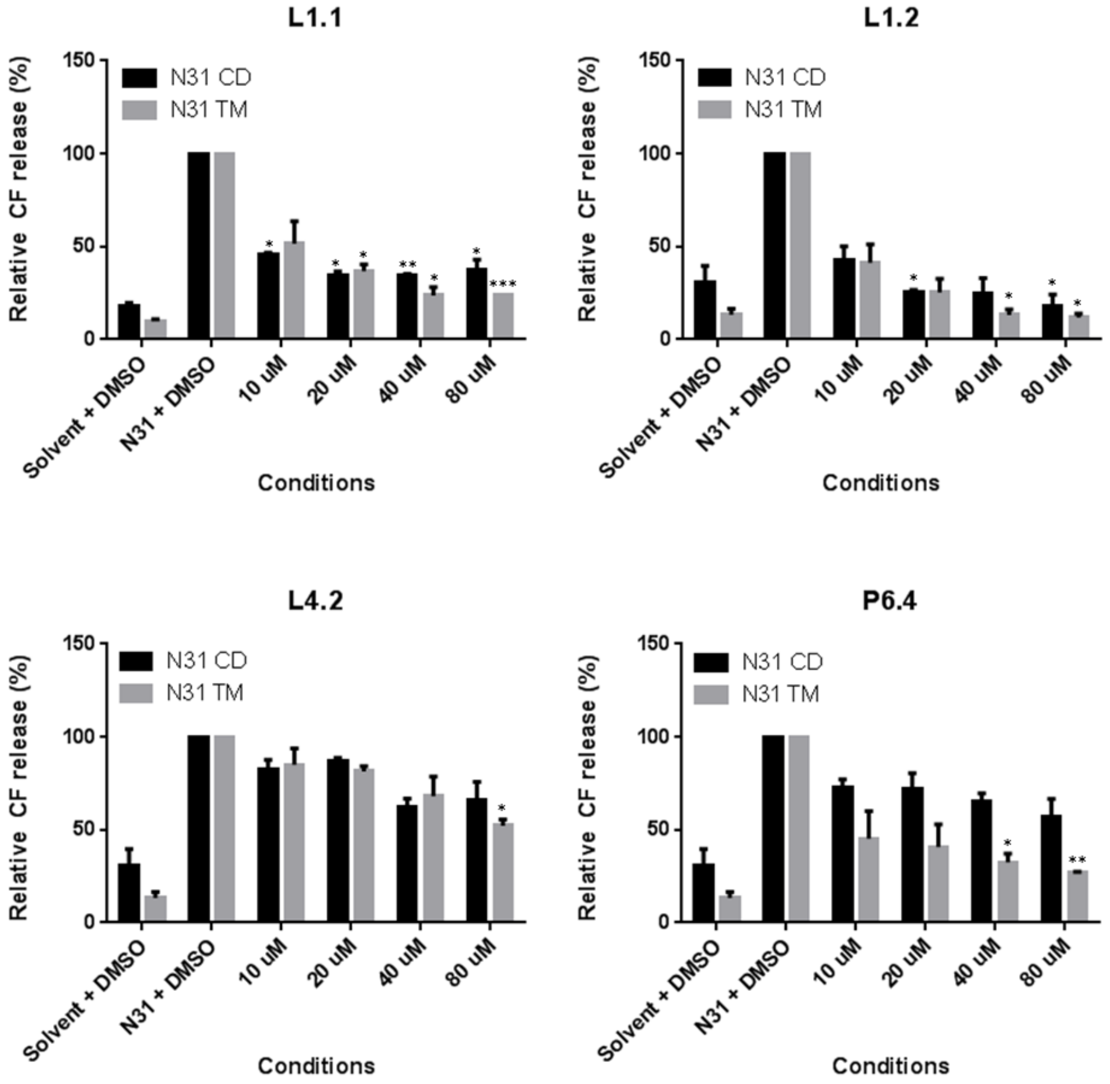

Figure 4.13 Dose dependent effects of unbiased compound analogues on the activity of transmembrane (TM) and conductance domain (CD), E195 M2 peptides.

Comparison of effects of the activity of two peptides, 40 nM N31 CD and 320 nM N31 TM. Compounds in 1 % v/v DMSO were preincubated with peptide in 5 % v/v MeOH, liposomes subtracted end points were normalised to N31 + DMSO control. Data is the average of two separate duplicate experiments. Errors bars represent standard error. Paired t-tests were used to determine statistical difference between DMSO and each concentration of compound (= p ≤ 0.05, ** = p ≤ 0.01, *** = p ≤ 0.001).*

In the 40 µM screen L4.2 had shown a preference for inhibiting N31 CD (Figure 4.12). However, this was not reproduced in the dose dependent experiments, where inhibitory activity is seen against both peptides, indicating lumenal binding. Similarly the inhibitory effects of P6.4 on both peptides in the single compound concentration screen were not reproduced. In the dose dependant experiment P6.4 only showed significant reduction in the activity of N31 TM (Figure 4.13). One explanation for this could be an ability of P6.4 to bind the partial peripheral binding site of the TM peptide. Alternatively the inhibitory effect of P6.4 might be due to differences in the tetramer conformation of the two peptides, with the TM channel being in a more open conformation due to the lack of stabilising helices.

4.5.2 Do unbiased compound analogues have improved effects against E195 virus titre?

Prior to assessing the effect of unbiased compound analogues on virus titre, the compounds were incubated with MDCK cells at concentrations of 20-160 µM for 48 hours to determine any effect on cellular metabolism via MTT assay (Figure 4.14). Of the compounds tested, L4.2 was the only one to have an adverse effect on cellular metabolism and this was only evident at the lowest concentration tested (Figure 4.14), as such this was thought to be an artefact. There was an increase in relative OD_{550} with L1.1 and L1.2, we have not been able to determine why this is, but they are not thought to be toxic. This was determined by carrying out, in parallel to the MTT assay, an assessment on the effects of L1.1, L1.2 and L4.2 on cell confluency. At the 48 hour time point, instead of adding the MTT reagent, cell confluency was assesses using an IncuCyte® ZOOM (Essen BioScience). None of the cell monolayers were affected by the presence of compound (Appendix Figure A. 4).

Re-optimisation of virus culture in Leeds demonstrated that experiments were more efficient with an increased MOI, as such the MOI increased ten-fold from 0.001 to 0.01. In order to make comparisons between previously tested compounds, it was necessary to test compound analogues alongside their parental unbiased compounds for effects on virus spread. Zanamivir, the licensed neuraminidase inhibitor, was included as a positive control in plaque assays, as pH1N1 swine ‘flu is sensitive to this antiviral (Dawood *et al.*, 2009). The data shown in Figure 4.15 is only from one assay where each condition was performed in triplicate. These results are representative, further repeats can be found in the appendix (Figure A.5).

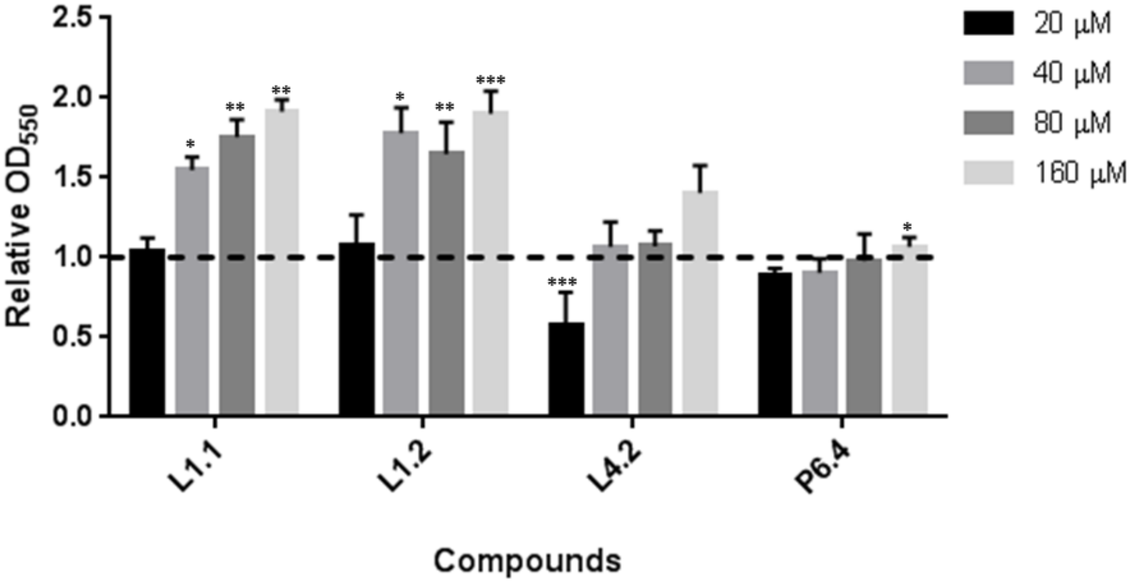

Figure 4.14 Analogues of L1, L4 and P6 do not exhibit adverse effects on MDCK cell metabolism.

Effect of increasing concentrations of novel non-adamantane compounds on MDCK cell metabolism, measured via MTT. Results were taken after 48 hr and normalised against the appropriate DMSO control (0.4-1.6 % v/v). Error bars represent standard deviation of three or four wells. Paired t-tests were carried out, on raw values, to assess statistical significance between DMSO and each compound (= p ≤ 0.05, ** = p ≤ 0.01, *** = p ≤ 0.001).*

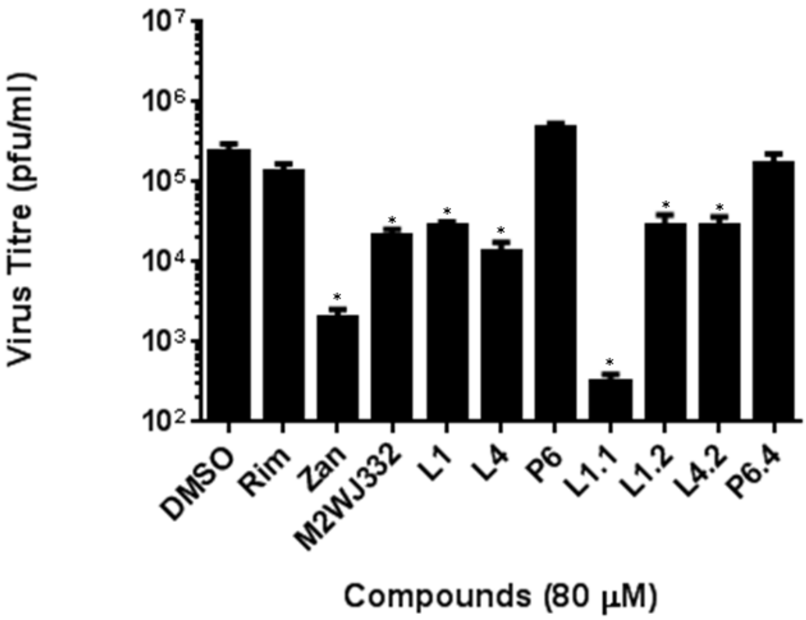

Figure 4.15 Effect of unbiased compounds and their analogues on E195 virus titre.

E195 virus titre is reduced by novel compounds at 24 hours post an infection of MOI 0.01. Results are representative of at least three independent experiments. Error bars represent standard deviation over three wells, paired t-tests were carried out to assess statistical significance between DMSO and compounds (= p ≤ 0.05).*

As seen in initial experiments carried out at Imperial College London (Figure 4.8), L1 and L4 both showed a significant reduction in virus titre, by at least a $\log_{10}$ reduction, at 24 hpi (Figure 4.15). However, P6 did not cause a reduction in virus titre (Figure 4.15) and across all repeats modest or no reduction in virus titre was observed (Figure A.5). This could perhaps be attributed to the increased MOI of 0.01.

The *in vitro* dye release assay was unable to detect any difference between the effects of L1 and two of its analogues, L1.1 or L1.2, on M2 mediated CF release (Figure 4.12 and Figure 4.13). However, when tested alongside one another in culture, L1.1 showed a dramatic improvement in effect against E195 virus (Figure 4.15), with a 1-2 $\log_{10}$ improvement compared to parental compound L1. It also was improved versus the licensed neuraminidase inhibitor zanamivir, which was used as a positive control.

Analogue L4.2 showed no difference compared to L4, with both having statistically significant effects. The effects of P6.4 were more reproducible compared to parental compound P4, but the effects were not statistically significant when compared to the DMSO control (Figure 4.15).

4.6 Effects of compounds derived from a biased screen on M2 channel activity and E195 virus titre

Compound effects on CD and TM N31 peptides were assessed by screening via the *in vitro* dye release assay, using a single concentration of 40 µM. Four of the 10 predicted lumenal binders, DL1, DL3, DL7 and DL11, reduced CF release mediated by both peptides. A further four, DL2, DL4, DL10 and DL12 reduced activity of TM peptide whilst either having no effect on CD peptide or causing “hyperactivation”. Hyperactivation, where there is an increase in relative fluorescence due to drug treatment, is an artefact that has previously been observed when using the dye release system (personal communication, Dr Stephen Griffin). The remaining two compounds, DL10 and DL17, had little effect on the CF release mediated by the TM peptide, but caused hyperactivation of N31 CD (Figure 4.16). Eighteen predicted peripheral binders were tested. Of these, only DP14 showed inhibitory effects against both peptides, whilst DP9 only showed effects on N31 CD (Figure 4.16). Many of the compounds also increased the relative CF release mediated by the N31 CD peptide, and others showed no effect on either peptide.

From the *in vitro* screen, any compounds seen to exert inhibitory effects (without evidence of hyperactivation), were taken forward to assess their effects on MDCK cell

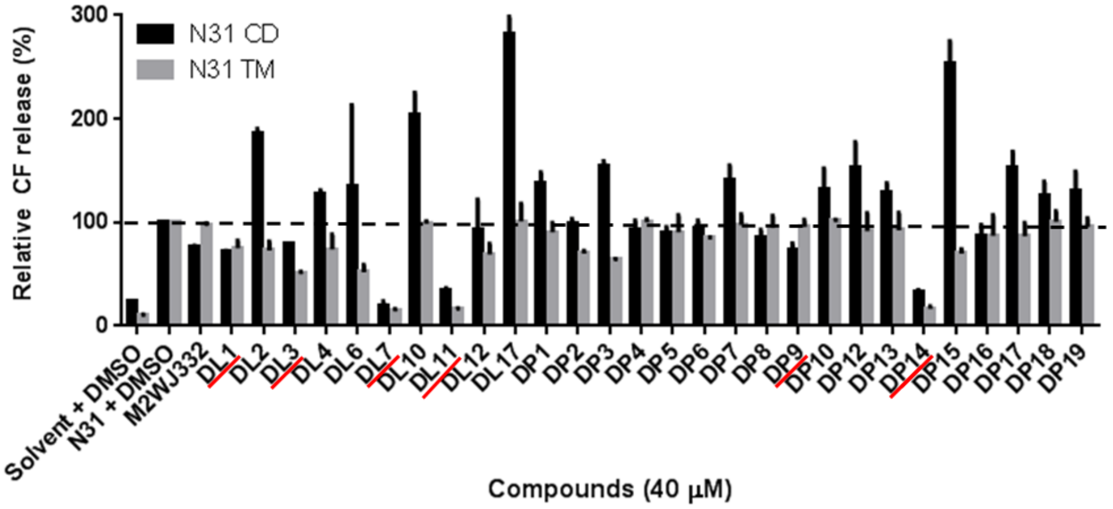

Figure 4.16 Effects of biased compounds on channel activity of transmembrane (TM) and conductance (CD) domain E195 M2 peptides *in vitro*.

Comparison of effects of the activity two peptides, 40 nM N31 CD and 320 nM N31 TM, a single concentration screen of all compounds. Compounds in 1 % v/v DMSO were preincubated with peptide in 5 % v/v MeOH, liposome subtracted end points were then normalised to N31 + DMSO control. Compound ID taken forward are underlined in red. Data is average of one duplicate experiment, error bars represent standard deviation.

metabolism (Figure 4.17A). Except for DL3, compounds were seen to exert no adverse effects. These compounds were then taken forward into virus culture, with reduction in virus titre assessed at 24 hpi (Figure 4.17B). Both DL7 and DP9 showed reproducible reductions in virus titre across three experiments; two further repeats can be found in the appendix (Figure A.6).

To ascertain more about the peptide preferences and potential binding of DL7 and DP9, these compounds were then tested at a range of concentrations against both N31 peptides *in vitro,* (Figure 4.18). From the original 40 µM screen, the effect of DL7 was similar on both peptides suggested it to be a lumenal binder (Figure 4.16), this was reproduced. At highest concentrations DL7 had a comparable inhibitory effect against both peptides, but at the lower concentrations the effect was greatest against the CD peptide (Figure 4.18). The ability to inhibit both peptides comparably at high concentration was also observed for P6 (Figure 4.11), so this result could be attributed to DL7 having the ability to bind the partial peripheral site present in the TM peptide when the compound is at a high enough concentration. Predicted peripheral binder, DP9 had little effect on the N31 TM peptide at any concentration, yet there was a dose dependent reduction in N31 CD mediated CF release up until 40 µM, supporting the predicted binding preference and showing a similar profile to M2WJ332 (Figure 4.10B). Increasing the concentration of DP9 to 80 µM did not improve the effect (Figure 4.18).

4.7 **Effect of non-adamantane compounds on S31 peptide**

Although the majority of circulating strains of IAVs are resistant to amantadine and rimantadine, an assessment to determine if novel non-adamantane compounds can also inhibit rimantadine-sensitive M2 was undertaken. As it was not possible to use a recombinant, rimantadine-sensitive N31S virus (personal communication, Dr Ruth Elderfield, Imperial College London), due to local risk assessments not permitting the use of genetically modified influenza, an N31S peptide was utilised in isolation. N31 CD and S31 CD peptides have comparable dose dependent effects of CF release from liposomes (Figure 4.9). The majority of compounds tested exerted similar effects on both peptides (Figure 4.19), except for M2JW332 and DP9, where there was a greater reduction in CF release mediated by the N31 CD peptide. The effects of compounds L1, L1.1, L1.2, L4 and DL7 achieved statistical significance, compared to the DMSO control ($p \leq 0.05$), yet this was not the case for L4.2, P6 and P6.4 which only achieved statistical significance against the S31 peptide. However, the data approached

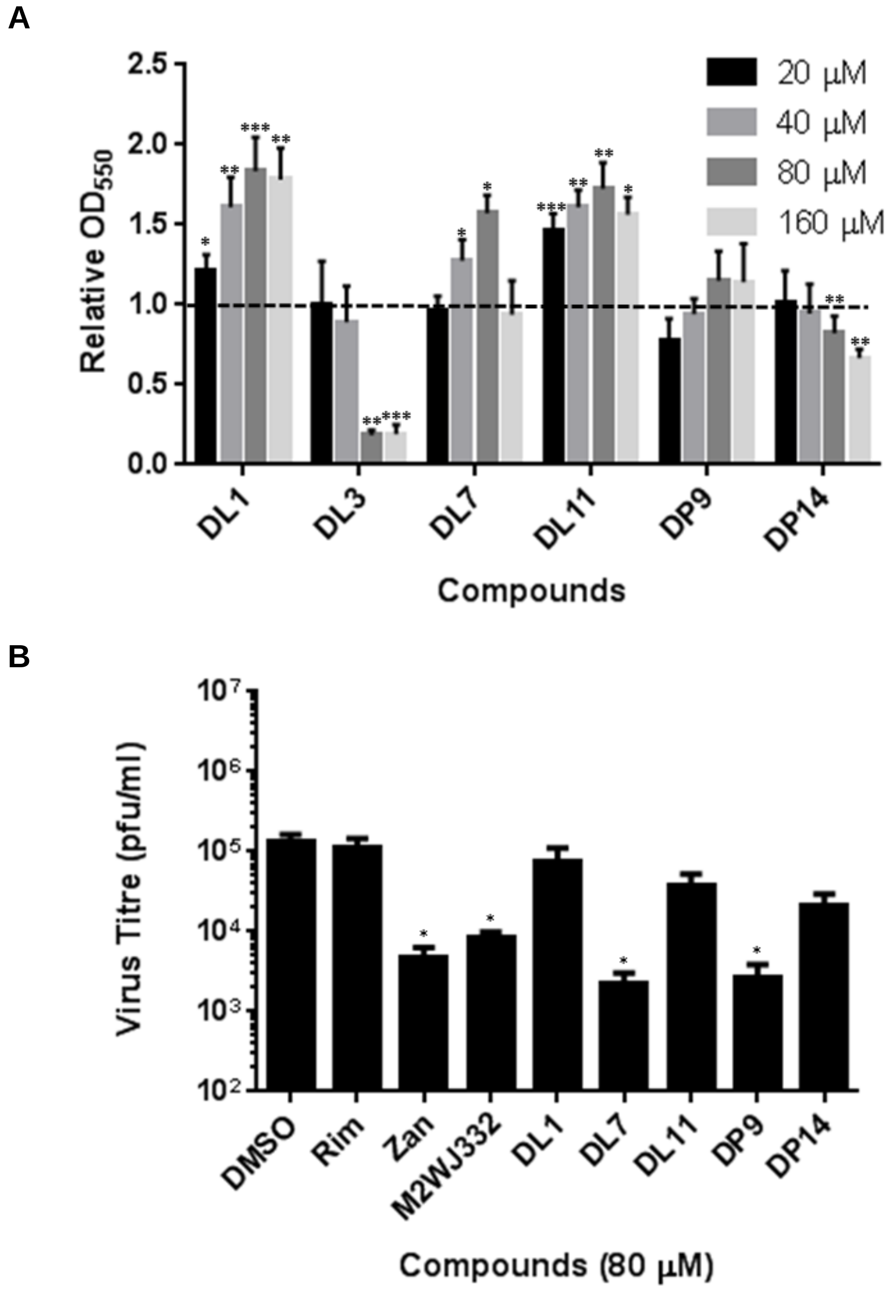

Figure 4.17 Biased screen compounds reduce E195 virus titre, without affecting MDCK cellular metabolism.

A) Effect of increasing concentrations of novel non-adamantane compounds on MDCK cell growth, measured via MTT. Results were taken after 48 hr and normalised against the appropriate DMSO control (0.4-1.6 % v/v). Error bars represent standard deviation of three or four wells. B) Effects of compounds on virus titre 24 hpi with virus added at an MOI of 0.01, data shown is of one experiment in triplicate, but is representative of 3 experimental repeats (see Appendix Figure A.6). Paired t-tests were carried out, on raw values, to assess statistical significance between DMSO and each compound (= p ≤ 0.05, ** = p ≤ 0.01, *** = p ≤ 0.001).*

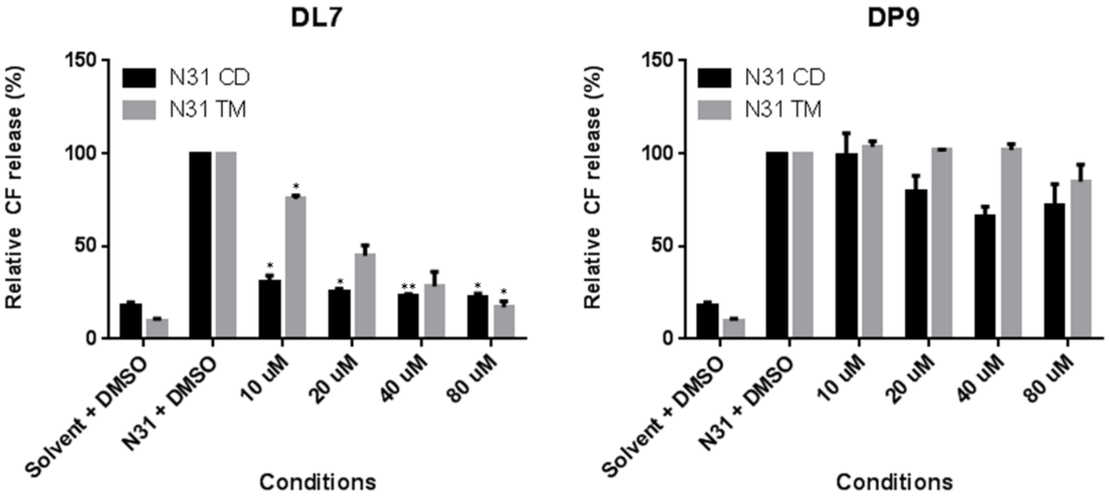

Figure 4.18 Dose dependent effects of biased screen compounds on CF release mediated by transmembrane (TM) and conductance (CD) domain E195 M2 peptides *in vitro*.

Comparison of effects of the activity two peptides, 40 nM N31 CD and 320 nM N31 TM. DL7 and DP9 in 1 % v/v DMSO were preincubated with peptide in 5 % v/v MeOH, liposome subtracted end point values were normalised to N31 + DMSO. Data is the average of two independent duplicate experiments. Errors bars represent standard error. Paired t-tests were used to determine statistical difference between N31 + DMSO and each concentration of compound (= p ≤ 0.05, ** = p ≤ 0.01).*

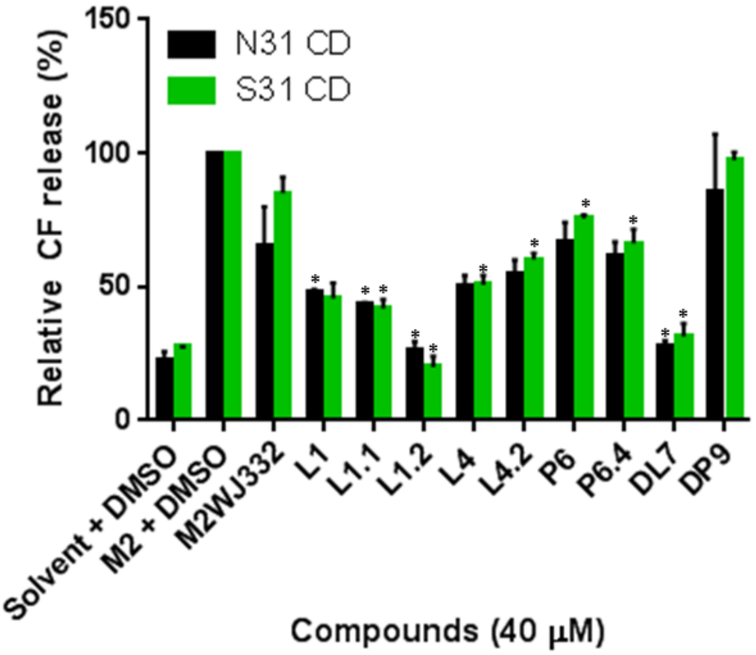

Figure 4.19 Comparison of compound effects against WT (N31) and mutated (S31) conductance domain M2 peptides activity *in vitro*.

Comparison of effects of the activity two peptides, 40 nM N31 CD and S31 TM. Compounds in 1 % v/v DMSO were preincubated with peptide in 5 % v/v MeOH, liposome subtracted end point values were normalised to peptide + DMSO. Data is the average of two independent duplicate experiments, errors bars represent standard error. Paired t-tests were carried out, on raw values, to assess statistical significance between M2 + DMSO and each compound (= p ≤ 0.05).*

significance for compounds L4 and L4.2 (p = 0.051 and 0.074), indicating further experimental repeats may have improved variability.

4.8 **Assessing potency of novel effective compounds**

Thus far, compounds were tested against E195 virus at a single screening concentration of 80 µM (Figure 4.8B, Figure 4.15 and Figure 4.17B), a value similar to that used by other groups (Balannik *et al.*, 2009; Wang *et al.*, 2013b). However, these results do not give a true indication of compound potency. In order to determine whether single compounds show promise as the basis of future therapies, IC_{50} values were determined. Compounds L1.1, DL7 and DP9 were selected primarily based upon reproducible effects in virus culture experiments (Figure 4.15 and Figure 4.17B). Virus was preincubated with compounds at a range of concentrations, spanning from 80 nM to 80 µM. After 30 minutes virus-compound mixtures were then used in a one hour infection, 24 hpi supernatants were serially diluted to establish the resultant infectious virus titre.

Virus titre was calculated as an average over three wells and converted to a percentage of DMSO control. Data was inputted into GraphPad (Prism), which was used to fit a sigmoidal curve (Figure 4.20) and calculate IC_{50} values (Table 4.2). M2WJ332, L1.1 and DL7 all had complete sigmoidal curves, so an accurate IC_{50} value could be calculated. All compound IC_{50}s were in the low micromolar range. Despite having very similar IC_{50}s, the 95 % confidence intervals varied between the compounds, with M2WJ332 having the narrowest (0.720 to 1.94) and L1.1 having the largest range (0.154 to 11.44). The confidence interval for L1.1 would likely have been reduced by the presence of a data point between 0.25 and 2.5 µM, between which the IC_{50} was calculated. On the other hand DP9 was not as potent against E195 virus and in order to establish a reliable IC_{50} value it would have been necessary to extend the concentrations beyond 80 µM. However, it was possible to say that the IC_{50} was greater than 25 µM, but below 80 µM.

As the calculated “top” and “bottom” of the curves varied between the compounds (Table 4.2), addition analysis was carried out for M2WJ332, L1.1 and DL7, where the top and bottom of the curves were forced to 100 and 0 %, respectively (Table 4.3). A slight increase in the IC_{50} values occurred when setting the new limits, but this also allowed for a more accurate calculation and comparison of IC_{90} values between compounds. As depicted from the titration of the compounds (Figure 4.20) and

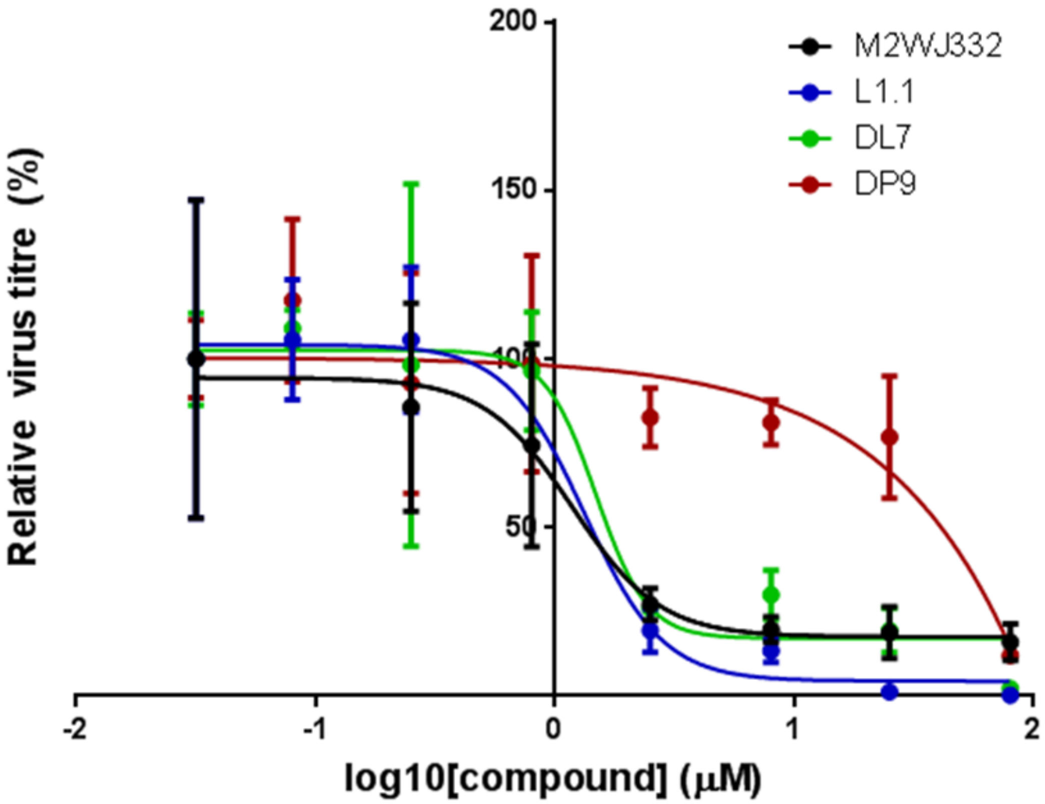

Figure 4.20 IC_{50} curves for novel M2 inhibitors against the E195 swine influenza.

Half log_{10} increments from 80 nM to 80 µM of novel compound were preincubated with E195 virus at an MOI of 0.01, prior to a one hour infection. The infectious supernatant at 24 hpi was titred via plaque assay; resultant titres were normalised to DMSO. Each condition was performed in triplicate wells in one experimental repeat. Error bars represent one standard deviation. GraphPad software was used to fit a sigmoidal IC_{50} curve to the data.

Compound	Calculated IC_{50} (µM)	Top of curve (relative virus titre %)	Bottom of curve (relative virus titre %)	95 % confidence interval
M2WJ332	1.183	94.38	17.55	0.720 to 1.94
L1.1	1.325	104.2	4.445	0.154 to 11.44
DL7	1.482	102.5	17.11	0.626 to 3.51
DP9	1372	99.97	-991.0	-

Table 4.2 Calculated IC_{50} values for novel M2 inhibitory compounds against E195 swine influenza.

Half $\log_{10}$ *increments from 80 nM to 80 µM of novel compound were each preincubated with E195 virus at an MOI of 0.01, prior to a one hour infection. GraphPad (Prism) software was used to fit a sigmoidal curve and determine* IC_{50} *values.*

Compounds	IC_{50} (µM)	IC_{90} (µM)
M2WJ332	1.668	20.54
L1.1	1.470	3.54
DL7	2.287	11.74

Table 4.3 Calculated IC_{50} and IC_{90} values for novel M2 inhibitory compounds against E195 swine influenza.

Half $\log_{10}$ *increments from 80 nM to 80 µM of novel compound were each preincubated with E195 virus at an MOI of 0.01, prior to a one hour infection. GraphPad (Prism) software was used to fit a sigmoidal curve, with the top and the bottom of the curves set to 100 and 0 %, respectively, and determine* IC_{50} *and* IC_{90} *values.*

previous 80 µM experiments (Figure 4.15), at higher concentrations L1.1 treatment results in a greater reduction in virus titre than the other compounds tested. This is also seen in the calculated IC_{90} values, where there is a greater spread compared to IC_{50} values, with the M2WJ332 IC_{90} five times that of L1.1.

4.9 **Discussion**

Novel non-adamantane compounds have been identified that affected M2 in isolation during *in vitro* assays, but also significantly reduced the infectious titre of rimantadine-resistant N31 IAV, which has not previously been demonstrated. In addition, through development of an *in vitro* assay utilising both N31 CD and TM peptides, distinct functional preferences were observed: compounds with an ability to inhibit CF release mediated by both peptides were denoted as lumenally targeted compounds whereas those with a preferential inhibition of the CD peptide were denoted as peripherally targeted compounds. Our data support the presence of two distinct binding sites on the M2 tetramer, both of which can be targeted separately with novel compounds.

Activation by protons has been shown to be required for the activity of M2 (Pinto *et al.*, 1992). This is achieved in acidic pH when a third H37 residue becomes protonated, $pK_a = 6.3$ (Hu *et al.*, 2006). As a result the gating residue W41 is rotated (Tang *et al.*, 2002), permitting conductance. M2 has also been shown to have a preference for conducting protons (Balannik *et al.*, 2010; Shimbo *et al.*, 1996); despite this M2 in liposomes was able to allow release of anionic CF in a dose dependent manner (Figure 4.3) (Aschi *et al.*, 2008). This release occurred at neutral pH, but was enhanced by acidic conditions (Figure 4.1). However, acidic pH quenches CF fluorescence (Massou *et al.*, 2000; StGelais *et al.*, 2007) and so it is necessary to readjust the buffer to neutral pH. As such experiments required additional manipulation, so we chose to carry out assays at neutral pH.

Previous viroporin studies, including those from our laboratory, using the CF dye release assay, have presented data as real time traces (Carter *et al.*, 2010; Foster *et al.*, 2011; StGelais *et al.*, 2007; Wetherill *et al.*, 2012) and calculated initial / reaction rates (StGelais *et al.*, 2009; StGelais *et al.*, 2007; Wetherill *et al.*, 2012). The real time traces provide a lot of information, including the maximum fluorescence reading, an indication of the rate of the reaction and the time taken, or whether a plateau of fluorescence is reached. Initial / reaction rates provide a means of interpreting the kinetics of the reaction, where many complex factors are at play, including oligomerisation, membrane insertion and opening of the channel complex. There is some inconsistency concerning the data used in the calculation of rates, where either arbitrarily using the values for the initial 5 or 6 minutes (StGelais *et al.*, 2009; StGelais *et al.*, 2007) or defining the linear section of the curve (Wetherill *et al.*, 2012). Whether the first experimental reading or a fluorescence reading of zero was used, in rate determination, can also have a great impact on the resultant calculated rate.

The *in vitro* activity of M2 peptides was much higher than other viroporins tested by dye release, including p7 and E5, which typically require a 37 ºC incubation to insert. As a result, nanomolar concentrations of M2 were used as opposed to 1 – 5 µM for other viroporins including p7 and E5 (StGelais *et al.*, 2009; Wetherill *et al.*, 2012). From the real time trace for M2 it was clear that it was not possible to capture the start of the reaction (Figure 4.3A), as the fluorescence value on the first reading was greater than the baseline of liposomes alone. As such, any determination of initial rate would not have been accurate. As each well of the plate was read individually and not simultaneously, a delay of up to 45 seconds between the reading of the first well and the last, potentially having the greatest impact at the start of the reaction, so the decision was taken to look at end point values instead.

Whilst adding increasingly complex functional groups to currently licensed (but not clinically useful antivirals), is helpful in respect to quickly identifying compounds with capabilities of effecting the growth of resistant virus stains (Wang *et al.*, 2013b; Wu *et al.*, 2014b), it does not contribute to answering the controversial mode of action questions that still exist around M2-adamantane binding. *In silico* docking gave predictions of the binding site preference of novel compounds and compounds were given a prefix of "L" or "DL" for predicted lumenal binders of the unbiased and biased screens, respectively. Similarly, prefixes "P" and "DP" were given to compounds predicted to preferentially bind to the peripheral binding sites. Compounds were chosen primarily upon *in silico* binding preference and selectivity, rather than necessarily their potency. Hence, compounds served as tools to further our understanding of M2 binding sites, and the mode of action for inhibitors, with the eventual aim of investigating potential combination therapies that may combat resistance.

An *in vitro* method with the ability to discriminate between the two proposed binding sites was required. The use of two different N31 peptides allowed, for the first time, direct comparison of the TM and CD peptides, allowing differential effects of compounds binding at each site. In order to directly compare both peptides, it was necessary to establish concentrations of peptides that gave comparable activity. The CD has a higher activity compared to the TM domain that is the minimal unit required for activity of M2, in oocytes (Ma *et al.*, 2009). Accordingly, titrations of the peptides revealed that for the same molar peptide concentration, CF release mediated by the TM peptide was significantly lower (Figure 4.9). Hence, peptides were normalised based upon activity, rather than concentration, as this likely reflects the number of inserted, functional channel complexes; 40 nM CD and 320 nM TM peptides were therefore used in inhibition studies. Whilst differences in peptide activity were not surprising based upon published data from oocytes, a number of factors may influence this *in vitro*. The additional residues of the CD peptide form helices with amphipathic properties, which are seen to orientate perpendicular to the TM helices (Schnell & Chou, 2008; Sharma *et al.*, 2010). This might allow interaction with the acidic lipids of the liposome, and so stabilise a more native form of the channel than is possible with the TM peptide (Sharma *et al.*, 2010). Structural studies have also shown that the diameter of the pore at neutral pH is larger for the TM peptide (Schnell & Chou, 2008; Stouffer *et al.*, 2008); this may conceivably affect the efficiency of oligomerisation and insertion into liposomes, as well as drug binding.

Using the CD and TM peptide system, it was possible to assign several compounds as having a functional preference for one or other binding site, which has not previously been attempted. Despite there being a published structure of M2WJ332 bound within the lumen of an M2 tetramer (Wang *et al.*, 2013b), M2WJ332 had a clear and reproducible functional preference for the peripheral binding site, demonstrated by a reduction in CF release mediated by the CD peptide (Figure 4.10B). By contrast, compounds L1 and L4 predicted by *in silico* docking to bind within the lumen (Figure 3.7), exerted effects upon both peptides (Figure 4.11). The peptide used for the 2LY0 structural study (aa 19-49) of M2WJ332 omitted a portion of the peripheral binding site, which was present in the CD peptide used in this study (aa 18-60). The omission of a portion of the peripheral binding site means that it was unlikely that the 2LY0 structure would be able to accommodate any peripheral binding. The electrophysiology data supporting the effects of M2WJ332 on M2 did not use a TM domain, but a full length M2 (Wang *et al.*, 2013b). Consequently functional binding at a particular site was not conclusively demonstrated.

Of the three unbiased compounds tested against both the CD and TM peptides, two were predicted lumenal binders (L1 and L4) and one a predicted peripheral binder (P6). In all studies, L1 and L4 exerted similarly significant effects on both peptides (Figure 4.11 and Figure 4.12), providing experimental support for their predicted binding within the lumen (Figure 3.7). However, the functional preference of P6 was not as clear cut. When tested at single concentration P6 demonstrated preference for inhibiting the CD peptide, suggesting binding at the periphery (Figure 4.12). However, during titrations of P6, this effect was not maintained, with similar reductions in the activity of both peptides at the highest concentrations of P6 (Figure 4.11). This could be explained by the *in silico* docking prediction simply being incorrect and P6 binding at the lumen. Alternatively, another explanation could be that P6 binds at the periphery, as it is the case that when the CD peptide as used there was a reduction in CF release, but at sufficiently high concentrations is able to bind to the partial peripheral binding site of the TM peptide. An account of binding to a peripheral site in the context of a TM peptide has been reported (Cady *et al.*, 2010), when high compound concentrations have been used.

From the biased screen of compounds identified by ROCS analysis of compound D (Section 3.5), many compounds were seen to affect CF release mediated by one or both peptides (Figure 4.16). Of these compounds one predicted lumenal (DL7) and one predicted peripheral (DP9) compound yielded reproducible and significant reductions in infectious E195 titre (Figure 4.17). In the 40 µM screen the predictions from *in silico* screening (Figure 3.9) held true and DL7 showed effects on both peptides, whilst DP9 had a preference for affecting the ion channel activity of only the CD peptide (Figure 4.16). Testing DL7 and DP9 across a range of concentrations, DP9 maintained a preference for the CD peptide (Figure 4.18). DL7, on the other hand, showed a preference of the CD peptide at low concentrations, but at 40 µM and above both peptides were affected to a similar extent (Figure 4.18). Following the reasoning discussed above for P6, compound DL7 could be considered as a peripheral binder, going against *in silico* predictions. Another possibility is that the primary binding site is within the lumen, but at high enough concentrations the peripheral site is also used, as suggested by Cady and colleagues for amantadine (Cady *et al.*, 2010); the different peptides may also exist in slightly different conformations within the system, as has been described for structural studies. Additionally, from this data it cannot be ruled out that DL7 binds at a third, undefined site, not taken into account by using the predefined lumenal and peripheral clip files. With the data available confidence in the functional peptide preference of DL7 and DP9 is reduced. It must be reiterated that the comparison of compound effects on the peptides can only be used as a guide to their site preference, just as the *in silico* docking provided predictions.

In some assays an increase in CF release was observed when compound was present. This hyperactivation could be attributed to the compound destabilising the liposomes, as seen for HMA, a published S31 M2 inhibitor (Balgi *et al.*, 2013), which resulted in a dose dependent increase in fluorescence readout (Appendix Figure A.7A) and even caused release of CF without M2 present (Figure A.7B). An increase in CF release was also observed for M2WJ332, in the biased compound *in vitro* screen, with the N31 TM peptide (Figure 4.16). In this case, the increase was clearly not due to M2WJ332 affecting the liposomes, as the same compound caused a reduction in fluorescence when incubated with the N31 CD peptide. It has been proposed that binding of rimantadine to the peripheral site of a closed tetramer makes it harder for the channel to open (Schnell & Chou, 2008). It could therefore be proposed that compound binding could also result in destabilisation of the closed channel structure, or stabilisation of the open structure, causing an increase in channel activity. If M2WJ332 was able to bind to the TM peptide, potentially at the partial peripheral site and cause a conformational change, meaning it remains in a more active configuration, this could explain the hyperactivation.

The premise of using TM and CD peptides as an indication of binding preference relied on lumenal compounds being able to inhibit both peptides, with peripheral compounds having a preference of the CD peptide. Compounds preferentially or only inhibiting the TM peptide, may be caused by conformational changes as a result of binding at the peripheral site, locking the channel in an open conformation. However, compounds exhibiting this effect do not fit into our system of binding site prediction, so as a result were not taken forward.

As cell death attributed to compound cytotoxicity could potentially be misinterpreted as CPE, cytotoxicity was investigated in isolation. Of all of the compounds tested, only L4.2 and DL3 were seen to cause a significant reduction in the MTT readout, compared to DMSO (Figure 4.14 and Figure 4.17A). For DL3 this occurred at 80 and 160 µM, and was accompanied by a visual disruption of the MDCK cell monolayer. For this reason DL3 was not taken forward. However, the reduction in cellular metabolism of L4.2, was only evident at the lowest concentration tested and was not accompanied by a cell death (Appendix Figure A. 4 and Figure A.8), so it was included for virus culture testing.

A number of compounds resulted in an apparent increase in relative cellular metabolism, evident as an increase in relative OD_{550}. Most notably, cells incubated with L1 at three out of the four concentrations tested had an OD_{550} measurement corresponding to at least a doubled relative metabolic rate. Analogues L1.1 and L1.2, at higher concentrations, also resulted in increased relative cell metabolism readouts (Figure 4.8A and Figure 4.14). Compounds did not affect the confluency of MDCK cells (Figure 4.14), measured using the IncuCyte® ZOOM both in parallel to the MTT assay (Appendix Figure A. 4), and measured on plaque assay producer plates (Appendix Figure A.8). It is known that some reducing compounds can interfere with MTT assays and lead to an increased absorbance. However, none of the compounds tested have strong acidic groups so this is unlikely to be the cause of the relative increase. There is the possibility that the compounds do have effects on cellular processes, such as autophagy. If treatment with compounds leads to an induction of autophagy, this could result in an MTT assay output that indicates an increase in metabolism.

After cytotoxic compounds were eliminated from further study, remaining compounds were taken forward into virus culture experiments. Almost all were seen to exert significant effects on titre. This unusually high hit rate could be attributed to our *in silico* screening and further refinement by dye release assay.

Initial virus inhibition studies, using unbiased compounds, involved taking supernatant at 24 and 48 hpi (Figure 4.8B), where 100 µl of this virus containing supernatant was removed to infect fresh cells, to determine the virus titre. The 100 µl was replenished with fresh media containing 80 µM compound at the 24 hr time point. The significant reduction in virus titre observed at 24 hpi was not maintained at 48 hpi. This could in part be due to the compound being metabolised by the cells and a decrease in relative compound : virus ratio. It was also noted that at 48 hpi there was evidence of high levels of CPE, with subtotal destruction of the monolayer, with the assay now being non-linear due to a decrease in viable cells. The absence of CPE at the earlier 24 hpi time point suggested that the calculated titre was solely as a result of non-lytic viral release after a complete cycle of replication. As significant effects were observed at 24 hpi, it was decided to only titre supernatants at this time point in subsequent plaque assays.

Through both our unbiased and biased compound screens (Sections 3.4 and 3.5), we identified novel compounds capable of exerting similar effects on virus titre as M2WJ332 (Figure 4.15 and Figure 4.17B). Undertaking SAR analysis on effective compounds identified compound L1.1, which had improved antiviral effects in the 80 µM screen, beyond those achieved with M2WJ332, or even the licensed antiviral zanamivir (Figure 4.15). This achievement is noteworthy, as this work was focussed on identifying compounds that could be used as tools to investigate the possibility of two druggable sites of M2, rather than simply finding highly potent compounds.

It is difficult to compare our results to those for adamantane derivatives, seen to reduce infectious virus titre of N31 viruses (Wang *et al.*, 2013a; Wang *et al.*, 2013b), due to the different IAV strains, MOI and compound concentrations used. M2WJ332 was included in our IC_{50} analysis to aid comparison between potency of novel adamantanes and adamantane derivatives. Despite the calculated IC_{50} values of the novel compounds not demonstrating any improvement compared to the amantadine analogue M2WJ332 (Figure 4.20), the IC_{90} value of novel compound L1.1 was calculated to more than a halflog$_{10}$ lower than that of M2WJ332. This could demonstrate an improved ability to reach saturation. In the literature, where EC_{50} values have been established via plaque assay against N31 viruses, the strains used are typically not those currently circulating, but instead A/WSN/1933 (H1N1) (Wang *et al.*, 2013a; Wang *et al.*, 2013b). The best EC_{50} values for the adamantane compounds were 153 nM and 3.2 µM, compared to 328 nM and 22.5 µM for adamantane against the WT S31 and S31N mutants, respectively (Wang *et al.*, 2013a; Wang *et al.*, 2013b). A separate study used a pH1N1 virus for its investigations of adamantane derivatives, with EC_{50} values for many compounds < 10 µM (Kolocouris *et al.*, 2014). These compounds were also tested against two different N31 strains of IAV. In general compounds showed efficacy against A/Puerto Rico/8/1934 (H1N1), but not against A/WSN/1933 (H1N1) (Kolocouris *et al.*, 2014). This further highlights the need to test compounds against clinically relevant strains of IAV.

The concept that M2 plays a role in maintaining the fusion competence of HA, as it is transported to the surface of an infected cell, was first demonstrated in H7 strains (Grambas & Hay, 1992; Sugrue *et al.*, 1990). Despite pH1N1 HA not containing a multibasic cleavage site, it has recently been shown that M2 was required during HA biosynthesis (Alvarado-Facundo *et al.*, 2015). Therefore, M2 inhibitors with activity against pH1N1 have the potential to affect not only virus entry, but also secretion. All investigations performed herein have assessed multicycle replication. A time of addition study in which compound was present during attachment/entry (pre-incubation and infection), replication (added 4-6 hpi) or throughout was unable to differentiate between the effects of compounds on entry and secretion (data not shown); this was attributed to allowing multiple cycles of replication to occur. Repeating this experiment, but looking at a single round infection would help to determine whether compounds affect virus entry and/or spread. Due to compounds abilities to reduce CF release from liposomes, their effect has been attributed to inhibiting the channel activity and related roles of M2 in the lifecycle. However, it has not been investigated whether compounds also effect the ion channel independent roles of M2, including those that result from interactions of M2 with endogenous proteins (Section 1.8.2)

In summary, the *in silico* work predictions of compound binding, combined with the development of *in vitro* assays using the CD and TM peptide have allowed assessment of functional preferences for either the lumenal or peripheral M2 binding site. This has yielded novel, non-adamantane compounds capable of reducing the infectious titre of rimantadine-resistant pH1N1 swine ‘flu, with potency comparable or superior to published adamantane derivative M2WJ332. Additionally, our *in vitro* work supports the presence of two binding sites on the M2 channel complex. This gives rise to the tantalizing possibility of targeting these two sites using combination, as a means of improving antiviral effects and mitigating viral resistance.

Chapter 5

Cell culture investigations of compound specificity

Chapter 5 Cell culture investigations of compound specificity

5.1 Introduction

From the original tens of thousands of novel non-adamantane compounds docked against the *in silico* E195 M2 homology model, a selection of compounds predicted to specifically bind to either the lumenal (Figure 3.7) or peripheral (Figure 3.8) binding site were taken forward into *in vitro* screening. Preliminary studies used an N31 CD peptide to identify compounds capable of affecting M2. Comparison with a second E195 N31 peptide, spanning only the residues of the TM domain of M2, meant it was possible to functionally discriminate preferences for either a lumenal, or peripheral M2 binding site; such a direct comparison has not been attempted previously in the reported literature. Compounds with the ability to affect CF release mediated by both peptides were designated as lumenally targeted, whereas compounds that preferentially affected the CD peptide, containing the entirety of the peripheral binding site, were designated as peripherally targeted. These data support the presence of two binding sites on M2 that can be targeted independently of one another. In some cases more complex phenotypes were observed, such as with DL7 (Figure 4.18), which could perhaps be explained by potential binding to the partial peripheral binding site present in the TM peptides or to different conformations of the tetramer.

To assess if an effect on M2 in isolation translated into a statistically significant reduction in E195 virus titre, compounds were tested at a single concentration and 24 hpi infectious titres were calculated (Figure 4.15 and Figure 4.17B). This led to the identification of the first non-adamantane compounds with an effect on rimantadine-resistant N31 IAV. Subsequently the potency of three novel non-adamantane compounds (L1.1, DL7 and DP9) and published adamantane M2 inhibitor M2WJ332 (Wang *et al.*, 2013b) was investigated, by means of determining their cell culture IC_{50} (Figure 4.20). Functional preferences of these compounds, determined by *in vitro* assays, indicated that L1.1 was a lumenally targeted compound (Figure 4.13), whilst DP9 was peripherally targeted (Figure 4.18), supporting *in silico* predictions (Figure 3.9). M2WJ332 also demonstrated a functional preference for peripheral binding (Figure 4.10B), in contrast to a previous TM peptide NMR structure, which supported lumenal binding (Wang *et al.*, 2013b). Novel compound DL7 did not exhibit an obvious peptide preference, with differential effects depending on the concertation of compound. These could potentially be due to an ability to bind the partial peripheral site present within the TM peptide at sufficiently high concentrations, or a difference in conformation of the channel between the two peptides. As a result the certainty of the predicted site of action for DL7 was diminished.

Despite *in vitro* data supporting the presence of two binding sites, corroboration via virus culture data was highly desirable. We hypothesised that compounds targeting the two proposed sites of M2 could be used in combination, with synergistic effects when two compounds targeted different sites, but antagonistic effects when two compounds compete for the same M2 binding site. Secondly, selection of specific M2 drug resistance, at positions corresponding to predicted binding sites, would provide evidence to support a particular mode of action.

5.2 **Drug combination assays**

The use of drug combinations is widespread in the clinic, with longstanding application in the treatments of diseases including cancer (Devita *et al.*, 1970; Frei *et al.*, 1958) and HIV (Hammer *et al.*, 1996). One aim of combinations is a reduction of the dose, and thereby related toxicities associated with specific drugs. However, another, perhaps most pertinent to the effective treatment of highly variable RNA viruses including HIV, is to minimise the risk and/or delay the onset of drug resistance. Like HIV, IAV viral replicase enzymes lack the proof-reading capability associated with cellular DNA polymerases; both viruses have very similar mutation rates (Sanjuan *et al.*, 2010). In the 1990s the first antiretroviral therapy (ART) trials combining two nucleoside analogues were undertaken, yielding improved responses compared to either drug as a monotherapy (Hammer *et al.*, 1996). One year later, the first HIV fixed-dose combination therapy “Combivir”, combining two nucleoside analogues, lamivudine and zidovudine, in one pill, was licensed by the FDA. In the ongoing battle against resistance, it is now common for HIV ART to comprise a minimum of three drugs, from at least two separate classes. This usually consists of two nucleoside analogues, plus either a protease inhibitor, integrase inhibitor or a non-nucleoside reverse-transcriptase inhibitor (Williams *et al.*, 2012).

Currently no influenza combination chemotherapies are used in the clinic, but trials have been carried out. Combinations of M2 and NA inhibitors have been tested with no evidence of synergistic effects seen, but resistance was reduced (Ison *et al.*, 2003; Morrison *et al.*, 2007). Efficacy of an oseltamivir-zanamivir combination has also been assessed for its ability to combat resistance in patients, but resulted in a reduction in clinical efficacy (Duval *et al.*, 2010), thought to be linked to zanamivir being able to bind to the catalytic pocket, before oseltamivir is metabolised and adsorbed through the digestive tract.

Additionally, double and triple drug combinations have been assessed for effects on influenza virus infections *in vitro*. Before NAI were discovered, combinations were carried out between M2 inhibitors and ribavirin, a synthetic nucleoside which inhibits viral RNA polymerases. It was found that, despite ribavirin having negligible effects in clinical trials, combination with either amantadine or rimantadine enhanced its antiviral activity *in vitro* (Hayden et al., 1980). Double combinations of an M2 inhibitor and a NAI have resulted in enhancements or additive effects against human strains of IAV (Govorkova *et al.*, 2004; Ilyushina *et al.*, 2006; Nguyen *et al.*, 2010). Combinations using amantadine, oseltamivir and ribavirin have also been carried out (Hoopes *et al.*, 2011; Nguyen *et al.*, 2010) and it was seen that triple combinations were more synergistic than any combinations of two compounds, even when tested against amantadine or oseltamivir-resistant IAV strains (Nguyen *et al.*, 2010). Compared to single agents or double combinations, triple regimes were also better at hindering the development of resistance (Hoopes *et al.*, 2011; Nguyen *et al.*, 2010).

Various potential outcomes exist when combining two or more compounds, which can depend on whether they target the same or different sites. “One-sided” effects, such as enhancement, can be determined by simply examining the change in percentage or fold changes in responses, yet the “mutual” effects of synergism and antagonism are determined by more complex means (Chou, 2006). The definition of the word synergy in the Oxford English Dictionary is “the interaction or cooperation of two or more organizations, substances, or other agents to produce a combined effect greater than the sum of their separate effects”. In biological and pharmacological terms the definition of synergy (Goldin & Mantel, 1957) and methods or algorithms for determining synergistic effects have not always been as clear (Greco *et al.*, 1995). Essentially synergy is defined by a more than additive effect, whilst antagonism is a less than additive effect. As such, the definition of an “additive effect” is key to understanding both phenomena.

In 1926, the term “isobole”, defining the connection of points of equal value (inhibition) on a graph with a line, was coined during investigation of the mathematics involved in combinations (Loewe & Muischnek, 1926). This laid the foundations for the Loewe additivity model, allowing interpretation of combinations of compounds as being synergistic, antagonistic or not interacting (additive). A second mathematical model for assessing combinations is the Bliss Independence model (Bliss, 1939). This does not take into account non-linear dose responses and as such, its definition of an additive effect is inaccurate when there are interactions between drugs. The combination index (CI) method of analysing drug combinations (Chou, 2006; 2010), has evolved from the Loewe additivity model. The ability to assess effects of compounds with non-linear dose responses and its incorporation of this method into the “CompuSyn” software (ComboSyn, Inc.) means this method is widely used and prompted us to use this package for the analysis of the work presented herein. For each given combination of two compounds the software will calculate a CI. It is this value that is used to quantify the combination as synergistic (C I< 1), additive (CI = 1) or antagonistic (C I> 1) (Chou, 2006).

Here, combinations were utilised to infer binding preference, predicted by *in silico* docking and *in vitro* peptide preference. Testing the potential presence of two binding sites on M2, relied upon the premise that if compounds A and B bound to the same site they would effectively be in competition, and could result in additive or antagonistic effects. If compound A bound at site x and compound B at site y, there is the potential that the effects would be additive or synergistic, as the binding of compound A to site x would not affect the ability of compound B binding to site y and vice versa. Thus, we hypothesised that we would be able to discriminate preferences due to their relative synergistic, additive, or antagonistic effects, however, such a simple discrimination is unlikely. Interpretation of the results might be complicated by there being four sites at the periphery, not simply one. In addition, it is thought that lumenal inhibitors work by physically occluding the lumen of open channels, whereas peripheral inhibitors bind allosterically, stabilising the closed conformation (Pielak *et al.*, 2009), As such it could be argued that it is not possible to simultaneously have inhibitors acting at different sites of M2. There is however evidence that does not fully support the differential binding preferences of lumenal and peripheral binding adamantanes. A structural study found that amantadine could bind simultaneously to the proposed lumenal and peripheral binding sites of an M2 tetramer, at neutral pH (Cady *et al.*, 2010), It must be noted that structural studies can provide evidence of compound binding and this does not necessarily correlate to inhibition. If a compound was to bind at either site, but not result in inhibition of the channel, then this would antagonise the effects of other inhibitors competing for the same site. Depending on the relative potencies and kinetics of inhibition, two compounds effective at the same site when used in combination could result in one-sided effects, but antagonism is also a possibility. Finally, novel lumenal and peripheral compounds may not necessarily be able to simultaneously bind the same M2 tetramer, but amongst the population of M2 channels, present within a cell, it is unlikely that all would be entirely in one state. Therefore, the presence of a compound able to bind open channels and a second able to bind closed channels should not be considered a disadvantage and could provide an advantage that might correspond to synergy.

To allow assessment of synergism, single compounds also needed to be tested across the same concentration range, which extended both above and below the IC_{50} (Chou, 2010). To analyse the data using CompuSyn software the relative virus titre (%) needed to be converted into an “effect”, on the scale of 0 to 1, with 0 indicating no change and 1 indicating complete inhibition; relative virus titre (%) was divided by 100 and then subtracted from 1, e.g. 100 % relative virus titre = 0 effect, 75 % relative virus titre = 0.25 effect, 10 % relative virus titre = 0.9 effect. These values of “effect” were then manually inputted into CompuSyn, first for each compound in isolation, then for each of the nine combinations of concentration. Resultant CI values were then used to identify each combination as either synergistic, additive or antagonistic.

Combination assays were plotted on 3D graphs, with the x-axis increasing concentrations of one compound, the y-axis increasing concentrations of the second compound and the z-axis for relative virus titre. The DMSO control was plotted at (0,0,100). The data was colour coded, increasing concentrations of single drug were shaded in darker shades of grey, synergistic combinations were green, additive combinations were orange and antagonistic combinations were red. Standard deviations, across three wells per condition, were calculated and a maximum error of 21 % relative virus titre was determined. However, it is not possible to plot error bars on 3D graphic representations in Excel 2010 (Microsoft Office) and as such none are shown on graphs.

5.2.1 Combination of predicted lumenally, and peripherally targeted compounds

The lumenally targeted compound L1.1 reproducibly exerted the most significant reductions in infectious virus titre (Figure 4.15 and Figure A.5) and had a low micromolar cell culture IC_{50} value (Figure 4.20). Thus, L1.1 was selected as the proof-of-principle lumenally targeted compound for combination experiments.

Of the novel non-adamantane compounds with statistically significant reductions in virus titre (Figure 4.15 and Figure 4.17B), only one (DP9) was classified as a peripheral binder based upon *in vitro* data (Figure 4.18). In virus culture, DP9 demonstrated a reduction in virus titre when used at a concentration of 80 µM (Figure 4.17B). However, the IC_{50} of DP9 could not be accurately calculated within the ranges tested (Figure

4.20), and so was ascribed as being 25 < IC_{50} < 80 μM. The adamantane analogue M2WJ332, contrary to the TM peptide NMR structural data (Wang *et al.*, 2013b), demonstrated a functional preference for the peripheral binding site *in vitro* (Figure 4.10B). The IC_{50} value calculated for M2WJ332 was much closer to that of L1.1 than that of DP9 (Figure 4.20), hence M2WJ332 was chosen alongside L1.1 for use in combination assays.

To assess effects of each compound in isolation and in combination, the selection of compound concentrations was important. Available stocks of compound dictated that three concentrations, plus a DMSO control could be tested. Based upon IC_{50}, the midpoint concentration was chosen as 1 μM, where a reduction in virus titre of approximately 50 % was expected; additionally 0.2 and 5 μM were chosen. Consistent with IC_{50} experiments, 1 μM M2WJ332 resulted in 56 % virus titre (Figure 5.1). However, L1.1 at 1 μM resulted in a virus titre of 72 %, only at 5 μM was the reduction greater than 50 % (Figure 5.1), fitting within the predicted confidence interval from previous titrations (Table 4.2). For both compounds in isolation there was little difference between the relative virus titres for 0.2 and 1 μM, but increasing the concentration to 5 μM led to more pronounced reductions in virus titre (Figure 5.1).

Encouragingly, combinations of compounds led to enhanced effects upon virus titre compared to that of single compounds at all concentrations tested (Figure 5.1), suggestive of at least additive effects. Analysis of CI values revealed that eight out of nine combinations were indeed synergistic, with only one, somewhat unexpectedly (1 μM M2WJ332 plus 0.2 μM L1.1), being antagonistic (Figure 5.1). Combinations with less than 1.5 μM total combined compound concentration reduced virus titre to 40-55 %, whereas those with total compound concentrations of 2 μM or above reduced virus titres to below 6 %. In four combinations titre was < 1 %, equivalent to a two-$\log_{10}$ reduction, representing a significant improvement on either compound in isolation. All but one of the CI values indicated that the combination of L1.1 and M2WJ332 was synergistic, suggestive that the act at different sites and consistent with the presence of two binding sites on M2.

5.2.2 Combination of two predicted peripherally targeted compounds

We next tested the effects of combining two predicted peripherally targeted compounds. It was hypothesised that two peripheral binding compounds would compete and as such the result would likely be additive or antagonistic. However, there are four peripheral binding sites present on each M2 tetramer (Schnell & Chou, 2008)

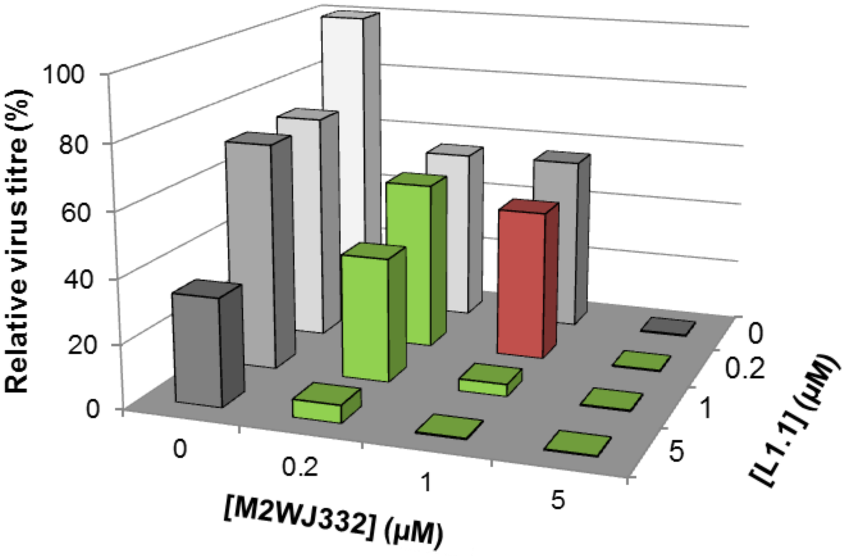

Figure 5.1 Effect of predicted peripheral targeting M2WJ332 in combination with predicted lumenal targeted compound L1.1 on E195 infectious virus titre 24 hpi.

M2WJ332 was preincubated in isolation or in combination with L1.1 at 0, 0.2, 1 and 5 µM, with E195 virus at MOI 0.01, prior to a one hour infection. 24 hpi virus titre was determined by plaque assay, resultant titres were normalised to DMSO control (0 µM, 0 µM). Each combination was carried out on triplicate wells and the titre was averaged across these and plotted. These average values were used for combination index (CI) analysis using CompuSyn software. Each combination point was given a CI value, this was used to colour the bars of the graph, synergistic (green) or antagonistic (red) combinations of compounds. Single compound data is shown in grey.

and it is not clear how many of these sites need to be occupied to achieve inhibition of channel activity and this has the potential to complicate interpretation of combination studies.

Our hypothesis states that two compounds targeting the same site should result in additive or antagonistic effects. Four out of nine combinations of M2WJ332 and DP9 were calculated to be antagonistic; in each case the addition of DP9 increased the virus titre compared to M2WJ332 in isolation (Figure 5.2), suggestive that the less potent DP9 competes with M2WJ332 and decreases its ability of reducing virus titre. However, the remaining five combinations resulted in a further decrease in virus titre compared to compounds in isolation; four conditions were synergistic and one was additive (Figure 5.2). Thus, whilst the combination of M2WJ332 and DP9 did not provide conclusive evidence to support that two peripherally targeted compounds might compete and result in antagonism, the average CI value across the nine combinations was 1, denoting an additive effect, which does not go against potential effects of two compounds acting at the same site. Interestingly, synergistic combinations occurred mainly at the lowest concentrations, whilst antagonistic combinations at the higher concentrations; thus, it was conceivable that a more complex explanation existed for these synergy profiles, potentially related to the presence of not one, but four peripheral binding sites or the differing potencies of the compounds.

5.2.3 Can combination experiments resolve the preferred binding site of DL7?

Thus far, combination experiments appeared generally consistent with our hypothesis. However, DL7 did not demonstrate a clear peptide preference *in vitro.* Compound DL7 caused a similar inhibition of CD and TM peptides at 40 µM or above, but at lower concentrations a preferential effect upon the CD peptide was observed (Figure 3.3). We reasoned that combinations of DL7 with M2WJ332 or L1.1 could help elucidate its preferred binding site. Should DL7 target the lumen it would likely result in synergistic combinations with M2WJ332, but additive or antagonistic combinations with L1.1, and vice versa.

Combinations of DL7 with L1.1 had an average CI value of 8.1, clearly demonstrating an overall antagonistic effect. These combinations led to unexpectedly low effects upon virus titre (Figure 5.3A), compared with previously determined IC_{50} values, despite testing across appropriate ranges (Table 4.2). Combinations involving the lowest concentration of DL7 showed no changes, in virus titre, when 0.2 or 5 µM L1.1 was

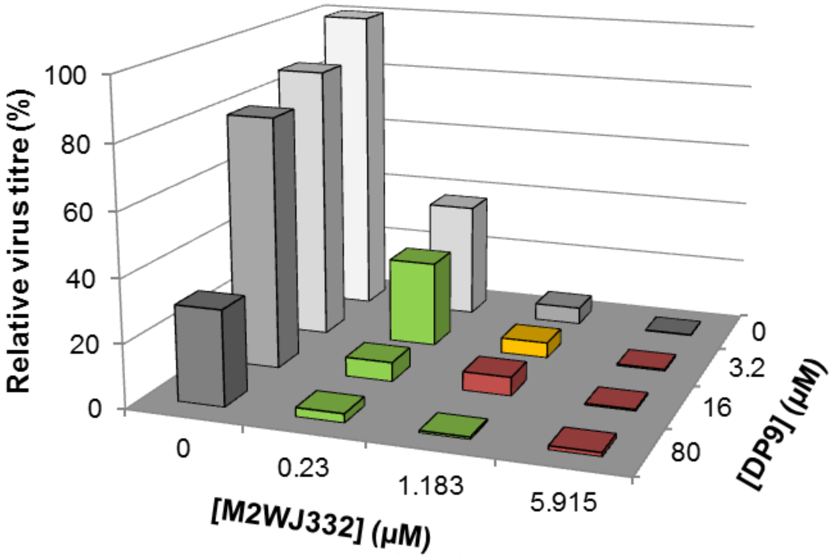

Figure 5.2 Effect of a combination of two predicted peripheral targeted compounds on E195 infectious virus titre 24 hpi.

M2WJ332 and DP9 were preincubated in isolation or in combination at concentrations of 0, 0.2, 1 and 5 µM, with E195 virus at MOI 0.01, prior to a one hour infection. 24 hpi virus titre was determined by plaque assay, resultant titres were normalised to DMSO control (0 µM, 0 µM). Each combination was carried out on triplicate wells and the titre was averaged across these and plotted. These average values were used for combination index (CI) analysis using CompuSyn software. Each combination point was given a CI value, this was used to colour the bars of the graph, synergistic (green), additive (orange) or antagonistic (red) combinations of compounds. Single compound data is shown in grey.

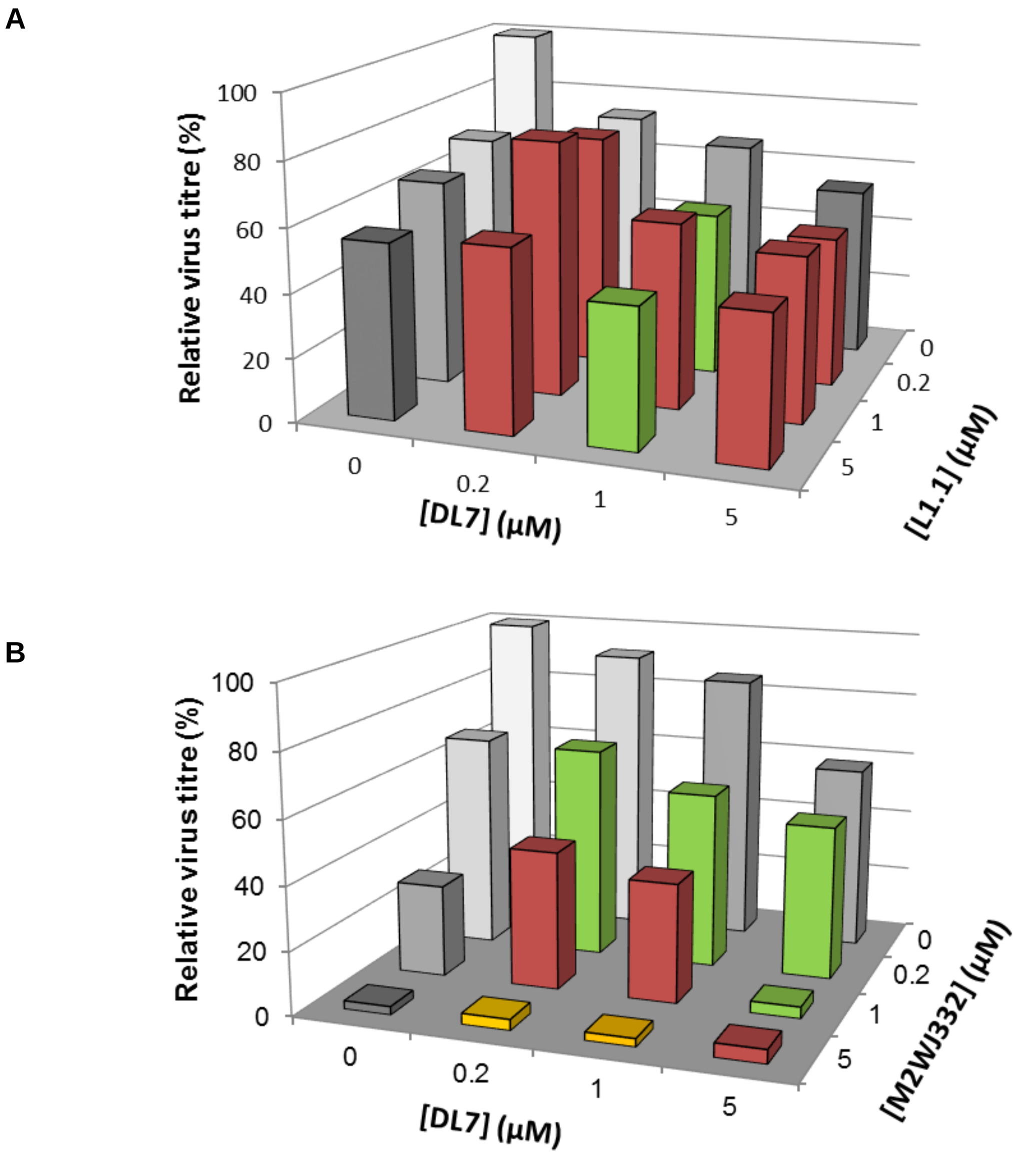

Figure 5.3 Effect of combining DL7 with predicted lumenal compound L1.1 and peripheral compound M2WJ332, on E195 infectious virus titre.

DL7 was preincubated with either A) L1.1 or B) M2WJ332 in combination at 0, 0.2, 1 and 5 µM, with E195 virus at MOI 0.01, prior to a one hour infection. 24 hpi virus titre was determined by plaque assay, resultant titres were normalised to DMSO control (0 µM, 0 µM). Each combination was carried out on triplicate wells and the titre was averaged across these and plotted. These average values were used for combination index (CI) analysis using CompuSyn software. Each combination point was given a CI value, this was used to colour the bars of the graph, synergistic (green), additive (orange) or antagonistic (red) combinations of compounds. Single compound data is shown in grey.

added, yet adding 1 µM L1.1 led to an increase (Figure 5.3A). Compound combinations involving 1 or 5 µM of DL7 resulted in improved effects on virus titre compared with either compound in isolation. However, only two of these combinations (1 µM DL7 with 0.2 or 5 µM L1.1) were calculated to be synergistic. The remaining seven combinations of DL7 and L1.1 resulted in antagonistic effects, despite four of these combinations resulting in improved effects on virus titre compared to compounds in isolation. This further demonstrates how it is not possible to infer mutual effects by a simple comparison of resultant titres (Figure 5.3A). Our hypothesis stated that if DL7 was a lumenal binding compound it would result in an additive or antagonistic combination with L1.1. The overall strong antagonism calculated for the combination suggest that both compounds do bind at the same site (Figure 5.3A) and DL7 was originally selected as a lumenally targeted compound (Section 2.2.2.2).

Combinations of DL7 with M2WJ332 also led to an overall antagonistic effect, with an average CI value of 1.1. Four of the nine individual CI values were synergistic, two were additive and three were antagonistic (Figure 5.3B). In all cases, the addition of M2WJ332 enhanced the effects of DL7 on virus titre (Figure 5.3B). However, this effect was “one-sided”; as the concentration of M2WJ332 increased above 0.2 µM, only one of the six conditions (5 µM M2WJ332 and 1 µM DL7) resulted in a decrease in virus titre compared to the equivalent concentration of M2WJ332 in isolation (Figure 5.3B).

From the combination of DL7 with L1.1 antagonistic CI values suggested that the compounds compete for the binding site. However, unlike when L1.1 was used in combination with predicted peripheral targeted compound M2WJ332 (Figure 5.1), the combination of DL7 with M2WJ332 was not a clear synergistic interaction. The effects were synergistic at lower concentrations of M2WJ332, but became antagonistic and additive at higher concentrations (Figure 5.3B), similar to that seen when M2WJ332 was used in combination with another predicted peripheral binder DP9 (Figure 5.2). It has not been possible to confidently assign DL7 as either a lumenally or peripherally targeted compound. It is possible that despite efforts to select specific compounds, DL7 may bind to both sites or potentially another site altogether.

5.2.4 Combinations of M2 and NA inhibitors

Zanamivir, a licensed NAI, was used as a positive control in plaque assays when screening novel M2 inhibitors (Figure 4.15 and Figure 4.17B). A combination of two antivirals targeting different proteins and/or parts of the IAV lifecycle is a useful comparison to combinations of M2 inhibitor, plus combinations of novel M2 inhibitors with NAI could be highly clinically relevant. Previous combination experiments were carried out using concentrations of compounds close to the calculated IC_{50} values in E195 virus culture (Table 4.2), so it was necessary to determine an IC_{50} for zanamivir. The published IC_{50} of zanamivir against pH1N1 is between 0.04 and 1.34 nM (Gubareva *et al.*, 2010; Sheu *et al.*, 2009). However, these values were determined using a chemiluminescent NAI assay, directly measuring NA enzyme activity, rather than viral infectivity via plaque assay, and also used a different pH1N1 isolate. The IC_{50} calculated for zanamivir by E195 plaque assay was 122 nM (Figure 5.4), with a 95 % confidence interval of 3.9 – 404 nM.

Combinations of L1.1 and zanamivir were assessed for their effects on E195 infectious virus titre. Previous combination studies involved two M2-targeted inhibitors with similar IC_{50} and analysis was scaled in the micromolar range. However, due to the IC_{50} value of zanamivir being over ten-fold lower than that of L1.1, analysis was initially done in terms of IC_{50} (0.2, 1 and 5), using the values calculated in GraphPad (L1.1 = 1.325 µM, zanamivir = 0.12 µM). Subsequently CompuSyn analysis was also repeated using raw concentrations and no change in CI values was observed (Appendix Table A.3 and Table A.4). Overall there was a trend to synergism with eight combinations showing enhanced effects compared to each compound in isolation. This is consistent with zanamivir and L1.1 targeting different proteins of IAV; the average CI value was 0.9 indicating slight synergism (Table 5.1).

Both compounds achieved a greater than 50 % reduction in virus titre with the highest concentration tested (Figure 5.5). All five of the combinations containing one or both of the compounds at its top concentration, plus the combination of 0.12 µM zanamivir and 1.325 µM L1.1, were calculated to be synergistic (Figure 5.5). The remaining three combinations, those with the lowest total compound concentrations (0.024 µM zanamivir with 0.265 or 1.135 µM L1.1 and 0.12 µM zanamivir with 0.265 µM L1.1), were antagonistic. Of all the combinations it was only the one involving the lowest concentrations of compound that did not result in an improved effect upon virus titre, compared to either in isolation (Figure 5.5).

5.2.5 Further analysis of combination indexes

None of the combination experiments undertaken involving M2 inhibitors resulted in exclusively synergistic or antagonistic effects. Instead the nine conditions within each experiments included both synergistic and antagonistic effects, and in some instances also examples of additive conditions. To generate a clearer picture of combination

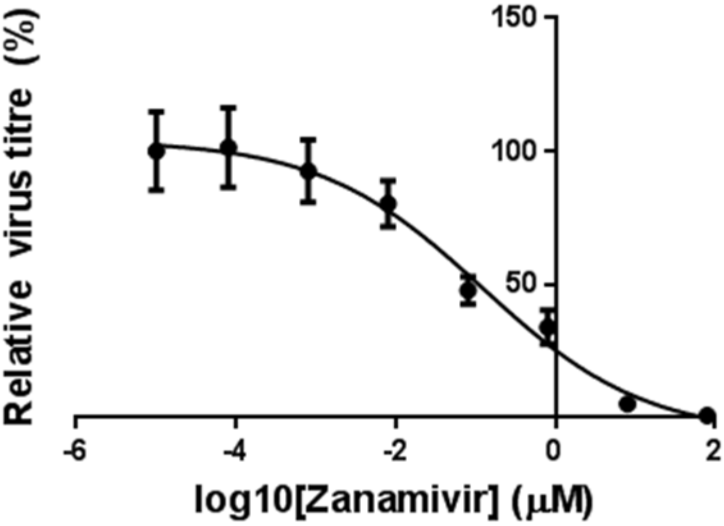

Figure 5.4 Zanamivir IC_{50} determination against E195 virus.

80 pM to 80 μM of zanamivir was preincubated with E195 virus applied to cells at an MOI of 0.01, prior to a one hour infection. The infectious supernatant at 24 hpi was titred via plaque assay, resultant titres were normalised to DMSO. Each condition was done in triplicate wells within the experiment, error bars represent standard deviation. GraphPad software was used to plot a sigmoidal IC_{50} *curve to the data.*

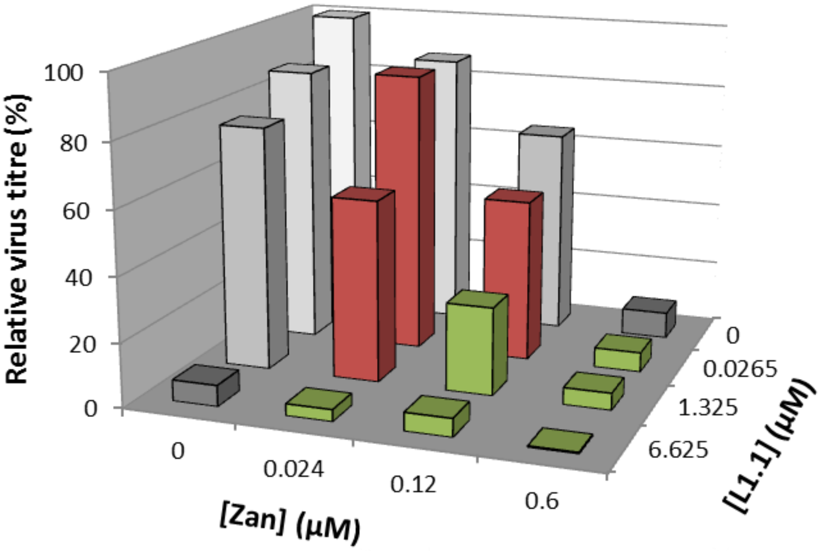

.

Figure 5.5 Effect of novel M2 inhibitor L1.1 in combination with neuraminidase inhibitor zanamivir on E195 infectious virus titre 24 hpi.

L1.1 and zanamivir (Zan) were preincubated in isolation or in combination at concentrations equivalent to 0, 0.2, 1 and 5 IC_{50}(s), with E195 virus at MOI 0.01, prior to a one hour infection. 24 hpi virus titre was determined by plaque assay, resultant titres were normalised to DMSO control (0 µM, 0 µM). Each combination was carried out on triplicate wells and the titre was averaged across these and plotted. These average values were used for combination index (CI) analysis using CompuSyn software. Each combination point was given a CI value, this was used to colour the bars of the graph, synergistic (green), additive (orange) or antagonistic (red) combinations of compounds. Single compound data is shown in grey.

effects, two methods were used in an attempt to generate an overall score across the nine conditions. First by averaging the individual CI values, and the second utilising a published grading of CI values (Chou, 2006).

An average of the nine CI values was made for each of the five combinations tested (Table 5.1). As observed from the individual CI values, overall the combination of the lumenal compound L1.1 with either peripheral compound M2WJ332 or NAI zanamivir was calculated to be synergistic, whereas in combination with DL7 it was antagonistic. These results support that L1.1 and DL7 bind M2 at an overlapping site, which differs to that bound by M2WJ332. Combinations of M2WJ332 with either DP9 or DL7, resulted in the most varied CI values (Figure 5.2 and Figure 5.3B). Averaging of CI values denoted the combination of M2WJ332 with another peripheral compound, DP9, as neither antagonistic, nor synergistic, but additive (Table 5.1).

The scale for synergy is 0 to 1, whereas the scale of antagonism is 1 to infinity, resulting in the possibility of highly antagonistic CI values skewing any averaged results. Due to this fact, a semi-quantitative means of interpreting CI values was also used, based upon the definitions of slight, moderate, substantial, strong and very strong antagonism or synergy (Chou, 2006). Each of the nine combinations within an experiment were denoted on a scale from very strong antagonism (- - - - -, - 5) through nearly additive (+ -, 0), to strong synergism (+++++, +5) (Appendix Table A.5) (Chou, 2006). An average of these taken, in order to eliminate the effect of very large CI values of antagonism (Table 5.2).

Semi-quantitative analysis did not change the grading of the combinations of M2WJ332 with either L1.1 or DP9, but resulted in a change from slight antagonism to nearly additive for its combination with DL7 (Table 5.2). The labelling of the combination of L1.1 with zanamivir remained as slight synergism. However, the level of antagonism with DL7 was reduced from strong to moderate (Table 5.2). Taking all analyses into account, the combination of L1.1 with M2WJ332 was the most representative of synergy, with the combination of L1.1 with zanamivir also being synergistic. The combination of L1.1 with DL7 was demonstrated to be antagonistic. These results support the prediction that L1.1 binds the same site as DL7, which is different than the site of action of M2WJ332. The combination of M2WJ332 and DL7 would therefore be anticipated to be synergistic, however this was not clearly demonstrated and the semi-quantitative analysis supported nearly additive effects. The results for M2WJ332 with DP9 also suggested a nearly additive effect of combination.

	M2WJ332 (P)	L1.1 (L)	DP9 (P)	DL7 (?)	Zanamivir (NA)
M2WJ332 (P)		0.7 Synergism	1.0 Nearly additive	1.1 Slight antagonism	
L1.1 (L)	0.7 Synergism			8.1 Strong antagonism	0.9 Slight synergism

Table 5.1 Average combination indexes for compound combinations

Detailed are the average values across the nine conditions for each of the five combinations of two compounds. The target of the compounds is given in parentheses, neuraminidase (NA), periphery (P) and lumen (L), or uncertain (?).

	M2WJ332 (P)	L1.1 (L)	DP9 (P)	DL7 (?)	Zanamivir (NA)
M2WJ332 (P)		+++ Synergism	+ - Nearly additive	+ - Nearly additive	
L1.1 (L)	+++ Synergism			- - Moderate antagonism	+ Slight synergism

Table 5.2 Average semi-quantitative grading of compound combination effects

Semi-quantitative grading across the nine conditions for each of the five combinations of two compounds was then averaged. The target of the compounds is given in parentheses, neuraminidase (NA), periphery (P) and lumen (L), or uncertain (?).

5.3 Generation of escape mutants to support predicted compound binding

Influenza A viruses readily mutate without external influences, due to the highly error prone polymerase (Drake, 1993; Parvin *et al.*, 1986). In addition to spontaneous events, selective pressure from the use of antivirals can result in the selection of mutations. Amantadine was first licensed for prophylactic treatment of IAV in 1966, but prior to this resistance was selected *in vitro* (Cochran et al., 1965) and soon after additionally using *in vivo* models (Oxford *et al.*, 1970). Resistance was identified to be due to four main point mutations (V27A, A30T, S31N and G34A) in the M2 proton channel (Hay *et al.*, 1985; Hay *et al.*, 1986), and was first noted in clinical isolates in the late 1980s (Belshe *et al.*, 1988; Pemberton *et al.*, 1986). Known resistance polymorphisms all lay within the transmembrane domain of the channel and span three helical turns (Pielak *et al.*, 2009; Schnell & Chou, 2008). However, this is too large a region for a single adamantane molecule to interact with all residues.

Selection of oseltamivir-resistant mutants was first observed when volunteers were infected with H1N1 IAV (Gubareva *et al.*, 2001); two of 54 volunteers had a H274Y mutation, conferring drug resistance. This polymorphism was also identified from human isolates of H1N1 in Europe during the winter of 2007/2008 (Lackenby *et al.*, 2008), whereas zanamivir resistance was seen in the clinic several years earlier when used for the treatment of IBV (Gubareva *et al.*, 1998).

The ability to identify potential resistance polymorphisms *in vitro* is widely applied in the field of influenza antiviral development; however, there is not one simple published method used for selection of resistant IAVs in cell culture. Some studies do not give a comprehensive description of their methodologies, whereas others are stricter. For example, to select NAI resistance, Colacino and colleagues state that viruses were passaged 6-8 times with increasing concentrations of inhibitor, until viruses were “able to replicate in normal inhibitory concentrations” of compound (Colacino *et al.*, 1997). However, after three rounds of plaque purification, the method did result in the isolation of virus which phenotypically, and genotypically, represented a resistant variant with a single nucleotide polymorphism. A similar method was used in another study for generating NAI resistance (Renzette *et al.*, 2014). In this case arbitrary $\log_{10}$ dilutions of the virus containing supernatants were made, when > 50 % CPE was observed. Similarly compound concentrations were increased with every passage, the first passage used a concentration equivalent to 1x median effective dose (ED_{50}), the second passage 4x ED_{50}, then two-fold increases for all subsequent passages

(Renzette *et al.*, 2014). Virus titres were subsequently calculated and MOIs of additional passages were determined to be between 0.00001 and 0.1, with an average MOI of 0.04.

A more rigorous approach was taken by Molla and colleagues. As above, serial passage with increasing concentrations of compound was conducted, in each instance waiting for the development of CPE (Molla *et al.*, 2002). This was repeated 14-15 times prior to plaque purification. Unlike the previously described methods, titres of virus-containing supernatants were calculated prior to continuation with the subsequent passage, in order to maintain an MOI of 0.05 pfu/ml (Molla *et al.*, 2002).

In vitro selection of resistant IAV variants had also been carried out using drug combinations (Hoopes *et al.*, 2011). Two methodologies were used, one of fixed compound concentration and a second of increasing concentration. In the first method, a fixed concentration of individual or combinations of inhibitors was used in a total of five serial passages, with each passage lasting three days. Infectious virus titres were then established and a defined MOI used for subsequent infections (Hoopes *et al.*, 2011). The second methodology had a less stringent schedule; passage occurred when 50 % CPE was observed and an arbitrary 1:1000 dilution of supernatant was also made, alongside either 1, 2 or 4-fold increases in compound concentration (Hoopes *et al.*, 2011).

The methods described so far for cell culture selection of resistant IAVs focus on serial passage on virus. A separate method involved infection at a low MOI and incubation with compound, followed by daily inspection for CPE. When CPE was observed, virus was plaque purified with and without compound. This method has been used to generate rimantadine resistance from a susceptible strain (personal communication, Dr Anika Singanayagam, Imperial College London). Similar methodologies have been utilised for amplification of resistant clinical isolates (Tamura *et al.*, 2013).

5.3.1 Optimisation of M2 sequencing from vRNA within infectious cell culture supernatants

The method of M2 sequencing was optimised for WT E195 virus stocks. E195 virus (10^6 pfu/ml) was clarified by centrifugation and vRNA isolated using a QIAamp Viral RNA Mini Kit (QIAGEN). SuperScript® III (SSCIII) was then used to reverse transcribe the vRNA into complementary DNA (cDNA), using a segment 7 specific primer (pH1N1_s7_fwd, Section 2.1.6). cDNA was subsequently amplified using the Phusion®

high fidelity polymerase (Phusion) (New England Biolabs) and E195 M2 specific primers (Section 2.1.6).

Initially, a universal segment 7 primer, (Flu_s7_fwd, Section 2.1.6) was used to prime reverse transcription reactions. The resultant cDNA was then amplified using three different segment 7 specific forward primers (pH1N1_s7_fwd, Flu_s7_fwd and pH1N1_s7_F2, Section 2.1.6) and universal segment 7 reverse primer Flu_s7_R2. Amplification was carried out using three different annealing temperatures, to optimise conditions. After 35 cycles the reaction was stopped and each sample was then subjected to agarose gel electrophoresis.

In seven out of the nine sample lanes, a single band was present at ~1000 bp (Figure 5.6); E195 IAV segment 7 is 1003 bp (Figure 1.3). A no SSCIII, negative control was included for each of the primer pairs, with Phusion cDNA amplification at an annealing temperature of 48 ºC. All negative control lanes were empty, showing there was no non-specific amplification and no DNA contamination. The universal segment 7 primer (Flu_s7_fwd), with an annealing temperature of 48 ºC, was only able to amplify segment 7 at 48 ºC (Figure 5.6).

5.3.2 Resistance selection following prolonged low MOI infection in presence of high compound concentrations

One method used to produce escape mutants involves a low MOI, high compound concentration infection, harvesting the virus when CPE is observed. Flasks were checked daily for observable CPE. As no CPE was observed, in any of the flasks, at 24 hpi, a 1 ml sample was removed and clarified. This was replaced with 1 ml of SF media containing 1 µg/ml TPCK and 80 µM compound or DMSO control. All flasks presented evidence of CPE at 48 hpi. The DMSO and rimantadine controls, plus the M2JW332 flask all had > 50 %CPE. Using such a high concentration of M2WJ332, it would be expected that you would get suppression of virus; therefore this high level of CPE could be indicative of resistance. In the L1.1 flask < 20 % CPE observed at 24 hpi, so only 1 ml of media was removed and replaced. The L1.1 flask showed > 50 % CPE at 72 hpi, so all virus containing supernatant was harvested and clarified at that time point. The 24 and 48 hpi supernatant from all conditions, additionally the 72 hpi L1.1 supernatant were assessed for sequence changes by Sanger sequencing. All conditions maintained WT sequence across all time points.

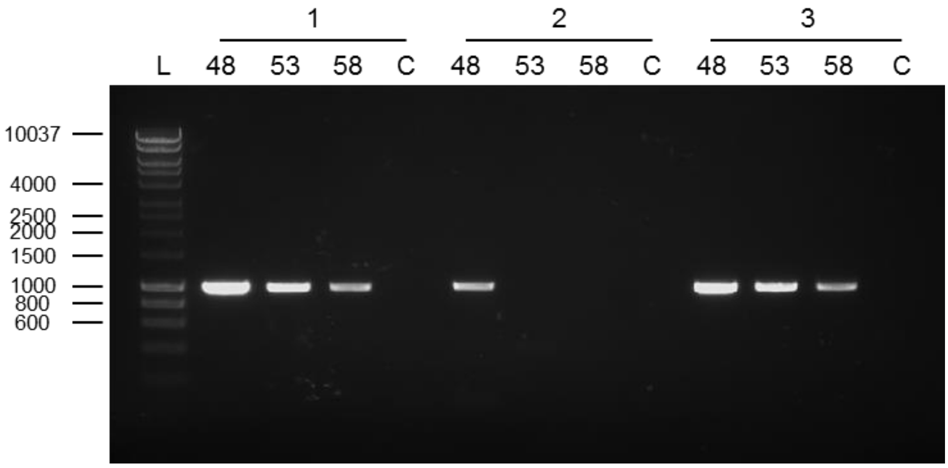
1
2
3
L
48
53
58
C
48
53
58
C
48
53
58
C
10037
4000
2500
2000
1500
1000
800
600

Figure 5.6 Optimisation of forward primer and annealing temperature.

An image of a 0.8 % agarose gel showing PCR amplified cDNA corresponding to segment 7 of E195 WT virus, alongside HyperLadder 1kb (L). cDNA was amplified using three annealing temperatures (48, 53 and 58 ºC) and three different forward primers pH1N1_s7_fwd (1), Flu_s7_fwd (2) and pH1N1_s7_F2 (3), included is a control (C) where no enzyme was present during the reverse transcription step previous to cDNA amplification.

5.3.3 Selection of resistance by serial passage in increasing concentration of compound

Serial passage of virus is a second method for generating escape mutants. There are a number of parts of the methodology that can be varied, such as whether to set an arbitrary time point for serial passage or an observation of CPE, constant or increasing compound concentrations and blind passage or set MOI for each passage. Hitherto plaque assay titres had been calculated 24 hpi in presence of compound, including when establishing IC_{50} values for novel compounds (Figure 4.20). As there had previously been no CPE observed at this time point, but significant reductions in virus titre were evident (Figure 4.15 and Figure 4.17B), an arbitrary time point of 24 hours was selected for passage.

Plaques form after 2-3 days of infection, meaning that, waiting to know the resultant titre after each drug treatment would mean 4 days between passages. Time restraints dictated that in order to carry out a large number of passages, the majority of serial passages were carried out blind (Figure 5.7), with an arbitrary 1/10th of the infectious supernatant used to infect fresh cells. Infectious virus titre was calculated at selected time points to allow the MOI to be re-normalised. In order to increase the selective pressure, it was decided to double the compound concentration in the media with every passage; once the screening concentration of 80 µM was reached this would be maintained for the rest of the experiment. Briefly, an initial MOI of 0.001, preincubated with 2.5 µM compound (zanamivir, rimantadine, M2WJ332, L1.1, DL7 and DMSO) was used for a one hour infection of MDCKs. Virus containing supernatant was removed and replaced with SF + compound + 1 µg/µl TPCK. 24 hpi infectious supernatant (SP-1) was removed and used for the subsequent one hour infection, without preincubation with increased compound concentration. Supernatant not used for the infection was clarified, snap frozen and stored at – 80 ºC, as described in section 2.6.2. After the one hour infection, virus supernatant was replaced with SF + 1µ g/µl TPCK and double the previous concentration of compound. SP-x nomenclature was used to identify the different samples, with SP-1 the supernatant taken 24 hours after the initial infection, SP-2 the supernatant taken 24 hours after SP-1 infection, and so on, until SP-14 (Figure 5.7).

Virus titres were established for SP-6, SP-7 and SP-14, in the presence of all compounds. Samples SP-6 and SP-7 were from two consecutive passages in the presence of 80 µM compound. Virus titres of samples treated with DMSO, zanamivir and M2WJ332 were consistent between SP-6 and SP-7, with DMSO and zanamivir at

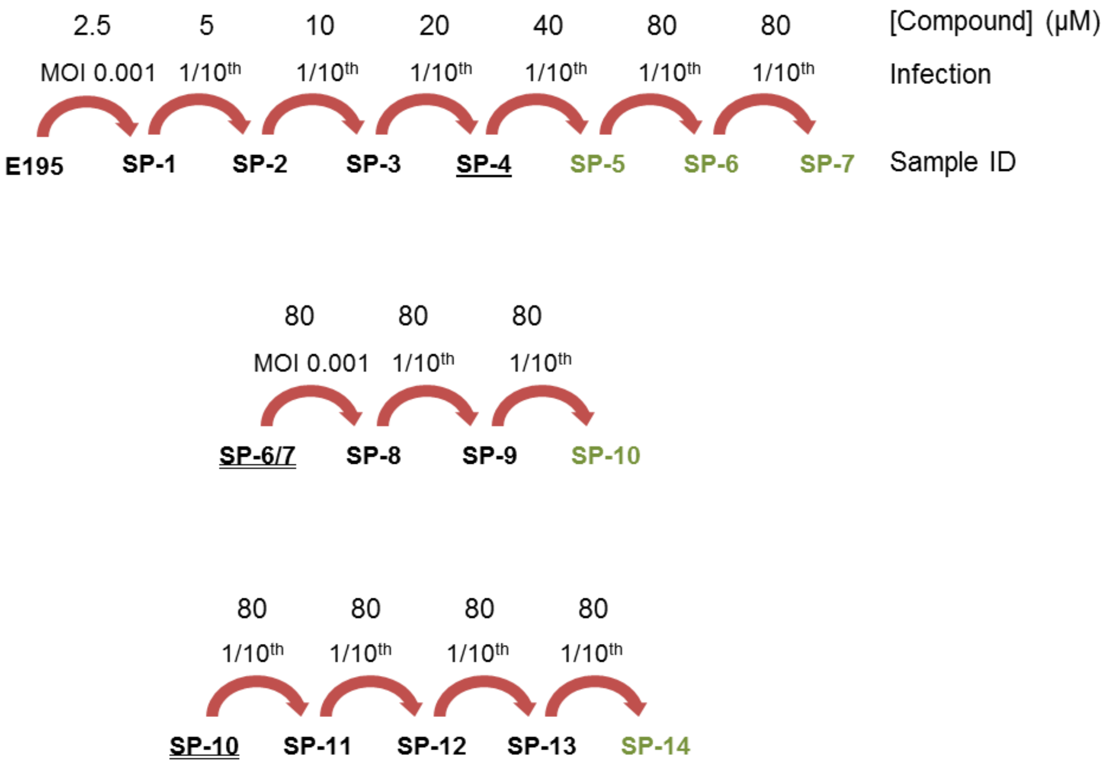
2.5
5
10
20
40
80
80
[Compound] (µM)
MOI 0.001
1/10th
1/10th
1/10th
1/10th
1/10th
1/10th
Infection
E195
SP-1
SP-2
SP-3
SP-4
SP-5
SP-6
SP-7
Sample ID
80
80
80
MOI 0.001
1/10th
1/10th
SP-6/7
SP-8
SP-9
SP-10
80
80
80
80
1/10th
1/10th
1/10th
1/10th
SP-10
SP-11
SP-12
SP-13
SP-14

Figure 5.7 Schematic representation of samples generated via serial passage method.

An initial infection of MDCK cells, using A/England/195/2009 (E195) was carried out in the presence of 2.5 µM of compound, at MOI 0.001, after 1 hr virus containing media was replaced with SF media containing 2.5 µM of compound and 1 µg/µl TPCK. 24 hpi 1/10th of this infectious supernatant (SP-1) was used to infect fresh cells, after a 1 hr infection, it was replaced with SF media containing twice the previous concentration of compound and 1 µg/µl TPCK. This process was repeated, increasing compound concentration to a maximum of 80 µM which was then maintained for the rest of the experiment. The virus titres of SP-6 and SP-7 were determined in order to re-normalise the subsequent infection to a MOI of 0.001. Sample IDs underlined once were stored at 4 ºC for at least 24 hr prior use, double underlined were clarified, snap frozen and then thawed prior to use and in green text have had the M2 protein sequenced.

10^4 pfu/ml and M2WJ332 at 10^5 pfu/ml (Figure 5.8). Between SP-6 and SP-7 the titre of the rimantadine treated virus increased by $\log_{10}$ (Figure 5.8), whereas there was a greater than $\log_{10}$ decrease in titre with L1.1 and DL7 treatments, with values of 10^3 pfu/ml. This reduced titre meant there was not enough virus to carry out a MOI 0.001 infection, so re-normalisation was carried out with SP-6 samples of L1.1 and DL7, whereas SP-7 was used for all other conditions. At the end of the experiment there was greater divergence in virus titres (Figure 5.8). The DMSO control had the highest titre, with zanamivir and DL7 also at 10^5 pfu/ml, whereas the titre for L1.1 was still low, at 10^3 pfu/ml. The virus titres for rimantadine and M2WJ332 both decreased between SP-7 and SP-14 to 10^4 pfu/ml. There was no general pattern in the change in virus titre from SP-6/7 to SP-14.

Viral RNA was isolated at a variety of time points (Figure 5.7) and resultant M2 cDNA sequenced. Across all of the time points examined there were no observed changes in the nucleotide sequence of M2 for (the novel non-adamantane) compounds L1.1 and DL7, or the controls DMSO, zanamivir and rimantadine. A polymorphism corresponding to residue 27 of M2 was detected at the earliest time point sequenced (day 5), during incubation with M2WJ332. At days 6 and 7 this was still observed with GTC (Valine) still dominant over the GCC (Alanine) minor species (Figure 5.9). At days 10 and 14 GCC was seen as the larger peak in the trace (Figure 5.9), suggesting that V27A was the dominant virus species. However, it should be noted that Sanger sequencing is not directly quantitative, making it unclear as to the precise composition of the viral population, for this reason samples have been sent for next generation sequencing (data not available at time of writing).

5.3.4 Plaque purification

The serial passage methodology described above (Section 5.3.3), resulted in generation of a mixed population for M2WJ332 treated virus (Figure 5.9); in order to isolate a single species the virus needed to be plaque purified. In this method virus containing supernatant was serially diluted and preincubated with compound prior to and during a one hour infection, which was then replaced with overlay media containing either the same concentration of compound, or DMSO.

The input virus for plaque purification was the SP-5 samples for rimantadine, M2WJ332 and L1.1 from the serial passage experiment. M2WJ332 and rimantadine were used at 20 and 80 µM, whereas L1.1 was used at 5, 20 and 40 µM as it was found to form crystals in the agar overlay when used at 80 µM, DMSO controls were also included for

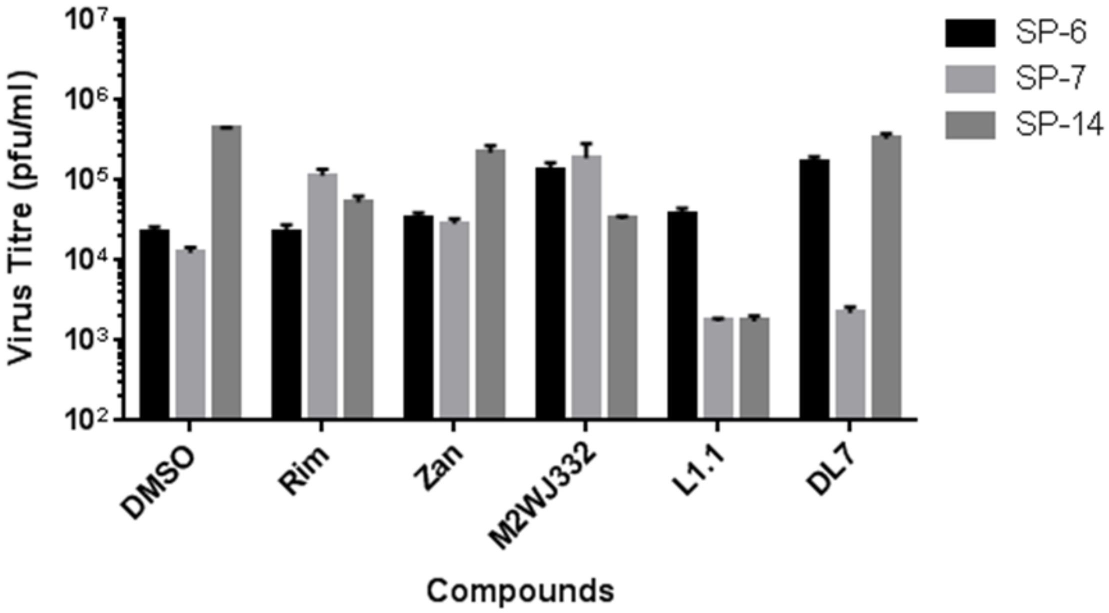

Figure 5.8 Virus titre of serial passage viruses samples SP-6, SP-7 and SP-14.

E195 infectious virus titres were calculated via plaque assay on the 24 hpi supernatants of samples SP-6, SP-7 and SP-14 of the serial passage experiment. Error bars represent standard deviation over three wells.

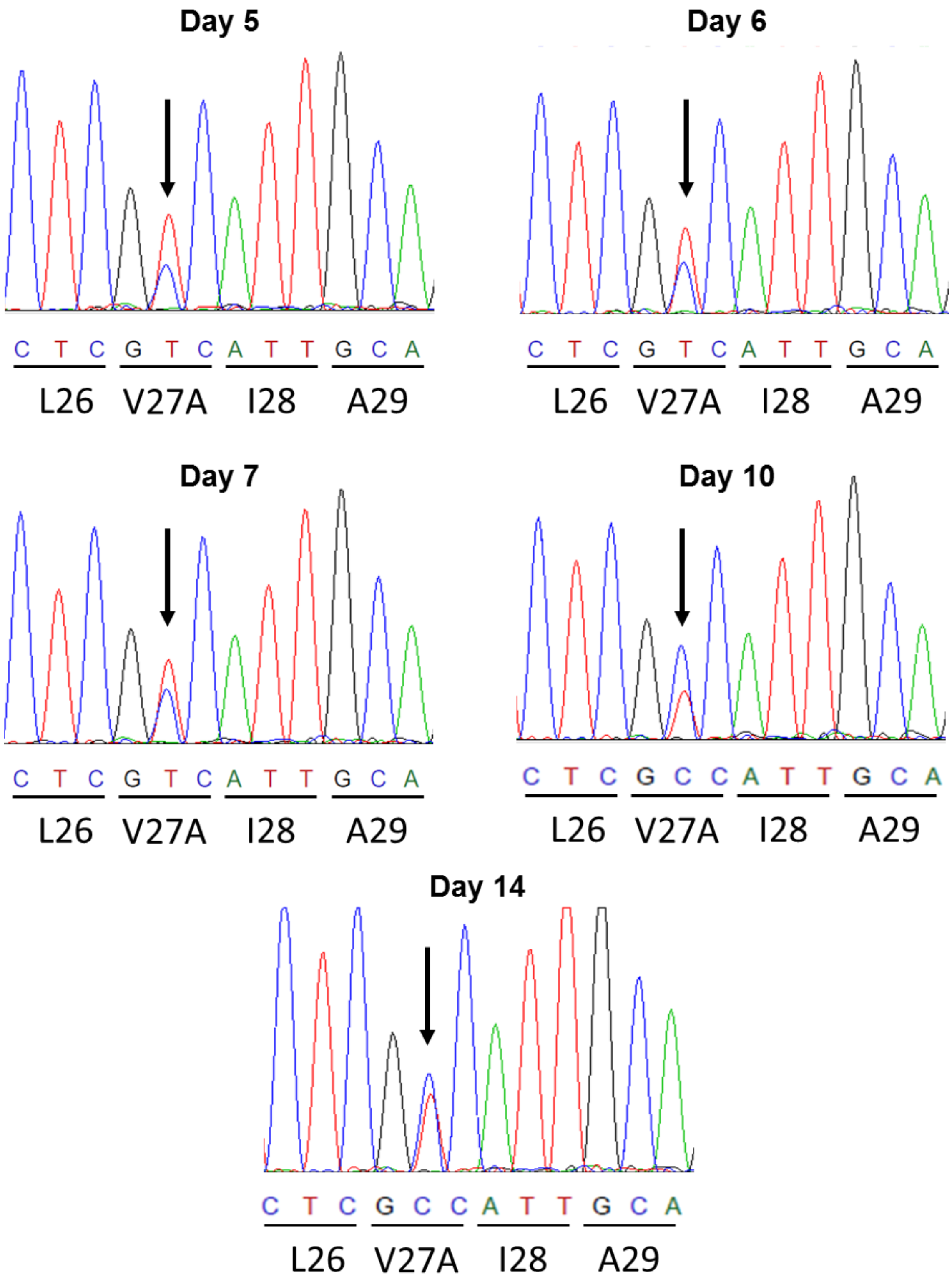

Figure 5.9 M2WJ332 serial passage M2 sequence on days 5, 6, 7, 10 and 14.

E195 virus was serially passaged with M2 targeted amantadine analogue M2WJ332. On days 5, 6, 7, 10 and 14 the vRNA was isolated from infectious supernatant and cDNA of segment 7 was sent for sequencing. A single nucleotide polymorphism at residue 27 (indicated by an arrow) was detected by ABI sequencing, at each time point.

each virus. Eight plaques from M2WJ332 at 20 µM and five plaques from L1.1 at each concentration (5, 20 and 40 µM), were picked 72 hpi and then the plates were fixed, stained and counted as normal. From this the titre was back calculated and relative virus titres plotted (Figure 5.10); input titres calculated from the DMSO controls were 9 $x10^4$, 1.75 $x10^5$ and 8.75 $x10^4$ pfu/ml for rimantadine, M2WJ332 and L1.1 treatment, respectively.

The agar plugs picked from the plates were incubated in SF media for 2 hours prior to infecting fresh cells, in the presence of compound. Media was harvested from cells when CPE was observed; for M2WJ332 this was 24 hpi and for L1.1 samples 48 hpi.

The presence of rimantadine did not exert a selective pressure on the SP-5 rimantadine virus (Figure 5.10), as E195 was inherently resistant; in fact the titre is slightly increased when rimantadine is present during the infection and in the overlay. The presence of either M2WJ332 or L1.1, with the corresponding serial passage virus samples, caused a reduction in relative virus titre, even at the lowest concentrations tested (Figure 5.10), suggestive of a selective pressure exerted by these compounds.

From 20 µM M2WJ332 samples, CPE was observed in seven out of eight samples at 24 hpi. In the presence of 40 µM L1.1 CPE was negligible in, whereas all samples from both 5 and 20 µM L1.1 displayed CPE at 48 hpi. Samples with observed CPE were clarified and taken forward for sequencing. All seven M2WJ332 virus samples were successfully isolated and segment 7 amplified as describe in Section 5.3.3. Sample 2 was selected for the initial sequencing, as it had the highest cDNA concentration. Both the forward and reverse primers, used for sequencing, confirmed that there was a single virus isolate present and that this contained the V27A polymorphism (Figure 5.11), in contrast to the mixed population seen in the serial passage experiments (Figure 5.9). The remaining six M2WJ332 samples also contained a single V27A population), demonstrating that the protocol was suitable for the selection of a potentially resistant variant from a mixed population. No sequence changes, in M2, were seen from four of the 20 µM and all five of the 5 µM L1.1 plaque purification samples.

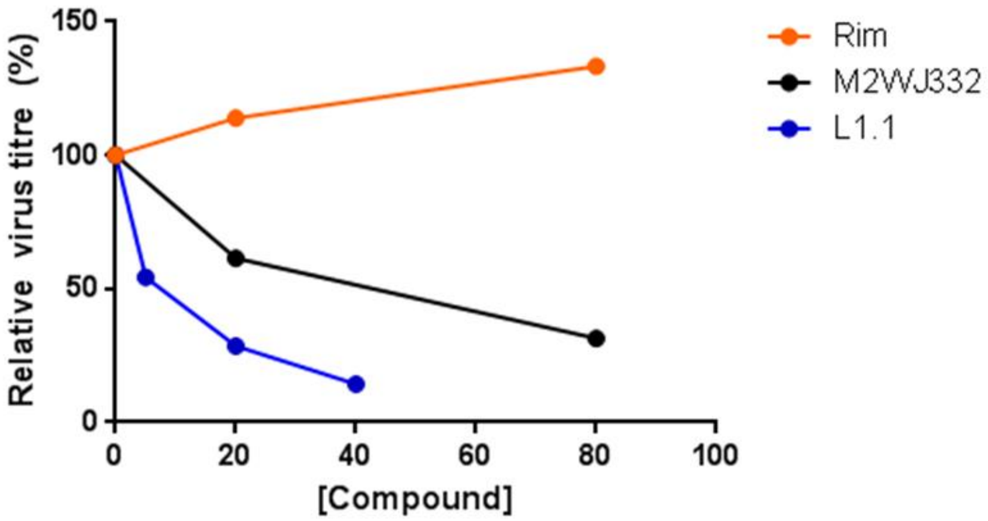

Figure 5.10 Effect of different concentrations of compound included in the overlay during plaque purification on E195 infectious virus titre.

SP-5 virus samples from viruses exposed to sequential treatment with rimantadine, M2WJ332 and L1.1 were preincubated with between 0 and 80 µM of the same respective compounds prior to a one hour infection. Compound was also added to the agar overlay. Resultant plaques were counted and normalised to the DMSO control for each virus.

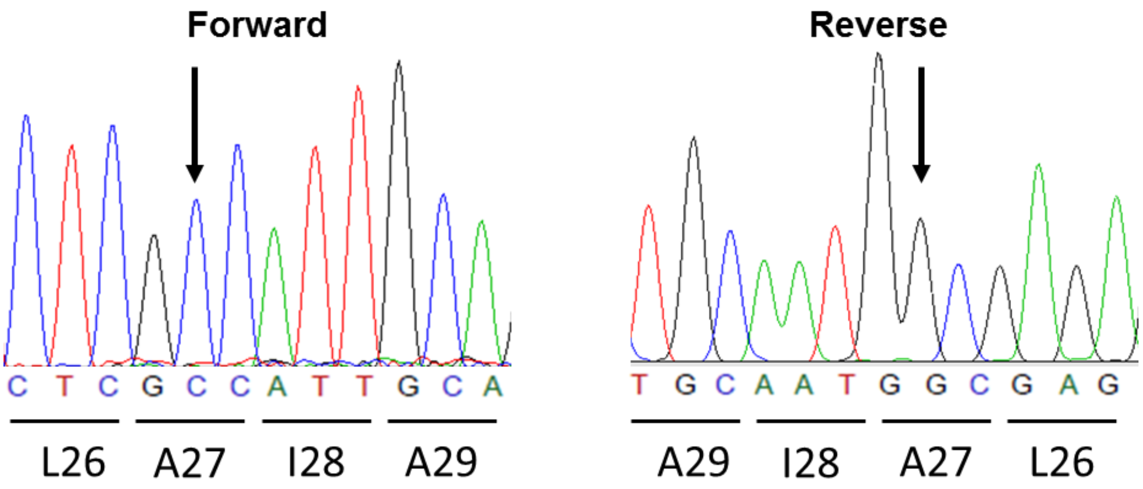

Figure 5.11 Plaque purification of M2WJ332 treated E195 virus.

E195 virus was serially passaged with increasing concentrations of M2 targeted amantadine analogue M2WJ332. The day 5 sample (SP-5) was used in a plaque purification protocol using 20 µM M2WJ332 during infection and in overlay media. Individual plaques were picked and virus bulked up in the presence of 20 µM compound, vRNA was isolated from infectious supernatant and cDNA of segment 7 was sent for sequencing. The virus isolate was seen to be a single population with, compared to WT, a single nucleotide polymorphism at residue 27 (indicated by an arrow) detected by ABI sequencing, using both forward and reverse primers.

5.4 **Discussion**

Through a process of virtual screening and *in vitro* testing, novel compounds predicted to target either the lumenal or peripheral binding site of the rimantadine-resistant N31 M2 proton channel were identified. Virus culture experiments, in which two M2 inhibitors were combined, supported the presence of two binding sites on the tetramer. *In vitro* established peptide preferences (Figure 4.10B, Figure 4.13 and Figure 4.18) were used to select compounds for combination studies. Synergistic effects were observed when a lumenal and a peripheral compound were combined (Figure 5.1). Whereas, two lumenally targeted compounds, predicted to bind at the same site, showed antagonistic effects, likely arising due to competition (Figure 5.2). Potential resistant variants were readily selected against predicted peripheral binding adamantane derivative M2WJ332 (Figure 5.9 and Figure 5.11). However, no resistance mutations were detected for novel non-adamantane compounds, whether predicted to bind either the peripheral or lumenal binding sites.

It had previously been reported that M2 and NA inhibitors can be used in combination to produce synergistic effects (Govorkova *et al.*, 2004; Ilyushina *et al.*, 2006; Nguyen *et al.*, 2010). We have shown that novel non-adamantane compounds can achieve synergy with a licensed NAI, against rimantadine-resistant N31 IAV (Figure 5.5). This shows that such combinations could still be clinically relevant, despite widespread resistance to amantadine and rimantadine.

Combinations of predicted lumenal compound L1.1 and peripheral compound M2WJ332 resulted in synergy in eight out of nine conditions tested (Figure 5.1), this trend to synergy supports the differential predicted binding preferences determined by *in vitro* experiments (Figure 4.10B and Figure 4.13). Combinations of zanamivir and L1.1, and DL7 and L1.1, resulted in a vast majority of combinations favouring synergy, or antagonism, respectively (Figure 5.3A and Figure 5.5).

The combination of M2WJ332 and novel compound DP9, both predicted, based upon *in vitro* peptide preference, to bind to the periphery of the M2 tetramer, resulted in an overall additive effect (Figure 5.2). These compounds are not seen be in direct competition and result in antagonism. A possible reason for this could be linked to there being four peripheral binding sites present on the M2 tetramer; it is unknown how many of these four sites are required to be bound by drug in order to inhibit the activity of the channel. It may be that more than one site needs to be occupied, or even all four. If there are not enough molecules of single compound, to occupy all the required number of binding sites, it could theoretically be complemented by the addition of a second compound, explaining the additive behaviour. Once at concentrations where the threshold required for inhibition is reached, i.e. sites are saturated, any further addition of compounds might interfere and result in antagonism. Another scenario, in which two peripherally targeted compounds do not directly compete, might be that the level of activity of M2 is reduced more by each additional binding site that is occupied by compound, in which case the kinetics of each compound, including on-rates and off-rates, needs to be taken into account. This would comprise follow on studies, such the NMR studies to be undertaken as part of a collaboration with Dr Jason Schnell at the University of Oxford.

Where possible the concentrations used during cell culture combination experiments were based upon previously calculated IC_{50} values (Figure 4.20 and Figure 5.4), as it was recommended to use concentrations that gave both less than and more than 50 % effect for CI analysis (Chou, 2010). The IC_{50} of DP9 could not be accurately determined, without increasing the concentration above 80 µM. Unlike the combination of L1.1 and M2WJ332, with similar calculated IC_{50} values, it was not considered appropriate to use equal concentrations for both compounds. Instead a top concentration of 80 µM was used for DP9 and IC_{50} adjusted concentrations used for M2WJ332, with five-fold dilutions for each. In accordance with previous experiments (Table 4.2), the concentration of DP9 required to cause a 50 % reduction in virus titre was between 16 and 80 µM (Figure 5.2). However, in this experiment as little as 0.23 µM of M2WJ332 reduced virus titre to below 50 % (Figure 5.2). This concentration was below the calculated 95 % confidence intervals for M2WJ332 IC_{50} (Table 4.2), demonstrating that in this particular experiment the effects of M2WJ332 were more potent. The resultant CI values may have been affected by the lack of data resulting in less than a 50 % effect. More rigorous determination of IC_{50} could have gone some way to alleviate this, along with combination experiments containing more than three concentrations of each compound. However, limited compound stocks dictated that this was not possible during this study, but future work should take this into consideration.

Thus far, virus culture experiments supported not only the presence of two binding sites on the M2 tetramer, but additionally supported the *in vitro* peptide preferences for novel compounds (Figure 4.10B, Figure 4.13 and Figure 4.18). One compound which did not demonstrate a clear peptide preference was DL7 (Figure 4.18), which was selected as a predicted lumenal binding compound from the biased *in silico* screen (Figure 3.9). Combinations of DL7 with either lumenal compound L1.1, or peripheral compound M2WJ332 were carried out to assess if a preferred binding site could be indicated. Moderate to strong antagonism was calculated for the combination of L1.1 and DL7 (Figure 5.2A and Table 5.1 and Table 5.2). The addition of a second compound did not result in additive effects, despite there being an improved effect on virus titre in some instances, supporting that they competed for the same lumenal binding site.

Unlike the combination of L1.1 with M2WJ332, which was calculated to be synergistic (Figure 5.1 and Table 5.1 and Table 5.2), DL7 in combination with M2WJ332 did not result in a clear demonstration of synergy, that might have been predicted for a lumenal and peripheral compound combination (Figure 5.3B). Instead, a broad range of CI values were calculated, for which average effects of slight antagonism or nearly additive were deduced (Table 5.1 and Table 5.2). This could in part be attributed to the expectation that lumenal and peripheral binders act on different forms of the channel, for example if DL7 stabilises the closed channel, then M2WJ332 will be unable to access and inhibit the lumen. When either 1 or 5 µM M2WJ332 was used in combination with DL7, all but one of the conditions resulted in an increase in virus titre compared to the equivalent concentration of M2WJ332 in isolation (Figure 5.3B). At equivalent concentrations M2WJ332 exerted a greater effect on virus titre compared to DL7 (Figure 5.3B), despite previous results indicating a similar IC_{50} values for both compounds (Table 4.2). As observed previously, the effect of M2WJ332 was heightened compared to the calculated IC_{50} (Figure 5.2). Whereas, DL7 had a lessened effect (Figure 5.3A), but this is within expected experimental variation. As seen in all other combination assays using M2WJ332, at concentrations of 5 µM of above the resultant relative virus titre is below 5% (Figure 5.1, Figure 5.2 and Figure 5.3B).

Taking into account the published grading scale (Chou, 2006) and the average CI values calculated (Table 5.1), the antagonism of M2WJ332 and DL7 was “slight”; whereas, for L1.1 and DL7 it was “strong”, therefore the relative antagonism of DL7 with L1.1 was greater than it was with M2WJ332. The main binding site for DL7 might be the lumen, however in addition, DL7 might have a low affinity for the peripheral binding site, such as that described by Cady and colleagues for amantadine (Cady *et al.*, 2010). This could explain why some antagonism was seen between DL7 and M2WJ332 despite the high level of antagonism with L1.1. Bearing in mind all of these interpretations, it is most likely that DL7 binds primarily at the same site as L1.1 and can therefore be considered to be a lumenal binding compound. We cannot discount the possibility DL7 binds at a third site, separate from those at which L1.1 and M2WJ332 are acting, or that the compounds are effective against different conformations of the M2 tetramer. In addition to its role as proton channel, different domains of M2 have been implicated with assembly and budding of virions and virulence (section 1.8.2). Despite DL7 and other novel compounds showing dose dependent effects in the CF dye release assay, it cannot be discounted that it causes a reduction in virus titre due to interrupting M2s interaction with other proteins. Through structural studies, to be carried out in collaboration with Dr Jason Schnell, we aim to gain a better insight into the binding of these novel compounds to a pH1N1 M2 CD tetramer.

Another means of validating drug binding is selection of resistance. A method utilising serial passage of virus and increasing concentrations of adamantane analogue M2WJ332 (Wang *et al.*, 2013b) was able to select mutant virus with a single nucleotide polymorphism in M2, V27A (Figure 5.9), which was subsequently plaque purified into a single virus isolate (Figure 5.11). Experiments to test the comparative sensitivity of this dual resistant (V27A/S31N) and the WT E195 (N31) virus to M2WJ332, have not yet been carried out, due to limited compound stocks and time constraints. It is therefore not possible to confirm that the V27A polymorphism does specifically confer resistance to M2WJ332. Nonetheless, during the plaque purification protocol, where the input contained a mixed population of both WT and V27A virus and M2WJ332 was present during infection and in the overlay media, all resultant isolates were found to contain a single species, V27A. This suggests that there was a selective pressure as a result of incubation with M2WJ332 and that the fitness cost of this mutation was low, with this polymorphism seen in nature. The use of a peptide containing the V27A mutation could also provide useful information on the effects this has on compound sensitivity.

As the polymorphism identified after incubation with M2WJ332 is also known to be associated with resistance to licensed adamantanes (amantadine and rimantadine), it suggests that the diversity between binding modes for these analogues is limited. It would be interesting to test the A/Puerto Rico/8/1934 (H1N1) strain, which naturally has V27A and S31N and was first detected in the human population before adamantanes were licensed. Strains such as this in nature would not be expected to be responsive to M2WJ332, and potentially other similar compounds that produce a V27A resistance polymorphism. Divergent chemical series, distinct from adamantanes may therefore generate alternative selective pressures, which may have a higher genetic barrier compared to V27A or S31N.

Long before the first report of binding of adamantane compounds at the peripheral site (Schnell & Chou, 2008), an allosteric mode of inhibition had been deliberated (Pinto & Lamb, 1995; Tosteson *et al.*, 1994). S31N and V27A mutations lead to destabilisation of the M2 tetramer structure (Pielak *et al.*, 2009), which was proposed to cause instability at the peripheral site and a reduced binding affinity, further supporting this mode of action for adamantanes. However, the V27A mutation has also been suggested to reduce the potential for hydrophobic contacts for compounds bound within the lumen (Pielak & Chou, 2010). M2WJ322, which has been classified as a peripheral binding compound, due to *in vitro* peptide preference (Figure 4.10B) and combination experiments in virus culture (Figure 5.1 and Figure 5.2), selected a V27A polymorphism. V27A lies within the lumen and as such this provides support for an allosteric method of inhibition and drug resistance for M2WJ332.

The same treatment regime that resulted in a V27A mutation, with increasing concentrations of M2WJ332, was carried out in parallel for novel non-adamantane compounds L1.1 and DL7, but no change from WT M2 sequence was observed. The lack of detection of any nucleotide changes in the M2 sequence for these compounds could be due to a number of factors. The sequencing method used may not have been able to detect a minor mutant population in a WT background, potentially resolvable via deep sequencing strategies. In the case of both serial passage with increasing concentration and low MOI, high compound concentration methodologies, the sequencing results presented are only for segment 7 and the M2 protein. As it has been demonstrated that the 2009 pH1N1 virus HA requires M2 during its trafficking to the cell surface (Alvarado-Facundo *et al.*, 2015), even after deep sequencing of M2 it would not be possible to definitively say that treatment with novel non-adamantane compounds had not generated escape mutants. In collaboration with Prof. Wendy Barclay (Imperial College London), SP-5 and SP-14 samples, as well as some of the plaque purified isolated, will have their matrix and HA proteins deep sequenced.

The serial passage methodology could be responsible for the lack of selection of resistant variants, as after each 24 hour incubation the resultant virus used to infect new cells was not preincubated with fresh compound, unlike the initial infection. As such only residual compound in the media was present during entry. As it is the entry step that would be most affected by M2 inhibitors (Davies *et al.*, 1964b; Kato & Eggers, 1969), lack of replenishment during this stage of the lifecycle may have resulted in reduced selective pressure, with a population of WT virus being able to infect and initiate replication. This carryover of WT virus, which could possess a replicative advantage compared to any resistant variants, would subsequently have been amplified by PCR; in hindsight preincubation should have taken place for the best chance of observing sequence changes. Although, the precedent of amantadine and our experience of M2WJ332 shows this is unique to novel compounds, indicative of higher genetic barrier to resistance. Additionally, plaque purification was employed to address the issue of mixed viral populations (Section 2.8.2), and allowed the successful isolation of V27A variants for M2WJ332 (Figure 5.11). This further demonstrated that the protocol applied could select and isolate escape mutants. Once again, a comparison of L1.1 sensitivity between WT E195 and L1.1 plaque purified isolate might give an indication on whether escape mutants had been generated.

As discussed previously, ambiguity surrounding the binding specificity of adamantane analogues (Section 3.3) meant novel chemical series investigated in this project moved away from this class of molecule. Removal of the hydrophobic adamantane cage might alter predicted binding modes. Alternatively, novel compounds could make a larger number or more extensive interactions with the M2 tetramer. This could mean that they require a more extreme change in the protein sequence to disrupt interactions, such as mutation of multiple residues, as opposed to the single polymorphisms required to confer adamantane resistance (Hay *et al.*, 1985; Hay *et al.*, 1986). It is possible that the rate of reversion to WT could be increased, due to increased fitness cost of the mutation, or the removal of selective pressure during the entry step in the serial passage procedure used.

Depending upon the nature or severity of amino acid changes necessary to disrupt binding, there could exist a higher genetic barrier to resistance for novel non-adamantane compounds compared with M2WJ332. As a result the frequency at which resistance to a drug, or class of drugs develops could be reduced (Luber, 2005). Novel compounds may have a different binding mode to adamantanes and resistance might be caused by mutations in different residues or could require a combination of polymorphisms. DL7 was selected for *in vitro* testing due to its predicted lumenal binding (Figure 3.9). It was predicted to partake in a π-π stacking interaction with H37 (Figure 3.10), a highly conserved residue due to its importance in channel activation (Wang *et al.*, 1995). Like its parental compound, L1.1 demonstrated an ability to affect both peptides *in vitro* supporting lumenal specificity (Figure 4.13). Combination assays provided further support that L1.1 and M2WJ332 act at different sites (Figure 5.1) and it is also likely that DL7 acts at the same site as L1.1 (Figure 5.3). If M2WJ332 is acting via an allosteric binding mechanism (Schnell & Chou, 2008; Tosteson *et al.*, 1994), but novel compounds bind the lumen, then it could be expected that this different binding mode would require different mutations to confer resistance. However, the controversy of amantadine and rimantadine binding is yet to be solved and as such it cannot be determined whether V27A mutations affect lumenal or peripheral binding of adamantanes.

During the plaque purification experiment, no reduction in virus titre was observed following rimantadine treatment (Figure 5.10), whereas both M2WJ332 and L1.1 caused a concentration dependent decrease in infectious virus titre. At equivalent molar concentrations of compound, L1.1 caused a greater reduction in titre, suggesting the virus was more sensitive (Figure 5.10), it is also a possibility that V27A that enters the cells could have reverted to V27. It must also be noted that the input titres were not equivalent, with the SP-5 M2WJ332 titre almost double that of either L1.1 or rimantadine (Section 5.3.4). Consistent with sequencing data (Figure 5.9), this suggests that at day 5 a minor population already existed that was resistant to M2WJ332, resulting in higher infectious virus titres. The reduction in the virus titre of the M2WJ332 SP-14 sample (Figure 5.8) does not fit with the theory of increased titres for resistant viruses, analysis of the virus titre of the samples between SP-7 and SP-14, especially those after the renormalisation, might shed light on why this was the case.

There are several known resistance mutations associated with the licensed adamantane inhibitors of M2 (Hay *et al.*, 1985; Hay *et al.*, 1986), all caused by a single nucleotide polymorphism. The V27A mutation generated due to serial passage of the E195 (N31) virus with M2WJ332 (Figure 5.9 and Figure 5.11) is one of these known polymorphisms. Dual amantadine resistance mutations have been identified, where a single isolate has both S31N and V27A polymorphisms; most isolates have been from swine, but dual mutations have also been identified at low frequencies in sequences from human isolates, including A/Puerto Rico/8/1934 (H1N1), but more frequently in strains circulating since 2000 (Durrant *et al.*, 2015; Furuse *et al.*, 2009; Garcia & Aris-Brosou, 2014). Recombinant IAVs with single and dual V27A/S31N mutations have been generated (Abed *et al.*, 2005), which in plaque assays has increased sensitivity to amantadine, relative to viruses containing one mutation in isolation. This suggests that the dual mutation virus is actually a less resistant virus strain, with the mutation not being synergistic with respect to resistance. However, the dual mutation also resulted in higher mortality rates in experimentally infected mice (Abed *et al.*, 2005), suggesting the strain does not have decreased fitness or virulence. It would be informative to test the potency of novel compounds against a dual mutant, but additionally a S31, V27A recombinant virus. Adamantane analogues have previously been identified as dual inhibitors of sensitive and resistant strains (Wang *et al.*, 2013a; Wu *et al.*, 2014b) and M2WJ332 has already been shown to be effective against both N31 and S31 CD peptides (Figure 4.19). Further testing of M2WJ332 against a recombinant E195 N31S virus would reveal if this compound could potentially be used against both rimantadine-sensitive and resistant strains. In addition, repeating the serial passage selection process using a recombinant E195 N31S virus might reveal if the V27A polymorphism is sufficient to cause resistance or potentially identify other resistance polymorphisms.

With an increase in the prevalence of IAVs with dual resistant V27A/S31N polymorphisms (Furuse *et al.*, 2009), novel M2 inhibitors would ideally be active against strains containing both polymorphism. A comparison of the sensitivity of WT

E195 and the V27A isolates, from plaque purification using M2WJ332 (Figure 5.11), to compounds L1.1, DL7 and DP9, could give an indication of whether the novel non-adamantane compounds could be effective against naturally occurring dual resistant strains. Additionally, using the dual resistant virus, as the basis of serial passage experiments, might allow selection of resistance against novel inhibitors not observed with WT E195. As discussed for M2WJ332, no experiment testing the sensitivity of the plaque purified L1.1 virus compared to WT E195 has been carried out, with time and compound stocks being limiting factors.

Looking at the prolonged infection experiments, where a low MOI was combined with a high compound concentration, there were no detectable sequence changes under any of the conditions (Section 5.3.2), although the planned deep sequencing may be able to reveal a minor resistant population. It can be concluded, at least in the case of M2WJ332 treatment, that the selective pressure on the virus was reduced in comparison to the serial passage experiments, in which resistance was detected (Figure 5.9). This was despite a higher concentration of M2WJ332 being used, than was required to cause sequence change in the serial passage experiment. It has not been investigated how long it takes for cellular catabolism to diminish the compound concentration in the media. Catabolism would decrease the effective concentration of M2WJ332, alleviating the selective pressure, compared to serial passage experiments with daily replenishment of compound.

During early experiments where MDCK cells were established as a cell line for investigating IAV infection in culture, a single replication cycle was measured to take between 8 and 10 hours (Gaush & Smith, 1968). However, a study looking at the time it takes infected MDCK cells to produce progeny virus revealed that this is somewhat dependent on input MOI (Abdoli *et al.*, 2013). Higher MOIs correlated to faster detection of progeny virus; the highest MOI tested was 1 and the lowest 0.0001, with virus detectable at 5 and 24 hpi, respectively (Abdoli *et al.*, 2013), after a one hour infection. They stated that an MOI of 0.01 was best for monitoring virus in MDCK cell culture, as unlike higher titres no unabsorbed virus is detectable at early time points and progeny virus was detectable at 8 hpi (Abdoli *et al.*, 2013). The MOI used in this method of generating escape mutants (MOI = 0.001), should mean that progeny virus will be released around 12 hpi (Abdoli *et al.*, 2013).

If the half-life of compounds in MDCK cells is shorter than 12 hours then it could be assumed that, using a prolonged infection setup, the effect of compounds on progeny virus will be reduced. As the experiment progresses and the effective drug concentration in the media is further diminished and the number of rounds of infection increases, there will become a point where subsequent rounds of infection will occur under reduced selective pressure. The first observation of CPE was at 48 hpi in the DMSO and rimantadine controls, as well as treatment with M2WJ332 (Section 5.3.2), but was delayed with L1.1 treatment. This might suggest that L1.1 has a longer half-life than M2WJ332, consistent with repeated observation that an 80 µM treatment with L1.1 had greater effects of infectious virus titre 24 hpi (Figure 4.13), despite similar potencies during *in vitro* dye release assays. All plaque assay experiments have examined multicycle replication and compounds were preincubated with virus and included in the media. Without dedicated time of addition and single round infection studies, it is therefore difficult to assess whether compound effects are due to a reduction in virus adsorption and entry during the one hour infection, or if effects are also linked to the role of pH1N1 M2 in protection of HA (Alvarado-Facundo *et al.*, 2015).

It must also be considered that the kinetics of the compounds, for example the reversibility of the inhibition and whether compounds bind the open, closed or both forms of the channel, are likely to play a part in the effects on infectivity. These factors have not been directly investigated in this work and as such effects can only be speculated on. Amantadine was first reported to be more effective against the closed form of channel (Wang *et al.*, 1993), consistent with the neutral pH, at which the majority of M2 tetramer structures with ligands bound are solved (Table 1.4). However, it was later demonstrated adamantanes can also inhibit in acidic conditions of pH 5.0 (Hu *et al.*, 2007b); the 3C9J structure solved at pH 5.3 still predicts amantadine binding (Stouffer *et al.*, 2008). NMR binding experiments involving novel compounds, under different conditions, could provide evidence of the preferred conformation of M2, for binding. Investigations of reversibility have not been carried out for novel compounds, but there has been some investigation into the reversibility of the effects of amantadine and rimantadine on IAVs. However, there are inconsistent findings, from being incomplete reversibility (Kato & Eggers, 1969) to readily reversed (Skehel *et al.*, 1978).

In summary, the synergistic effects of predicted lumenal and peripheral binding M2 inhibitors provide evidence of the presence of more than one druggable binding site on the tetramer. There is also the potential for novel M2 inhibitors to be used in combination therapy with licensed NAIs, potentially providing a means to help combat antiviral resistance. A common rimantadine-resistance polymorphism was readily selected via serial passage with adamantane compound M2WJ332 and was isolated in all samples after plaque purification. However, under the same conditions, no mutations were detected within the M2 sequence with novel compounds, indicating the potential that new classes of compound have a different mode of action or higher barrier to resistance.

Chapter 6

Reconciliation of *in silico* work and final discussion

Chapter 6 Reconciliation of *in silico* work and final discussion

6.1 Reconciliation of *in silico* work

In silico homology models and compound docking studies have significant limitations, with output predictions that must be experimentally tested. The E195 M2 homology model was used to identify compounds with a predicted preference for either the proposed lumenal or peripheral binding site (Figure 3.7, Figure 3.8 and Figure 3.9), and many of these predictions were supported by functional peptide preferences upon testing *in vitro* (Figure 4.11 and Figure 4.18). More importantly, compounds were also able to reduce the infectious titre of E195 virus in culture (Figure 4.15 and Figure 4.17B) and use of compounds in combination supported the presence of two druggable sites on M2 (Section 5.2). Computational analysis of drug combination experiments revealed that treatment of virus with M2WJ332 and L1.1 resulted in synergistic effects (Figure 5.1), consistent with them targeting different binding sites. Despite this, further *in silico* work was carried out to assess whether the system used could have been improved.

As previously mentioned (Section 3.2) the 2RLF structure (Schnell & Chou, 2008), based upon A/Udorn/307/1972 (H3N2) M2 CD tetramer, was selected for the basis of our homology model. This was due to its inclusion of residues attributed to both proposed lumenal and complete peripheral binding sites, as well as the presence of a ligand. Our 2RLF-based E195 M2 homology model was first used during the initial unbiased screen (Section 3.4). It was also used in the subsequent studies including analogues (Section 3.6) and biased *in silico* screening (Section 3.5), to allow comparisons between the compounds from each screen.

One method used to validate our octanol homology model was to re-dock rimantadine, the original ligand from the 2RLF structure (Schnell & Chou, 2008), using the peripheral clip file. Rimantadine was predicted to bind to the peripheral site of the pH1N1 M2 homology model (Figure 6.1B), the resultant eHiTS score of -2.587 showed the binding was lower affinity than the novel unbiased predicted lumenal binders (Appendix Table A.6). The docking pose of rimantadine to the homology model closely reflected what was seen in the original NMT structure, with the methyl group predicted to make polar interactions with D44 (Figure 6.1C) as seen for 2RLF (Schnell & Chou, 2008). However, additional contacts with residues R45 and W41, seen via NMR were not

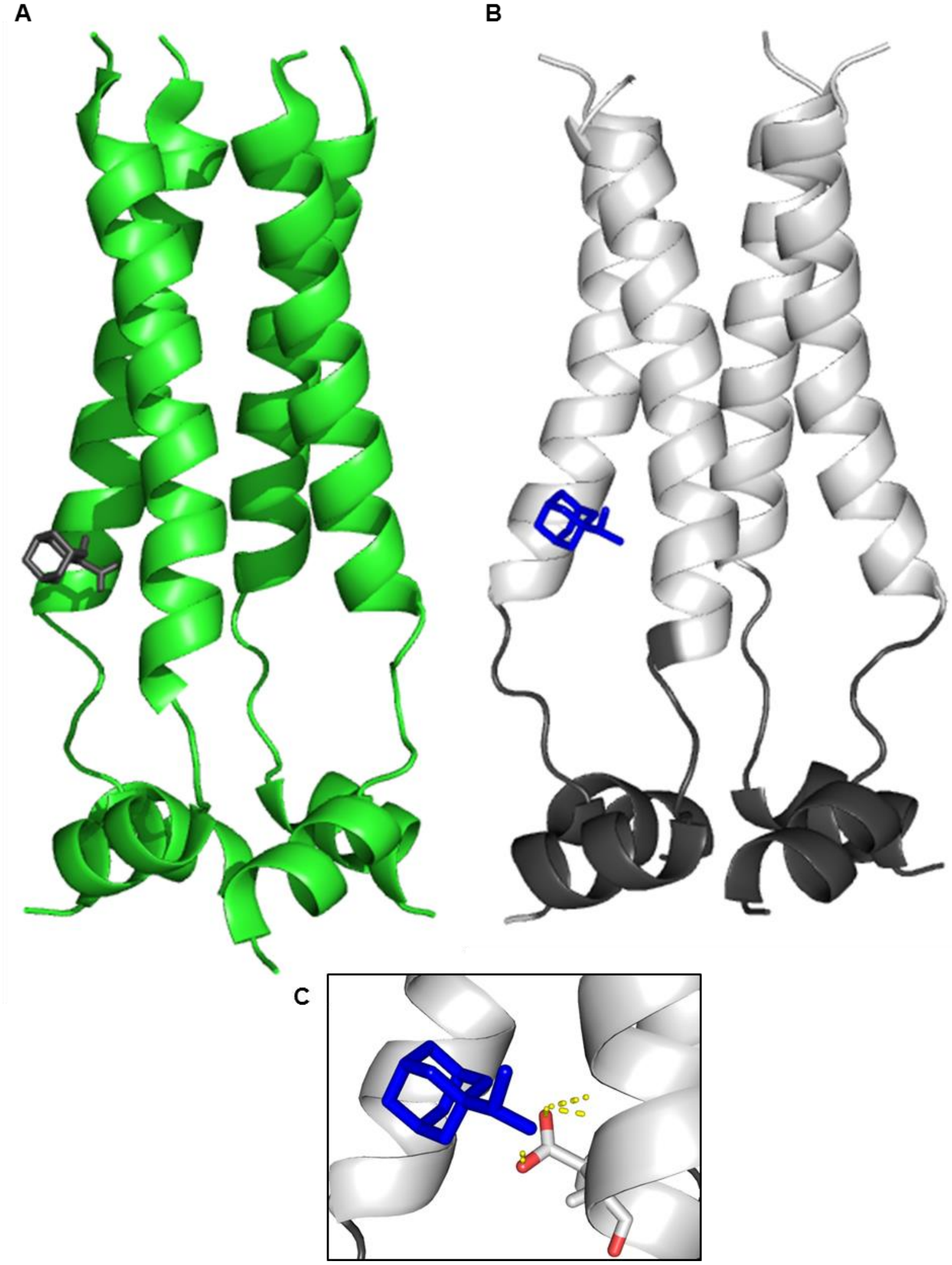

Figure 6.1 Comparison of predicted rimantadine docking to E195 homology model and the original 2RLF structure.

A) The 2RLF NMR structure (H3N2), with a single rimantadine ligand shown. B) The E195 homology model of M2 with predicted peripheral binding rimantadine, C) zoomed in on peripheral site, showing D44 as a stick and predicted polar contacts as yellow dashed lines.

identified from the docking pose, as discussed in Section 3.2 W41 residues in the homology model are rotated towards the lumen, further away from the peripheral binding pocket, so this may attribute for the lack of further interactions between rimantadine and M2 at this site.

6.1.1 Membrane minimised E195 M2 homology model

The original E195 M2 homology model (Figure 3.1B), based upon the published structure 2RLF (Schnell & Chou, 2008), was minimised in an octanol environment. Although this has the ability to mimic the membrane bilayer, upon reflection it was thought it might have been more appropriate to use a true membrane environment. For this reason the same homology model was then re-minimised in a membrane environment, with a lipid bilayer spanning the TM residues (Figure 6.2A). The two models were overlaid, using the “superposition” tool in Maestro (Figure 6.2B). There was high complementarity between the two 3D models, with an alignment score of 0.119 and a RMSD of 1.721 Å. These scores are better than those when overlaying the 2RLF published structure with the octanol minimised homology model (Section 3.2), suggesting that there is little difference between the two 2RLF-based E195 M2 homology models. The position of the C-terminal aliphatic helices have altered slightly (Figure 6.2B), with them being shifted towards the membrane interface in the membrane minimised structure, potentially due to interactions of the protein with the lipids and stabilising the tetramer (Sharma *et al.*, 2010).

The original unbiased *in silico* screen identified compounds L1-7 and P1-6 as preferentially binding to the lumenal and peripheral binding sites, respectively. These compounds were docked against the 2RLF-based E195 membrane minimised model, using new clip files. Comparing the eHiTS scores for P1-6 docked against the peripheral binding site of each model (Table 6.1), the values are all the more negative, translating to a decrease in predicted log IC_{50}. This can be explained by the fact that with the tetramer now spanning a lipid membrane the peripheral binding site was now recognised as a hydrophobic region as opposed to in the octanol environment, when a hydrophobic penalty would have been applied to molecules docking at this site. Additionally, any interactions between the lipid membrane and the aliphatic helices in the membrane minimised model, bringing them into closer proximity, might result in slight changes in the shape of the peripheral site. These changes could strengthen interactions already predicted in the octanol minimised model, or permit additional interactions not seen previously, due to the reduced distances between atoms.

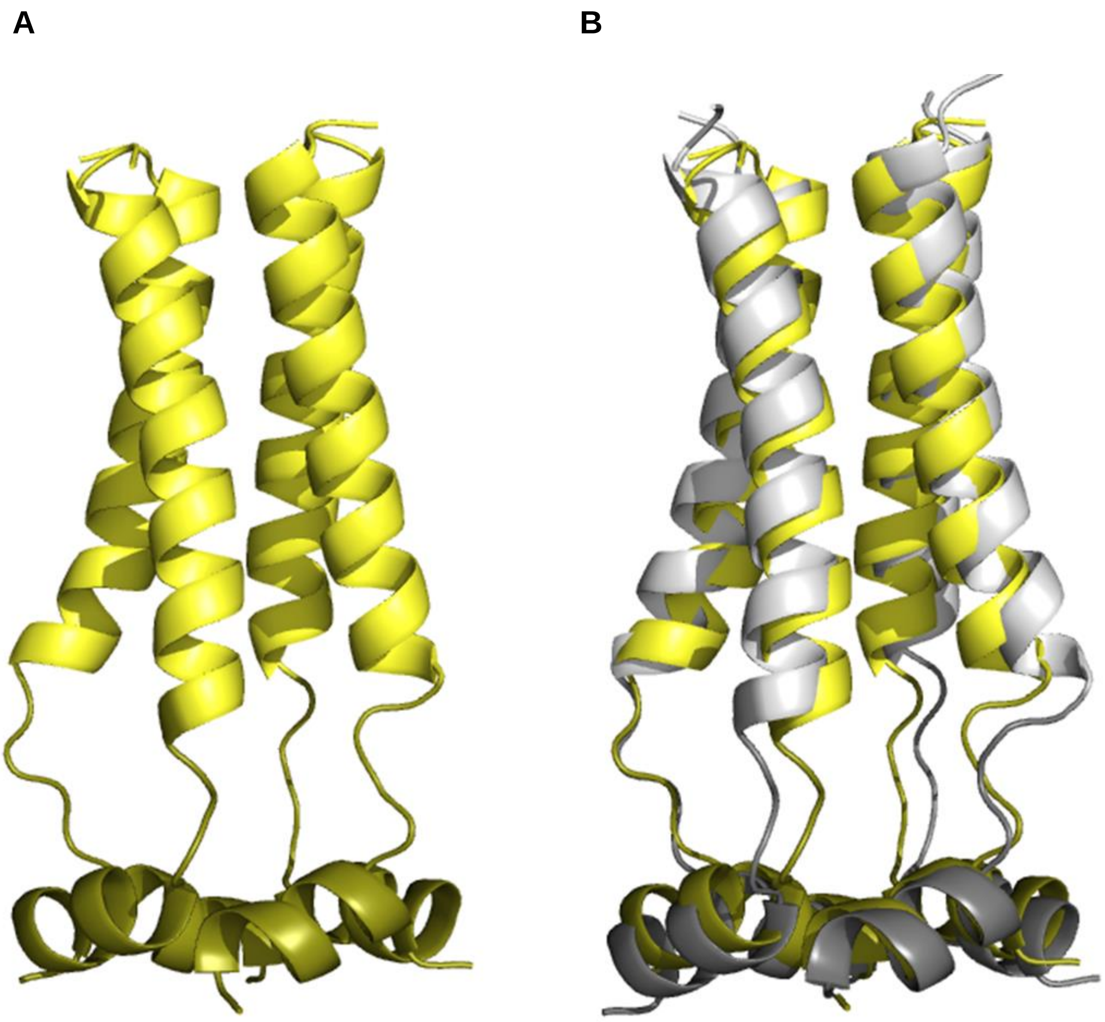

Figure 6.2 Structures of the A/Udorn/307/1972 (H3N2) 2RLF-based A/England/195/2009 (H1N1) (E195) M2 homology models minimised in either octanol or membrane environments.

The original E195 M2 conductance domain homology model was energy minimised in an octanol environment, it was subsequently re-minimised in a membrane environment. Cartoon representations of the A) membrane minimised E195 M2 homology model and B) an overlay of the two models (octanol – grey and membrane – yellow).

Compound ID	eHiTS Score	
	Octanol	**Membrane**
L1	-5.138	-2.882
L2	-4.988	-3.631
L3	-4.827	-4.655
L4	-5.233	-5.899
L5	-5.108	-6.782
L6	-4.805	-7.561
L7	-4.603	-4.873
P1	-4.211	-5.500
P2	-4.785	-5.341
P3	-5.427	-7.503
P4	-4.421	-8.414
P5	-4.308	-8.703
P6	-4.122	-8.358

Table 6.1 Comparison of the binding of unbiased compounds to the A/England/195/2009 (H1N1) (E195) M2 homology model minimised in an octanol environment and a lipid membrane.

The 2RLF-based E195 M2 homology model was energy minimised in both an octanol and a lipid membrane environment, the eHiTS scores, representing binding energy are compared for unbiased compounds at both sites, L and P compounds at the lumenal and peripheral binding sites respectively.

For P2, this was a modest change of less than a $\log_{10}$; whereas, for the others the change was greater and in the case of P5 and P6 values have gone from the range of – 4 to – 8, equating to a change in IC_{50} from 10-100 µM to 1 – 10 nM. The range of scores was much smaller for the octanol minimised model, whereas with the membrane minimised model the scores spanned $3\log_{10}$, with an improved score not clearly correlating to improved activity in either dye release or virus culture experiments (Figure 4.7 and Figure 4.8B). Out of these predicted peripheral binding compounds, *in vitro* peptide preference was only investigated for compound P6. It was seen that at 20 µM and above, P6 was able to significantly reduce CF release mediated by the longer CD peptide, but unlike M2WJ332 which showed no significant effects against the TM peptide (Figure 4.12B), above 40 µM P6 did cause a significant reduction CF release by the TM peptide (Figure 4.13). These data indicated that P6 is a peripheral binder that at high concentrations can exert effects at the partial peripheral site present when using the TM peptide. The improved eHiTS score of P6, in the membrane minimised E195 M2 homology model (Table 6.1), might reflect the favourable binding of P6 at this site, even if it is only partially intact.

A clear trend between eHiTS scores for the two homology models was not apparent when looking at the lumenal binding site (Table 6.1). Of the seven L compounds three scores are increased, two decreased and two remain relatively unchanged. The most dramatic changes were for L1 which has eHiTS scores of -5.138 and -2.882 and L6 with -4.805 and -7.561 from the octanol and membrane minimised models, respectively. These two compounds exerted similar reductions in infectious virus titre, when used at 80 µM (Figure 4.8). The two homology models had less variation at the N-terminal portion of the conductance domain, as such it could be expected that as a result the differences between binding would not be as pronounced compared to at the peripheral binding site.

6.1.2 A homology model based upon a structure solved in a lipid environment

Many of the M2 ion channel structures, including those that sparked the controversy over the drug binding site (Schnell & Chou, 2008; Stouffer *et al.*, 2008), were solved in the presence of detergents that form “bilayer-like” environments. In the virion and during the IAV lifecycle M2 resides in lipid membrane, as such experimental structures solved in lipid bilayer environments are thought provide more native conformations of the tetramer (Cady *et al.*, 2009; Sharma *et al.*, 2010). An E195 M2 homology model based upon the PDB 2L0J (Sharma *et al.*, 2010), solved in a lipid bilayer, was generated to assess whether such a model could provide improved prediction of *in vitro* site preferences (Figure 3.1B and Figure 6.2B).

The 2L0J-based E195 M2 homology model was minimised in an octanol environment, as it was seen that this provided a good mimic of the membrane environment (Section 6.1.1). The 3D structures of 2L0J and its E195 M2 homology model are shown individually and overlaid in Figure 6.3, the alignment score between the two was 0.124 and RMSD 1.520 Å. From the overlaid image (Figure 6.3C), the homology model structure TM helices are seen to be tilted further away from the vertical TM axis, compared to the original 2L0J structure. A second difference between the two structures is with the C-terminal aliphatic helices, where in the E195 M2 homology model they lie more perpendicular to the vertical TM axis. However, the right angle between the two helices of each of the four chains remains, suggesting this change was due to the tilt of the TM helices (Figure 6.3).

Compared to the results of the overlay between 2RLF and the 2RLF-based E195 M2 octanol homology model (Sections 3.2 and 6.1.1), there is better alignment between 2L0J and its respective homology model. Both 2RLF and 2L0J structures used A/Udorn/307/1972 (H3N2) M2, so this difference cannot be attributed to the number of substitutions required to change the template to the target sequence. Consequently an overlay of the two octanol homology models was carried out, this produced an alignment score of 0.816 and a RMSD of 4.360 Å, suggesting there was not good agreement between the two homology models. These discrepancies bring into question the dependability of the predicted docking of novel compounds to the 2RLF E195 M2 homology model. However, it must be reiterated that *in silico* docking was always seen as a prediction that needed to be tested experimentally, and it was seen that *in vitro* work largely supported docking predictions to the 2RLF homology model (Figure 4.11 and Figure 4.16).

In order to assess the predicted binding of novel compounds to the 2L0J-based E195 M2 homology model clip files were generated for the two predicted binding sites and a selection of compounds were docked to each site. The resultant eHiTS scores are given in Table 6.2, alongside scores for the 2RLF-based E195 M2 octanol minimised homology model. In all instances, except for L4.4 at the lumenal binding site, the eHiTS score was less negative for the 2L0J-based homology model, denoting weaker binding interactions than determined for the 2RLF-based homology model (Table 6.2). The average eHiTS scores within each homology model varied little between the two sites, for 2L0J -2.73 and -2.77 and 2RLF -3.89 and -3.74 for lumenal and peripheral binding sites respectively.

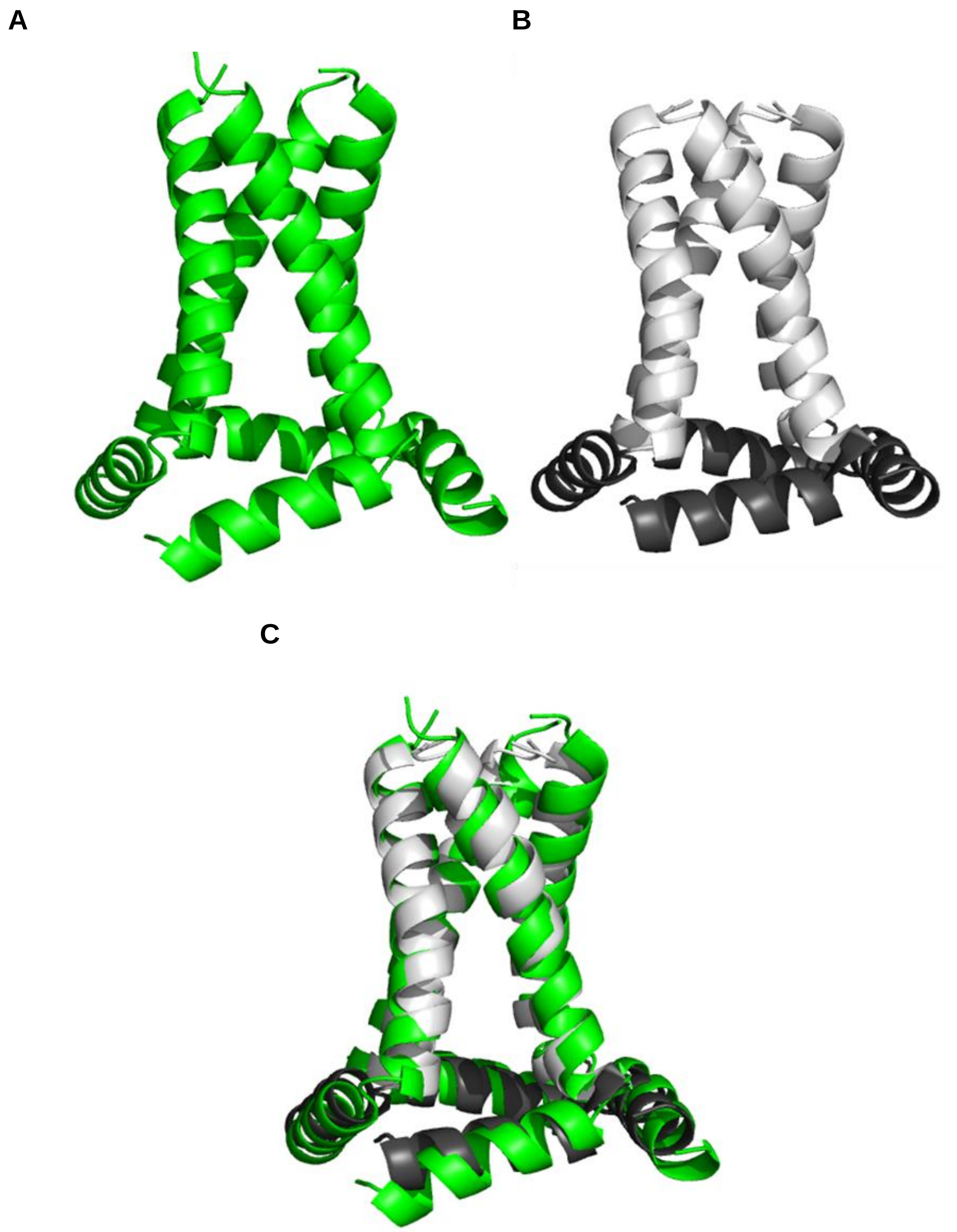

Figure 6.3 Structures of the conductance domain of the 2L0J structure and 2L0J-based A/England/195/2009 (H1N1) (E195) M2 homology model.

The 2L0J structure was solved, in a lipid environment, using the conductance domain (aa 22-62) of A/Udorn/307/1972 (H3N2) M2. A/England/195/2009 (H1N1) (E195) homology was generated from 2L0J and minimised in an octanol environment. Cartoon representations of the A) 2L0J, B) 2L0J-based E915 M2 homology model (residues 22-46 light grey and 47-62 dark grey) and C) an overlay of the two structures.

Compound ID	**eHiTS Score**			
	2L0J model		**2RLF model**	
	Lumen	**Periphery**	**Lumen**	**Periphery**
M2WJ332	-3.06	-2.74	-4.55	-3.54
L1.1	-2.47	-0.58	-3.68	-3.11
L4	-3.05	-3.32	-5.23	-
L4.2	-3.10	-2.84	-3.94	-3.40
L4.4	-3.12	-3.16	-3.04	-3.48
P6	-3.00	-3.60	-	-4.12
P6.4	-1.57	-2.81	-1.80	-3.55
DL7	-2.99	-3.05	-4.98	-
DP9	-2.24	-2.86	-	-5.00

Table 6.2 Docking scores for novel compounds at each of the two proposed binding sites of the 2L0J- and 2RLF-based E195 M2 homology models.

The E195 M2 homology models based upon the 2L0J and 2RLF structures were energy minimised in an octanol environment and compounds docked against the proposed lumenal and peripheral binding sites. eHiTS scores are arbitrary scores generated based upon interactions with the protein, cases where docking was not re-analysed are denoted by '-'.

Against both homology models, L1.1 is predicted to have the weakest peripheral binding of all of the compounds investigated. However, when taking into account the eHiTS score, it is drastically worse for the 2L0J-based homology model, with a score of just -0.58, compared to -3.11 for the 2RLF-based homology model (Table 6.2). The *in vitro* peptide studies, where L1.1 significantly reduced CF release mediated by both the CD and TM peptides, support the predicted lumenal binding (Figure 4.15).

Maestro analysis revealed all compounds made polar interactions to the peripheral binding site of the 2L0J-based homology model (Figure A.12, Figure A.13, Figure A.14 and Figure A.15). Those compounds which were docked to the peripheral site of the 2RLF-based homology model also made polar interaction at this site (Figure 3.11, Figure 3.15, Figure 3.16 and Figure 3.17). Adamantane compound M2WJ332 is predicted to make a combination of hydrogen bonds, salt bridges, as well as π-π and π-cation interactions with residues D44, R45 and F48 to the 2RLF-based homology model (Figure A.15B). In addition to these residues, M2WJ332 is predicted to interact with residue Y52 in the 2L0J-based homology model (Figure A.12). Fewer interaction are predicted between M2WJ332 and the lumenal binding site, where both homology models predicted hydrogen bonds to N31 and a second interaction to either V27 or H37, for the 2L0J and 2RLF-based models, respectively (Figure A.9 and Figure A.15A). The 2LY0 structure published for M2WJ332 shows the compound interacting via hydrogen bonds to two of the N31 residues (Wang *et al.*, 2013b). Only in the 2L0J-based homology model are specific interactions predicted to the lumenal residue V27 (Figure A.12), the residue for which a polymorphism was selected after serial passage with M2WJ332 (Figure 5.9). If the V27A polymorphism does confer resistance to M2WJ332, it is at the moment unclear if this would be due to disruption of the binding at the lumenal binding site or via allosteric effects on the peripheral binding site. The sidechain of alanine is less bulky than that of valine; therefore it is unlikely that this would obstruct compound binding. The V27A polymorphism could, in theory, decrease the number of interactions between a lumenal binding compound and the tetramer, but the NMR does not suggest it is important for binding (Wang *et al.*, 2013b). However, it has been suggested that a V27A mutation can destabilise the tetramer bundle, affecting the proposed peripheral binding site and increase the channel opening (Pielak & Chou, 2010; Pielak *et al.*, 2009).

Biased compound DP9 was predicted to be a peripherally targeted compound from *in silico* docking to the 2RLF-homology model (Figure 3.11) and of the compounds analysed in this section it had the greatest eHiTS score at this site (Table 6.2). During *in vitro* dye release experiments DP9 demonstrated a preference for inhibiting the CD peptide (Figure 4.18). Low level effects on the TM peptide were seen at high concentrations of DP9, this could perhaps be attributed to weaker binding to partial peripheral site present with the shorter peptide. Combination experiments in virus culture using DP9 and M2WJ332, another predicted peripheral binding compound, did not result in the predicted antagonistic effects (Figure 5.2). The reasons for the additive and synergistic effects of the combination have been discussed previously (Section 5.4). When docked against the 2L0J-based homology model the score at the peripheral site was much reduced (-5.00 to -2.86), and it was no longer the best scoring compound at this site (Table 6.2). It is not possible to compare the scores for DP9 at both sites of the 2L0J homology model to determine a preferential binding site. However, of the compounds docked, DP9 has a below average eHiTS score at the lumenal binding site, as such it is unlikely that binding to this site is the cause of the effects seen in combination assays (Figure 5.2).

Comparing between the two homology models, the 2L0J-based model predicted fewer interactions to the lumenal binding site for compounds DL7, L4.2 and P6.4 (Figure A.9, Figure A.10 and Figure A.11). In the case of DL7 and P6.4 in the 2RLF-based homology model a π-π stacking interaction was predicted for each compound to the lumenal binding site (Figure 3.10 and Figure 3.14), with no such interactions were predicted when docking to the 2L0J-based E195 M2 homology model (Figure A.9 and Figure A.11). Likewise, a hydrogen bond predicted to occur between L4.2 and the lumenal binding site of the 2RLF-based E195 M2 homology model (Figure 3.13), was not predicted when docking was performed against the 2L0J-based E195 M2 homology model (Figure A.10).

In vitro dye release assay experiments were unable to define the site preference of the biased compound DL7 (Figure 4.18), which was selected as a lumenally targeted compound from *in silico* docking against the 2RLF E195 M2 homology model (Figure 3.10). Combination assays were used in an attempt to determine the site preference of DL7 (Section 5.2.3). Although the combination with predicted lumenally targeted compound L1.1 was calculated to be antagonistic (Figure 5.3A), the effects combined with the predicted peripheral compound M2WJ332 were less clear (Figure 5.3B). On balance it was decided that DL7 was most likely a lumenally targeted compound, but the potential that it weakly binds more than one site, or binds another distinct site cannot be entirely ruled out (Section 5.4). When compared to the other compounds docked to the 2L0J-based homology model, at both sites, the eHiTS score for DL7 was roughly mid-table; this was compared to being the second best scoring compound at the lumenal site of the 2RLF-based homology model (Table 6.2). The intention of the biased screen was to use compound D as a starting point, to generate series of compounds with specific preference for either the lumenal or peripheral binding sites.

Despite these efforts, perhaps DL7 is an example where this specificity has not been completely achieved. It is possible that DL7 has a preference for the lumenal binding site, but also has an ability to weakly bind at the periphery, as described for amantadine in structural studies (Cady *et al.*, 2010).

6.1.3 Discussion

The relative merit of the 2RLF-based E195 octanol-minimised M2 homology model was assessed, by generation of two additional homology models. Firstly, a model using the original homology model, but minimised in a membrane environment (Figure 6.2), with a second model based upon a structure of M2 solved in lipid bilayers (Sharma *et al.*, 2010) (Figure 6.3). The limited difference between the 2RLF-based homology models minimised in octanol or a membrane bilayer (Figure 6.2), demonstrated the good mimic the octanol environment provided. Although the conformation of M2 tetramers solved in lipid bilayers are thought to better resemble the native protein (Cady *et al.*, 2009; Sharma *et al.*, 2010), the use of the 2L0J as the basis of a homology model for E195 M2 generally resulted in lower docking score compared to the original 2RLF-based E195 M2 homology model (Table 6.2). At the lumenal binding site fewer specific interactions between compounds and the protein were predicted (Figure A.9, Figure A.10 and Figure A.11). Taking this into account, alongside the observation that compounds identified by docking to the 2RLF-based E195 M2 homology model had significant effects against M2 peptides *in vitro* (Figure 4.6, Figure 4.7 and Figure 4.16) and reduced infectious titre of E195 in culture (Figure 4.15, Figure 4.17B and Figure 4.20), justifies the use of the 2RLF-based homology model.

6.2 **Final discussion**

Controversy over the drug binding site of M2 antivirals was highlighted by the simultaneous publication of two tetramer structures with adamantane compounds bound. One structure demonstrated lumenal binding of a single amantadine molecule (Stouffer *et al.*, 2008) and the other four rimantadine molecules bound around the periphery of the channel complex (Schnell & Chou, 2008). As a consequence of the almost ubiquitous prevalence of M2-resistant strains, currently licensed adamantane based antivirals amantadine and rimantadine are no longer recommended for the treatment of IAV. Despite the urgent need for antivirals targeting resistant strains, there has been minimal investigation into the potential of the two proposed binding sites.

This study has demonstrated the ability to target the lumenal and peripheral binding sites of pH1N1 "swine" influenza M2 independently, with specifically targeted compounds. These compounds are distinct from the licensed adamantanes and are the first such compounds to demonstrate an antiviral effect on a resistant strain containing the N31 polymorphism.

In the absence of structural information of the pH1N1 M2, a homology model was generated *in silico* to allow for virtual high throughput screening of novel compound libraries. This model used the published structure 2RLF (Schnell & Chou, 2008) as a template and was able to investigate binding at both the lumenal and peripheral binding sites.

An *in vitro* assay was developed to assess the functional preferences of novel compounds. By utilising two different peptides, one spanning only the transmembrane domain and a second, longer conductance domain peptide with additional C-terminal residues, it was possible to distinguish between lumenal and peripheral binding. Both TM and CD peptides contained the lumenal binding site, whilst only the CD peptide contained the entirety of the peripheral binding site and as such peripherally targeted compounds would preferentially inhibit only CD peptide. Distinct functional preferences were observed for many of the novel compounds, largely supporting *in silico* binding predictions. In addition, the adamantane derivative M2WJ332 (Wang *et al.*, 2013b) was used in this experimental system and in contrast to structural data demonstrating lumenal binding, it exerted a functional preference for the peripheral binding site.

Despite novel compounds being selected purely on having an *in silico* preference for one or other binding site, we were able to identify compounds with substantial efficacy against pH1N1 in culture, that is comparable to adamantane analogues and licensed NAI zanamivir. Compounds with functional preferences for either the lumenal or peripheral binding sites, both had appreciable IC_{50} values and as such were exploited in combination studies.

A combination of predicted lumenally targeted compound L1.1 and peripherally targeted M2WJ332 resulted in synergistic effects on the infectious titre of pH1N1. Conversely, a combination of L1.1 with a second predicted lumenally targeted compound resulted in antagonistic effects, likely due to competing for the same binding site. These data not only provided support for the presence of two druggable sites, but also demonstrated the potential for exploiting both with the potential to help combat resistance. Further to this, novel compound L1.1 was shown to have synergistic effects when used with zanamivir, signifying a possible clinical application of combination therapies.

Due to the high prevalence of adamantane resistance in circulating strains, caused by a number of single polymorphisms, it was decided to try and select resistance to novel compounds. Adamantane compound M2WJ332 is effective against rimantadine-resistant N31 strains of influenza, but resistance to this compound was readily selected and identified to be caused by a second known rimantadine resistance polymorphism (V27A). Even before adamantane compounds were first used V27A/S31N dual mutants existed (Furuse *et al.*, 2009), further demonstrating the limited fitness cost these changes have on IAVs and emphasising the necessity to move away from adamantane compounds. Conversely, under the same conditions, no M2 sequence polymorphisms were detected for novel non-adamantane compounds, indicating a potential higher genetic barrier to resistance with novel compound classes.

In summary, non-adamantane compounds identified via a rational, structure-guided *in silico* docking regime have been shown to be efficacious against rimantadine-resistant pH1N1 swine flu. The presence of two druggable sites and subsequently the benefit of targeting both sites in combination have been demonstrated. Work using recombinant viruses or purified V27A/S31N isolates is desirable to supplement these data. In addition, deep sequencing M2 and HA is being undertaken (Imperial College London), to further investigate the mode of action and resistance to compounds. Shortly, this work will also be supplemented by structural information on the binding of novel compounds, with Dr Jason Schnell (University of Oxford) undertaking NMR studies using a pH1N1 system. These findings have the potential to pave the way for drug-discovery programmes, using novel compound classes targeting the two sites of M2, in a bid to combat antiviral resistance.

Chapter 7

References

Chapter 7 References

Abdoli, A., Soleimanjahi, H., Kheiri, M. T., Jamali, A. & Jamaati, A. (2013). Determining influenza virus shedding at different time points in Madin-Darby canine kidney cell line. *Cell Journal (Yakhteh)* **15**, 130.

Abed, Y., Goyette, N. & Boivin, G. (2005). Generation and characterization of recombinant influenza A (H1N1) viruses harboring amantadine resistance mutations. *Antimicrobial Agents & Chemotherapy* **49**, 556-559.

Acharya, R., Carnevale, V., Fiorin, G., Levine, B. G., Polishchuk, A. L., Balannik, V., Samish, I., Lamb, R. A., Pinto, L. H. & DeGrado, W. F. (2010). Structure and mechanism of proton transport through the transmembrane tetrameric M2 protein bundle of the influenza A virus. *Proceedings of the National Academy of Sciences* **107**, 15075-15080.

Akari, H., Bour, S., Kao, S., Adachi, A. & Strebel, K. (2001). The Human Immunodeficiency Virus Type 1 Accessory Protein Vpu Induces Apoptosis by Suppressing the Nuclear Factor κB–dependent Expression of Antiapoptotic Factors. *The Journal of experimental medicine* **194**, 1299-1312.

Aldabe, R., Barco, A. & Carrasco, L. (1996). Membrane permeabilization by poliovirus proteins 2B and 2BC. *Journal of Biological Chemistry* **271**, 23134-23137.

Allen, H., McCauley, J., Waterfield, M. & Gething, M.-J. (1980). Influenza virus RNA segment 7 has the coding capacity for two polypeptides. *Virology* **107**, 548-551.

Almond, J. (1977). A single gene determines the host range of influenza virus. *Nature* **270**, 617-618.

Alvarado-Facundo, E., Gao, Y., Ribas-Aparicio, R. M., Jiménez-Alberto, A., Weiss, C. D. & Wang, W. (2015). Influenza virus M2 protein ion channel activity helps to maintain pandemic 2009 H1N1 virus hemagglutinin fusion competence during transport to the cell surface. *Journal of virology* **89**, 1975-1985.

Ambrose, C. S., Levin, M. J. & Belshe, R. B. (2011). The relative efficacy of trivalent live attenuated and inactivated influenza vaccines in children and adults. *Influenza and other respiratory viruses* **5**, 67-75.

Amorim, M. J., Bruce, E. A., Read, E. K., Foeglein, Á., Mahen, R., Stuart, A. D. & Digard, P. (2011). A Rab11-and microtubule-dependent mechanism for cytoplasmic transport of influenza A virus viral RNA. *Journal of virology* **85**, 4143-4156.

An, L., Liu, R., Tang, W., Wu, J.-G. & Chen, X. (2014). Screening and identification of inhibitors against influenza A virus from a US Drug Collectionof 1280 drugs. *Antiviral Research*.

Andreas, L. B., Reese, M., Eddy, M. T., Gelev, V., Ni, Q. Z., Miller, E. A., Emsley, L., Pintacuda, G., Chou, J. J. & Griffin, R. G. (2015). Structure and Mechanism of the Influenza-A M218-60 Dimer of Dimers. *Journal of the American Chemical Society*.

Archetti, I. & Horsfall, F. L. (1950). Persistent antigenic variation of influenza A viruses after incomplete neutralization in ovo with heterologous immune serum. *The Journal of experimental medicine* **92**, 441-462.

Arnold, K., Bordoli, L., Kopp, J. & Schwede, T. (2006). The SWISS-MODEL workspace: a web-based environment for protein structure homology modelling. *Bioinformatics* **22**, 195-201.

Aschi, M., D'Archivio, A. A., Fontana, A. & Formiglio, A. (2008). Physicochemical properties of fluorescent probes: experimental and computational determination of the overlapping p K a values of carboxyfluorescein. *The Journal of organic chemistry* **73**, 3411-3417.

Atkins, E., Tatineni, R., Li, H., Gretch, D., Harris, M. & Griffin, S. (2014). The stability of secreted, acid-labile H77/JFH-1 hepatitis C virus (HCV) particles is altered by patient isolate genotype 1a p7 sequences. *Virology* **448**, 117-124.

Balannik, V., Carnevale, V., Fiorin, G., Levine, B. G., Lamb, R. A., Klein, M. L., Degrado, W. F. & Pinto, L. H. (2010). Functional studies and modeling of pore-lining residue mutants of the influenza a virus M2 ion channel. *Biochemistry* **49**, 696-708.

Balannik, V., Wang, J., Ohigashi, Y., Jing, X., Magavern, E., Lamb, R. A., Degrado, W. F. & Pinto, L. H. (2009). Design and pharmacological characterization of inhibitors of amantadine-resistant mutants of the M2 ion channel of influenza A virus. *Biochemistry* **48**, 11872-11882.

Balgi, A. D., Wang, J., Cheng, D. Y. H., Ma, C., Pfeifer, T. A., Shimizu, Y., Anderson, H. J., Pinto, L. H., Lamb, R. A., DeGrado, W. F. & Roberge, M. (2013). Inhibitors of the Influenza A Virus M2 Proton Channel Discovered Using a High-Throughput Yeast Growth Restoration Assay. *PLoS ONE* **8**, e55271.

Baranovich, T., Wong, S.-S., Armstrong, J., Marjuki, H., Webby, R. J., Webster, R. G. & Govorkova, E. A. (2013). T-705 (favipiravir) induces lethal mutagenesis in influenza A H1N1 viruses in vitro. *Journal of virology* **87**, 3741-3751.

Barría, M. I., Garrido, J. L., Stein, C., Scher, E., Ge, Y., Engel, S. M., Kraus, T. A., Banach, D. & Moran, T. M. (2013). Localized mucosal response to intranasal live attenuated influenza vaccine in adults. *Journal of Infectious Diseases* **207**, 115-124.

Barry, D. W., Staton, E. & Mayner, R. E. (1974). Inactivated influenza vaccine efficacy: diminished antigenicity of split-product vaccines in mice. *Infection and immunity* **10**, 1329-1336.

Baum, L. & Paulson, J. (1989). Sialyloligosaccharides of the respiratory epithelium in the selection of human influenza virus receptor specificity. *Acta histochemica Supplementband* **40**, 35-38.

Baum, L. G. & Paulson, J. C. (1991). The N2 neuraminidase of human influenza virus has acquired a substrate specificity complementary to the hemagglutinin receptor specificity. *Virology* **180**, 10-15.

Baumert, T. F., Schuster, C., Cosset, F.-L., Dubuisson, J., Hofmann, M., Tautz, N., Zeisel, M. B. & Thimme, R. (2016). Addressing the Next Challenges: a Summary of the 22nd International Symposium on Hepatitis C Virus and Related Viruses. *Journal of hepatology*.

Beale, R., Wise, H., Stuart, A., Ravenhill, B. J., Digard, P. & Randow, F. (2014). A LC3-Interacting Motif in the Influenza A Virus M2 Protein Is Required to Subvert Autophagy and Maintain Virion Stability. *Cell host & microbe* **15**, 239-247.

Bean, B., Moore, B., Sterner, B., Peterson, L., Gerding, D. & Balfour, H. (1982). Survival of influenza viruses on environmental surfaces. *Journal of infectious diseases* **146**, 47-51.

Bean, W. & Simpson, R. W. (1976). Transcriptase activity and genome composition of defective influenza virus. *Journal of virology* **18**, 365-369.

Belshe, R., Smith, M. H., Hall, C., Betts, R. & Hay, A. (1988). Genetic basis of resistance to rimantadine emerging during treatment of influenza virus infection. *Journal of virology* **62**, 1508-1512.

Belshe, R. B., Mendelman, P. M., Treanor, J., King, J., Gruber, W. C., Piedra, P., Bernstein, D. I., Hayden, F. G., Kotloff, K. & Zangwill, K. (1998). The efficacy of live attenuated, cold-adapted, trivalent, intranasal influenzavirus vaccine in children. *New England Journal of Medicine* **338**, 1405-1412.

Bentham, M. J., Foster, T. L., McCormick, C. & Griffin, S. (2013). Mutations in hepatitis C virus p7 reduce both the egress and infectivity of assembled particles via impaired proton channel function. *Journal of General Virology* **94**, 2236-2248.

Berthoud, T. K., Hamill, M., Lillie, P. J., Hwenda, L., Collins, K. A., Ewer, K. J., Milicic, A., Poyntz, H. C., Lambe, T. & Fletcher, H. A. (2011). Potent CD8+ T-cell immunogenicity in humans of a novel heterosubtypic influenza A vaccine, MVA− NP+ M1. *Clinical infectious diseases* **52**, 1-7.

Betakova, T., Ciampor, F. & Hay, A. J. (2005). Influence of residue 44 on the activity of the M2 proton channel of influenza A virus. *Journal of General Virology* **86**, 181-184.

Birnkrant, D. & Cox, E. (2009). The emergency use authorization of peramivir for treatment of 2009 H1N1 influenza. *New England Journal of Medicine* **361**, 2204-2207.

Black, R. A., Rota, P. A., Gorodkova, N., Cramer, A., Klenk, H.-D. & Kendal, A. P. (1993a). Production of the M2 protein of influenza A virus in insect cells is enhanced in the presence of amantadine. *Journal of general virology* **74**, 1673-1677.

Black, R. A., Rota, P. A., Gorodkova, N., Klenk, H.-D. & Kendal, A. P. (1993b). Antibody response to the M2 protein of influenza A virus expressed in insect cells. *Journal of general virology* **74**, 143-146.

Bliss, C. (1939). The toxicity of poisons applied jointly1. *Annals of applied biology* **26**, 585-615.

Blumenthal, R., Weinstein, J. N., Sharrow, S. O. & Henkart, P. (1977). Liposome--lymphocyte interaction: saturable sites for transfer and intracellular release of liposome contents. *Proceedings of the National Academy of Sciences* **74**, 5603-5607.

BMJ (2013). First probable person to person transmission of new bird flu virus in China. *British Medical Journal* **347**, f4752.

Boone, S. A. & Gerba, C. P. (2005). The occurrence of influenza A virus on household and day care center fomites. *Journal of Infection* **51**, 103-109.

Boson, B., Granio, O., Bartenschlager, R. & Cosset, F.-L. (2011). A concerted action of hepatitis C virus p7 and nonstructural protein 2 regulates core localization at the endoplasmic reticulum and virus assembly. *PLoS Pathogens* **7**, e1002144.

Bour, S., Perrin, C., Akari, H. & Strebel, K. (2001). The human immunodeficiency virus type 1 Vpu protein inhibits NF-κB activation by interfering with βTrCP-mediated degradation of IκB. *Journal of Biological Chemistry* **276**, 15920-15928.

Brankston, G., Gitterman, L., Hirji, Z., Lemieux, C. & Gardam, M. (2007). Transmission of influenza A in human beings. *The Lancet infectious diseases* **7**, 257-265.

Bridges, C. B., Lim, W., Hu-Primmer, J., Sims, L., Fukuda, K., Mak, K., Rowe, T., Thompson, W. W., Conn, L. & Lu, X. (2002). Risk of influenza A (H5N1) infection among poultry workers, Hong Kong, 1997–1998. *Journal of Infectious Diseases* **185**, 1005-1010.

Bukreyev, A., Whitehead, S. S., Murphy, B. R. & Collins, P. L. (1997). Recombinant respiratory syncytial virus from which the entire SH gene has been deleted grows efficiently in cell culture and exhibits site-specific attenuation in the respiratory tract of the mouse. *Journal of virology* **71**, 8973-8982.

Bullough, P. A., Hughson, F. M., Skehel, J. J. & Wiley, D. C. (1994). Structure of influenza haemagglutinin at the pH of membrane fusion. *Nature* **371**, 37-43.

Burgui, I., Aragon, T., Ortín, J. & Nieto, A. (2003). PABP1 and eIF4GI associate with influenza virus NS1 protein in viral mRNA translation initiation complexes. *Journal of General Virology* **84**, 3263-3274.

Butler, J., Hooper, K. A., Petrie, S., Lee, R., Maurer-Stroh, S., Reh, L., Guarnaccia, T., Baas, C., Xue, L. & Vitesnik, S. (2014). Estimating the Fitness Advantage Conferred by Permissive Neuraminidase Mutations in Recent Oseltamivir-Resistant A (H1N1) pdm09 Influenza Viruses. *PLoS Pathogens* **10**, e1004065.

Cady, S. D., Mishanina, T. V. & Hong, M. (2009). Structure of amantadine-bound M2 transmembrane peptide of influenza A in lipid bilayers from magic-angle-spinning solid-state NMR: the role of Ser31 in amantadine binding. *Journal of molecular biology* **385**, 1127-1141.

Cady, S. D., Schmidt-Rohr, K., Wang, J., Soto, C. S., Degrado, W. F. & Hong, M. (2010). Structure of the amantadine binding site of influenza M2 proton channels in lipid bilayers. *Nature* **463**, 689-692.

Cannell, J., Vieth, R., Umhau, J., Holick, M., Grant, W., Madronich, S., Garland, C. & Giovannucci, E. (2006). Epidemic influenza and vitamin D. *Epidemiology and infection* **134**, 1129-1140.

Carrasco, L. (1978). Membrane leakiness after viral infection and a new approach to the development of antiviral agents. *Nature* **272**, 694-699.

Carrasco, L. (2001). Human immunodeficiency virus type 1 VPU protein affects Sindbis virus glycoprotein processing and enhances membrane permeabilization. *Virology* **279**, 201-209.

Carrere-Kremer, S., Montpellier-Pala, C., Cocquerel, L., Wychowski, C., Penin, F. & Dubuisson, J. (2002). Subcellular localization and topology of the p7 polypeptide of hepatitis C virus. *Journal of Virology* **76**, 3720-3730.

Carter, S. D., Dent, K. C., Atkins, E., Foster, T. L., Verow, M., Gorny, P., Harris, M., Hiscox, J. A., Ranson, N. A., Griffin, S. & Barr, J. N. (2010). Direct visualization of the small hydrophobic protein of human respiratory syncytial virus reveals the structural basis for membrane permeability. *FEBS Letters* **584**, 2786-2790.

Cases, C. (1998). Isolation of avian influenza A (H5N1) viruses from humans—Hong Kong, May-December 1997. *JAMA* **279**, 263.

Cass, L. M., Efthymiopoulos, C. & Bye, A. (1999). Pharmacokinetics of zanamivir after intravenous, oral, inhaled or intranasal administration to healthy volunteers. *Clinical pharmacokinetics* **36**, 1-11.

Castrucci, M. R., Donatelli, I., Sidoli, L., Barigazzi, G., Kawaoka, Y. & Webster, R. G. (1993). Genetic reassortment between avian and human influenza A viruses in Italian pigs. *Virology* **193**, 503-506.

Chan, P. K. (2002). Outbreak of avian influenza A (H5N1) virus infection in Hong Kong in 1997. *Clinical Infectious Diseases* **34**, S58-S64.

Chen, B. J., Leser, G. P., Jackson, D. & Lamb, R. A. (2008). The Influenza Virus M2 Protein Cytoplasmic Tail Interacts with the M1 Protein and Influences Virus Assembly at the Site of Virus Budding. *Journal of Virology* **82**, 10059-10070.

Chen, W., Calvo, P. A., Malide, D., Gibbs, J., Schubert, U., Bacik, I., Basta, S., O'Neill, R., Schickli, J. & Palese, P. (2001). A novel influenza A virus mitochondrial protein that induces cell death. *Nature medicine* **7**, 1306-1312.

Cheong, H.-K., Cheong, C. & Choi, B.-S. (1996). Secondary structure of the panhandle RNA of influenza virus A studied by NMR spectroscopy. *Nucleic acids research* **24**, 4197-4201.

Cherkasov, A., Muratov, E. N., Fourches, D., Varnek, A., Baskin, I. I., Cronin, M., Dearden, J., Gramatica, P., Martin, Y. C. & Todeschini, R. (2014). QSAR modeling: where have you been? Where are you going to? *Journal of medicinal chemistry* **57**, 4977-5010.

Cheung, C.-L., Rayner, J. M., Smith, G. J., Wang, P., Naipospos, T., Zhang, J., Yuen, K.-Y., Webster, R. G., Peiris, J. M. & Guan, Y. (2006). Distribution of amantadine-resistant H5N1 avian influenza variants in Asia. *Journal of Infectious Diseases* **193**, 1626-1629.

Chou, T.-C. (2006). Theoretical basis, experimental design, and computerized simulation of synergism and antagonism in drug combination studies. *Pharmacological reviews* **58**, 621-681.

Chou, T.-C. (2010). Drug combination studies and their synergy quantification using the Chou-Talalay method. *Cancer research* **70**, 440-446.

Chu, C., Dawson, I. & Elford, W. (1949). Filamentous forms associated with newly isolated influenza virus. *The Lancet* **253**, 602-603.

Ciampor, F., Bayley, P., Nermut, M., Hirst, E., Sugrue, R. & Hay, A. (1992). Evidence that the amantadine-induced, M2-mediated conversion of influenza A virus hemagglutinin to the low pH conformation occurs in an acidic trans Golgi compartment. *Virology* **188**, 14-24.

Claas, E. C., Osterhaus, A. D., Van Beek, R., De Jong, J. C., Rimmelzwaan, G. F., Senne, D. A., Krauss, S., Shortridge, K. F. & Webster, R. G. (1998). Human influenza A H5N1 virus related to a highly pathogenic avian influenza virus. *The Lancet* **351**, 472-477.

Clarke, D., Griffin, S., Beales, L., Gelais, C. S., Burgess, S., Harris, M. & Rowlands, D. (2006). Evidence for the formation of a heptameric ion channel complex by the hepatitis C virus p7 protein in vitro. *Journal of Biological Chemistry* **281**, 37057-37068.

Cochran, K. W., Maassab, H. F., Tsunoda, A. & Berlin, B. S. (1965). Studies on the antiviral activity of amantadine hydrochloride. *Annals of the New York Academy of Sciences* **130**, 432-439.

Cohen, E. A., Terwilliger, E. F., Sodroski, J. G. & Haseltine, W. A. (1988). Identification of a protein encoded by the vpu gene of HIV-1. *Nature* **334**, 532-534.

Colacino, J. M., Laver, W. G. & Air, G. M. (1997). Selection of influenza A and B viruses for resistance to 4-guanidino-Neu5Ac2en in cell culture. *Journal of Infectious Diseases* **176**, S66-S68.

Coleman, M., Dowdle, W., Pereira, H., Schild, G. & Chang, W. (1968). The HONG KONG/68 influenza A2 variant. *The Lancet* **292**, 1384-1386.

Collins, P. L. & Mottet, G. (1993). Membrane orientation and oligomerization of the small hydrophobic protein of human respiratory syncytial virus. *Journal of General Virology* **74**, 1445-1450.

Compans, R. W. & Duesberg, P. H. (1972). Structure of the ribonucleoprotein of influenza virus. *Journal of Virology* **10**, 795-800.

Control, C. f. D. & Prevention (2008). Update: influenza activity--United States, September 28-November 29, 2008. *MMWR Morbidity and mortality weekly report* **57**, 1329.

Cook, G. A., Dawson, L. A., Tian, Y. & Opella, S. J. (2013). Three-Dimensional Structure and Interaction Studies of Hepatitis C Virus p7 in 1,2-Dihexanoyl- sn -glycero-3-phosphocholine by Solution Nuclear Magnetic Resonance. *Biochemistry* **52**, 5295-5303.

Cordes, F. S., Kukol, A., Forrest, L. R., Arkin, I. T., Sansom, M. S. P. & Fischer, W. B. (2001). The structure of the HIV-1 Vpu ion channel: modelling and simulation studies. *Biochimica et Biophysica Acta (BBA) - Biomembranes* **1512**, 291-298.

Davies, B. E. (2010). Pharmacokinetics of oseltamivir: an oral antiviral for the treatment and prophylaxis of influenza in diverse populations. *Journal of antimicrobial chemotherapy* **65**, ii5-ii10.

Davies, W., Grunert, R., Haff, R., McGahen, J., Neumayer, E., Paulshock, M., Watts, J., Wood, T., Hermann, E. & Hoffmann, C. (1964a). Antiviral activity of 1-adamantanamine (amantadine). *Science* **144**, 862-863.

Davies, W. L., Grunert, R. R., Haff, R. F., McGahen, J. W., Neumayer, E. M., Paulshock, M., Watts, J. C., Wood, T. R., Hermann, E. C. & Hoffmann, C. E. (1964b). Antiviral Activity of 1-Adamantanamine (Amantadine). *Science* **144**, 862-863.

Dawood, F., Jain, S., Finelli, L., Shaw, M., Lindstrom, S. & Garten, R. (2009). Emergence of a Novel Swine-Origin Influenza A (H1N1) Virus in Humans. *N Engl J Med* **360**, 2605-2465.

Dawson, I. a. & Elford, W. (1949). The investigation of influenza and related viruses in the electron microscope, by a new technique. *Microbiology* **3**, 298-311.

De Filette, M., Jou, W. M., Birkett, A., Lyons, K., Schultz, B., Tonkyro, A., Resch, S. & Fiers, W. (2005). Universal influenza A vaccine: optimization of M2-based constructs. *Virology* **337**, 149-161.

De La Luna, S., Fortes, P., Beloso, A. & Ortín, J. (1995). Influenza virus NS1 protein enhances the rate of translation initiation of viral mRNAs. *Journal of virology* **69**, 2427-2433.

Desselberger, U., Nakajima, K., Alfino, P., Pedersen, F. S., Haseltine, W. A., Hannoun, C. & Palese, P. (1978). Biochemical evidence that" new" influenza virus strains in nature may arise by recombination (reassortment). *Proceedings of the National Academy of Sciences* **75**, 3341-3345.

Desselberger, U., Racaniello, V. R., Zazra, J. J. & Palese, P. (1980). The 3'and 5'-terminal sequences of influenza A, B and C virus RNA segments are highly conserved and show partial inverted complementarity. *Gene* **8**, 315-328.

Devita, V. T., Serpick, A. A. & Carbone, P. P. (1970). Combination chemotherapy in the treatment of advanced Hodgkin's disease. *Annals of Internal Medicine* **73**, 881-895.

Dias, A., Bouvier, D., Crépin, T., McCarthy, A. A., Hart, D. J., Baudin, F., Cusack, S. & Ruigrok, R. W. (2009). The cap-snatching endonuclease of influenza virus polymerase resides in the PA subunit. *Nature* **458**, 914-918.

Dong, G., Peng, C., Luo, J., Wang, C., Han, L., Wu, B., Ji, G. & He, H. (2015). Adamantane-resistant influenza a viruses in the world (1902–2013): Frequency and distribution of M2 gene mutations. *PloS one* **10**, e0119115.

Dong, H., Fiorin, G., DeGrado, W. F. & Klein, M. L. (2013). Exploring histidine conformations in the M2 channel lumen of the influenza A virus at neutral pH via molecular simulations. *The journal of physical chemistry letters* **4**, 3067-3071.

Drake, J. W. (1993). Rates of spontaneous mutation among RNA viruses. *Proceedings of the National Academy of Sciences* **90**, 4171-4175.

Du, B., Wolf, A., Lee, S. & Terwilliger, E. (1993). Changes in the host range and growth potential of an HIV-1 clone are conferred by the vpu gene. *Virology* **195**, 260-264.

Du, Q.-S., Huang, R.-B., Wang, S.-Q. & Chou, K.-C. (2010). Designing inhibitors of M2 proton channel against H1N1 swine influenza virus. *PLoS ONE [Electronic Resource]* **5**, e9388.

Duesberg, P. H. (1968). The RNA's of influenza virus. *Proc Nat Acad Sci USA* **59**, 930-937.

Duff, K. C. & Ashley, R. H. (1992). The transmembrane domain of influenza A M2 protein forms amantadine-sensitive proton channels in planar lipid bilayers. *Virology* **190**, 485-489.

Duque, M. D., Ma, C., Torres, E., Wang, J., Naesens, L., Juárez-Jiménez, J., Camps, P., Luque, F. J., DeGrado, W. F., Lamb, R. A., Pinto, L. H. & Vázquez, S. (2011). Exploring the Size Limit of Templates for Inhibitors of the M2 Ion Channel of Influenza A Virus. *J Med Chem* **54**, 2646-2657.

Durrant, M. G., Eggett, D. L. & Busath, D. D. (2015). Investigation of a recent rise of dual amantadine-resistance mutations in the influenza A M2 sequence. *BMC genetics* **16**, S3.

Duval, X., Van Der Werf, S., Blanchon, T., Mosnier, A., Bouscambert-Duchamp, M., Tibi, A., Enouf, V., Charlois-Ou, C., Vincent, C. & Andreoletti, L. (2010). Efficacy of oseltamivir-zanamivir combination compared to each monotherapy for seasonal influenza: a randomized placebo-controlled trial. *PLoS Med* **7**, e1000362.

Eisfeld, A. J., Kawakami, E., Watanabe, T., Neumann, G. & Kawaoka, Y. (2011). RAB11A is essential for transport of the influenza virus genome to the plasma membrane. *Journal of virology* **85**, 6117-6126.

Eisfeld, A. J., Neumann, G. & Kawaoka, Y. (2015). At the centre: influenza A virus ribonucleoproteins. *Nature Reviews Microbiology* **13**, 28-41.

Ewart, G., Sutherland, T., Gage, P. & Cox, G. (1996). The Vpu protein of human immunodeficiency virus type 1 forms cation-selective ion channels. *Journal of virology* **70**, 7108-7115.

Ewart, G. D., Mills, K., Cox, G. B. & Gage, P. W. (2002). Amiloride derivatives block ion channel activity and enhancement of virus-like particle budding caused by HIV-1 protein Vpu. *European Biophysics Journal* **31**, 26-35.

Farooqui, A., Huang, L., Wu, S., Cai, Y., Su, M., Lin, P., Chen, W., Fang, X., Zhang, L. & Liu, Y. (2015). Assessment of antiviral properties of Peramivir against H7N9 avian influenza virus in an experimental mouse model. *Antimicrobial agents and chemotherapy* **59**, 7255-7264.

Feng, J., Zhang, M., Mozdzanowska, K., Zharikova, D., Hoff, H., Wunner, W., Couch, R. B. & Gerhard, W. (2006). Influenza A virus infection engenders a poor antibody response against the ectodomain of matrix protein 2. *Virology journal* **3**, 1.

Fiore, A. E., Fry, A., Shay, D., Gubareva, L., Bresee, J. S., Uyeki, T. M., Centers for Disease, C. & Prevention (2011). Antiviral agents for the treatment and chemoprophylaxis of influenza --- recommendations of the Advisory Committee on Immunization Practices (ACIP). *Morbidity & Mortality Weekly Report Recommendations & Reports* **60**, 1-24.

Fleet, G. W., Karpas, A., Dwek, R. A., Fellows, L. E., Tyms, A., Petursson, S., Namgoong, S. K., Ramsden, N. G., Smith, P. W. & Son, J. C. (1988). Inhibition of HIV replication by amino-sugar derivatives. *FEBS letters* **237**, 128-132.

Fodor, E., Pritlove, D. C. & Brownlee, G. G. (1994). The influenza virus panhandle is involved in the initiation of transcription. *Journal of virology* **68**, 4092-4096.

Fodor, E., Seong, B. L. & Brownlee, G. G. (1993). Photochemical cross-linking of influenza A polymerase to its virion RNA promoter defines a polymerase binding site at residues 9 to 12 of the promoter. *Journal of General Virology* **74**, 1327-1333.

Foster, T. L., Thompson, G. S., Kalverda, A. P., Kankanala, J., Bentham, M., Wetherill, L. F., Thompson, J., Barker, A. M., Clarke, D., Noerenberg, M., Pearson, A. R., Rowlands, D. J., Homans, S. W., Harris, M., Foster, R. & Griffin, S. (2014). Structure-guided design affirms inhibitors of hepatitis C virus p7 as a viable class of antivirals targeting virion release. *Hepatology* **59**, 408-422.

Foster, T. L., Verow, M., Wozniak, A. L., Bentham, M. J., Thompson, J., Atkins, E., Weinman, S. A., Fishwick, C., Foster, R., Harris, M. & Griffin, S. (2011). Resistance mutations define specific antiviral effects for inhibitors of the hepatitis C virus p7 ion channel. *Hepatology* **54**, 79-90.

Foster, T. L. G., Stephen D.C (unpublished).

Franchi, L., Eigenbrod, T., Muñoz-Planillo, R. & Nuñez, G. (2009). The inflammasome: a caspase-1-activation platform that regulates immune responses and disease pathogenesis. *Nature immunology* **10**, 241-247.

Francis Jr, T., Salk, J. E., Pearson, H. E. & Brown, P. N. (1945). Protective effect of vaccination against induced influenza A. *Journal of Clinical Investigation* **24**, 536.

Francis, T. & Magill, T. (1937). The antibody response of human subjects vaccinated with the virus of human influenza. *The Journal of experimental medicine* **65**, 251-259.

Francis, T., Salk, J. E. & Brace, W. M. (1946). The protective effect of vaccination against epidemic influenza B. *Journal of the American Medical Association* **131**, 275-278.

Frei, E., Holland, J. F., Schneiderman, M. A., Pinkel, D., SELKIRK, G., FREIREICH, E. J., SILVER, R. T., GOLD, G. L. & REGELSON, W. (1958). A comparative study of two regimens of combination chemotherapy in acute leukemia. *Blood* **13**, 1126-1148.

Fuentes, S., Tran, K. C., Luthra, P., Teng, M. N. & He, B. (2007). Function of the Respiratory Syncytial Virus Small Hydrophobic Protein. *Journal of Virology* **81**, 8361-8366.

Fujii, K., Fujii, Y., Noda, T., Muramoto, Y., Watanabe, T., Takada, A., Goto, H., Horimoto, T. & Kawaoka, Y. (2005). Importance of both the coding and the segment-specific noncoding regions of the influenza A virus NS segment for its efficient incorporation into virions. *Journal of virology* **79**, 3766-3774.

Fujii, Y., Goto, H., Watanabe, T., Yoshida, T. & Kawaoka, Y. (2003). Selective incorporation of influenza virus RNA segments into virions. *Proceedings of the National Academy of Sciences* **100**, 2002-2007.

Furuse, Y., Suzuki, A. & Oshitani, H. (2009). Large-scale sequence analysis of M gene of influenza A viruses from different species: mechanisms for emergence and spread of amantadine resistance. *Antimicrobial Agents & Chemotherapy* **53**, 4457-4463.

Furuta, Y., Gowen, B. B., Takahashi, K., Shiraki, K., Smee, D. F. & Barnard, D. L. (2013). Favipiravir (T-705), a novel viral RNA polymerase inhibitor. *Antiviral research* **100**, 446-454.

Gack, M. U., Albrecht, R. A., Urano, T., Inn, K.-S., Huang, I.-C., Carnero, E., Farzan, M., Inoue, S., Jung, J. U. & García-Sastre, A. (2009). Influenza A virus NS1 targets the ubiquitin ligase TRIM25 to evade recognition by the host viral RNA sensor RIG-I. *Cell host & microbe* **5**, 439-449.

Gamblin, S., Haire, L., Russell, R., Stevens, D., Xiao, B., Ha, Y., Vasisht, N., Steinhauer, D., Daniels, R. & Elliot, A. (2004). The structure and receptor binding properties of the 1918 influenza hemagglutinin. *Science* **303**, 1838-1842.

Gan, S. W., Ng, L., Lin, X., Gong, X. & Torres, J. (2008). Structure and ion channel activity of the human respiratory syncytial virus (hRSV) small hydrophobic protein transmembrane domain. *Protein Science* **17**, 813-820.

Gan, S. W., Tan, E., Lin, X., Yu, D., Wang, J., Tan, G. M. Y., Vararattanavech, A., Yeo, C. Y., Soon, C. H., Soong, T. W., Pervushin, K. & Torres, J. (2012). The Small Hydrophobic Protein of the Human Respiratory Syncytial Virus Forms Pentameric Ion Channels. *Journal of Biological Chemistry* **287**, 24671-24689.

Gannagé, M., Dormann, D., Albrecht, R., Dengjel, J., Torossi, T., Rämer, P. C., Lee, M., Strowig, T., Arrey, F. & Conenello, G. (2009). Matrix protein 2 of influenza A virus blocks autophagosome fusion with lysosomes. *Cell host & microbe* **6**, 367-380.

Gao, R., Cao, B., Hu, Y., Feng, Z., Wang, D., Hu, W., Chen, J., Jie, Z., Qiu, H. & Xu, K. (2013). Human infection with a novel avian-origin influenza A (H7N9) virus. *New England Journal of Medicine* **368**, 1888-1897.

Garcí, A., Egorov, A., Matassov, D., Brandt, S., Levy, D. E., Durbin, J. E., Palese, P. & Muster, T. (1998). Influenza A virus lacking the NS1 gene replicates in interferon-deficient systems. *Virology* **252**, 324-330.

Garcia, V. & Aris-Brosou, S. (2014). Comparative dynamics and distribution of influenza drug resistance acquisition to protein M2 and neuraminidase inhibitors. *Molecular biology and evolution* **31**, 355-363.

Gaush, C. R. & Smith, T. F. (1968). Replication and plaque assay of influenza virus in an established line of canine kidney cells. *Applied microbiology* **16**, 588-594.

Gentzsch, J., Brohm, C., Steinmann, E., Friesland, M., Menzel, N., Vieyres, G., Perin, P. M., Frentzen, A., Kaderali, L. & Pietschmann, T. (2013). Hepatitis C Virus p7 is Critical for Capsid Assembly and Envelopment. *PLoS Pathogens* **9**, e1003355.

George, K. S. (2012). Diagnosis of influenza virus. *Influenza Virus: Methods and Protocols*, 53-69.

Gervais, C., Do, F., Cantin, A., Kukolj, G., White, P. W., Gauthier, A. & Vaillancourt, F. H. (2011). Development and validation of a high-throughput screening assay for the hepatitis C virus p7 viroporin. *Journal of Biomolecular Screening* **16**, 363-369.

Gieswein, C. E., Sharom, F. J. & Wildeman, A. G. (2003). Oligomerization of the E5 protein of human papillomavirus type 16 occurs through multiple hydrophobic regions. *Virology* **313**, 415-426.

Glück, R., Mischler, R., Brantschen, S., Just, M., Althaus, B. & Cryz Jr, S. (1992). Immunopotentiating reconstituted influenza virus virosome vaccine delivery system for immunization against hepatitis A. *Journal of Clinical Investigation* **90**, 2491.

Goldin, A. & Mantel, N. (1957). The employment of combinations of drugs in the chemotherapy of neoplasia: a review. *Cancer research* **17**, 635-654.

Goodsell, D. S. & Olson, A. J. (1990). Automated docking of substrates to proteins by simulated annealing. *Proteins: Structure, Function, and Bioinformatics* **8**, 195-202.

Goto, H., Muramoto, Y., Noda, T. & Kawaoka, Y. (2013). The genome-packaging signal of the influenza A virus genome comprises a genome incorporation signal and a genome-bundling signal. *Journal of virology* **87**, 11316-11322.

Goulet, M.-L., Olagnier, D., Xu, Z., Paz, S., Belgnaoui, S. M., Lafferty, E. I., Janelle, V., Arguello, M., Paquet, M. & Ghneim, K. (2013). Systems analysis of a RIG-I agonist inducing broad spectrum inhibition of virus infectivity. *PLoS Pathog* **9**, e1003298.

Govorkova, E. A., Baranovich, T., Seiler, P., Armstrong, J., Burnham, A., Guan, Y., Peiris, M., Webby, R. J. & Webster, R. G. (2013). Antiviral resistance among highly pathogenic influenza A (H5N1) viruses isolated worldwide in 2002-2012 shows need for continued monitoring. *Antiviral Research*.

Govorkova, E. A., Fang, H.-B., Tan, M. & Webster, R. G. (2004). Neuraminidase inhibitor-rimantadine combinations exert additive and synergistic anti-influenza virus effects in MDCK cells. *Antimicrobial agents and chemotherapy* **48**, 4855-4863.

Grambas, S. & Hay, A. (1992). Maturation of influenza A virus hemagglutinin—estimates of the pH encountered during transport and its regulation by the M2 protein. *Virology* **190**, 11-18.

Greco, W. R., Bravo, G. & Parsons, J. C. (1995). The search for synergy: a critical review from a response surface perspective. *Pharmacological reviews* **47**, 331-385.

Grice, A. L., Kerr, I. D. & Sansom, M. S. P. (1997). Ion channels formed by HIV-1 Vpu: a modelling and simulation study. *FEBS Letters* **405**, 299-304.

Griffin, S., Stgelais, C., Owsianka, A. M., Patel, A. H., Rowlands, D. & Harris, M. (2008). Genotype-dependent sensitivity of hepatitis C virus to inhibitors of the p7 ion channel. *Hepatology* **48**, 1779-1790.

Griffin, S. D. C. (2004). A conserved basic loop in hepatitis C virus p7 protein is required for amantadine-sensitive ion channel activity in mammalian cells but is dispensable for localization to mitochondria. *Journal of General Virology* **85**, 451-461.

Griffin, S. D. C., Beales, L. P., Clarke, D. S., Worsfold, O., Evans, S. D., Jaeger, J., Harris, M. P. G. & Rowlands, D. J. (2003). The p7 protein of hepatitis C virus forms an ion channel that is blocked by the antiviral drug, Amantadine. *FEBS Letters* **535**, 34-38.

Griffin, S. D. C., Harvey, R., Clarke, D. S., Barclay, W. S., Harris, M. & Rowlands, D. J. (2004). A conserved basic loop in hepatitis C virus p7 protein is required for amantadine-sensitive ion channel activity in mammalian cells but is dispensable for localization to mitochondria. *Journal of General Virology* **85**, 451-461.

Gubareva, L. V., Kaiser, L. & Hayden, F. G. (2000). Influenza virus neuraminidase inhibitors. *The Lancet* **355**, 827-835.

Gubareva, L. V., Kaiser, L., Matrosovich, M. N., Soo-Hoo, Y. & Hayden, F. G. (2001). Selection of influenza virus mutants in experimentally infected volunteers treated with oseltamivir. *Journal of Infectious Diseases* **183**, 523-531.

Gubareva, L. V., Matrosovich, M. N., Brenner, M. K., Bethell, R. C. & Webster, R. G. (1998). Evidence for zanamivir resistance in an immunocompromised child infected with influenza B virus. *Journal of Infectious Diseases* **178**, 1257-1262.

Gubareva, L. V., Trujillo, A. A., Okomo-Adhiambo, M., Mishin, V. P., Deyde, V. M., Sleeman, K., Nguyen, H. T., Sheu, T. G., Garten, R. J., Shaw, M. W., Fry, A. M. & Klimov, A. I. (2010). Comprehensive assessment of 2009 pandemic influenza A (H1N1) virus drug susceptibility in vitro. *Antiviral Therapy* **15**, 1151-1159.

Hagen, N., Bayer, K., Rosch, K. & Schindler, M. (2014). The Intraviral Protein Interaction Network of Hepatitis C Virus. *Molecular & Cellular Proteomics* **13**, 1676-1689.

Halbert, C. L. & Galloway, D. A. (1988). Identification of the E5 open reading frame of human papillomavirus type 16. *Journal of virology* **62**, 1071-1075.

Hamilton, B. S., Chung, C., Cyphers, S. Y., Rinaldi, V. D., Marcano, V. C. & Whittaker, G. R. (2014). Inhibition of influenza virus infection and hemagglutinin cleavage by the protease inhibitor HAI-2. *Biochemical and biophysical research communications* **450**, 1070-1075.

Hammer, S. M., Katzenstein, D. A., Hughes, M. D., Gundacker, H., Schooley, R. T., Haubrich, R. H., Henry, W. K., Lederman, M. M., Phair, J. P. & Niu, M. (1996). A trial comparing nucleoside monotherapy with combination therapy in HIV-infected adults with CD4 cell counts from 200 to 500 per cubic millimeter. *New England Journal of Medicine* **335**, 1081-1090.

Hamre, D., Loosli, C. G. & Gerber, P. (1958). Antigenic variants of influenza A virus (PR8 strain) III. Serological relationships of a line of variants derived in sequence in mice given homologous vaccine. *The Journal of experimental medicine* **107**, 829-844.

Haqshenas, G., Mackenzie, J. M., Dong, X. & Gowans, E. J. (2007). Hepatitis C virus p7 protein is localized in the endoplasmic reticulum when it is encoded by a replication-competent genome. *Journal of General Virology* **88**, 134-142.

Hay, A., Wolstenholme, A., Skehel, J. & Smith, M. H. (1985). The molecular basis of the specific anti-influenza action of amantadine. *The EMBO journal* **4**, 3021.

Hay, A., Zambon, M., Wolstenholme, A., Skehel, J. & Smith, M. (1986). Molecular basis of resistance of influenza A viruses to amantadine. *Journal of Antimicrobial Chemotherapy* **18**, 19-29.

Hayden, F. & Croisier, A. (2005). Transmission of avian influenza viruses to and between humans. *Journal of Infectious Diseases* **192**, 1311-1314.

Hayden, F., Douglas, R. & Simons, R. (1980). Enhancement of activity against influenza viruses by combinations of antiviral agents. *Antimicrobial agents and chemotherapy* **18**, 536-541.

Heggeness, M. H., Smith, P., Ulmanen, I., Krug, R. M. & Choppin, P. W. (1982). Studies on the helical nucleocapsid of influenza virus. *Virology* **118**, 466-470.

Hemmes, J., Winkler, K. & Kool, S. (1960). Virus survival as a seasonal factor in influenza and poliomyelitis.

Herfst, S., Schrauwen, E. J., Linster, M., Chutinimitkul, S., de Wit, E., Munster, V. J., Sorrell, E. M., Bestebroer, T. M., Burke, D. F. & Smith, D. J. (2012). Airborne transmission of influenza A/H5N1 virus between ferrets. *science* **336**, 1534-1541.

Herz, C., Stavnezer, E., Krug, R. M. & Gurney Jr, T. (1981). Influenza virus, an RNA virus, synthesizes its messenger RNA in the nucleus of infected cells. *Cell* **26**, 391-400.

Hirata, N., Suizu, F., Matsuda-Lennikov, M., Edamura, T., Bala, J. & Noguchi, M. (2014). Inhibition of Akt kinase activity suppresses entry and replication of influenza virus. *Biochemical and Biophysical Research Communications*.

Hoffmann, C., Neumayer, E. M., Haff, R. & Goldsby, R. (1965). Mode of action of the antiviral activity of amantadine in tissue culture. *Journal of bacteriology* **90**, 623-628.

Hoopes, J. D., Driebe, E. M., Kelley, E., Engelthaler, D. M., Keim, P. S., Perelson, A. S., Rong, L., Went, G. T. & Nguyen, J. T. (2011). Triple combination antiviral drug (TCAD) composed of amantadine, oseltamivir, and ribavirin impedes the selection of drug-resistant influenza A virus. *PLoS One* **6**, e29778.

Hope-Simpson, R. (1981). The role of season in the epidemiology of influenza. *Journal of Hygiene* **86**, 35-47.

Hornung, V., Ellegast, J., Kim, S., Brzózka, K., Jung, A., Kato, H., Poeck, H., Akira, S., Conzelmann, K.-K. & Schlee, M. (2006). 5'-Triphosphate RNA is the ligand for RIG-I. *Science* **314**, 994-997.

Hout, D. R., Gomez, M. L., Pacyniak, E., Gomez, L. M., Inbody, S. H., Mulcahy, E. R., Culley, N., Pinson, D. M., Powers, M. F., Wong, S. W. & Stephens, E. B. (2005). Scrambling of the amino acids within the transmembrane domain of Vpu results in a simian-human immunodeficiency virus (SHIVTM) that is less pathogenic for pig-tailed macaques. *Virology* **339**, 56-69.

Hsu, K., Han, J., Shinlapawittayatorn, K., Deschenes, I. & Marbán, E. (2010). Membrane potential depolarization as a triggering mechanism for Vpu-mediated HIV-1 release. *Biophysical journal* **99**, 1718-1725.

Hsu, M.-T., Parvin, J. D., Gupta, S., Krystal, M. & Palese, P. (1987). Genomic RNAs of influenza viruses are held in a circular conformation in virions and in infected cells by a terminal panhandle. *Proceedings of the National Academy of Sciences* **84**, 8140-8144.

Hu, J., Asbury, T., Achuthan, S., Li, C., Bertram, R., Quine, J. R., Fu, R. & Cross, T. A. (2007a). Backbone Structure of the Amantadine-Blocked Trans-Membrane Domain M2 Proton Channel from Influenza A Virus. *Biophysical Journal* **92**, 4335-4343.

Hu, J., Fu, R. & Cross, T. A. (2007b). The chemical and dynamical influence of the anti-viral drug amantadine on the M 2 proton channel transmembrane domain. *Biophysical journal* **93**, 276-283.

Hu, J., Fu, R., Nishimura, K., Zhang, L., Zhou, H. X., Busath, D. D., Vijayvergiya, V. & Cross, T. A. (2006). Histidines, heart of the hydrogen ion channel from influenza A virus: Toward an understanding of conductance and proton selectivity. *Proceedings of the National Academy of Sciences* **103**, 6865-6870.

Hu, W., Zeng, S., Li, C., Jie, Y., Li, Z. & Chen, L. (2010). Identification of hits as matrix-2 protein inhibitors through the focused screening of a small primary amine library. *Journal of Medicinal Chemistry* **53**, 3831-3834.

Hurt, A., Selleck, P., Komadina, N., Shaw, R., Brown, L. & Barr, I. (2007). Susceptibility of highly pathogenic A (H5N1) avian influenza viruses to the neuraminidase inhibitors and adamantanes. *Antiviral research* **73**, 228-231.

Hurt, A. C., Holien, J. K., Parker, M., Kelso, A. & Barr, I. G. (2009). Zanamivir-resistant influenza viruses with a novel neuraminidase mutation. *Journal of virology* **83**, 10366-10373.

Hussain, S., Miller, J., Harvey, D., Gu, Y., Rosenthal, P., Zitzmann, N. & McCauley, J. (2014). Strain-specific antiviral activity of iminosugars against human influenza A viruses. *Journal of Antimicrobial Chemotherapy*, dku349.

Ichinohe, T., Pang, I. K. & Iwasaki, A. (2010). Influenza virus activates inflammasomes via its intracellular M2 ion channel. *Nature immunology* **11**, 404-410.

Ilyushina, N. A., Bovin, N. V., Webster, R. G. & Govorkova, E. A. (2006). Combination chemotherapy, a potential strategy for reducing the emergence of drug-resistant influenza A variants. *Antiviral Research* **70**, 121-131.

Imai, M., Watanabe, T., Hatta, M., Das, S. C., Ozawa, M., Shinya, K., Zhong, G., Hanson, A., Katsura, H. & Watanabe, S. (2012). Experimental adaptation of an influenza H5 HA confers respiratory droplet transmission to a reassortant H5 HA/H1N1 virus in ferrets. *Nature* **486**, 420-428.

Inamdar, P., Bhandari, S., Sonawanw, B., Hole, A. & Jadhav, C. (2014). Structure Optimization of Neuraminidase Inhibitors as Potential Anti-Influenza (H1N1Inhibitors) Agents Using QSAR and Molecular Docking Studies. *Iranian Journal of Pharmaceutical Research* **13**, 49-65.

Ison, M. G., Nagy-Agren, S., Paya, C., Steigbigel, R., Elliott, M., Weiss, H. L. & Hayden, F. G. (2003). Safety and efficacy of nebulized zanamivir in hospitalized patients with serious influenza. *Antiviral therapy* **8**, 183-190.

Ito, T., Couceiro, J. N. S., Kelm, S., Baum, L. G., Krauss, S., Castrucci, M. R., Donatelli, I., Kida, H., Paulson, J. C. & Webster, R. G. (1998). Molecular basis for the generation in pigs of influenza A viruses with pandemic potential. *Journal of virology* **72**, 7367-7373.

Iwasaki, A. & Pillai, P. S. (2014). Innate immunity to influenza virus infection. *Nature Reviews Immunology* **14**, 315-328.

Jacob, G. S. & Bryant, M. L. (1993). Iminosugar glycosylation inhibitors as anti-HIV agents. *Perspectives in Drug Discovery and Design* **1**, 211-224.

Jagger, B. W., Wise, H. M., Kash, J. C., Walters, K.-A., Wills, N. M., Xiao, Y.-L., Dunfee, R. L., Schwartzman, L. M., Ozinsky, A., Bell, G. L., Dalton, R. M., Lo, A., Efstathiou, S., Atkins, J. F., Firth, A. E., Taubenberger, J. K. & Digard, P. (2012). An Overlapping Protein-Coding Region in Influenza A Virus Segment 3 Modulates the Host Response. *Science* **337**, 199-204.

Jirasko, V., Montserret, R., Appel, N., Janvier, A., Eustachi, L., Brohm, C., Steinmann, E., Pietschmann, T., Penin, F. & Bartenschlager, R. (2008). Structural and Functional Characterization of Nonstructural Protein 2 for Its Role in Hepatitis C Virus Assembly. *Journal of Biological Chemistry* **283**, 28546-28562.

Jirasko, V., Montserret, R., Lee, J. Y., Gouttenoire, J., Moradpour, D., Penin, F. & Bartenschlager, R. (2010). Structural and functional studies of nonstructural protein 2 of the hepatitis C virus reveal its key role as organizer of virion assembly. *PLoS Pathogens* **6**, e1001233.

Johansson, B. E. & Cox, M. M. (2011). Influenza viral neuraminidase: the forgotten antigen. *Expert review of vaccines* **10**, 1683-1695.

Johnson, N. P. & Mueller, J. (2002). Updating the accounts: global mortality of the 1918-1920" Spanish" influenza pandemic. *Bulletin of the History of Medicine* **76**, 105-115.

Jones, C. T., Murray, C. L., Eastman, D. K., Tassello, J. & Rice, C. M. (2007). Hepatitis C virus p7 and NS2 proteins are essential for production of infectious virus. *Journal of Virology* **81**, 8374-8383.

Kakisaka, M., Sasaki, Y., Yamada, K., Kondoh, Y., Hikono, H., Osada, H., Tomii, K., Saito, T. & Aida, Y. (2015). A Novel Antiviral Target Structure Involved in the RNA Binding, Dimerization, and Nuclear Export Functions of the Influenza A Virus Nucleoprotein. *PLOS Pathog* **11**, e1005062.

Karle, I. L., Perozzo, M. A., Mishra, V. K. & Balaram, P. (1998). Crystal structure of the channel-forming polypeptide antiamoebin in a membrane-mimetic environment. *Proceedings of the National Academy of Sciences* **95**, 5501-5504.

Karplus, M. & McCammon, J. A. (2002). Molecular dynamics simulations of biomolecules. *Nature Structural & Molecular Biology* **9**, 646-652.

Karron, R. A., Buonagurio, D. A., Georgiu, A. F., Whitehead, S. S., Adamus, J. E., Clements-Mann, M. L., Harris, D. O., Randolph, V. B., Udem, S. A. & Murphy, B. R. (1997). Respiratory syncytial virus (RSV) SH and G proteins are not essential for viral replication in vitro: clinical evaluation and molecular characterization of a cold-passaged, attenuated RSV subgroup B mutant. *Proceedings of the National Academy of Sciences* **94**, 13961-13966.

Kato, N. & Eggers, H. J. (1969). Inhibition of uncoating of fowl plague virus by l-adamantanamine hydrochloride. *Virology* **37**, 632-641.

Kawaoka, Y., Krauss, S. & Webster, R. G. (1989). Avian-to-human transmission of the PB1 gene of influenza A viruses in the 1957 and 1968 pandemics. *Journal of virology* **63**, 4603-4608.

Kerkau, T., Bacik, I., Bennink, J. R., Yewdell, J. W., Hünig, T., Schimpl, A. & Schubert, U. (1997). The human immunodeficiency virus type 1 (HIV-1) Vpu protein interferes with an early step in the biosynthesis of major histocompatibility complex (MHC) class I molecules. *The Journal of experimental medicine* **185**, 1295-1306.

Khoury, G., Ewart, G., Luscombe, C., Miller, M. & Wilkinson, J. (2010). Antiviral efficacy of the novel compound BIT225 against HIV-1 release from human macrophages. *Antimicrobial agents and chemotherapy* **54**, 835-845.

Kilbourne, E. D. (1976). Comparative efficacy of neuraminidase-specific and conventional influenza virus vaccines in induction of antibody to neuraminidase in humans. *Journal of infectious diseases* **134**, 384-394.

Kim, M.-C., Lee, Y.-N., Hwang, H. S., Lee, Y.-T., Ko, E.-J., Jung, Y.-J., Cho, M. K., Kim, Y.-J., Lee, J. S., Ha, S.-H. & Kang, S.-M. (2014). Influenza M2 virus-like particles confer a broader range of cross protection to the strain-specific pre-existing immunity. *Vaccine* **32**, 5824-5831.

Kim, M. C., Song, J. M., Eunju, O., Kwon, Y. M., Lee, Y. J., Compans, R. W. & Kang, S. M. (2012). Virus-like Particles Containing Multiple M2 Extracellular Domains Confer Improved Cross-protection Against Various Subtypes of Influenza Virus. *Molecular Therapy*.

Klenk, H.-D., Rott, R. & Becht, H. (1972). On the structure of the influenza virus envelope. *Virology* **47**, 579-591.

Klenk, H.-D., Rott, R., Orlich, M. & Blödorn, J. (1975). Activation of influenza A viruses by trypsin treatment. *Virology* **68**, 426-439.

Kobasa, D., Kodihalli, S., Luo, M., Castrucci, M. R., Donatelli, I., Suzuki, Y., Suzuki, T. & Kawaoka, Y. (1999). Amino acid residues contributing to the substrate specificity of the influenza A virus neuraminidase. *Journal of virology* **73**, 6743-6751.

Kochs, G., García-Sastre, A. & Martínez-Sobrido, L. (2007). Multiple anti-interferon actions of the influenza A virus NS1 protein. *Journal of virology* **81**, 7011-7021.

Kolocouris, A., Tzitzoglaki, C., Johnson, F. B., Zell, R., Wright, A. K., Cross, T. A., Tietjen, I., Fedida, D. & Busath, D. D. (2014). Aminoadamantanes with persistent in vitro efficacy against H1N1 (2009) influenza A. *Journal of medicinal chemistry* **57**, 4629-4639.

Krammer, F., Pica, N., Hai, R., Margine, I. & Palese, P. (2013). Chimeric hemagglutinin influenza virus vaccine constructs elicit broadly protective stalk-specific antibodies. *Journal of virology* **87**, 6542-6550.

Krawczyk, E., Suprynowicz, F. A., Sudarshan, S. R. & Schlegel, R. (2010). Membrane orientation of the human papillomavirus type 16 E5 oncoprotein. *Journal of virology* **84**, 1696-1703.

Kuchipudi, S. V., Nelli, R., White, G. A., Bain, M., Chang, K. C. & Dunham, S. (2009). Differences in influenza virus receptors in chickens and ducks: implications for interspecies transmission. *Journal of molecular and genetic medicine: an international journal of biomedical research* **3**, 143.

Kurtz, S., Luo, G., Hahnenberger, K. M., Brooks, C., Gecha, O., Ingalls, K., Numata, K. & Krystal, M. (1995). Growth impairment resulting from expression of influenza virus M2 protein in Saccharomyces cerevisiae: identification of a novel inhibitor of influenza virus. *Antimicrobial agents and chemotherapy* **39**, 2204-2209.

Lackenby, A., Hungnes, O., Dudman, S., Meijer, A., Paget, W., Hay, A. & Zambon, M. (2008). Emergence of resistance to oseltamivir among influenza A(H1N1) viruses in Europe. *Peer-reviewed European information on communicable disease surveillance and control* **13**, 113-114.

Lama, J. & Carrasco, L. (1992). Expression of poliovirus nonstructural proteins in Escherichia coli cells. Modification of membrane permeability induced by 2B and 3A. *Journal of Biological Chemistry* **267**, 15932-15937.

Lamb, R. A. & Choppin, P. W. (1979). Segment 8 of the influenza virus genome is unique in coding for two polypeptides. *Proceedings of the National Academy of Sciences* **76**, 4908-4912.

Lamb, R. A. & Lai, C.-J. (1981). Conservation of the influenza virus membrane protein (M 1) amino acid sequence and an open reading frame of RNA segment 7 encoding a second protein (M 2) in H1N1 and H3N2 strains. *Virology* **112**, 746-751.

Lamb, R. A., Lai, C. J. & Choppin, P. W. (1981). Sequences of mRNAs derived from genome RNA segment 7 of influenza virus: colinear and interrupted mRNAs code for overlapping proteins. *Proceedings of the National Academy of Sciences of the United States of America* **78**, 4170-4174.

Lamb, R. A., Zebedee, S. L. & Richardson, C. D. (1985). Influenza virus M2 protein is an integral membrane protein expressed on the infected-cell surface. *Cell* **40**, 627-633.

Laver, W. & Webster, R. (1968). Selection of antigenic mutants of influenza viruses. Isolation and peptide mapping of their hemagglutinating proteins. *Virology* **34**, 193-202.

Lazarowitz, S. G. & Choppin, P. W. (1975). Enhancement of the infectivity of influenza A and B viruses by proteolytic cleavage of the hemagglutinin polypeptide. *Virology* **68**, 440-454.

Le Goffic, R., Pothlichet, J., Vitour, D., Fujita, T., Meurs, E., Chignard, M. & Si-Tahar, M. (2007). Cutting Edge: Influenza A virus activates TLR3-dependent inflammatory and RIG-I-dependent antiviral responses in human lung epithelial cells. *The Journal of Immunology* **178**, 3368-3372.

Lee, L. Y.-H., Simmons, C., de Jong, M. D., Chau, N. V. V., Schumacher, R., Peng, Y. C., McMichael, A. J., Farrar, J. J., Smith, G. L. & Townsend, A. R. (2008). Memory T cells established by seasonal human influenza A infection cross-react with avian influenza A (H5N1) in healthy individuals. *The Journal of clinical investigation* **118**, 3478-3490.

Lee, S. M.-Y. & Yen, H.-L. (2012). Targeting the host or the virus: current and novel concepts for antiviral approaches against influenza virus infection. *Antiviral research* **96**, 391-404.

Leechanachai, P., Banks, L., Moreau, F. & Matlashewski, G. (1992). The E5 gene from human papillomavirus type 16 is an oncogene which enhances growth factor-mediated signal transduction to the nucleus. *Oncogene* **7**, 19-25.

Leneva, I. A., Russell, R. J., Boriskin, Y. S. & Hay, A. J. (2009). Characteristics of arbidol-resistant mutants of influenza virus: implications for the mechanism of anti-influenza action of arbidol. *Antiviral research* **81**, 132-140.

Leptak, C., y Cajal, S. R., Kulke, R., Horwitz, B., Riese, D., Dotto, G. P. & DiMaio, D. (1991). Tumorigenic transformation of murine keratinocytes by the E5 genes of bovine papillomavirus type 1 and human papillomavirus type 16. *Journal of virology* **65**, 7078-7083.

Li, H., Atkins, E., Bruckner, J., McArdle, S., Qiu, W. C., Thomassen, L. V., Scott, J., Shuhart, M. C., Livingston, S., Townshend-Bulson, L., McMahon, B. J., Harris, M., Griffin, S. & Gretch, D. R. (2012). Genetic and functional heterogeneity of the hepatitis C virus p7 ion channel during natural chronic infection. *Virology* **423**, 30-37.

Li, S., Sieben, C., Ludwig, K., Höfer, C. T., Chiantia, S., Herrmann, A., Eghiaian, F. & Schaap, I. A. (2014a). pH-Controlled Two-Step Uncoating of Influenza Virus. *Biophysical Journal* **106**, 1447-1456.

Li, X. & Palese, P. (1994). Characterization of the polyadenylation signal of influenza virus RNA. *Journal of virology* **68**, 1245-1249.

Li, Y., To, J., Verdià-Baguena, C., Dossena, S., Surya, W., Huang, M., Paulmichl, M., Liu, D. X., Aguilella, V. M. & Torres, J. (2014b). Inhibition of the human respiratory syncytial virus small hydrophobic protein and structural variations in a bicelle environment. *Journal of virology* **88**, 11899-11914.

Lillie, P. J., Berthoud, T. K., Powell, T. J., Lambe, T., Mullarkey, C., Spencer, A. J., Hamill, M., Peng, Y., Blais, M.-E. & Duncan, C. J. (2012). Preliminary assessment of the efficacy of a t-cell–based influenza vaccine, MVA-NP+ M1, in humans. *Clinical infectious diseases*, cis327.

Lin, C., Lindenbach, B. D., Pragai, B. M., McCourt, D. W. & Rice, C. M. (1994). Processing in the hepatitis C virus E2-NS2 region: identification of p7 and two distinct E2-specific products with different C termini. *Journal of virology* **68**, 5063-5073.

Lin, L., Liu, Q., Berube, N., Detmer, S. & Zhou, Y. (2012). 5′-Triphosphate-short interfering RNA: potent inhibition of influenza A virus infection by gene silencing and RIG-I activation. *Journal of virology* **86**, 10359-10369.

Lin, Q., Lin, Z., Chiu, A. P. & He, D. (2016). Seasonality of Influenza A (H7N9) Virus in China—Fitting Simple Epidemic Models to Human Cases. *PloS one* **11**, e0151333.

Lin, T.-I., Heider, H. & Schroeder, C. (1997). Different modes of inhibition by adamantane amine derivatives and natural polyamines of the functionally reconstituted influenza virus M2 proton channel protein. *Journal of general virology* **78**, 767-774.

Lipinski, C. A., Lombardo, F., Dominy, B. W. & Feeney, P. J. (2012). Experimental and computational approaches to estimate solubility and permeability in drug discovery and development settings. *Advanced drug delivery reviews* **64**, 4-17.

Loewe, S. & Muischnek, H. (1926). Effect of combinations: mathematical basis of the problem. *Naunyn Schmiedebergs Arch Exp Pathol Pharmakol* **114**, 313–326.

Long, J. S., Giotis, E. S., Moncorgé, O., Frise, R., Mistry, B., James, J., Morisson, M., Iqbal, M., Vignal, A. & Skinner, M. A. (2016). Species difference in ANP32A underlies influenza A virus polymerase host restriction. *Nature* **529**, 101-104.

Loo, Y.-M. & Gale, M. (2011). Immune signaling by RIG-I-like receptors. *Immunity* **34**, 680-692.

López-Martínez, R., Ramírez-Salinas, G. L., Correa-Basurto, J. & Barrón, B. L. (2013). Inhibition of influenza A virus infection in vitro by peptides designed in silico. *PloS one* **8**, e76876.

Loregian, A., Mercorelli, B., Nannetti, G., Compagnin, C. & Palù, G. (2014). Antiviral strategies against influenza virus: towards new therapeutic approaches. *Cellular and Molecular Life Sciences*, 1-25.

Lowen, A. C., Mubareka, S., Steel, J. & Palese, P. (2007). Influenza virus transmission is dependent on relative humidity and temperature. *PLoS Pathog* **3**, e151.

Luber, A. D. (2005). Genetic barriers to resistance and impact on clinical response. *Journal of the International AIDS Society* **7**, 69.

Luik, P., Chew, C., Aittoniemi, J., Chang, J., Wentworth, P., Jr., Dwek, R. A., Biggin, P. C., Venien-Bryan, C. & Zitzmann, N. (2009). The 3-dimensional structure of a hepatitis C virus p7 ion channel by electron microscopy. *Proceedings of the National Academy of Sciences of the United States of America* **106**, 12712-12716.

Lund, J. M., Alexopoulou, L., Sato, A., Karow, M., Adams, N. C., Gale, N. W., Iwasaki, A. & Flavell, R. A. (2004). Recognition of single-stranded RNA viruses by Toll-like receptor 7. *Proceedings of the National Academy of Sciences of the United States of America* **101**, 5598-5603.

Luscombe, C. A., Huang, Z., Murray, M. G., Miller, M., Wilkinson, J. & Ewart, G. D. (2010). A novel Hepatitis C virus p7 ion channel inhibitor, BIT225, inhibits bovine viral diarrhea virus in vitro and shows synergism with recombinant interferon-alpha-2b and nucleoside analogues. *Antiviral Research* **86**, 144-153.

Ma, C., Fiorin, G., Carnevale, V., Wang, J., Lamb, R. A., Klein, M. L., Wu, Y., Pinto, L. H. & DeGrado, W. F. (2013). Asp44 Stabilizes the Trp41 Gate of the M2 Proton Channel of Influenza A Virus. *Structure* **21**, 2033-2041.

Ma, C., Polishchuk, A. L., Ohigashi, Y., Stouffer, A. L., Schon, A., Magavern, E., Jing, X., Lear, J. D., Freire, E., Lamb, R. A., DeGrado, W. F. & Pinto, L. H. (2009). Identification of the functional core of the influenza A virus A/M2 proton-selective ion channel. *Proceedings of the National Academy of Sciences* **106**, 12283-12288.

Ma, Y., Anantpadma, M., Timpe, J. M., Shanmugam, S., Singh, S. M., Lemon, S. M. & Yi, M. (2011). Hepatitis C virus NS2 protein serves as a scaffold for virus assembly by interacting with both structural and nonstructural proteins. *Journal of Virology* **85**, 86-97.

Maeda, T. & Ohnishi, S.-i. (1980). Activation of influenza virus by acidic media causes hemolysis and fusion of erythrocytes. *FEBS letters* **122**, 283-287.

Maldarelli, F., Chen, M., Willey, R. L. & Strebel, K. (1993). Human immunodeficiency virus type 1 Vpu protein is an oligomeric type I integral membrane protein. *Journal of virology* **67**, 5056-5061.

Margine, I., Krammer, F., Hai, R., Heaton, N. S., Tan, G., Andrews, S., Runstadler, J., Wilson, P., Albrecht, R. & Garcia-Sastre, A. (2013). Hemagglutinin stalk-based universal vaccine constructs protect against group 2 influenza A viruses. *Journal of virology* **87**, 10435-10446.

Markwell, D. D. & Shortridge, K. F. (1982). Possible waterborne transmission and maintenance of influenza viruses in domestic ducks. *Applied and Environmental Microbiology* **43**, 110-115.

Martin, K. & Helenius, A. (1991). Transport of incoming influenza virus nucleocapsids into the nucleus. *Journal of Virology* **65**, 232-244.

Martínez-Gil, L., Ayllon, J., Ortigoza, M. B., García-Sastre, A., Shaw, M. L. & Palese, P. (2012). Identification of small molecules with type I interferon inducing properties by high-throughput screening. *PLoS One* **7**, e49049.

Massin, P., Van der Werf, S. & Naffakh, N. (2001). Residue 627 of PB2 is a determinant of cold sensitivity in RNA replication of avian influenza viruses. *Journal of virology* **75**, 5398-5404.

Massou, S., Albigot, R. & Prats, M. (2000). Carboxyfluorescein fluorescence experiments. *Biochemical education* **28**, 171-173.

Matlin, K. S., Reggio, H., Helenius, A. & Simons, K. (1981). Infectious entry pathway of influenza virus in a canine kidney cell line. *The Journal of cell biology* **91**, 601-613.

Matrosovich, M., Gambaryan, A., Teneberg, S., Piskarev, V., Yamnikova, S., Lvov, D., Robertson, J. & Karlsson, K.-A. (1997). Avian influenza A viruses differ from human viruses by recognition of sialyloligosaccharides and gangliosides and by a higher conservation of the HA receptor-binding site. *Virology* **233**, 224-234.

McCammon, J. A., Gelin, B. R. & Karplus, M. (1977). Dynamics of folded proteins. *Nature* **267**, 585-590.

McGeoch, D., Fellner, P. & Newton, C. (1976). Influenza virus genome consists of eight distinct RNA species. *Proceedings of the National Academy of Sciences* **73**, 3045-3049.

McKeage, K. (2013). Inactivated quadrivalent split-virus seasonal influenza vaccine (Fluarix® quadrivalent): a review of its use in the prevention of disease caused by influenza A and B. *Drugs* **73**, 1587-1594.

McKimm-Breschkin, J., Trivedi, T., Hampson, A., Hay, A., Klimov, A., Tashiro, M., Hayden, F. & Zambon, M. (2003). Neuraminidase sequence analysis and susceptibilities of influenza virus clinical isolates to zanamivir and oseltamivir. *Antimicrobial agents and chemotherapy* **47**, 2264-2272.

McKimm-Breschkin, J. L. (2013). Influenza neuraminidase inhibitors: antiviral action and mechanisms of resistance. *Influenza and other respiratory viruses* **7**, 25-36.

McMichael, A. J., Gotch, F. M., Noble, G. R. & Beare, P. A. (1983). Cytotoxic T-cell immunity to influenza. *New England Journal of Medicine* **309**, 13-17.

Mehle, A. & Doudna, J. A. (2009). Adaptive strategies of the influenza virus polymerase for replication in humans. *Proceedings of the National Academy of Sciences* **106**, 21312-21316.

Mehnert, T., Routh, A., Judge, P. J., Lam, Y. H., Fischer, D., Watts, A. & Fischer, W. B. (2007). Biophysical characterization of Vpu from HIV-1 suggests a channel-pore dualism. *Proteins* **70**, 1488-1497.

Melton, J. V., Ewart, G. D., Weir, R. C., Board, P. G., Lee, E. & Gage, P. W. (2002). Alphavirus 6K Proteins Form Ion Channels. *Journal of Biological Chemistry* **277**, 46923-46931.

Memoli, M. J., Hrabal, R. J., Hassantoufighi, A., Eichelberger, M. C. & Taubenberger, J. K. (2010). Rapid selection of oseltamivirand peramivir-resistant pandemic H1N1 virus during therapy in 2 immunocompromised hosts. *Clinical infectious diseases* **50**, 1252-1255.

Mibayashi, M., Martínez-Sobrido, L., Loo, Y.-M., Cárdenas, W. B., Gale, M. & García-Sastre, A. (2007). Inhibition of retinoic acid-inducible gene I-mediated induction of beta interferon by the NS1 protein of influenza A virus. *Journal of virology* **81**, 514-524.

Mischler, R. & Metcalfe, I. C. (2002). Inflexal® V a trivalent virosome subunit influenza vaccine: production. *Vaccine* **20**, B17-B23.

Mitchell, C. A. & Guerin, L. (1972). Influenza A of human, swine, equine and avian origin: comparison of survival in aerosol form. *Canadian Journal of comparative Medicine* **36**, 9.

Mizushima, H., Hijikata, M., Asabe, S.-i., Hirota, M., Kimura, K. & Shimotohno, K. (1994). Two hepatitis C virus glycoprotein E2 products with different C termini. *Journal of virology* **68**, 6215-6222.

Molla, A., Kati, W., Carrick, R., Steffy, K., Shi, Y., Montgomery, D., Gusick, N., Stoll, V. S., Stewart, K. D. & Ng, T. I. (2002). In vitro selection and characterization of influenza A (A/N9) virus variants resistant to a novel neuraminidase inhibitor, A-315675. *Journal of virology* **76**, 5380-5386.

Montaville, P. & Jamin, N. (2010). Determination of membrane protein structures using solution and solid-state NMR. *Membrane protein structure determination: methods and protocols*, 261-282.

Morens, D. M., Taubenberger, J. K. & Fauci, A. S. (2008). Predominant role of bacterial pneumonia as a cause of death in pandemic influenza: implications for pandemic influenza preparedness. *Journal of Infectious Diseases* **198**, 962-970.

Morrison, D., Roy, S., Rayner, C., Amer, A., Howard, D., Smith, J. R. & Evans, T. G. (2007). A randomized, crossover study to evaluate the pharmacokinetics of amantadine and oseltamivir administered alone and in combination. *PLoS One* **2**, e1305.

Mould, J. A., Li, H.-C., Dudlak, C. S., Lear, J. D., Pekosz, A., Lamb, R. A. & Pinto, L. H. (2000). Mechanism for proton conduction of the M2 ion channel of influenza A virus. *Journal of Biological Chemistry* **275**, 8592-8599.

Mounts, A. W., Kwong, H., Izurieta, H. S., Ho, Y.-y., Au, T.-k., Lee, M., Bridges, C. B., Williams, S. W., Mak, K. H. & Katz, J. M. (1999). Case-control study of risk factors for avian influenza A (H5N1) disease, Hong Kong, 1997. *Journal of Infectious Diseases* **180**, 505-508.

Muramoto, Y., Noda, T., Kawakami, E., Akkina, R. & Kawaoka, Y. (2013). Identification of novel influenza A virus proteins translated from PA mRNA. *Journal of virology* **87**, 2455-2462.

Murray, J. L., McDonald, N. J., Sheng, J., Shaw, M. W., Hodge, T. W., Rubin, D. H., O'Brien, W. A. & Smee, D. F. (2012). Inhibition of influenza A virus replication by antagonism of a PI3K-AKT-mTOR pathway member identified by gene-trap insertional mutagenesis. *Antiviral Chemistry and Chemotherapy* **22**, 205-215.

Neil, S. J. D., Zang, T. & Bieniasz, P. D. (2008). Tetherin inhibits retrovirus release and is antagonized by HIV-1 Vpu. *Nature* **451**, 425-430.

Neirynck, S., Deroo, T., Saelens, X., Vanlandschoot, P., Jou, W. M. & Fiers, W. (1999). A universal influenza A vaccine based on the extracellular domain of the M2 protein. *Nature medicine* **5**, 1157-1163.

Nguyen, J. T., Hoopes, J. D., Le, M. H., Smee, D. F., Patick, A. K., Faix, D. J., Blair, P. J., De Jong, M. D., Prichard, M. N. & Went, G. T. (2010). Triple combination of amantadine, ribavirin, and oseltamivir is highly active and synergistic against drug resistant influenza virus strains in vitro. *PLoS One* **5**, e9332.

Nishimura, K., Kim, S., Zhang, L. & Cross, T. (2002). The closed state of a H+ channel helical bundle combining precise orientational and distance restraints from solid state NMR. *Biochemistry* **41**, 13170-13177.

Noda, T., Sagara, H., Yen, A., Takada, A., Kida, H., Cheng, R. H. & Kawaoka, Y. (2006). Architecture of ribonucleoprotein complexes in influenza A virus particles. *Nature* **439**, 490-492.

O'Neill, R. E., Jaskunas, R., Blobel, G., Palese, P. & Moroianu, J. (1995). Nuclear import of influenza virus RNA can be mediated by viral nucleoprotein and transport factors required for protein import. *Journal of Biological Chemistry* **270**, 22701-22704.

O'Neill, R. E., Talon, J. & Palese, P. (1998). The influenza virus NEP (NS2 protein) mediates the nuclear export of viral ribonucleoproteins. *The EMBO journal* **17**, 288-296.

Ortigoza, M. B., Dibben, O., Maamary, J., Martinez-Gil, L., Leyva-Grado, V. H., Abreu Jr, P., Ayllon, J., Palese, P. & Shaw, M. L. (2012). A novel small molecule inhibitor of influenza A viruses that targets polymerase function and indirectly induces interferon. *PLoS Pathog* **8**, e1002668.

Osterhaus, A., Rimmelzwaan, G., Martina, B., Bestebroer, T. & Fouchier, R. (2000). Influenza B virus in seals. *Science* **288**, 1051-1053.

OuYang, B., Xie, S., Berardi, M. J., Zhao, X., Dev, J., Yu, W., Sun, B. & Chou, J. J. (2013). Unusual architecture of the p7 channel from hepatitis C virus. *Nature* **498**, 521-525.

Oxford, J., Logan, I. & Potter, C. (1970). Passage of influenza strains in the presence of aminoadamantane. *Annals of the New York Academy of Sciences* **173**, 300-313.

Oxford, J., Schild, G., Potter, C. & Jennings, R. (1979). The specificity of the anti-haemagglutinin antibody response induced in man by inactivated influenza vaccines and by natural infection. *Journal of Hygiene* **82**, 51-61.

Palese, P. & Schulman, J. (1976). Differences in RNA patterns of influenza A viruses. *Journal of virology* **17**, 876-884.

Palese, P., Tobita, K., Ueda, M. & Compans, R. W. (1974). Characterization of temperature sensitive influenza virus mutants defective in neuraminidase. *Virology* **61**, 397-410.

Paniker, C. (1968). Serological relationships between the neuraminidases of influenza viruses. *Journal of General Virology* **2**, 385-394.

Park, E. K., Castrucci, M. R., Portner, A. & Kawaoka, Y. (1998). The M2 ectodomain is important for its incorporation into influenza A virions. *Journal of virology* **72**, 2449-2455.

Park, S. H., Mrse, A. A., Nevzorov, A. A., Mesleh, M. F., Oblatt-Montal, M., Montal, M. & Opella, S. J. (2003). Three-dimensional Structure of the Channel-forming Trans-membrane Domain of Virus Protein “u” (Vpu) from HIV-1. *Journal of Molecular Biology* **333**, 409-424.

Parvin, J. D., Moscona, A., Pan, W., Leider, J. & Palese, P. (1986). Measurement of the mutation rates of animal viruses: influenza A virus and poliovirus type 1. *Journal of Virology* **59**, 377-383.

Patterson, S., Oxford, J. & Dourmashkin, R. (1979). Studies on the mechanism of influenza virus entry into cells. *Journal of General Virology* **43**, 223-229.

Paul, M. & Jabbar, M. A. (1997). Phosphorylation of both phosphoacceptor sites in the HIV-1 Vpu cytoplasmic domain is essential for Vpu-mediated ER degradation of CD4. *Virology* **232**, 207-216.

Pavlovic, D., Neville, D. C. A., Argaud, O., Blumberg, B., Dwek, R. A., Fischer, W. B. & Zitzmann, N. (2003). The hepatitis C virus p7 protein forms an ion channel that is inhibited by long-alkyl-chain iminosugar derivatives. *Proceedings of the National Academy of Sciences of the United States of America* **100**, 6104-6108.

Pemberton, R., Jennings, R., Potter, C. & Oxford, J. (1986). Amantadine resistance in clinical influenza A (H3N2) and (H1N1) virus isolates. *Journal of Antimicrobial Chemotherapy* **18**, 135-140.

Perez, M., García-Barreno, B., Melero, J. A., Carrasco, L. & Guinea, R. (1997). Membrane Permeability Changes Induced in Escherichia coliby the SH Protein of Human Respiratory Syncytial Virus. *Virology* **235**, 342-351.

Peterson, E., Ryser, T., Funk, S., Inouye, D., Sharma, M., Qin, H., Cross, T. A. & Busath, D. D. (2011). Functional reconstitution of influenza A M2 (22–62). *Biochimica et Biophysica Acta (BBA)-Biomembranes* **1808**, 516-521.

Pielak, R. M. & Chou, J. J. (2010). Solution NMR structure of the V27A drug resistant mutant of influenza A M2 channel. *Biochemical and biophysical research communications* **401**, 58-63.

Pielak, R. M. & Chou, J. J. (2011). Influenza M2 proton channels. *Biochimica et Biophysica Acta (BBA)-Biomembranes* **1808**, 522-529.

Pielak, R. M., Schnell, J. R. & Chou, J. J. (2009). Mechanism of drug inhibition and drug resistance of influenza A M2 channel. *Proceedings of the National Academy of Sciences* **106**, 7379-7384.

Pim, D., Collins, M. & Banks, L. (1992). Human papillomavirus type 16 E5 gene stimulates the transforming activity of the epidermal growth factor receptor. *Oncogene* **7**, 27-32.

Pinto, L. H., Holsinger, L. J. & Lamb, R. A. (1992). Influenza virus M2 protein has ion channel activity. *Cell* **69**, 517-528.

Pinto, L. H. & Lamb, R. A. (1995). Understanding the mechanism of action of the anti-influenza virus drug amantadine. *Trends in microbiology* **3**, 271.

Pinto, L. H. & Lamb, R. A. (2006). The M2 proton channels of influenza A and B viruses. *Journal of Biological Chemistry* **281**, 8997-9000.

Pons, M. W. (1977). Early RNA synthesis in influenza virus-infected cells. *Virology* **76**, 855-859.

Pons, M. W. & Hirst, G. K. (1968). Polyacrylamide gel electrophoresis of the replicative form of influenza virus RNA. *Virology* **35**, 182-184.

Premkumar, A., Horan, C. R. & Gage, P. W. (2005). Dengue Virus M Protein C-Terminal Peptide (DVM-C) Forms Ion Channels. *J Membrane Biol* **204**, 33-38.

Premkumar, A., Wilson, L., Ewart, G. D. & Gage, P. W. (2004). Cation-selective ion channels formed by p7 of hepatitis C virus are blocked by hexamethylene amiloride. *FEBS Letters* **557**, 99-103.

Pulendran, B. & Maddur, M. S. (2014). Innate immune sensing and response to influenza. In *Influenza Pathogenesis and Control-Volume II*, pp. 23-71: Springer.

Pyle, G. F. (1986). *The diffusion of influenza: patterns and paradigms*: Rowman & Littlefield.

Ranjan, P., Jayashankar, L., Deyde, V., Zeng, H., Davis, W. G., Pearce, M. B., Bowzard, J. B., Hoelscher, M. A., Jeisy-Scott, V. & Wiens, M. E. (2010). 5'PPP-RNA induced RIG-I activation inhibits drug-resistant avian H5N1 as well as 1918 and 2009 pandemic influenza virus replication. *Virology journal* **7**, 1.

Renzette, N., Caffrey, D. R., Zeldovich, K. B., Liu, P., Gallagher, G. R., Aiello, D., Porter, A. J., Kurt-Jones, E. A., Bolon, D. N. & Poh, Y.-P. (2014). Evolution of the influenza A virus genome during development of oseltamivir resistance in vitro. *Journal of virology* **88**, 272-281.

Rey-Carrizo, M., Barniol-Xicota, M., Ma, C., Frigolé-Vivas, M., Torres, E., Naesens, L., Llabrés, S., Juárez-Jiménez, J., Luque, F. J., DeGrado, W. F., Lamb, R. A., Pinto, L. H. & Vázquez, S. (2014). Easily Accessible Polycyclic Amines that Inhibit the Wild-Type and Amantadine-Resistant Mutants of the M2 Channel of Influenza A Virus. *J Med Chem* **57**, 5738-5747.

Rey-Carrizo, M., Torres, E., Ma, C., Barniol-Xicota, M., Wang, J., Wu, Y., Naesens, L., DeGrado, W. F., Lamb, R. A., Pinto, L. H. & Vázquez, S. (2013). 3-Azatetracyclo[5.2.1.1 5,8 .0 1,5]undecane Derivatives: From Wild-Type Inhibitors of the M2 Ion Channel of Influenza A Virus to Derivatives with Potent Activity against the V27A Mutant. *J Med Chem* **56**, 9265-9274.

Richardson, J. & Akkina, R. (1991). NS2 protein of influenza virus is found in purified virus and phosphorylated in infected cells. *Archives of virology* **116**, 69-80.

Robb, N. C., Smith, M., Vreede, F. T. & Fodor, E. (2009). NS2/NEP protein regulates transcription and replication of the influenza virus RNA genome. *Journal of general virology* **90**, 1398-1407.

Robertson, J. S. (1979). 5′ and 3′ terminal nucleotide sequences of the RNA genome segments of influenza virus. *Nucleic acids research* **6**, 3745-3758.

Rogers, G. N. & Paulson, J. C. (1983). Receptor determinants of human and animal influenza virus isolates: differences in receptor specificity of the H3 hemagglutinin based on species of origin. *Virology* **127**, 361-373.

Rossman, J. S., Jing, X., Leser, G. P., Balannik, V., Pinto, L. H. & Lamb, R. A. (2010). Influenza virus m2 ion channel protein is necessary for filamentous virion formation. *Journal of virology* **84**, 5078-5088.

Rossman, J. S., Leser, G. P. & Lamb, R. A. (2012). Filamentous influenza virus enters cells via macropinocytosis. *Journal of virology* **86**, 10950-10960.

Rowse, M., Qiu, S., Tsao, J., Xian, T., Khawaja, S., Yamauchi, Y., Yang, Z., Wang, G. & Luo, M. (2015a). Characterization of potent fusion inhibitors of influenza virus. *PloS one* **10**, e0122536.

Rowse, M., Qiu, S., Tsao, J., Yamauchi, Y., Wang, G. & Luo, M. (2015b). Reduction of influenza virus envelope's fusogenicity by viral fusion inhibitors. *ACS Infectious Diseases* **2**, 47-53.

Ruben, F. L. & Jackson, G. G. (1972). A new subunit influenza vaccine: acceptability compared with standard vaccines and effect of dose on antigenicity. *Journal of Infectious Diseases* **125**, 656-664.

Rückle, A., Haasbach, E., Julkunen, I., Planz, O., Ehrhardt, C. & Ludwig, S. (2012). The NS1 protein of influenza A virus blocks RIG-I-mediated activation of the noncanonical NF-κB pathway and p52/RelB-dependent gene expression in lung epithelial cells. *Journal of virology* **86**, 10211-10217.

Saito, R., Sakai, T., Sato, I., Sano, Y., Oshitani, H., Sato, M. & Suzuki, H. (2003). Frequency of amantadine-resistant influenza A viruses during two seasons featuring cocirculation of H1N1 and H3N2. *Journal of Clinical Microbiology* **41**, 2164-2165.

Sakaguchi, T., Tu, Q., Pinto, L. H. & Lamb, R. A. (1997). The active oligomeric state of the minimalistic influenza virus M2 ion channel is a tetramer. *Proceedings of the National Academy of Sciences* **94**, 5000-5005.

Sakai, A., Claire, M. S., Faulk, K., Govindarajan, S., Emerson, S. U., Purcell, R. H. & Bukh, J. (2003). The p7 polypeptide of hepatitis C virus is critical for infectivity and contains functionally important genotype-specific sequences. *Proceedings of the National Academy of Sciences of the United States of America* **100**, 11646-11651.

Samji, T. (2009). Influenza A: understanding the viral life cycle. *The Yale journal of biology and medicine* **82**, 153.

Sanders, C. R. & Sönnichsen, F. (2006). Solution NMR of membrane proteins: practice and challenges. *Magnetic Resonance in Chemistry* **44**, S24-S40.

Sanjuan, R., Nebot, M. R., Chirico, N., Mansky, L. M. & Belshaw, R. (2010). Viral mutation rates. *Journal of virology* **84**, 9733-9748.

Saunier, B., Triyatni, M., Ulianich, L., Maruvada, P., Yen, P. & Kohn, L. D. (2003). Role of the asialoglycoprotein receptor in binding and entry of hepatitis C virus structural proteins in cultured human hepatocytes. *Journal of Virology* **77**, 546-559.

Schlee, M., Roth, A., Hornung, V., Hagmann, C. A., Wimmenauer, V., Barchet, W., Coch, C., Janke, M., Mihailovic, A. & Wardle, G. (2009). Recognition of 5′ triphosphate by RIG-I helicase requires short blunt double-stranded RNA as contained in panhandle of negative-strand virus. *Immunity* **31**, 25-34.

Schmidt, A., Schwerd, T., Hamm, W., Hellmuth, J. C., Cui, S., Wenzel, M., Hoffmann, F. S., Michallet, M.-C., Besch, R. & Hopfner, K.-P. (2009). 5′-triphosphate RNA requires base-paired structures to activate antiviral signaling via RIG-I. *Proceedings of the National Academy of Sciences* **106**, 12067-12072.

Schnell, J. R. & Chou, J. J. (2008). Structure and mechanism of the M2 proton channel of influenza A virus. *Nature* **451**, 591-595.

Scholtissek, C., Bürger, H., Kistner, O. & Shortridge, K. (1985). The nucleoprotein as a possible major factor in determining host specificity of influenza H3N2 viruses. *Virology* **147**, 287-294.

Scholtissek, C., Rohde, W. v., Von Hoyningen, V. & Rott, R. (1978). On the origin of the human influenza virus subtypes H2N2 and H3N2. *Virology* **87**, 13-20.

Schroeder, C., Ford, C. M., Wharton, S. A. & Hay, A. J. (1994). Functional reconstitution in lipid vesicles of influenza virus M2 protein expressed by baculovirus: evidence for proton transfer activity. *Journal of General Virology* **75**, 3477-3484.

Schroeder, C., Heider, H., Möncke-Buchner, E. & Lin, T.-I. (2005). The influenza virus ion channel and maturation cofactor M2 is a cholesterol-binding protein. *European Biophysics Journal* **34**, 52-66.

Schubert, U., Bour, S., Ferrer-Montiel, A. V., Montal, M., Maldarell, F. & Strebel, K. (1996a). The two biological activities of human immunodeficiency virus type 1 Vpu protein involve two separable structural domains. *Journal of virology* **70**, 809-819.

Schubert, U., Ferrer-Montiel, A. V., Oblatt-Montal, M., Henklein, P., Strebel, K. & Montal, M. (1996b). Identification of an ion channel activity of the Vpu transmembrane domain and its involvement in the regulation of virus release from HIV-1-infected cells. *FEBS Letters* **398**, 12-18.

Schulman, J. & Kilbourne, E. (1969). Independent variation in nature of hemagglutinin and neuraminidase antigens of influenza virus: distinctiveness of hemagglutinin antigen of Hong Kong/68 virus. *Proceedings of the National Academy of Sciences* **63**, 326-333.

Schulman, J. L. & Kilbourne, E. D. (1962). Airborne transmission of influenza virus infection in mice.

Schwarz, G., Zong, R.-t. & Popescu, T. (1992). Kinetics of melittin induced pore formation in the membrane of lipid vesicles. *Biochimica et Biophysica Acta (BBA)-Biomembranes* **1110**, 97-104.

Scott, C. & Griffin, S. (2015). Viroporins: structure, function and potential as antiviral targets. *Journal of General Virology* **96**, 2000-2027.

Seong, B. L. & Brownlee, G. (1992). A new method for reconstituting influenza polymerase and RNA in vitro: a study of the promoter elements for cRNA and vRNA synthesis in vitro and viral rescue in vivo. *Virology* **186**, 247-260.

Shaman, J. & Kohn, M. (2009). Absolute humidity modulates influenza survival, transmission, and seasonality. *Proceedings of the National Academy of Sciences* **106**, 3243-3248.

Sharma, M., Yi, M., Dong, H., Qin, H., Peterson, E., Busath, D. D., Zhou, H. X. & Cross, T. A. (2010). Insight into the Mechanism of the Influenza A Proton Channel from a Structure in a Lipid Bilayer. *Science* **330**, 509-512.

Sharpe, S., Yau, W.-M. & Tycko, R. (2006). Structure and Dynamics of the HIV-1 Vpu Transmembrane Domain Revealed by Solid-State NMR with Magic-Angle Spinning †. *Biochemistry* **45**, 918-933.

Sheu, T., Garten, R., Smith, C., Barnes, J., Myrick, A., Hillman, M., Shaw, M., Bridges, C. & Klimov, A. (2009). Update: drug susceptibility of swine-origin influenza A (H1N1) viruses, April 2009. *Morbidity and Mortality Weekly Report* **58**.

Shimbo, K., Brassard, D. L., Lamb, R. A. & Pinto, L. H. (1996). Ion selectivity and activation of the M2 ion channel of influenza virus. *Biophysical Journal* **70**, 1335-1346.

Shinya, K., Ebina, M., Yamada, S., Ono, M., Kasai, N. & Kawaoka, Y. (2006). Avian flu: influenza virus receptors in the human airway. *Nature* **440**, 435-436.

Shinya, K., Hamm, S., Hatta, M., Ito, H., Ito, T. & Kawaoka, Y. (2004). PB2 amino acid at position 627 affects replicative efficiency, but not cell tropism, of Hong Kong H5N1 influenza A viruses in mice. *Virology* **320**, 258-266.

Sissoko, D., Laouenan, C., Folkesson, E., M'Lebing, A.-B., Beavogui, A.-H., Baize, S., Camara, A.-M., Maes, P., Shepherd, S. & Danel, C. (2016). Experimental Treatment with Favipiravir for Ebola Virus Disease (the JIKI Trial): A Historically Controlled, Single-Arm Proof-of-Concept Trial in Guinea. *PLoS Med* **13**, e1001967.

Skehel, J. J. (1972). Polypeptide synthesis in influenza virus-infected cells. *Virology* **49**, 23-36.

Skehel, J. J., Hay, A. J. & Armstrong, J. A. (1978). On the mechanism of inhibition of influenza virus replication by amantadine hydrochloride. *Journal of General Virology* **38**, 97-110.

Smith, W., Andrewes, C. & Laidlaw, P. (1933). A virus obtained from influenza patients. *The Lancet* **222**, 66-68.

Soundararajan, V., Tharakaraman, K., Raman, R., Raguram, S., Shriver, Z., Sasisekharan, V. & Sasisekharan, R. (2009). Extrapolating from sequence—the 2009 H1N1'swine'influenza virus. *Nature biotechnology* **27**, 510-513.

Stanley, W. (1945). The preparation and properties of influenza virus vaccines concentrated and purified by differential centrifugation. *The Journal of experimental medicine* **81**, 193-218.

Stauffer, S., Feng, Y., Nebioglu, F., Heilig, R., Picotti, P. & Helenius, A. (2014). Stepwise priming by acidic pH and a high K+ concentration is required for efficient uncoating of influenza A virus cores after penetration. *Journal of virology* **88**, 13029-13046.

Steel, J., Lowen, A. C., Mubareka, S. & Palese, P. (2009). Transmission of influenza virus in a mammalian host is increased by PB2 amino acids 627K or 627E/701N. *PLoS Pathog* **5**, e1000252.

Steel, J., Lowen, A. C., Wang, T. T., Yondola, M., Gao, Q., Haye, K., García-Sastre, A. & Palese, P. (2010). Influenza virus vaccine based on the conserved hemagglutinin stalk domain. *MBio* **1**, e00018-00010.

Steinmann, E., Penin, F., Kallis, S., Patel, A. H., Bartenschlager, R. & Pietschmann, T. (2007a). Hepatitis C virus p7 protein is crucial for assembly and release of infectious virions. *PLoS Pathogens* **3**, e103.

Steinmann, E., Whitfield, T., Kallis, S., Dwek, R. A., Zitzmann, N., Pietschmann, T. & Bartenschlager, R. (2007b). Antiviral effects of amantadine and iminosugar derivatives against hepatitis C virus. *Hepatology* **46**, 330-338.

Stevens, J., Blixt, O., Paulson, J. C. & Wilson, I. A. (2006). Glycan microarray technologies: tools to survey host specificity of influenza viruses. *Nature Reviews Microbiology* **4**, 857-864.

Stewart, S. M., Wu, W.-H., Lalime, E. N. & Pekosz, A. (2010). The cholesterol recognition/interaction amino acid consensus motif of the influenza A virus M2 protein is not required for virus replication but contributes to virulence. *Virology* **405**, 530-538.

StGelais, C., Foster, T. L., Verow, M., Atkins, E., Fishwick, C. W. G., Rowlands, D., Harris, M. & Griffin, S. (2009). Determinants of hepatitis C virus p7 ion channel function and drug sensitivity identified in vitro. *Journal of Virology* **83**, 7970-7981.

StGelais, C., Tuthill, T., Clarke, D., Rowlands, D., Harris, M. & Griffin, S. (2007). Inhibition of hepatitis C virus p7 membrane channels in a liposome-based assay system. *Antiviral Research* **76**, 48-58.

Stieneke-Gröber, A., Vey, M., Angliker, H., Shaw, E., Thomas, G., Roberts, C., Klenk, H. & Garten, W. (1992). Influenza virus hemagglutinin with multibasic cleavage site is activated by furin, a subtilisin-like endoprotease. *The EMBO journal* **11**, 2407.

Stouffer, A. L., Acharya, R., Salom, D., Levine, A. S., Di Costanzo, L., Soto, C. S., Tereshko, V., Nanda, V., Stayrook, S. & DeGrado, W. F. (2008). Structural basis for the function and inhibition of an influenza virus proton channel. *Nature* **451**, 596-599.

Straight, S. W., Hinkle, P. M., Jewers, R. J. & McCance, D. (1993). The E5 oncoprotein of human papillomavirus type 16 transforms fibroblasts and effects the downregulation of the epidermal growth factor receptor in keratinocytes. *Journal of virology* **67**, 4521-4532.

Strebel, K., Klimkait, T. & Martin, M. (1988). A novel gene of HIV-1, vpu, and its 16-kilodalton product. *Science* **241**, 1221-1223.

Subbarao, E. & Murphy, B. (1993). A single amino acid in the PB2 gene of influenza A virus is a determinant of host range. *Journal of virology* **67**, 1761-1764.

Subbarao, K., Klimov, A., Katz, J., Regnery, H., Lim, W., Hall, H., Perdue, M., Swayne, D., Bender, C. & Huang, J. (1998). Characterization of an avian influenza A (H5N1) virus isolated from a child with a fatal respiratory illness. *Science* **279**, 393-396.

Subczynski, W. K., Wojas, J., Pezeshk, V. & Pezeshk, A. (1998). Partitioning and localization of spin-labeled amantadine in lipid bilayers: an EPR study. *Journal of Pharmaceutical Sciences* **87**, 1249-1254.

Sugrue, R., Bahadur, G., Zambon, M., Hall-Smith, M., Douglas, A. & Hay, A. (1990). Specific structural alteration of the influenza haemagglutinin by amantadine. *The EMBO journal* **9**, 3469.

Sugrue, R. & Hay, A. (1991). Structural characteristics of the M2 protein of influenza a viruses: Evidence that it forms a tetrameric channel. *Virology* **180**, 617-624.

Suprynowicz, F. A., Krawczyk, E., Hebert, J. D., Sudarshan, S. R., Simic, V., Kamonjoh, C. M. & Schlegel, R. (2010). The Human Papillomavirus Type 16 E5 Oncoprotein Inhibits Epidermal Growth Factor Trafficking Independently of Endosome Acidification. *Journal of Virology* **84**, 10619-10629.

Suzuki, T., Orba, Y., Okada, Y., Sunden, Y., Kimura, T., Tanaka, S., Nagashima, K., Hall, W. W. & Sawa, H. (2010). The Human Polyoma JC Virus Agnoprotein Acts as a Viroporin. *PLoS Pathog* **6**, e1000801.

Takeda, M., Pekosz, A., Shuck, K., Pinto, L. H. & Lamb, R. A. (2002). Influenza a virus M2 ion channel activity is essential for efficient replication in tissue culture. *Journal of Virology* **76**, 1391-1399.

Tamura, D., Nguyen, H. T., Sleeman, K., Levine, M., Mishin, V. P., Yang, H., Guo, Z., Okomo-Adhiambo, M., Xu, X. & Stevens, J. (2013). Cell culture-selected substitutions in influenza A (H3N2) neuraminidase affect drug susceptibility assessment. *Antimicrobial agents and chemotherapy* **57**, 6141-6146.

Tang, Y., Zaitseva, F., Lamb, R. A. & Pinto, L. H. (2002). The gate of the influenza virus M2 proton channel is formed by a single tryptophan residue. *Journal of Biological Chemistry* **277**, 39880-39886.

Taubenberger, J. K., Reid, A. H., Lourens, R. M., Wang, R., Jin, G. & Fanning, T. G. (2005). Characterization of the 1918 influenza virus polymerase genes. *Nature* **437**, 889-893.

Tedbury, P., Welbourn, S., Pause, A., King, B., Griffin, S. & Harris, M. (2011). The subcellular localization of the hepatitis C virus non-structural protein NS2 is regulated by an ion channel-independent function of the p7 protein. *Journal of General Virology* **92**, 819-830.

Teissier, E., Zandomeneghi, G., Loquet, A., Lavillette, D., Lavergne, J.-P., Montserret, R., Cosset, F.-L., Böckmann, A., Meier, B. H. & Penin, F. (2011). Mechanism of inhibition of enveloped virus membrane fusion by the antiviral drug arbidol. *PloS one* **6**, e15874.

Thomas, F. & Magill, T. (1936). Vaccination of human subjects with virus of human influenza. *Experimental Biology and Medicine* **33**, 604-606.

Thomaston, J. L., Alfonso-Prieto, M., Woldeyes, R. A., Fraser, J. S., Klein, M. L., Fiorin, G. & DeGrado, W. F. (2015). High-resolution structures of the M2 channel from influenza A virus reveal dynamic pathways for proton stabilization and transduction. *Proceedings of the National Academy of Sciences* **112**, 14260-14265.

Thomaston, J. L. & DeGrado, W. F. (2016). Crystal structure of the drug-resistant S31N influenza M2 proton channel. *Protein Science*.

Thompson, C. I., Barclay, W. S., Zambon, M. C. & Pickles, R. J. (2006). Infection of human airway epithelium by human and avian strains of influenza a virus. *Journal of virology* **80**, 8060-8068.

Tintori, C., Laurenzana, I., Fallacara, A. L., Kessler, U., Pilger, B., Stergiou, L. & Botta, M. (2014). High-throughput docking for the identification of new influenza A virus polymerase inhibitors targeting the PA–PB1 protein–protein interaction. *Bioorganic & medicinal chemistry letters* **24**, 280-282.

Tong, S., Li, Y., Rivailler, P., Conrardy, C., Castillo, D. A. A., Chen, L.-M., Recuenco, S., Ellison, J. A., Davis, C. T. & York, I. A. (2012). A distinct lineage of influenza A virus from bats. *Proceedings of the National Academy of Sciences* **109**, 4269-4274.

Tong, S., Zhu, X., Li, Y., Shi, M., Zhang, J., Bourgeois, M., Yang, H., Chen, X., Recuenco, S. & Gomez, J. (2013). New world bats harbor diverse influenza A viruses. *PLoS Pathog* **9**, e1003657.

Torres, E., Leiva, R., Gazzarrini, S., Rey-Carrizo, M., Frigolé-Vivas, M., Moroni, A., Naesens, L. & Vázquez, S. (2014). Azapropellanes with anti-influenza a virus activity. *ACS medicinal chemistry letters* **5**, 831-836.

Tosteson, M., Pinto, L., Holsinger, L. & Lamb, R. (1994). Reconstitution of the influenza virus M2 ion channel in lipid bilayers. *The Journal of membrane biology* **142**, 117-126.

Townsend, A. & Skehel, J. (1982). Influenza A specific cytotoxic T-cell clones that do not recognize viral glycoproteins. *Nature* **300**, 655-657.

Tran, L., Choi, S. B., Al-Najjar, B. O., Yusuf, M., Wahab, H. A. & Le, L. (2011). Discovery of potential M2 channel inhibitors based on the amantadine scaffold via virtual screening and pharmacophore modeling. *Molecules* **16**, 10227-10255.

Treanor, J. J., Tierney, E. L., Zebedee, S. L., Lamb, R. A. & Murphy, B. R. (1990). Passively transferred monoclonal antibody to the M2 protein inhibits influenza A virus replication in mice. *Journal of virology* **64**, 1375-1377.

Tu, Q., Pinto, L. H., Luo, G., Shaughnessy, M. A., Mullaney, D., Kurtz, S., Krystal, M. & Lamb, R. A. (1996). Characterization of inhibition of M2 ion channel activity by BL-1743, an inhibitor of influenza A virus. *Journal of virology* **70**, 4246-4252.

Valle, G. F. & Banks, L. (1995). The human papillomavirus (HPV)-6 and HPV-16 E5 proteins co-operate with HPV-16 E7 in the transformation of primary rodent cells. *Journal of General Virology* **76**, 1239-1245.

Van Noorden, R. (2014). Report disputes benefit of stockpiling Tamiflu. *Nature*.

van Riel, D., den Bakker, M. A., Leijten, L. M., Chutinimitkul, S., Munster, V. J., de Wit, E., Rimmelzwaan, G. F., Fouchier, R. A., Osterhaus, A. D. & Kuiken, T. (2010). Seasonal and pandemic human influenza viruses attach better to human upper respiratory tract epithelium than avian influenza viruses. *The American journal of pathology* **176**, 1614-1618.

Van Riel, D., Munster, V. J., De Wit, E., Rimmelzwaan, G. F., Fouchier, R. A., Osterhaus, A. D. & Kuiken, T. (2006). H5N1 virus attachment to lower respiratory tract. *Science* **312**, 399-399.

Virelizier, J.-L. (1975). Host defenses against influenza virus: the role of anti-hemagglutinin antibody. *The Journal of Immunology* **115**, 434-439.

von Itzstein, M., Wu, W.-Y., Kok, G. B., Pegg, M. S., Dyason, J. C., Jin, B., Van Phan, T., Smythe, M. L., White, H. F. & Oliver, S. W. (1993). Rational design of potent sialidase-based inhibitors of influenza virus replication. *Nature* **363**, 418-423.

Vyas, V., Ukawala, R., Ghate, M. & Chintha, C. (2012). Homology modeling a fast tool for drug discovery: current perspectives. *Indian journal of pharmaceutical sciences* **74**, 1.

Wack, A., Baudner, B. C., Hilbert, A. K., Manini, I., Nuti, S., Tavarini, S., Scheffczik, H., Ugozzoli, M., Singh, M. & Kazzaz, J. (2008). Combination adjuvants for the induction of potent, long-lasting antibody and T-cell responses to influenza vaccine in mice. *Vaccine* **26**, 552-561.

Wang, C., Lamb, R. A. & Pinto, L. H. (1995). Activation of the M2 ion channel of influenza virus: a role for the transmembrane domain histidine residue. *Biophysical Journal* **69**, 1363-1371.

Wang, C., Takeuchi, K., Pinto, L. & Lamb, R. (1993). Ion channel activity of influenza A virus M2 protein: characterization of the amantadine block. *Journal of virology* **67**, 5585-5594.

Wang, H., Feng, Z., Shu, Y., Yu, H., Zhou, L., Zu, R., Huai, Y., Dong, J., Bao, C. & Wen, L. (2008). Probable limited person-to-person transmission of highly pathogenic avian influenza A (H5N1) virus in China. *The Lancet* **371**, 1427-1434.

Wang, J., Cady, S. D., Balannik, V., Pinto, L. H., DeGrado, W. F. & Hong, M. (2009). Discovery of Spiro-Piperidine Inhibitors and Their Modulation of the Dynamics of the M2 Proton Channel from Influenza A Virus. *J Am Chem Soc* **131**, 8066-8076.

Wang, J., Ma, C., Fiorin, G., Carnevale, V., Wang, T., Hu, F., Lamb, R. A., Pinto, L. H., Hong, M., Klein, M. L. & DeGrado, W. F. (2011). Molecular dynamics simulation directed rational design of inhibitors targeting drug-resistant mutants of influenza A virus M2. *Journal of the American Chemical Society* **133**, 12834-12841.

Wang, J., Ma, C., Wang, J., Jo, H., Canturk, B., Fiorin, G., Pinto, L. H., Lamb, R. A., Klein, M. L. & DeGrado, W. F. (2013a). Discovery of Novel Dual Inhibitors of the Wild-Type and the Most Prevalent Drug-Resistant Mutant, S31N, of the M2 Proton Channel from Influenza A Virus. *Journal of Medicinal Chemistry* **56**, 2804-2812.

Wang, J., Wu, Y., Ma, C., Fiorin, G., Wang, J., Pinto, L. H., Lamb, R. A., Klein, M. L. & Degrado, W. F. (2013b). Structure and inhibition of the drug-resistant S31N mutant of the M2 ion channel of influenza A virus. *Proceedings of the National Academy of Sciences of the United States of America* **110**, 1315-1320.

Watanabe, T., Watanabe, S., Ito, H., Kida, H. & Kawaoka, Y. (2001). Influenza A virus can undergo multiple cycles of replication without M2 ion channel activity. *Journal of Virology* **75**, 5656-5662.

Watanabe, T., Watanabe, S., Noda, T., Fujii, Y. & Kawaoka, Y. (2003). Exploitation of nucleic acid packaging signals to generate a novel influenza virus-based vector stably expressing two foreign genes. *Journal of virology* **77**, 10575-10583.

Weber, M., Sediri, H., Felgenhauer, U., Binzen, I., Bänfer, S., Jacob, R., Brunotte, L., García-Sastre, A., Schmid-Burgk, J. L. & Schmidt, T. (2015). Influenza virus adaptation PB2-627K modulates nucleocapsid inhibition by the pathogen sensor RIG-I. *Cell host & microbe* **17**, 309-319.

Webster, R. & Laver, W. (1967). Preparation and properties of antibody directed specifically against the neuraminidase of influenza virus. *The Journal of Immunology* **99**, 49-55.

Webster, R., Morita, M., Pridgen, C. & Tumova, B. (1976). Ortho-and paramyxoviruses from migrating feral ducks: characterization of a new group of influenza A viruses. *Journal of General Virology* **32**, 217-225.

Webster, R. G., Yakhno, M., Hinshaw, V. S., Bean, W. J. & Murti, K. C. (1978). Intestinal influenza: replication and characterization of influenza viruses in ducks. *Virology* **84**, 268-278.

Wells, W. & Brown, H. (1936). Recovery of influenza virus suspended in air and its destruction by ultraviolet radiation. *American Journal of Epidemiology* **24**, 407-413.

Wetherill, L. F., Holmes, K. K., Verow, M., Muller, M., Howell, G., Harris, M., Fishwick, C., Stonehouse, N., Foster, R., Blair, G. E., Griffin, S. & Macdonald, A. (2012). High-Risk Human Papillomavirus E5 Oncoprotein Displays Channel-Forming Activity Sensitive to Small-Molecule Inhibitors. *Journal of Virology* **86**, 5341-5351.

White, J., Matlin, K. & Helenius, A. (1981). Cell fusion by Semliki Forest, influenza, and vesicular stomatitis viruses. *The Journal of cell biology* **89**, 674-679.

WHO (1980). A revision of the system of nomenclature for influenza viruses: a WHO memorandum. *Bulletin of the World Health Organisation* **58**, 585-591.

Willey, R., Maldarelli, F., Martin, M. & Strebel, K. (1992). Human immunodeficiency virus type 1 Vpu protein induces rapid degradation of CD4. *Journal of virology* **66**, 7193-7200.

Williams, I., Churchill, D., Anderson, J., Boffito, M., Bower, M., Cairns, G., Cwynarski, K., Edwards, S., Fidler, S. & Fisher, M. (2012). British HIV Association guidelines for the treatment of HIV-1-positive adults with antiretroviral therapy 2012. *HIV medicine* **13**, 1-6.

Williams, R. C. & Wyckoff, R. W. (1945). Electron Shadow-Micrography of Virus Particles. *Experimental Biology and Medicine* **58**, 265-270.

Wiltgen, M. & Tilz, G. P. (2009). Homology modelling: a review about the method on hand of the diabetic antigen GAD 65 structure prediction. *Wiener Medizinische Wochenschrift* **159**, 112-125.

Winkler, D. A. (2002). The role of quantitative structure-activity relationships (QSAR) in biomolecular discovery. *Briefings in bioinformatics* **3**, 73-86.

Winter, G. & Fields, S. (1980). Cloning of influenza cDNA into M13: the sequence of the RNA segment encoding the A/PR/8/34 matrix protein. *Nucleic acids research* **8**, 1965-1974.

Wise, H. M., Foeglein, A., Sun, J., Dalton, R. M., Patel, S., Howard, W., Anderson, E. C., Barclay, W. S. & Digard, P. (2009). A complicated message: Identification of a novel PB1-related protein translated from influenza A virus segment 2 mRNA. *Journal of virology* **83**, 8021-8031.

Wozniak, A. L., Griffin, S., Rowlands, D., Harris, M., Yi, M., Lemon, S. M. & Weinman, S. A. (2010). Intracellular proton conductance of the hepatitis C virus p7 protein and its contribution to infectious virus production. *PLoS Pathogens* **6**, e1001087.

Wu, N. C., Young, A. P., Al-Mawsawi, L. Q., Olson, C. A., Feng, J., Qi, H., Chen, S.-H., Lu, I.-H., Lin, C.-Y. & Chin, R. G. (2014a). High-throughput profiling of influenza A virus hemagglutinin gene at single-nucleotide resolution. *Scientific reports* **4**.

Wu, S.-F., Lee, C.-J., Liao, C.-L., Dwek, R. A., Zitzmann, N. & Lin, Y.-L. (2002). Antiviral effects of an iminosugar derivative on flavivirus infections. *Journal of virology* **76**, 3596-3604.

Wu, Y., Canturk, B., Jo, H., Ma, C., Gianti, E., Klein, M. L., Pinto, L. H., Lamb, R. A., Fiorin, G., Wang, J. & DeGrado, W. F. (2014b). Flipping in the Pore: Discovery of Dual Inhibitors That Bind in Different Orientations to the Wild-Type versus the Amantadine-Resistant S31N Mutant of the Influenza A Virus M2 Proton Channel. *J Am Chem Soc* **136**, 17987-17995.

Wu, Y., Wu, Y., Tefsen, B., Shi, Y. & Gao, G. F. (2014c). Bat-derived influenza-like viruses H17N10 and H18N11. *Trends in microbiology* **22**, 183-191.

Yan, Z., Zhang, L., Fu, H., Wang, Z. & Lin, J. (2014). Design of the influenza virus inhibitors targeting the PA endonuclease using 3D-QSAR modeling, side-chain hopping, and docking. *Bioorganic & medicinal chemistry letters* **24**, 539-547.

Yang, Y., Halloran, M. E., Sugimoto, J. D. & Longini Jr, I. M. (2007). Detecting human-to-human transmission of avian influenza A (H5N1). *Emerg Infect Dis* **13**, 1348-1353.

Yasuda, J., Nakada, S., Kato, A., Toyoda, T. & Ishihama, A. (1993). Molecular assembly of influenza virus: association of the NS2 protein with virion matrix. *Virology* **196**, 249-255.

Yewdell, J. W., Bennink, J. R., Smith, G. L. & Moss, B. (1985). Influenza A virus nucleoprotein is a major target antigen for cross-reactive anti-influenza A virus cytotoxic T lymphocytes. *Proceedings of the National Academy of Sciences* **82**, 1785-1789.

Yi, M., Cross, T. A. & Zhou, H.-X. (2008). A secondary gate as a mechanism for inhibition of the M2 proton channel by amantadine. *The Journal of Physical Chemistry B* **112**, 7977-7979.

Yu, H. B. & Finlay, B. B. (2008). The caspase-1 inflammasome: a pilot of innate immune responses. *Cell host & microbe* **4**, 198-208.

Yuanji, G., Fengen, J., Ping, W., Min, W. & Jiming, Z. (1983). Isolation of influenza C virus from pigs and experimental infection of pigs with influenza C virus. *Journal of General Virology* **64**, 177-182.

Zebedee, S. L. & Lamb, R. A. (1988). Influenza A virus M2 protein: monoclonal antibody restriction of virus growth and detection of M2 in virions. *Journal of Virology* **62**, 2762-2772.

Zhao, X., Li, C., Zeng, S. & Hu, W. (2011). Discovery of highly potent agents against influenza A virus. *European Journal of Medicinal Chemistry* **46**, 52-57.

Zitzmann, N., Mehta, A. S., Carrouée, S., Butters, T. D., Platt, F. M., McCauley, J., Blumberg, B. S., Dwek, R. A. & Block, T. M. (1999). Imino sugars inhibit the formation and secretion of bovine viral diarrhea virus, a pestivirus model of hepatitis C virus: implications for the development of broad spectrum anti-hepatitis virus agents. *Proceedings of the National Academy of Sciences* **96**, 11878-11882.

Zou, P., Wu, F., Lu, L., Huang, J.-H. & Chen, Y.-H. (2009). The cytoplasmic domain of influenza M2 protein interacts with caveolin-1. *Archives of biochemistry and biophysics* **486**, 150-154.

Zsoldos, Z., Reid, D., Simon, A., Sadjad, B. S. & Peter Johnson, A. (2006). eHiTS: an innovative approach to the docking and scoring function problems. *Current Protein and Peptide Science* **7**, 421-435.

Appendix

Appendix

Appendix A Supplementary Data

ID	eHiTS Score	Dipole-dipole		π-π	H Bond
		N31	H37	H37	N31
DL1	-4.694	ABD	-	-	-
DL2	-5.111	AB	AD	-	-
DL3	-5.095	CD	BCD	C	-
DL4	-4.782	ACD	-	-	-
DL5	-5.586	ACD	-	-	-
DL6	-4.942	ACD	CD	-	-
DL7	-4.982	AC	ABCD	C	-
DL8	-4.899	BCD	CD	-	-
DL9	-4.735	CD	BC	-	-
DL10	-4.848	AC	BCD	-	-
DL11	-5.163	ABD	C	-	-
DL12	-4.678	ACD	CD	-	D
DL13	-4.591	BD	CD	-	-
DL14	-5.290	CD	BC	-	-
DL15	-5.183	ACD	C	-	-
DL16	-5.301	BCD	BCD	-	-
DL17	-5.481	B	AD	-	-

Table A.1 Interactions between DL compounds and the lumenal binding site of the E195 M2 homology model.

List of interactions between unbiased compound and the M2 lumenal binding site. Each interaction has a type (polar / π-π / hydrogen (H) bond), residue (N31 / H37) and chain (A / B / C / D) detailed.

ID	eHiTS Score	Salt bridge	π-cation		π-π			H Bond	
		D44	R45	F48	W41	R45	F48	W41	R45
DP1	-5.179	D	A	D	-	-	D	-	-
DP2	-5.173	-	A	-	-	-	D	-	-
DP3	-5.230	-	AA	-	-	-	-	-	-
DP4	-4.583	-	AA	-	-	-	-	-	-
DP5	-5.411	D	A	-	-	-	-	-	-
DP6	-4.580	D	A	-	-	-	-	-	-
DP7	-5.345	D	AA	-	-	-	-	-	-
DP8	-5.435	-	-	-	D	A	-	A	-
DP9	-4.986	-	-	-	A	-	D	A	-
DP10	-5.159	-	A	-	-	-	D	-	-
DP11	-4.815	-	A	-	A	-	-	-	A
DP12	-5.627	-	A	-	A	-	D	-	-
DP13	-4.623	-	A	-	-	-	D	-	-
DP14	-6.157	-	A		D	AA	D	-	-
DP15	-4.886	-	A	-	-	A	D	-	-
DP16	-4.610	-	A	-	-	A	-	A	-
DP17	-4.901	-	A	-	-	-	-	A	-
DP18	-4.590	D	AA	-	-	-	-	-	-
DP19	-4.598	D	-	D	A	-	-	-	-

Table A.2 Interactions between DP compounds and the peripheral binding site of the E195 M2 homology model.

List of interactions between unbiased compound and the M2 peripheral binding site, between chains A and D. Each interaction has a type (salt bridge / π – cation / π-π / hydrogen (H) bond), residue (W41 / D44 / R45 / F48) and chain (A / D) detailed. (AA, denotes two interactions of the same kind to one residue and chain).

[Zan] (IC_{50})	[L1.1] (IC_{50})	Effect	CI
0.2	0.2	0.11765	1.61056
0.2	1.0	0.43137	1.40759
0.2	5.0	0.96324	0.44305
1.0	0.2	0.49020	1.12490
1.0	1.0	0.72549	0.92395
1.0	5.0	0.94314	0.72235
5.0	0.2	0.93824	0.69035
5.0	1.0	0.94706	0.70560
5.0	5.0	0.99539	0.19121

Table A.3 Combination Indexes calculated for the combination of zanamivir and L1.1 when calculated using IC_{50} concentrations.

[Zan] (uM)	[L1.1] (uM)	Effect	CI
0.0242	0.265	0.11765	1.61159
0.0242	1.325	0.43137	1.40874
0.0242	6.625	0.96324	0.44329
0.12	0.265	0.49020	1.12256
0.12	1.325	0.72549	0.92382
0.12	6.625	0.94314	0.72283
0.6	0.265	0.93824	0.69275
0.6	1.325	0.94706	0.70795
0.6	6.625	0.99539	0.19219

Table A.4 Combination Indexes calculated for the combination of zanamivir and L1.1 when calculated using micromolar concentrations.

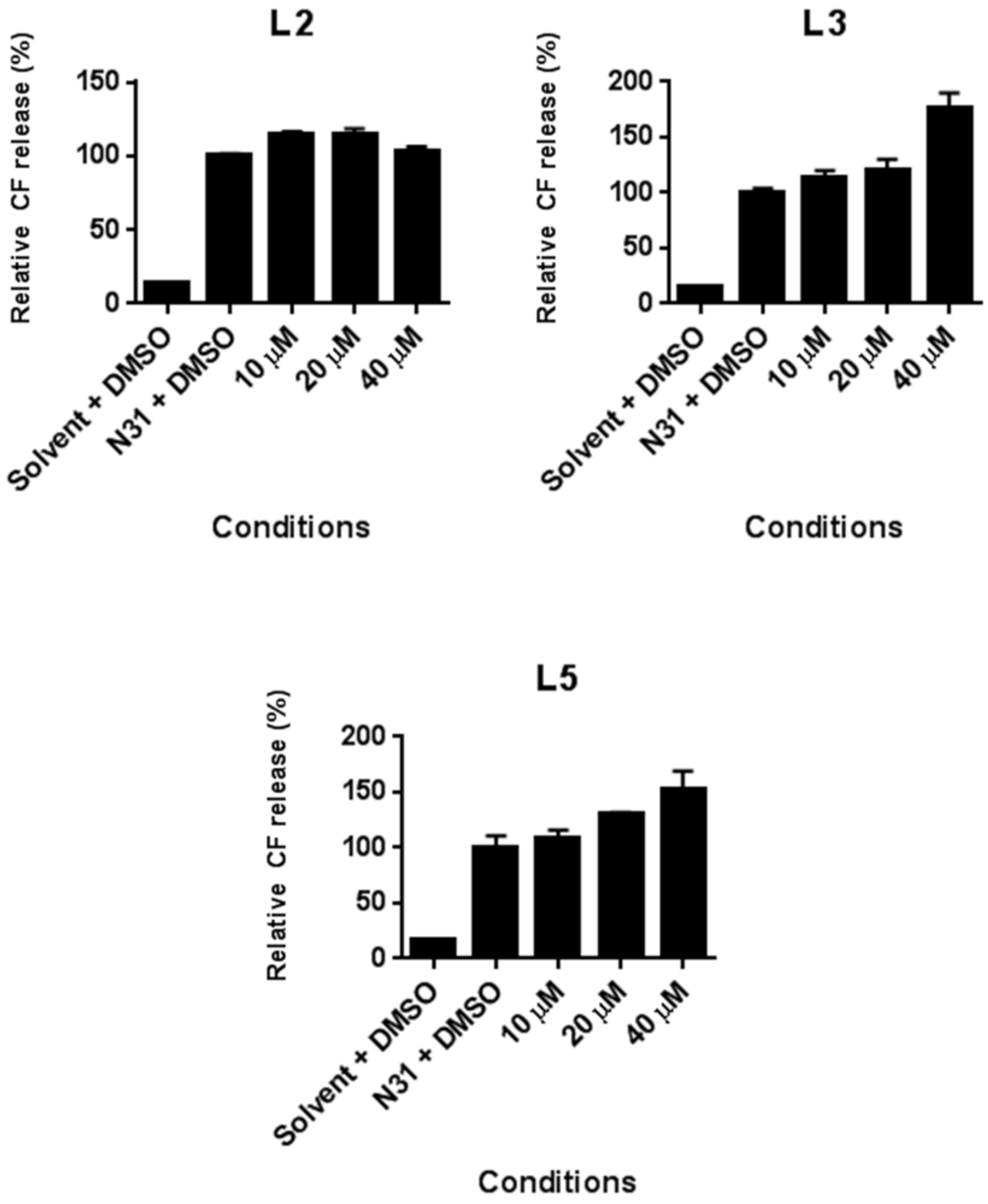

Figure A.1 Effect of predicted lumenal binding compounds on CF release mediated by an E195 N31 CD peptide.

Increasing concentrations of predicted lumenal targeting compounds L2, L3 and L5 (10, 20, and 40 µM, 1 % v/v DMSO) were preincubated with 25 nM N31 CD peptide (5 %v/v MeOH). CF release from liposomes was then measured by fluorimetry (λex = 485 nm, λem = 520 nm). End point values, with liposomes alone subtracted, then normalised to peptide + DMSO (N31 + DMSO) and relative CF release plotted. Error bars represent standard deviation of the mean, from duplicate wells of a single experiment.

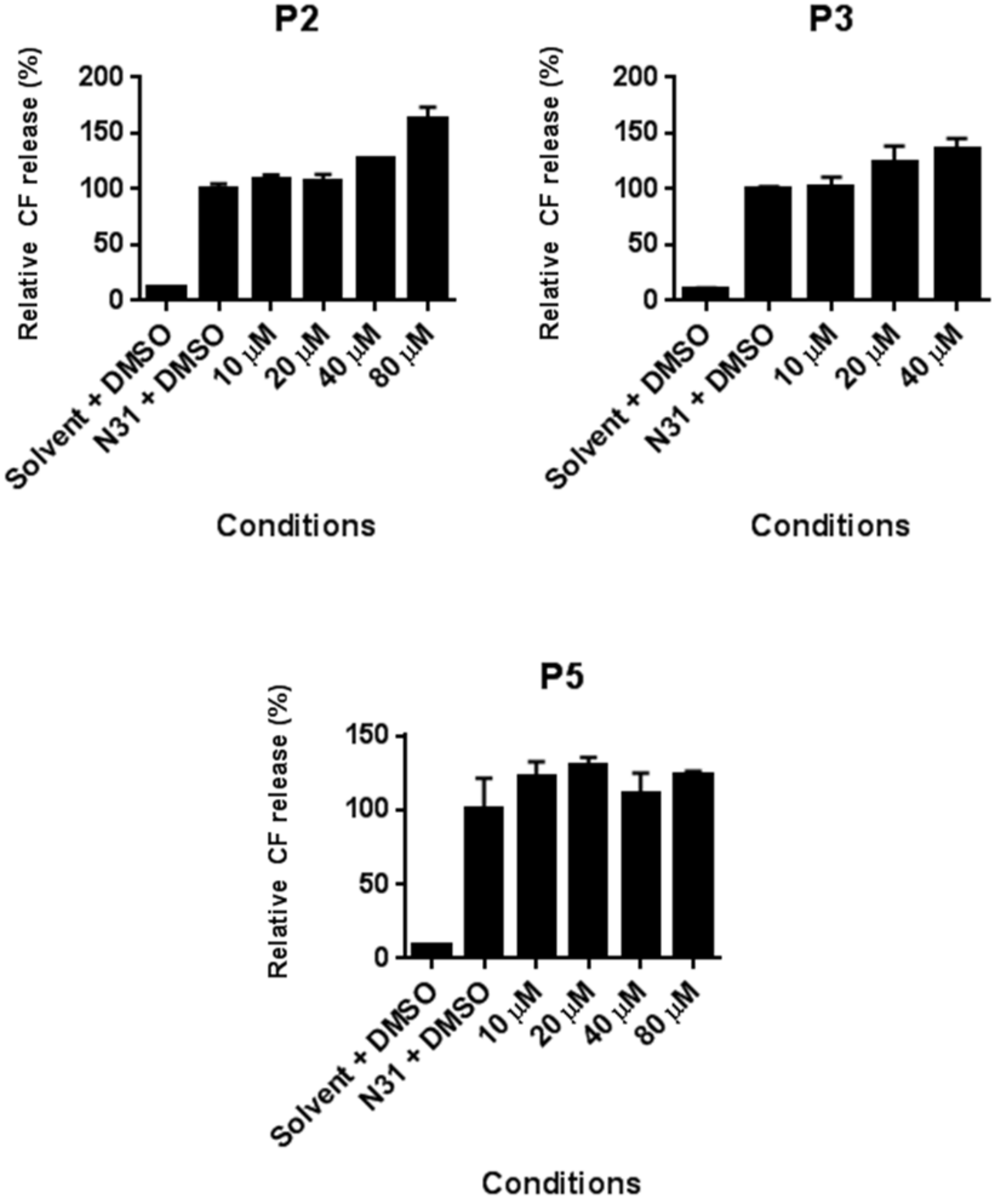

Figure A.2 Effect of predicted peripheral binding compounds CF release mediated by an E195 N31 CD peptide.

Increasing concentrations of predicted peripheral targeting compounds P2, P3 and P5 (10, 20, 40 and 80 µM, 1 % v/v DMSO) were preincubated with 25 nM N31 CD peptide (5 %v/v MeOH). CF release from liposomes was then measured by fluorimetry (λex = 485 nm, λem = 520 nm). End point values, with liposomes alone subtracted, then normalised to peptide + DMSO (N31 + DMSO) and relative CF release plotted. Error bars represent standard deviation of the mean, from duplicate wells of a single experiment.

L1

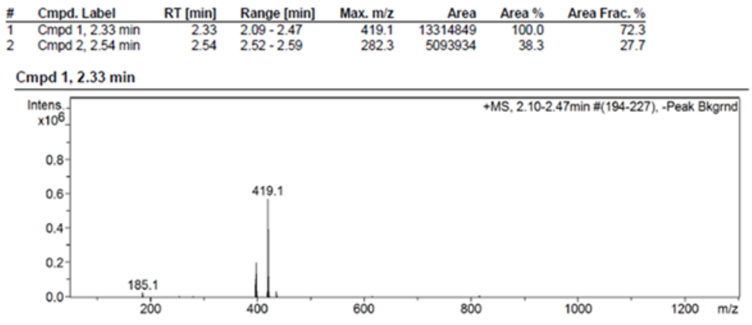

#	Cmpd. Label	RT [min]	Range [min]	Max. m/z	Area	Area %	Area Frac. %
1	Cmpd 1, 2.33 min	2.33	2.09 - 2.47	419.1	13314849	100.0	72.3
2	Cmpd 2, 2.54 min	2.54	2.52 - 2.59	282.3	5093934	38.3	27.7

Cmpd 1, 2.33 min

Intens.
x10^6
+MS, 2.10-2.47min #(194-227), -Peak Bkgrnd
0.8
0.6
0.4
0.2
0.0
419.1
185.1
200
400
600
800
1000
1200
m/z

L4

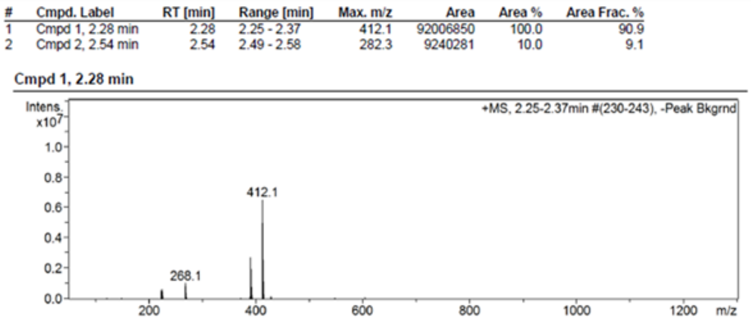

#	Cmpd. Label	RT [min]	Range [min]	Max. m/z	Area	Area %	Area Frac. %
1	Cmpd 1, 2.28 min	2.28	2.25 - 2.37	412.1	92006850	100.0	90.9
2	Cmpd 2, 2.54 min	2.54	2.49 - 2.58	282.3	9240281	10.0	9.1

Cmpd 1, 2.28 min

Intens.
x10^7
+MS, 2.25-2.37min #(230-243), -Peak Bkgrnd
1.0
0.8
0.6
0.4
0.2
0.0
412.1
268.1
200
400
600
800
1000
1200
m/z

P1

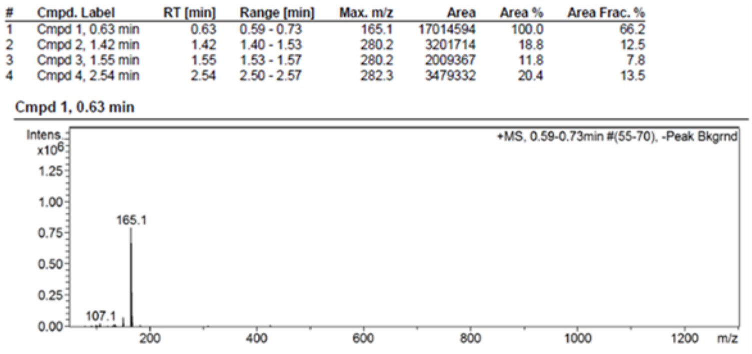

#	Cmpd. Label	RT [min]	Range [min]	Max. m/z	Area	Area %	Area Frac. %
1	Cmpd 1, 0.63 min	0.63	0.59 - 0.73	165.1	17014594	100.0	66.2
2	Cmpd 2, 1.42 min	1.42	1.40 - 1.53	280.2	3201714	18.8	12.5
3	Cmpd 3, 1.55 min	1.55	1.53 - 1.57	280.2	2009367	11.8	7.8
4	Cmpd 4, 2.54 min	2.54	2.50 - 2.57	282.3	3479332	20.4	13.5

Cmpd 1, 0.63 min

Intens.
x10^6
+MS, 0.59-0.73min #(55-70), -Peak Bkgrnd
1.25
1.00
0.75
0.50
0.25
0.00
165.1
107.1
200
400
600
800
1000
1200
m/z

P6

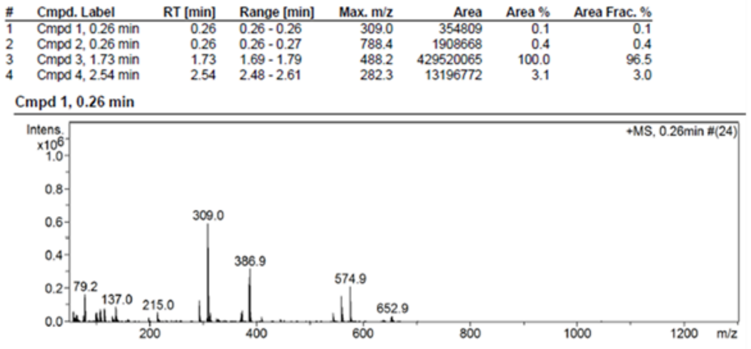

#	Cmpd. Label	RT [min]	Range [min]	Max. m/z	Area	Area %	Area Frac. %
1	Cmpd 1, 0.26 min	0.26	0.26 - 0.26	309.0	354809	0.1	0.1
2	Cmpd 2, 0.26 min	0.26	0.26 - 0.27	788.4	1908668	0.4	0.4
3	Cmpd 3, 1.73 min	1.73	1.69 - 1.79	488.2	429520065	100.0	96.5
4	Cmpd 4, 2.54 min	2.54	2.48 - 2.61	282.3	13196772	3.1	3.0

Cmpd 1, 0.26 min

Intens.
x10^6
+MS, 0.26min #(24)
1.0
0.8
0.6
0.4
0.2
0.0
309.0
386.9
574.9
79.2
137.0
215.0
652.9
200
400
600
800
1000
1200
m/z

Figure A.3 Assessment of L1, L4, P1 and P6 compound purity.

Compound purity was assessed via Liquid Chromatography Mass Spectrometry analysis and carried out by Dr Charlotte Revill.

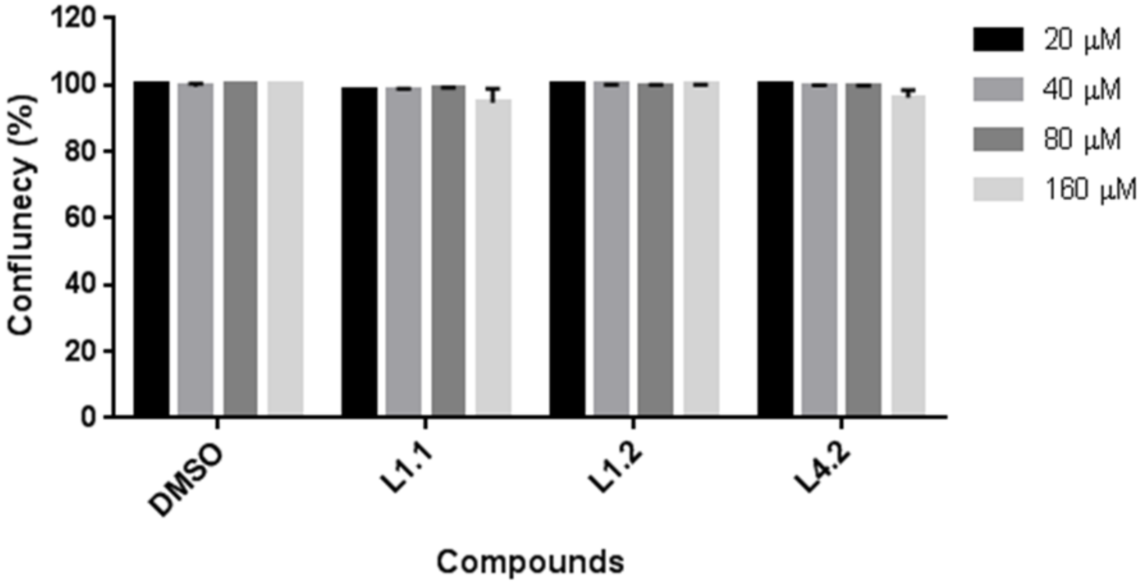

Figure A. 4 Effect of compound analogues on MDCK cell confluency after a 48 hour incubation.

Effect of increasing concentrations (20, 40, 80 and 160 µM) of novel non-adamantane compounds on MDCK cell confluency. Measurements were made after 48 hr, using the IncuCyte® ZOOM. Error bars represent standard deviation of four wells within one experiment.

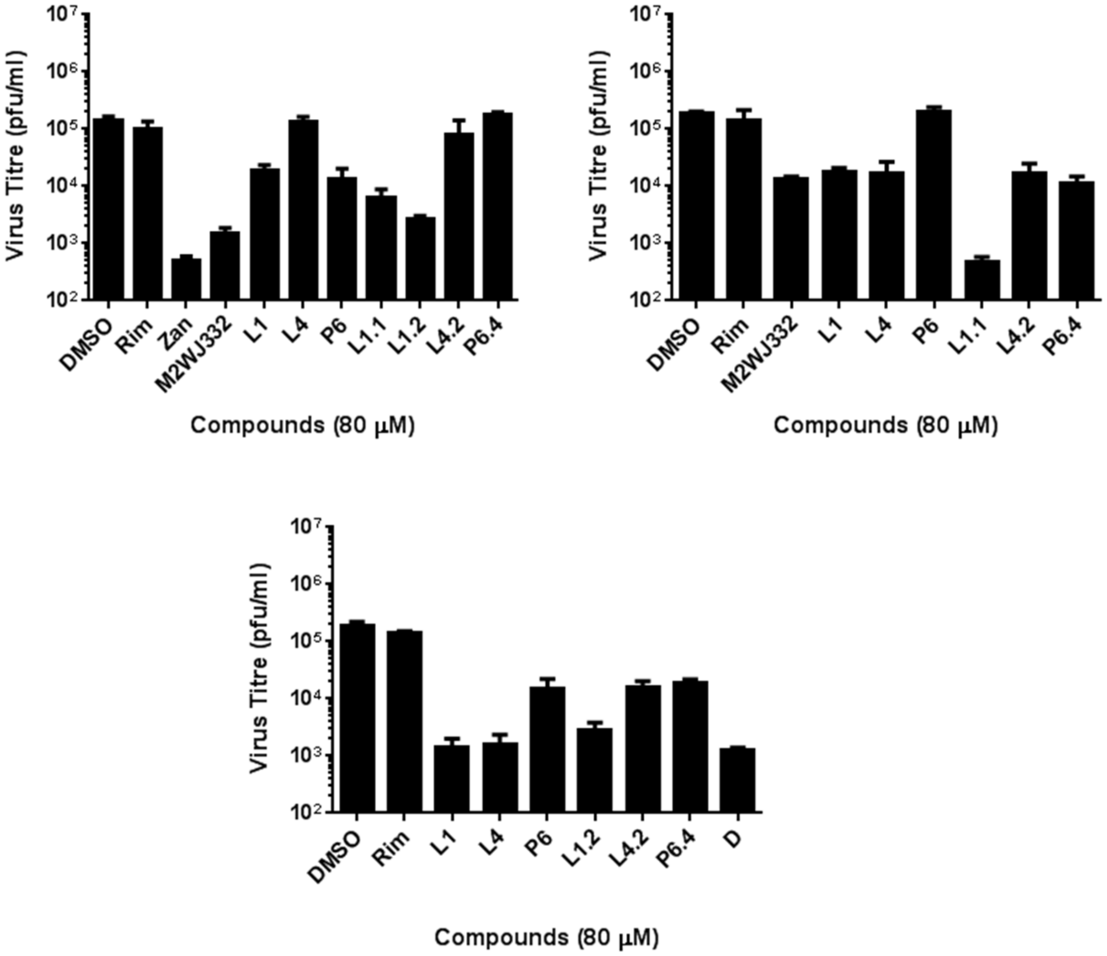

Figure A.5 Effect of L1, L4, P6 and selected analogues on infectious E195 virus titre.

E195 infectious virus titre is reduced by novel compounds at 24 hours post an infection of MOI 0.01, each graph represents data from an independent experiment. Error bars represent standard deviation over three wells.

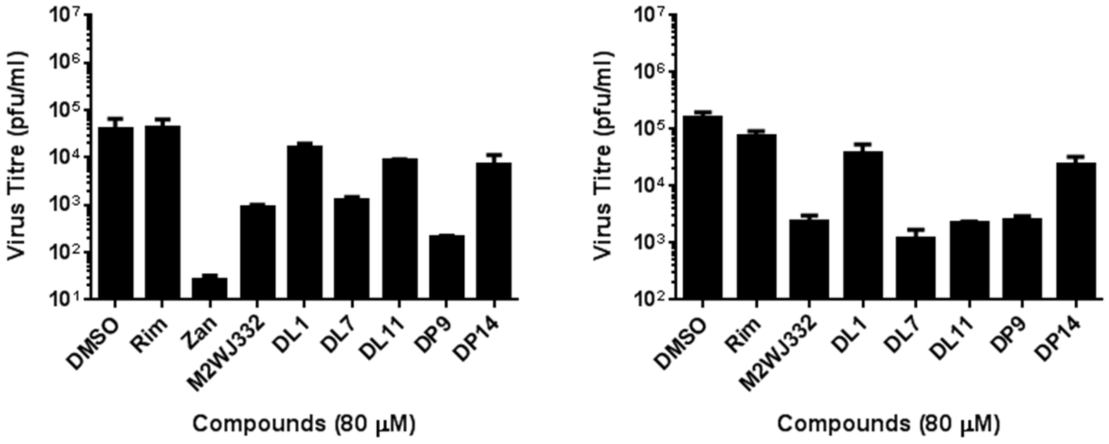

Figure A.6 Effect of biased compounds on E195 virus titre.

E195 infectious virus titre is reduced by novel compounds at 24 hours post an infection of MOI 0.01, each graph represents data from an independent experiment. Error bars represent standard deviation over three wells.

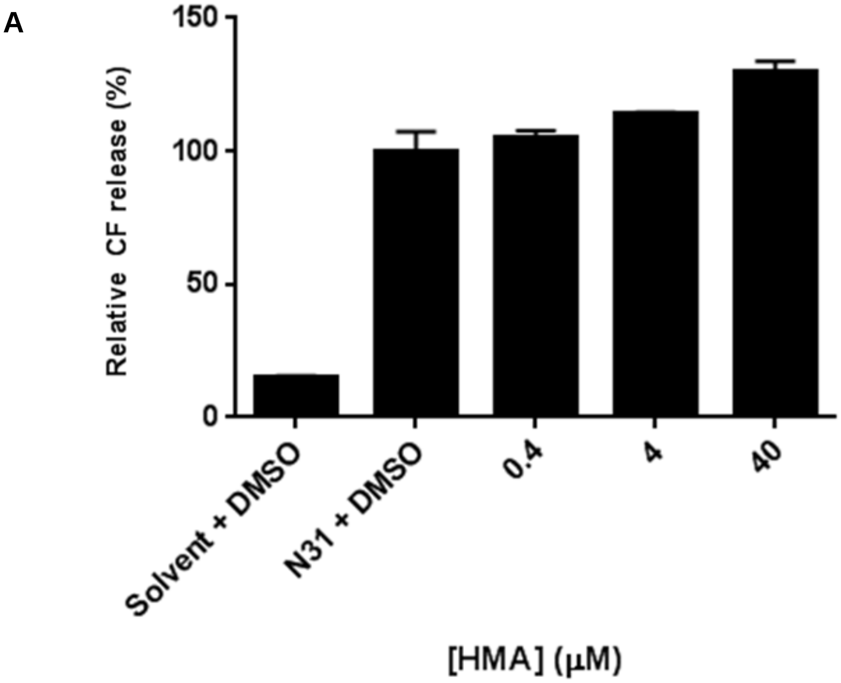

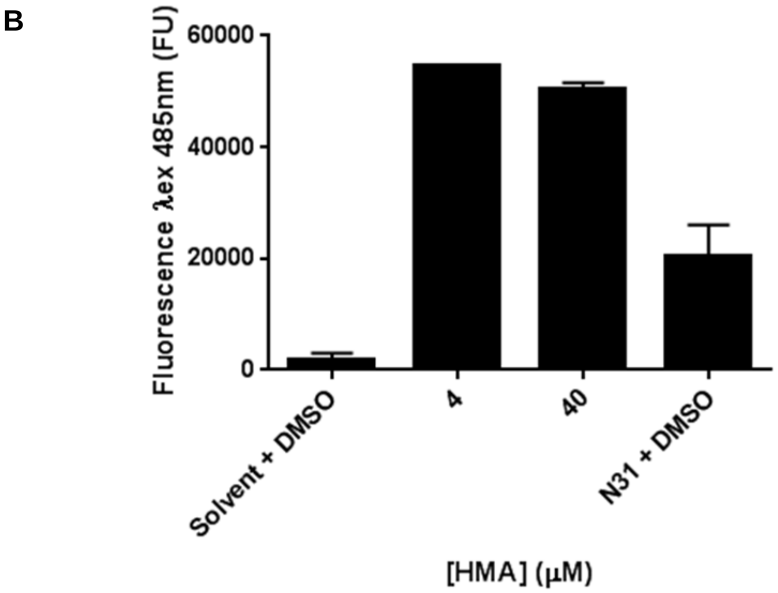

Figure A.7 Effect of HMA on the CF release mediated by an E195 N31 CD peptide.

Increasing concentrations of HMA (1 % v/v DMSO) were preincubated with A) 25 nM N31 CD peptide or B) solvent control (5 %v/v MeOH). CF release from liposomes was then measured by fluorimetry (λex = 485 nm, λem = 520 nm). End point values, with liposomes alone subtracted. For the experiment testing the effect of HMA against M2 these results were then normalised to N31 + DMSO and relative CF release plotted. Error bars represent standard deviation of the mean, from duplicate wells of a single experiment.

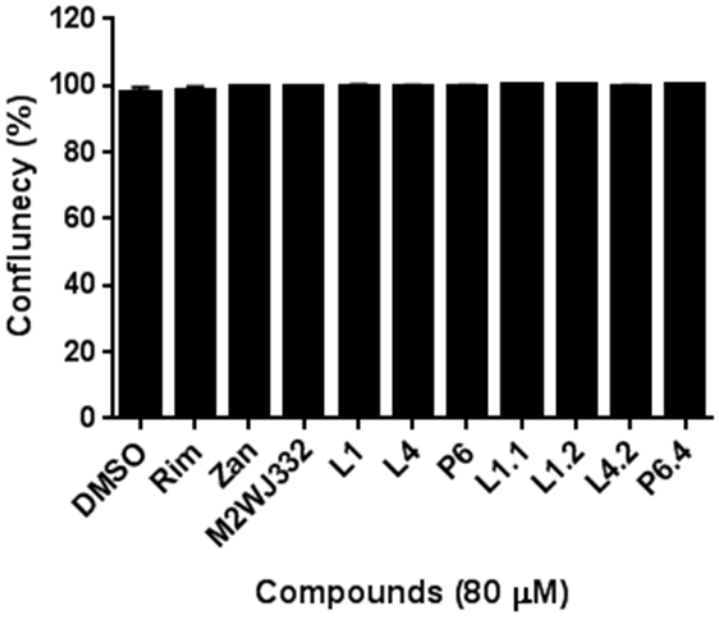

Figure A.8 MDCK cell confluency is unaffected by MOI 0.01 with 80 µM novel compound over 24 hours.

After the initial 24 hour infection at MOI 0.01, with compounds present at 80 µM, the producer plate was fixed (4 % PFA). Cell confluency was measured using the IncuCyte® ZOOM. Error bars represent standard deviation of three wells within one experiment.

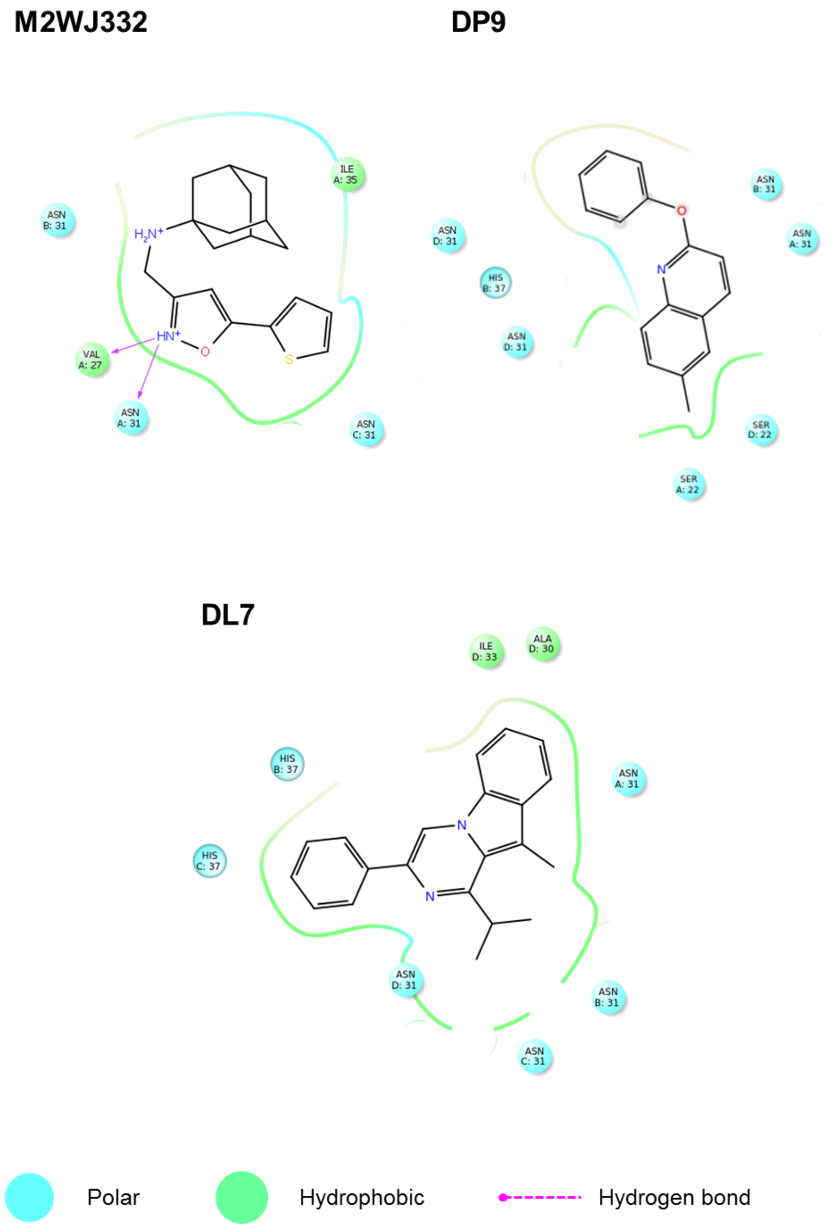
M2WJ332
DP9
DL7
ILE A: 35
ASN B: 31
H_2N^+
HN^+
O
S
VAL A: 27
ASN A: 31
ASN C: 31
ASN B: 31
ASN A: 31
ASN D: 31
HIS B: 37
ASN D: 31
O
N
SER D: 22
SER A: 22
ILE D: 33
ALA D: 30
HIS B: 37
ASN A: 31
HIS C: 37
N
N
ASN D: 31
ASN B: 31
ASN C: 31
Polar
Hydrophobic
Hydrogen bond

Figure A.9 Predicted interactions between compounds M2WJ332, DL7 and DP9, and the lumenal binding site of the 2L0J E195 M2 homology model.

2D structures of M2WJ332, DP9 and DL7 and residues (circles) of the M2 tetramer they interact with are shown. Amino acids involved in interactions with compounds are coloured as being either hydrophobic (lime green) or polar (light blue), they are labelled with the three letter code, chain and residue number and hydrogen bond (magenta lines) interactions are highlighted.

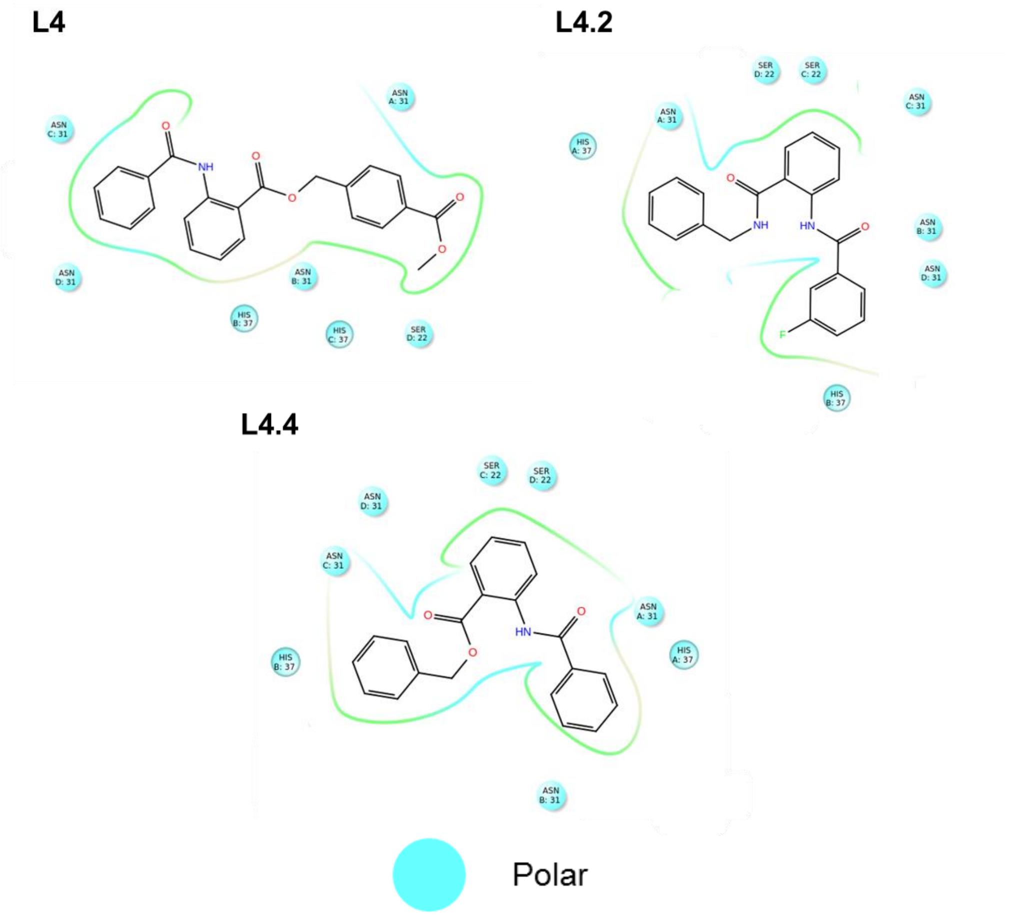
L4

L4.2

L4.4

ASN C: 31
ASN A: 31
ASN D: 31
ASN B: 31
HIS B: 37
HIS C: 37
SER D: 22
NH
O
SER D: 22
SER C: 22
ASN A: 31
ASN C: 31
HIS A: 37
NH
HN
F
ASN B: 31
ASN D: 31
HIS B: 37
SER C: 22
SER D: 22
ASN D: 31
ASN C: 31
HN
ASN A: 31
HIS B: 37
HIS A: 37
ASN B: 31
Polar

Figure A.10 Predicted interactions between novel compound L4 and its analogues L4.2 and L4.4 and the lumenal binding site of the 2L0J E195 M2 homology model.

2D structures of L4 and its analogues L4.2 and L4.4, and polar residues (light blue circles) of the M2 tetramer they interact with are shown.

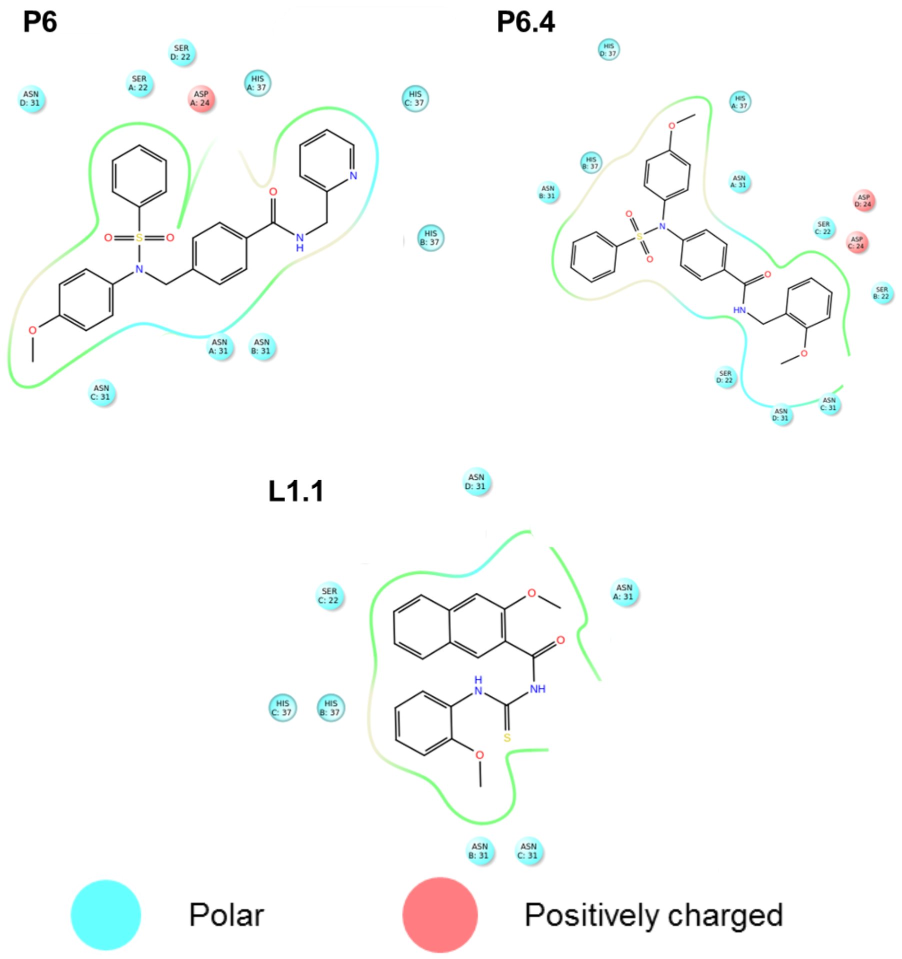
P6
SER D: 22
SER A: 22
ASP A: 24
HIS A: 37
ASN D: 31
HIS C: 37
HIS B: 37
ASN A: 31
ASN B: 31
ASN C: 31
P6.4
HIS D: 37
HIS A: 37
HIS B: 37
ASN B: 31
ASN A: 31
ASP D: 24
SER C: 22
ASP C: 24
SER B: 22
SER D: 22
ASN D: 31
ASN C: 31
L1.1
ASN D: 31
SER C: 22
ASN A: 31
HIS C: 37
HIS B: 37
ASN B: 31
ASN C: 31
Polar
Positively charged

Figure A.11 Predicted interactions between novel compounds P6, P6.4 and L1.1, and the lumenal binding site of the 2L0J E195 M2 homology model.

2D structures of P6, P6.4 and L1.1, and residues (circles) of the M2 tetramer they interact with are shown. Amino acids involved in interactions with compounds are coloured as being either polar (light blue) or positively charged (red), they are labelled with the three letter code, chain and residue number.

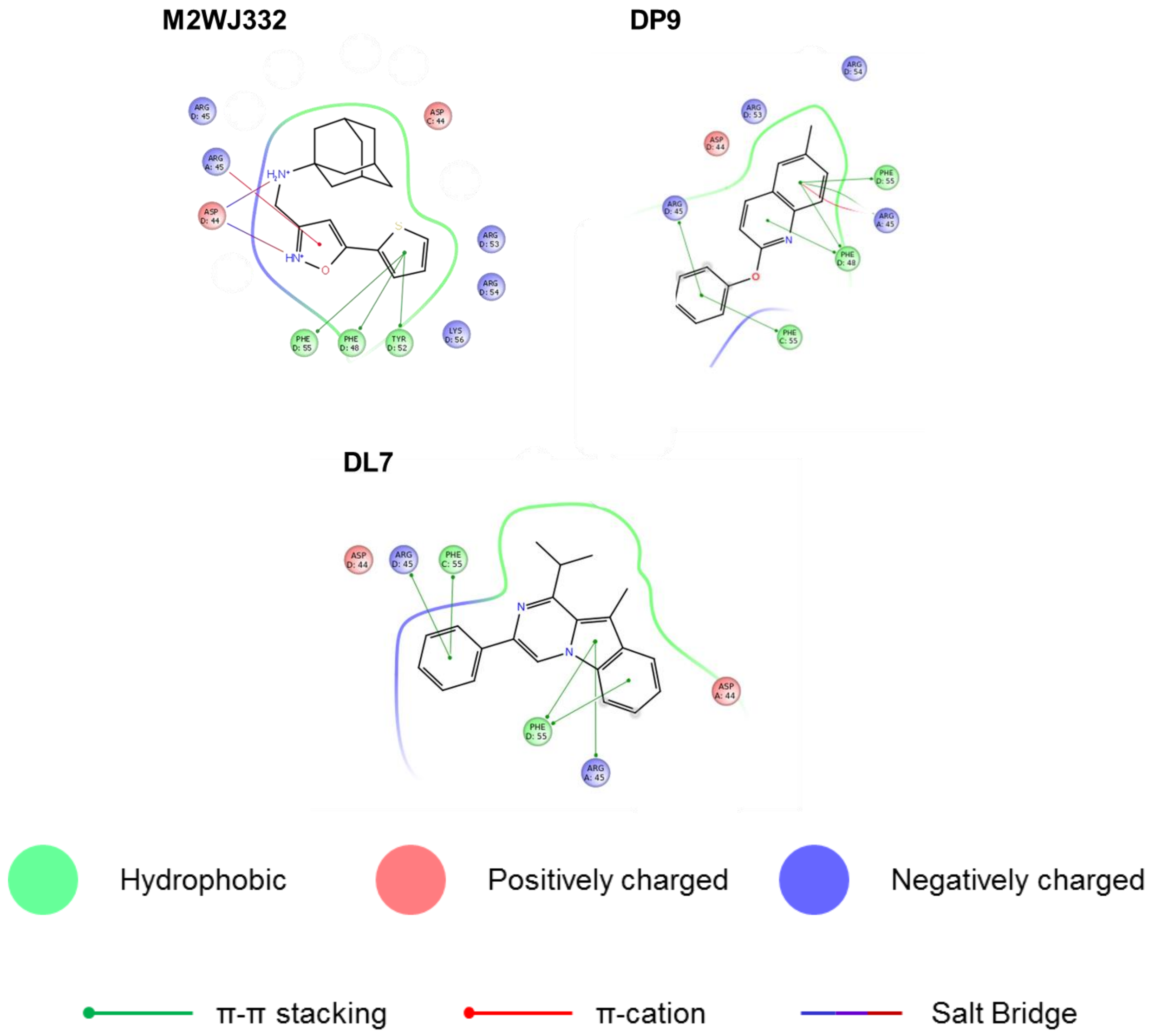
M2WJ332
ARG D: 45
ARG A: 45
ASP D: 44
ASP C: 44
H2N+
HN+
O
S
ARG D: 53
ARG D: 54
LYS D: 56
PHE D: 55
PHE D: 48
TYR D: 52
DP9
ARG D: 54
ARG D: 53
ASP D: 44
ARG D: 45
PHE D: 55
ARG A: 45
PHE D: 48
N
O
PHE C: 55
DL7
ASP D: 44
ARG D: 45
PHE C: 55
N
N
ASP A: 44
PHE D: 55
ARG A: 45
Hydrophobic
Positively charged
Negatively charged
π-π stacking
π-cation
Salt Bridge

Figure A.12 Predicted interactions between compounds M2WJ332, DL7 and DP9, and the peripheral binding site of the 2L0J E195M2 homology model.

2D structures of M2WJ332, DP9 and DL7 and residues (circles) of the M2 tetramer they interact with are shown. π-π stacking (green lines), π-cation (red lines) and salt bridges (blue and red lines) interactions are highlighted. Amino acids involved in interactions with compounds are coloured as being either hydrophobic (green), negatively (blue) or positively charged (red), they are labelled with the three letter code, chain and residue number.

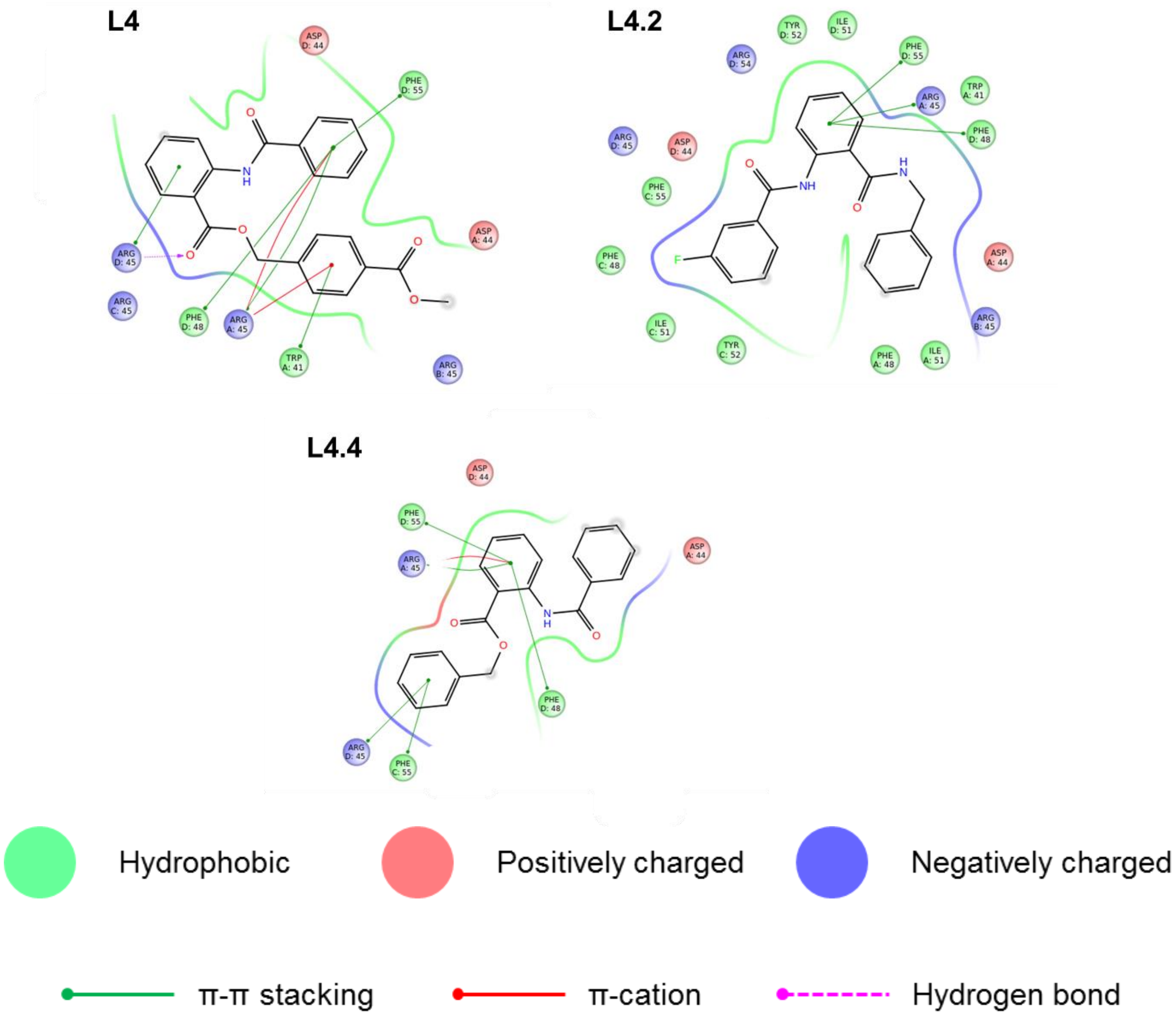
L4
ASP D: 44
PHE D: 55
ASP A: 44
ARG D: 45
ARG C: 45
PHE D: 48
ARG A: 45
TRP A: 41
ARG B: 45
L4.2
TYR D: 52
ILE D: 51
ARG D: 54
PHE D: 55
TRP A: 41
ARG A: 45
PHE D: 48
ARG D: 45
ASP D: 44
PHE C: 55
PHE C: 48
ASP A: 44
ILE C: 51
TYR C: 52
PHE A: 48
ILE A: 51
ARG B: 45
L4.4
ASP D: 44
PHE D: 55
ARG A: 45
ASP A: 44
PHE D: 48
ARG D: 45
PHE C: 55
Hydrophobic
Positively charged
Negatively charged
π-π stacking
π-cation
Hydrogen bond

Figure A.13 Predicted interactions between novel compound L4 and its analogues L4.2 and L4.4 and the peripheral binding site of the 2L0J E195 M2 homology model.

2D structures of L4 and its analogues L4.2 and L4.4, and residues (circles) of the M2 tetramer they interact with are shown. π-π stacking (green lines), π-cation (red lines) and hydrogen bond (magenta lines) interactions are highlighted. Amino acids involved in interactions with compounds are coloured as being either hydrophobic (green), positively (red) or negatively charged (blue), they are labelled with the three letter code, chain and residue number.

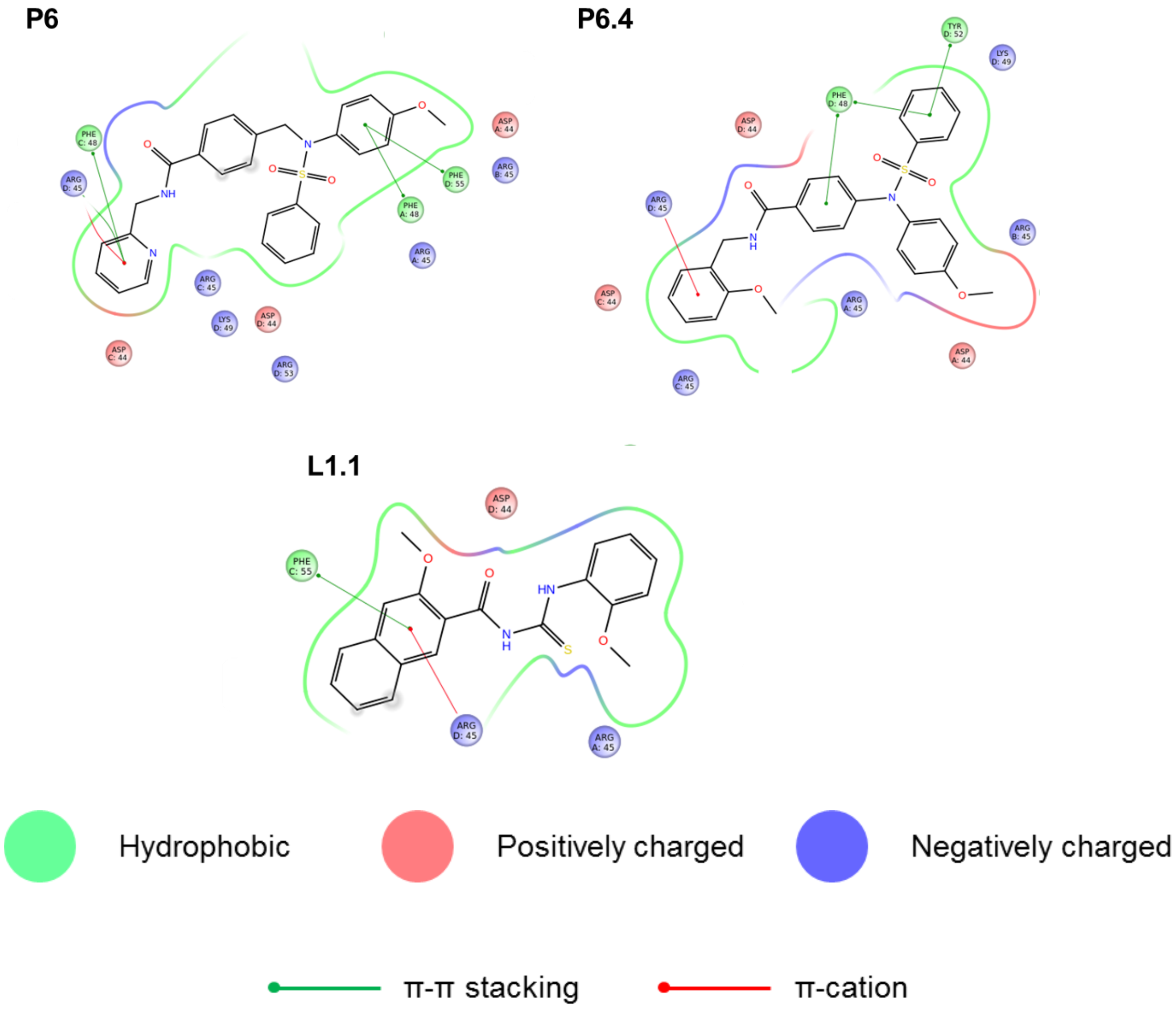
P6
PHE C: 48
ARG D: 45
O
NH
N
N
O
S
O
O
ASP A: 44
ARG B: 45
PHE D: 55
PHE A: 48
ARG A: 45
ARG C: 45
LYS D: 49
ASP D: 44
ASP C: 44
ARG D: 53
P6.4
TYR D: 52
LYS D: 49
PHE D: 48
ASP D: 44
ARG D: 45
ASP C: 44
ARG C: 45
ARG A: 45
ARG B: 45
ASP A: 44
L1.1
ASP D: 44
PHE C: 55
HN
N H
S
ARG D: 45
ARG A: 45
Hydrophobic
Positively charged
Negatively charged
π-π stacking
π-cation

Figure A.14 Predicted interactions between novel compounds P6, P6.4 and L1.1, and the peripheral binding site of the 2L0J E195 M2 homology model.

2D structures of P6, P6.4 and L1.1, and residues (circles) of the M2 tetramer they interact with are shown. π-π stacking (green lines) and π-cation (red lines) interactions are highlighted. Amino acids involved in interactions with compounds are coloured as being either hydrophobic (green), positively (red) or negatively charged (blue), they are labelled with the three letter code, chain and residue number.

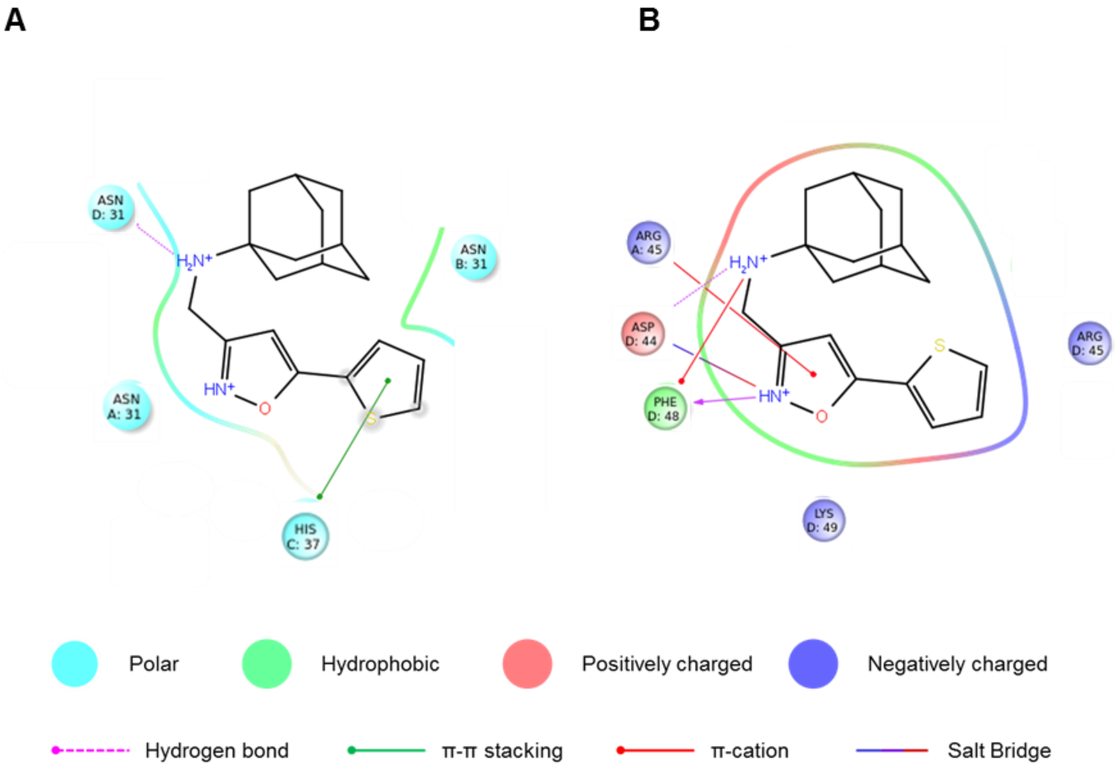
A
B
ASN D: 31
ASN B: 31
ASN A: 31
HIS C: 37
H2N+
HN+
O
S
ARG A: 45
ASP D: 44
PHE D: 48
ARG D: 45
LYS D: 49
Polar
Hydrophobic
Positively charged
Negatively charged
Hydrogen bond
π-π stacking
π-cation
Salt Bridge

Figure A.15 Predicted interactions between M2WJ332 and the lumenal binding and peripheral binding sites of the 2RLF E195 M2 homology model.

2D structure of M2WJ332 and residues (circles) of the M2 tetramer the compound interacts with at the A) lumenal and B) peripheral binding site are shown. Hydrogen bonds (magenta lines), π-π stacking (green lines), π-cation (red lines) and salt bridge (blue and red lines) interactions are highlighted. Amino acids involved in interactions with compounds are coloured as being either polar (light blue), hydrophobic (green), positively (red) or negatively charged (blue), they are labelled with the three letter code, chain and residue number.

Appendix B Recipes

B.1 Carboxyfluorescein (CF) buffer

50 mM CF, 10 mM HEPES (pH 7.4) and 107 mM NaCl

B.2 Liposome assay buffer

10 mM HEPES (pH 7.4) and 107 mM NaCl

B.3 Cell culture media

Dulbecco's modified eagles medium (DMEM), 10 % v/v fetal calf serum (FCS), 1x non-essential amino acids (NEAA), 1 Uml-1 Penicillin and 0.5 mg Streptomycin

B.4 Freezing media

DMEM, 20 % v/v FCS and 10 % DMSO

B.5 Serum free (SF) media

DMEM, 1x NEAA, 1 Uml-1 Penicillin and 0.5 mg Streptomycin

B.6 Overlay media

Modified eagles medium (MEM), 0.3 % v/v BSA (fraction V), 2.8 nM L-Glutamine, 0.2 % v/v $NaHCO_2$, 14 mM HEPES, 0.001 % v/v Dextran, 0.1x Penicillin and 0.1x Streptomycin

B.7 Viral RNA extraction buffers

B.7.1 Lysis buffer (AVL)

Composition unknown (confidential). Component guanidine isothiocyanate denatures the proteins and inactivates the virus, whilst with the addition of carrier RNA stabilises vRNA

B.7.2 Wash buffer 1 (AW1) (concentrate)

Composition unknown (confidential), suspected to contain 1M Guanidine Hydrochloride

B.7.3 Wash buffer 2 (AW2) (concentrate)

Composition unknown (confidential), contains sodium azide as a preservative

B.7.4 Elution buffer (AVE)

RNase free water containing 0.04% sodium azide as a preservative

B.8 5x Superscript III (SSCIII) first strand buffer

250 mM Tris-HCl (pH 8.3), 375 mM KCl, 15 mM MgCl2

B.9 PCR purification buffers

B9.1 Binding buffer (PB)

Composition unknown (confidential), suspected to contains 30 % isopropanol and 5 M guanidine hydrochloride

B9.2 Elution buffer (PE)

Composition unknown (confidential), suspected to be 10 mM Tris-HCl pH 7.5 and 80% ethanol

B.10 50x Tris-acetate-EDTA (TAE)

2 M Tris base, 5.7 % v/v glacial acetic acid, 50 mM EDTA

Appendix C Description and semi-quantitative analysis of compound combinations

Range of CI values	Description	Graded symbols
< 0.10	Very strong synergism	+++++
0.10-0.30	Strong synergism	++++
0.30-0.70	Synergism	+++
0.70-0.85	Moderate synergism	++
0.85-0.90	Slight synergism	+
0.90-1.10	Nearly additive	+ -
1.10-1.20	Slight antagonism	-
1.20-1.45	Moderate antagonism	- -
1.45-3.3	Antagonism	- - -
3.3-10	Strong antagonism	- - - -
>10	Very strong antagonism	- - - - -

Table A.5 Interpretation of combination index values.

Combination index (CI) values have been attributed to a scale of synergism and antagonism and also a semi-quantitative scale. Adapted from (Chou, 2006).

Appendix D Summary of compound effects

ID, CB ID	**Structure**	**L / P**	**eHiTS score**	***In vitro* activity (40 µM)**			**Virus culture**	
				N31 CD	N31 TM	S31 CD	80 µM	IC$_{50}$ (µM)
Rim, -	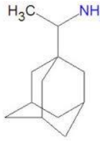	L	-2.487	73.3 ^{D}	-	56.6 ^{E}	10^{0}	-
		P	-2.925					
HMA, -	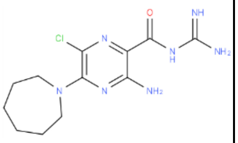	-	-	>100^{A}	-	-	-	-
D, 5354112	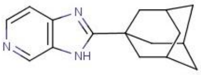	L	-3.841	53.5 ^{E}	-	-	$10^{-1\ F}$	-
		P	-2.949				10^{-2}	
H, 5680218	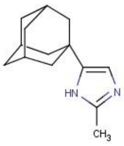	L	-3.593	79.2 ^{A}	-	-	10^{-2} ^{F}	-
		P	-3.000					
M2WJ332, -	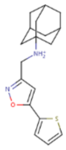	L	-3.992	61.9 ^{B}	>100 ^{B}	85.0	10^{-1} - 10^{-2}	1.183
		P	-3.430	58.4 ^{C}	99.0 ^{C}			
L1, 6622092	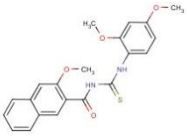	L	-5.138	37.9 ^{A}	-	45.6	$10^{-1\ F}$	-
				31.8 ^{B}	19.8 ^{B}		10^{-1} - 10^{-2}	
				24.4 ^{C}	21.7 ^{C}			
L2, 6553988	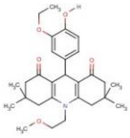	L	-4.988	>100^{A}	-	-	-	-
L3, 5523006	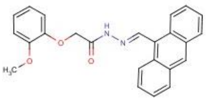	L	-4.827	>100^{A}	-	-	-	-
L4, 7636415	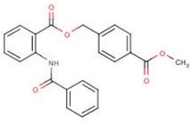	L	-5.233	59.9 ^{A}	-	50.7	$10^{-1\ F}$	-
				38.0 ^{B}	44.6 ^{B}		10^{0} – 10^{-2}	
				42.4 ^{C}	44.0 ^{C}			

L5, 5561699	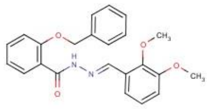	L	-5.108	>100^{A}	-	-	-	-
L6, 5525030	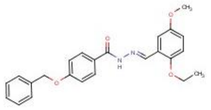	L	-4.805	26.2 ^{A}	-	-	10^{-1} ^{F}	-
L7, 7774661	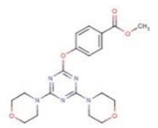	L	-4.603	95.0 ^{A}	-	-	10^{-1} ^{F}	-
P1, 7267124	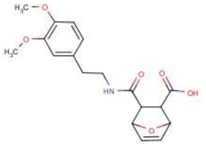	P	-4.211	52.9 ^{A}	-	-	10^{-1} ^{F}	-
P2, 5739630	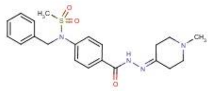	P	-4.785	>100^{A}	-	-	-	-
P3, 5114273	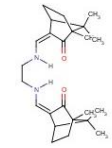	P	-5.427	>100^{A}	-	-	-	-
P4, 7612059	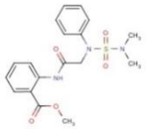	P	-4.421	25.3 ^{A}	-	-	10^{-0} ^{F}	-
P5, 5565578	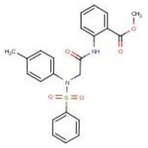	P	-4.308	>100^{A}	-	-	-	-
P6, 6424106	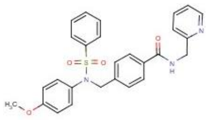	P	-4.122	73.0 ^{A}	-	75.6	10^{-1} ^{F}	-
				50.2 ^{B}	75.8 ^{B}		10^{0} – 10^{-2}	
				35.4 ^{C}	45.5 ^{C}			
L1.1, 6607593	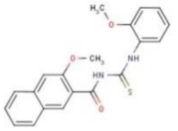	L	-3.682	32.8 ^{B}	22.0 ^{B}	41.8	10^{1} – 10^{-3}	1.325
		P	-3.113	34.5 ^{C}	23.7 ^{C}			
L1.2, 6598617	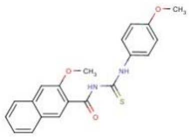	L	-3.152	26.3 ^{B}	18.2 ^{B}	19.9	10^{-1} – 10^{-2}	-
		P	-3.112	25.0 ^{C}	13.2 ^{C}			
L1.3, 6945470	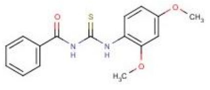	L	-2.797	61.8 ^{B}	85.4 ^{B}	-	-	-
		P	-2.784					

L1.4, 7642465	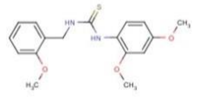	L	-3.519	77.8 ^{B}	84.4 ^{B}	-	-	-
		P	-2.707					
L4.1, 6302982	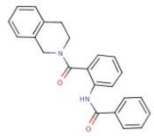	L	-3.615	>100 ^{B}	>100 ^{B}	-	-	-
		P	-3.958					
L4.2, 7999011	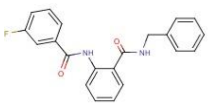	L	-3.942	47.2 ^{B}	84.5 ^{B}	60.1	$10^{0} – 10^{-1}$	-
		P	-3.400	62.6 ^{C}	68.2 ^{C}			
L4.3, 5128188	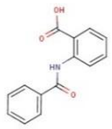	L	-4.033	>100 ^{B}	>100 ^{B}	-	-	-
		P	-3.333					
L4.4, 7749703	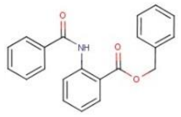	L	-3.038	51.0 ^{B}	69.3 ^{B}	-	-	-
		P	-3.483					
P6.1, 6479640	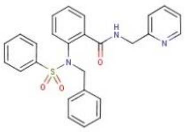	L	-4.919	>100 ^{B}	>100 ^{B}	-	-	-
		P	-4.9					
P6.2, 6470103	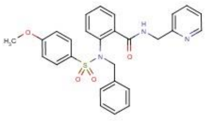	L	-3.275	93.8 ^{B}	>100 ^{B}	-	-	-
		P	-4.542					
P6.3, 5732197	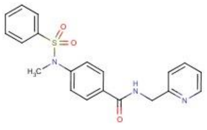	L	-4.546	>100 ^{B}	>100 ^{B}	-	-	-
		P	-4.097					
P6.4, 5861836	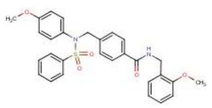	L	-1.803	37.7 ^{B}	34.3 ^{B}	66.3	$10^{0} – 10^{-1}$	-
		P	-3.551	65.4 ^{C}	32.6 ^{C}			
DL1, 5315243	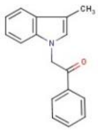	L	-4.694	72.2 ^{B}	75.2 ^{B}	-	10^{0}	-
DL2, 5923305	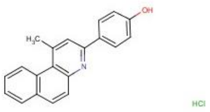	L	-5.111	>100 ^{B}	72.8 ^{B}	-	-	-
DL3, 5631260	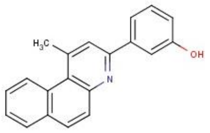	L	-5.095	78.7 ^{B}	50.5 ^{B}	-	-	-

DL4, 9033942	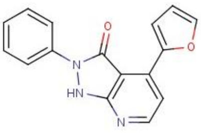	L	-4.782	>100 ^{B}	74.1 ^{B}	-	-	-
DL5, 5676101	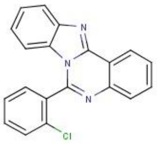	L	-5.586	-	-	-	-	-
DL6, 9119119	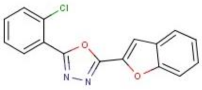	L	-4.942	>100 ^{B}	51.8 ^{B}	-	-	-
DL7, 5712740	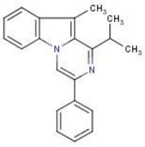	L	-4.982	19.5 ^{B} 23.5 ^{C}	15.0 ^{B} 28.7 ^{C}	31.3	$10^{-1} – 10^{-2}$	1.482
DL8, 5213091	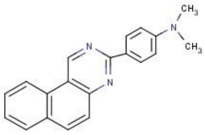	L	-4.899	-	-	-	-	-
DL9, 5215423	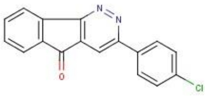	L	-4.735	-	-	-	-	-
DL10, 5737287	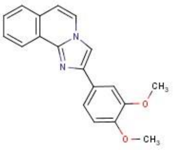	L	-4.848	>100 ^{B}	99.0 ^{B}	-	-	-
DL11, 7640329	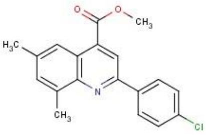	L	-5.163	35.0 ^{B}	16.2 ^{B}	-	$10^{0} – 10^{-1}$	-
DL12, 7229212	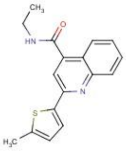	L	-4.678	93.4 ^{B}	69.0 ^{B}	-	-	-
DL13, 6631391	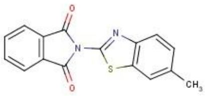	L	-4.591	-	-	-	-	-
DL14, 5401629	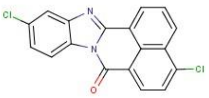	L	-5.290	-	-	-	-	-
DL15, 6872928	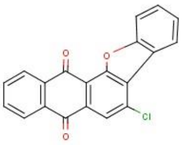	L	-5.183	-	-	-	-	-

DL16, 7361170	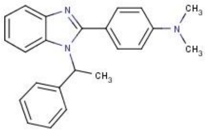	L	-5.301	-	-	-	-	-
DL17, 6690543	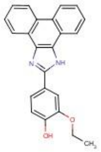	L	-5.481	>100 ^{B}	>100 ^{B}	-	-	-
DP1, 6449207	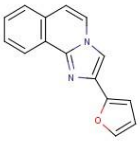	P	-5.179	>100 ^{B}	90.6 ^{B}	-	-	-
DP2, 30091343	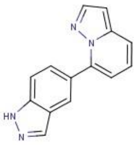	P	-5.173	98.8 ^{B}	70.0 ^{B}	-	-	-
DP3, 21992432	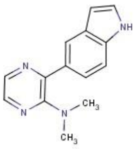	P	-5.230	>100 ^{B}	63.9 ^{B}	-	-	-
DP4, 7916732	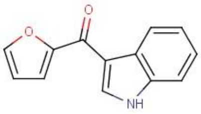	P	-4.583	93.4 ^{B}	>100 ^{B}	-	-	-
DP5, 5141622	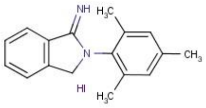	P	-5.411	90.4 ^{B}	90.5 ^{B}	-	-	-
DP6, 5120994	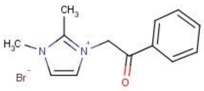	P	-4.580	95.0 ^{B}	85.6 ^{B}	-	-	-
DP7, 5121141	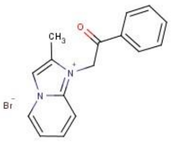	P	-5.345	>100 ^{B}	97.7 ^{B}	-	-	-
DP8, 7547759	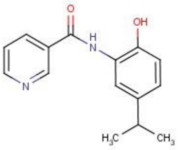	P	-5.435	84.8 ^{B}	95.0 ^{B}	-	-	-
DP9, 5107631	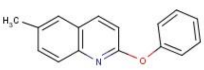	P	-4.986	74.2 ^{B} 65.8 ^{C}	95.9 ^{B} >100 ^{C}	97.4	$10^{-1} – 10^{-2}$	> 25
DP10, 65195788	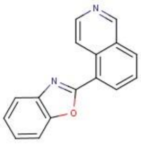	P	-5.159	>100 ^{B}	>100 ^{B}	-	-	-

DP11, 78296026	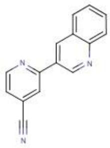	P	-4.815	-	-	-	-	-
DP12, 7750337	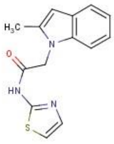	P	-5.627	>100 ^{B}	91.6 ^{B}	-	-	-
DP13, 5175182	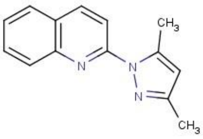	P	-4.623	>100 ^{B}	92.9 ^{B}	-	-	-
DP14, 5108039	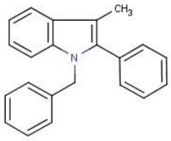	P	-6.157	32.7 ^{B}	16.7 ^{B}	-	10^{0}	-
DP15, 9059508	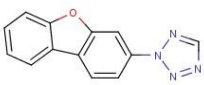	P	-4.886	>100 ^{B}	70.0 ^{B}	-	-	-
DP16, 5302843	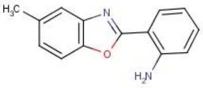	P	-4.610	87.2 ^{B}	87.1 ^{B}	-	-	-
DP17, 9207910	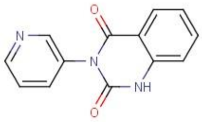	P	-4.901	>100 ^{B}	86.7 ^{B}	-	-	-
DP18, 5760804	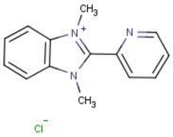	P	-4.590	>100 ^{B}	>100 ^{B}	-	-	-
DP19, 5356162	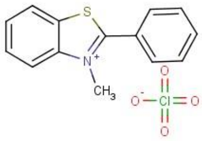	P	-4.598	>100 ^{B}	95.7 ^{B}	-	-	-

Table A.6 Summary of compound data.

A summary of data generated during in vitro in vitro dye release experiments and plaque assays for novel compounds, alongside previously identified adamantane or amiloride derivatives. The compound ID and ChemBridge (CB) ID are listed where appropriate, along with the molecular structure. Where established the eHiTS scores achieved when docking the compound against the 2RLF-based E195 M2 homology model lumenal (L) or peripheral (P) binding site is stated. Dye release data are given for each peptide, as a percentage relative to the DMSO control. Different experiments are denoted by superscripts: $^{'A'}$ - 25 nM N31 peptide screens, $^{'B'}$ - 40 µM screen, $^{'C'}$ - compound titration. In the case where a higher concentration of compound was used these results are denoted by $^{'D'}$ - 200 µM compound, 40 nM peptide or $^{'E'}$ - 50 µM compound, 25 nM peptide. Plaque assay screening data are given as scientific notation changes relative to the DMSO control. Results marked with $^{'F'}$, denote they were carried out at Imperial College London using a MOI of 0.0001. Compound IC_{50} results are given in µM. When there is no experimental data this is denoted by '-'.